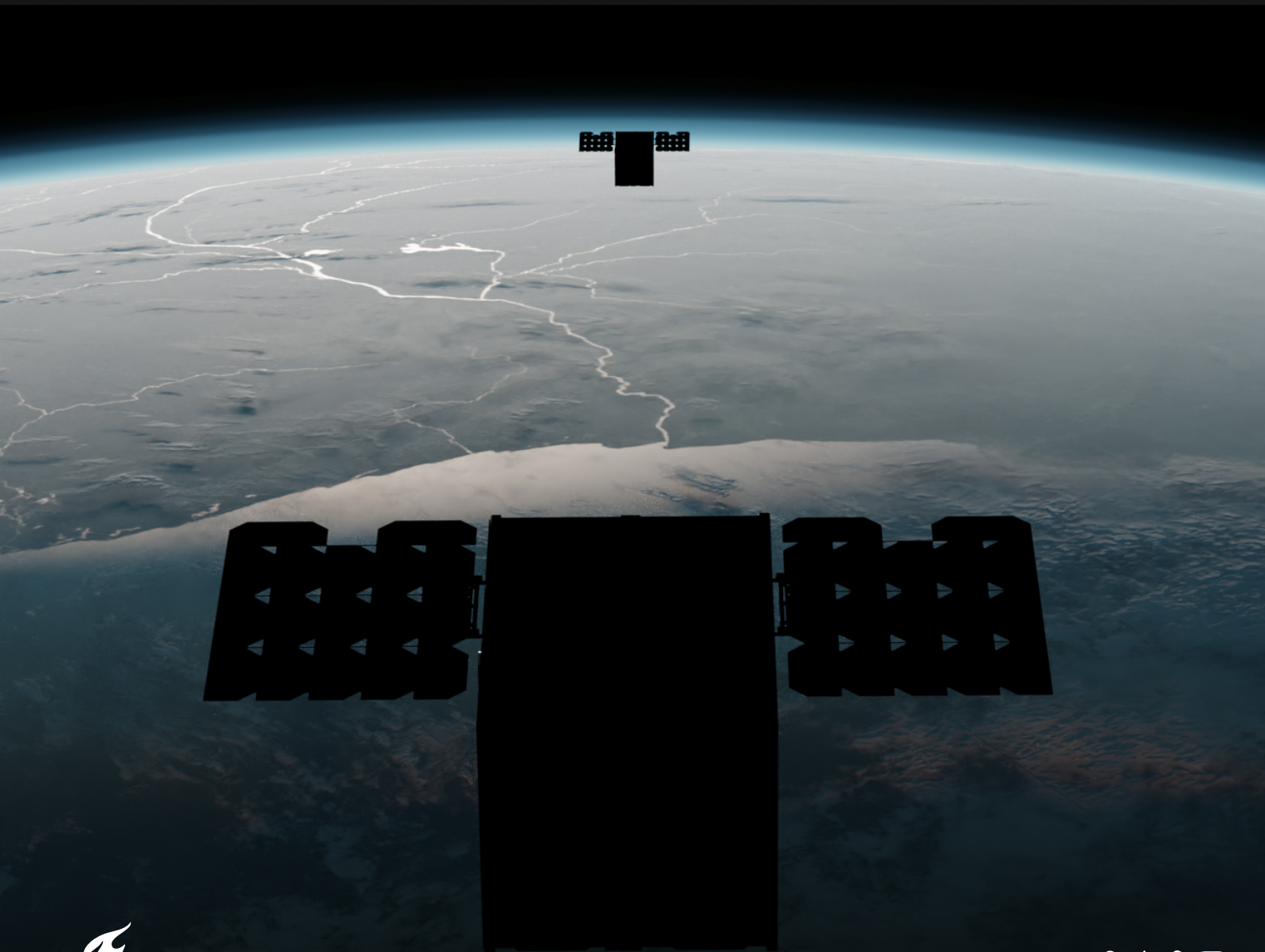


Constellation for Aerosol Surveillance around the Equator

Final Report

Design Synthesis Exercise (AE3200)

Group 16



This page has been intentionally left blank.

Constellation for Aerosol Surveillance around the Equator

Final Report

by

Group 16

Jasper Jeuken	4856716
Efe Kulaksizoglu	4650409
Freek Kunz	4829409
Rudolf Maununen	4803930
Tijs Peeters	4874110
Jakub Plutecki	4838513
Ties Rozema	4672496
Noah van Santen	4838750
Remi Storme	4682793

Principal Tutors:	Dr. ir. J.M. Kuiper - AE Prof. dr. ir. H.W.J. Russchenberg - CiTG
Coaches:	Ourania Altiparmaki & Jesse Reusen
Teaching Assistant:	Lorenza Mottinelli
Institution:	Delft University of Technology, Faculty of Aerospace Engineering
Location:	Delft, the Netherlands
Project Duration:	April 2021 - July 2021

Preface

The following report has been authored by a team of 9 Aerospace Engineering students as part of their final Bachelor's project at Delft University of Technology. In this final project, we are presented with the opportunity of collaborating as a group to improve our skills in project management, aerospace design and systems engineering.

This report has a target audience of engineers, managers and academics with a fundamental technical understanding of aerospace engineering. Herein, it shall be assumed that the reader possesses a Bachelor's degree level of knowledge in aerospace systems, as well as in relevant engineering sub-disciplines.

We would like to extend our gratitude to staff members Dr. Ir. Hans Kuiper, Prof. Dr. Ir. Herman Russchenberg, Ourania Altiparmaki MSc., and Jesse Reusen MSc., as well as our teaching assistant Lorenza Mottinelli BSc. for their continued support and guidance during this design synthesis exercise. We would also like to thank Ir. Joris Melkert for coordinating the project, and Jurrien Vos BSc. for contributing valuable expertise.

Furthermore, we also wish to thank Dr. Martijn Smit (SRON), Dr. Andrew Bell (TNO), and Prof. Dr. Giampiero Gerini (TNO) for providing knowledge and insights supporting the completion of this report.

*Group 16
Delft, June 2021*

Summary

This report presents the final report for the Constellation for Aerosol Surveillance around the Equator (CASE) mission as written by Group 16 as part of the Design Synthesis Exercise (DSE) from the Faculty of Aerospace Engineering (AE) of Delft University of Technology. The team has been assigned to design an Earth-observing aerosol detection system over a period of ten weeks. The aim of this project is to find a higher performance, more sustainable and more cost effective solution for aerosol detection, compared to the alternatives currently available. This was done by analyzing the alternatives for the spectro-polarimeter payload and the observation platform.

This report is written to outline the final design stage of the CASE mission. It continues where the Midterm Report concluded, with a final design concept and preliminary subsystems. These subsystems are now elaborated upon in further detail, sizing the individual components that the satellite will host. This allows for an accurate resource and budget estimation to be performed, resulting in the CASE spacecraft possessing the following details. The TNO optical metasurfaces based spectro-polarimeter will be hosted on a constellation of 3 spacecraft, in an equatorial orbit. Each spacecraft will have a 12U CubeSat structure with a total mass of 12.451 kg and a total cost of 32 M€. The contributions of each subsystem to these final characteristics can be found in their respective subsections. The total cost of the mission including supporting ground stations and launch has also been estimated to require 120 M€. Furthermore, each spacecraft has an estimated reliability of 81.5%, while the launcher possesses a reliability of 85%.

Contributing factors to the final design such as risk, sustainability and profitability are also elaborated upon to provide a holistic assessment of the CASE mission. Sustainability is essential to ensure that an ethical philosophy has been employed, and that the sustainability requirements are respected. The adherence to requirements has also been confirmed in a compliance and feasibility analysis.

The marketability and profitability have also been investigated in substantial detail. To maximize the marketability and interest to investors, a collection of renders have been produced in line with the final configuration; to ensure the design has accurately converged to its final version, a sensitivity analysis was performed to visualize the effects of varied inputs. Also, to confirm that the calculations and analyses leading to the final design are reputable, significant stress has been placed on the verification and validation of those methods.

Delving into the individual subsystems, each has been sized down to its individual components or subcomponents, allowing for an accurate sizing of the final design. The telemetry, tracking & command and guidance, navigation & control subsystems could be sized from the data rate. For the former, a Hyperion Technologies CubeCat laser communications system was selected with a mirror based coarse pointing assembly for bi-directional pointing. For the guidance, navigation & control subsystem, a global navigation satellite system patch antenna and receiver from ISISpace were chosen. The remaining subsystems were also sized simultaneously, and iteratively. The propulsion system was designed with a Tethers Unlimited HYDROS-C engine, favoured for its sustainability and green fuel usage. The command & data handling subsystem was equipped with an ISISpace on-board computer processing unit. The passive thermal control varies per subsystem, but consists of a multi-layer insulation constructed from a variety of materials, depending on the subsystem in question. Graphite fiber thermal straps are also included to facilitate necessary heat distribution across the components. The former is supplied by Frako-Term while the latter are provided by Technology Applications, Inc. The spacecraft will be covered with the black lacquer of Paladin, to ensure the desired internal temperature range. The attitude determination & control subsystem then consists of an assembly of magnetorquers, star trackers and sun sensors. The magnetorquers serve as the actuators of the spacecraft and are acquired from Hyperion, while the two sensor types (star and sun) are obtained from OCE Technologies and NEEDRONIX, respectively. The electrical power subsystem comprises of a solar array, battery, and power conditioning & distribution unit. The solar array uses the QJ Solar Cell 4G32C supplied by Azur Space; the OPTIMUS-40 battery from AAC Clyde Space was selected as the battery component; the PCDU was selected to be the STARBUCK-NANO-PLUS, also from AAC Clyde Space. Finally, Rocket Lab's Electron Rocket was chosen as the launcher.

Contents

Preface	i	9.4 Final Concept	36
Summary	ii	10 Astrodynamic Characteristics	38
Abbreviations	v	10.1 Orbit Characteristics & ΔV Budget . . .	38
List of Figures	vi	10.2 Points of Interest	39
List of Tables	vii	10.3 Results	41
1 Introduction	1	10.4 Risk	43
2 Project Objectives	2	10.5 Sustainability	44
3 User Requirements & Constraints	3	11 Payload Subsystem	45
3.1 Stakeholder Requirements	3	11.1 Optical Metasurfaces Based Spectro- Polarimeter	45
3.2 Mission Requirements	4	11.2 Configuration Trade-Off	46
3.3 System Requirements	5	11.3 Instrument Characteristics	49
3.4 Subsystem Requirements	6	11.4 Verification and Validation	50
4 Market Analysis	11	11.5 Risk	51
4.1 Earth Observation and Aerosol Detection	11	11.6 Sustainability	51
4.2 Target Locations	12	12 Propulsion Subsystem	52
4.3 Market Positioning	14	12.1 Subsystem Selection	52
5 Technical Risk Assessment	18	12.2 Sizing	54
5.1 System-level Technical Risk Analysis . .	18	12.3 Verification and Validation	57
5.2 Risk Maps & Mitigation Strategies	19	12.4 Risk	57
5.3 Subsystem-level Technical Risk Analysis	21	12.5 Sustainability	57
6 Sustainable Development Strategy	23	13 Command & Data Handling Subsystem	58
6.1 Sustainability Definition	23	13.1 Data Handling Block Diagram	58
6.2 Mission Life Cycle Assessment	23	13.2 Processing Requirements	59
6.3 Subsystem Life Cycle Assessment	25	13.3 Component Selection	62
7 RAMS Characteristics	26	13.4 Spacecraft Data Bus	63
7.1 Reliability	26	13.5 Verification and Validation	63
7.2 Availability	29	13.6 Risk	64
7.3 Maintainability	29	13.7 Sustainability	64
7.4 Safety	30	14 Thermal Subsystem	65
7.5 Conclusion	30	14.1 Temperature Requirements	65
8 Verification & Validation	31	14.2 Active Control	66
8.1 System-level V&V	31	14.3 Passive Control	66
8.2 Subsystem-level V&V	32	14.4 Verification and Validation	69
9 Preliminary Design Overview	33	14.5 Risk	69
9.1 Observation Platform	33	14.6 Sustainability	69
9.2 Preliminary Design Concepts	34	15 Tracking, Telemetry & Command Subsystem	70
9.3 Trade-off Summary	35	15.1 Data Generation and Transmission	70
		15.2 Selection of a Laser Communication System	70
		15.3 Coarse Pointing Assembly	71
		15.4 Verification and Validation	73
		15.5 Risk	73
		15.6 Sustainability	73
		16 Attitude Determination & Control Subsystem	75
		16.1 Sensors	75
		16.2 Actuators	77
		16.3 ADCS Overview	81
		16.4 Verification and Validation	81
		16.5 Risk	82
		16.6 Sustainability	82
		17 Guidance, Navigation & Control Subsystem	83
		17.1 GNSS Receiver	83

17.2 GNSS Antenna	83	21.5 Risk	108
17.3 Verification and Validation	84	21.6 Sustainability	108
17.4 Risk	84		
17.5 Sustainability	84	22 Configuration & Layout	109
18 Electrical Power Subsystem	85	22.1 Outer Envelope	109
18.1 Subsystem Selection	85	22.2 Component Configuration	110
18.2 Verification and Validation	89	22.3 Cabling Harness	112
18.3 Risk	89		
18.4 Sustainability	90	23 Final Design Overview	114
		23.1 Subsystem Design	114
19 Structural & Material Characteristics	91	23.2 Hardware/Electrical Block Diagram . . .	116
19.1 Primary Structure Selection	91	23.3 Software Diagram	117
19.2 Payload Platform	94	23.4 Operations & Logistic Concept Description	117
19.3 Launcher Integration	96		
19.4 Verification and Validation	96	24 Compliance Matrix & Feasibility Analysis	119
19.5 Risk	97		
19.6 Sustainability	97	25 Sensitivity Analysis	121
		25.1 Change in Dry Mass	121
20 Launch Vehicle Selection	98	25.2 Change in Volume	121
20.1 Launch Vehicle Data & Justification . . .	98	25.3 Change in Power Consumption	122
20.2 Dedicated Launch Justification	99		
20.3 Launcher Trade-off	99	26 Cost Breakdown Structure & Profitability	124
20.4 Sensitivity Analysis	100	26.1 Cost Breakdown Structure	124
20.5 Deployer Selection	100	26.2 Profitability Analysis	126
20.6 Verification and Validation	101		
20.7 Risk	101	27 Conclusion	128
20.8 Sustainability	102		
		Personal Communication	129
21 Ground Segment	103	Bibliography	131
21.1 Ground Station Network	103		
21.2 Availability Estimation	105	A Organizational Structure, Functional &	
21.3 Locations	106	Post-DSE Diagrams	131
21.4 Verification and Validation	108	B Second Moment of Area	137

Abbreviations

Abbreviation	Definition
ADCS	Attitude Determination & Control System
AE	Aerospace Engineering
AHP	Analytic Hierarchy Process
AOD	Aerosol Optical Depth
AT	Acceptance Testing
BATV	Battery Voltage
BER	Bit Error Rate
BCR	Battery Charge Regulator
BOL	Begin Of Life
CAD	Computer-Aided Design
CASE	Constellation for Aerosol Surveillance around the Equator
CDH	Command & Data Handling
CI	Consistency Index
CiTG	Civil Engineering and Geosciences
COTS	Commercial Off-The-Shelf
CPA	Coarse Pointing Assembly
CR	Consistency Ratio
DOA	Dead On Arrival
DOD	Depth Of Discharge
DSE	Design Synthesis Exercise
EDLK/EDL	Aluminized Polyester and Chemical Fiber Spacer
ELK/EL	Aluminium Foil and Chemical Fiber Spacer
EOL	End of Life
EPS	Electrical Power System
ESA	European Space Agency
FOV	Field Of View
FWHM	Full Width at Half Maximum
GEO	Geostationary Orbit
GFTS	Graphite Fibre Thermal Straps
GLONASS	GLObalnaja NAvigatsionnaja Spoetnikovaja Sistema
GNC	Guidance, Navigation & Control
GNSS	Global Navigation Satellite System
GPS	Global Positioning System
GS	Ground Station
GSD	Ground Sampling Distance
GTO	Geostationary Transfer Orbit
ID	Identifier
I ² C	Inter Integrated Circuit
I/O	Input/Output
IPS	Instructions Per Second
LCA	Life Cycle Assessment
LEO	Low Earth Orbit
LNCH	Launch
LV	Launch Vehicle
MIS	Mission

Abbreviation	Definition
MLI	Multi Layer Insulation
MMOI	Mass Moment Of Inertia
MNS	Mission Need Statement
MOCET	Mission Operations Cost Estimation Tool
MPPT	Maximum Power Point Tracking
MS	Margin of Safety
NASA	National Aeronautics and Space Administration
NGO	Non-Governmental Organization
OBC	On-Board Computing
OS	Operating System
PCB	Printed Circuit Board
PCU	Power Conditioning Unit
PCDU	Power Conditioning and Distribution Unit
PDU	Power Distribution Unit
PL	Payload
POI	Point of Interest
POS	Project Objective Statement
PROP	Propulsion
PTD-1	Pathfinder Technology Demonstration 1
QT	Qualification Testing
RAMS	Reliability, Availability, Maintainability and Safety
R&D	Research and Development
RF	Radio Frequency
ROI	Return on Investment
RSK	Risk
SEE	Single Event Effects
SNR	Signal-to-Noise Ratio
SoH	State of Health
SPI	Serial Peripheral Interface
SSA	Single Scattering Albedo
SSO	Sun-Synchronous Orbit
SRON	Netherlands Institute for Space Research
ST	Stakeholder
STR	Structures
SYS	System
SWOT	Strengths, Weaknesses, Opportunities, Threats
TBD	To Be Defined
TC	Thermal Control
TNO	Netherlands Organisation for Applied Scientific Research
TRL	Technological Readiness Level
TT&C	Telemetry, Tracking & Command
TUI	Tethers Unlimited, Inc.
UN	United Nations
V&V	Verification & Validation
WWF	World Wide Fund for Nature

List of Figures

4.1	Market segmentation for small satellites	11	14.2	Temperature range of solar panels over β -angle. 67
4.2	Net official development aid received	14	14.3	Schematic of GFTS configuration. 68
5.1	Risk map before mitigation. 20		15.1	CubeCat by Hyperion Technologies. 71
5.2	Risk map after mitigation. 21		15.2	Mirror based CPA 72
7.1	CubeSat failure by subsystem after injection . 26		15.3	Risley prism based CPA 72
7.2	Reliability estimation of CubeSats over one year 27		16.1	Magnetic field around the equator at 500 km altitude 79
7.3	NASA reliability estimate 28		19.1	12-Unit CubeSat structure from ISISpace. . . 91
9.1	Schematic visualisations of the design concepts 34		19.2	Free body diagram of the payload platform. . 95
9.2	Preliminary render of the subsystem layout in the satellite 37		19.3	Payload integration into the launch vehicle . . 96
10.1	Visualisation of the final orbit 38		20.1	12U QuadPack by ISISpace for CubeSat deployment 101
10.2	ΔV budget at various altitudes 39		21.1	Relationship between contact time and different GS latitudes 104
10.3	Differences in swath coverage depending on target selection 41		21.2	Average annual afternoon data of cloud coverage across Earth based on daily measurements 105
10.4	Off-nadir pointing required for measurements at varying latitudes 42		21.3	Example reliability calculations for a configuration with five GSs 106
10.5	Spatial density of LEO space debris 43		21.4	Overview of 7 GS locations and their slant range 107
11.1	Mean absolute errors of aerosol optical depth and single scattering albedo 46		22.1	Factors contributing to the outer envelope of the CASE spacecraft 109
11.2	Retrieval noise and regularization error on the retrieved optical thickness of aerosols 49		22.2	Positioning of solar arrays on the spacecraft. . 110
11.3	Schematic 3D render of the angled payload structure 50		22.3	Placement of the payload, propulsion, and telecommunications subsystems 111
12.1	Water electrolysis rocket propulsion diagram 53		22.4	Positioning of components with outside view. 111
12.2	HYDROS-C engine dimensions 56		22.5	Positioning of the processing unit, battery units, and magnetorquers. 112
13.1	Data flow block diagram for the space and ground segments 59		22.6	Positioning of PCDUs and GNSS receiver. . . 112
14.1	Temperature range over β -angle 67		22.7	Final configuration of the spacecraft. 112
			22.8	Assumed cabling between two connectors compared to the straight line distance. 113
			23.1	Hardware/Electrical Block Diagram. 116
			23.2	Software diagram. 117
			23.3	Logistic diagram. 118
			26.1	Cost Breakdown Structure. 125
			26.2	Fund Allocation. 126
			B.1	Cross sections of the primary 12U structure. . 137
			B.2	Cross sections shapes with dimensions in mm. 137

List of Tables

3.1	Abbreviations used in the requirement IDs. . .	3
4.1	Strengths, Weaknesses, Opportunities, Threats (SWOT) Analysis	16
8.1	Verification & validation strategies shown for each subsystem.	32
9.1	Trade-off between a stratospheric balloon and satellite constellation	33
9.2	Design option specification.	34
9.1	Assessment of grading criteria per design concept for trade-off	34
9.2	Weights assigned to each trade-off criteria . .	35
9.3	Trade-off results, score per criterion.	35
9.4	Overview of change in relative importance factors for sensitivity analysis.	36
9.5	New concept scores after adding the final design	36
10.1	Summary of orbital characteristics.	38
10.2	ΔV budget of the spacecraft.	39
10.3	Specification of the mission targets, divided into three categories based on their priority. .	40
10.4	Properties of the measurements during the orbit	41
10.5	Time between measurements and the required pointing change.	42
11.1	Requirements Optical Metasurfaces Based Spectro-Polarimeter from TNO	45
11.2	Options considered for the payload instrument configuration.	47
11.3	Assessment of the criteria for each of the payload configuration options.	48
11.4	Weights assigned to each criteria	48
11.5	Scores for each of the payload configuration options	48
11.6	Payload configuration sensitivity analysis . .	49
11.7	Properties Gpixel GSENSE400BSI Cooled Back illuminated USB3 camera	50
11.8	Payload instrument properties.	51
12.1	Properties of the HYDROS-C water propulsion unit	54
12.2	HYDROS-C Sizing for the CASE mission. .	56
13.1	Contributions to the required throughput of the processing unit	60
13.2	Estimation of the number of words per second m [28].	61

13.3	Contributions to the required data storage capacity.	62
13.4	Properties of the selected processing unit . . .	62
13.5	Connections between various subsystem components and the CDH subsystem	63
14.1	Operating temperatures of the spacecraft components.	65
14.2	Multi-layer insulation properties.	68
14.3	Properties Graphite Fiber Thermal Straps. . .	68
15.1	Payload measurement time vs downlink data rate.	70
15.2	Various optical communication systems . . .	71
15.3	Properties of the CubeCat	71
16.1	List of star trackers and their most important parameters.	76
16.2	List of sun sensors and their most important parameters.	77
16.3	Latitude, longitude and their difference between Nairobi and Singapore	77
16.4	Magnetic dipole moment required for the magnetorquer for pitch yaw and rolling motion. .	80
16.5	Properties of the different ADCS parts	81
17.1	Various GNSS receivers	83
17.2	Various GNSS antennas.	84
18.1	Parameters and intermediate results used for solar array sizing.	86
18.2	Properties of the selected solar cell.	87
18.3	Parameters and intermediate results used for battery sizing.	88
18.4	Properties of the selected battery.	88
18.5	Properties of the selected PCDU.	89
19.1	Properties of the selected 12U structure from ISISpace.	92
19.2	Properties of the Aluminum 7075-T6	92
19.3	Loads experienced by the spacecraft during CASE mission.	93
19.4	Geometrical properties of the 12U CubeSat. .	93
19.5	Structural analysis results of the primary structure.	94
19.6	Properties of the Aluminum 2014-T6.	95
19.7	Structural analysis results of the payload platform.	95
19.8	Verification tests on structural model.	96
20.1	Assessment of the criteria for launcher selection.	98
20.2	Weights assigned to each criteria.	99
20.3	Scores for each launcher.	100
20.4	Launch vehicle sensitivity analysis	100
21.1	Availability for different numbers of GSs. . .	106
21.2	Selected GS locations around the equator. . .	107
21.3	Contingency factor for GS contact.	107

22.1 Properties of the cabling harness in the space-craft.	113	25.1 Dry mass sensitivity analysis.	121
23.1 Summary of the components selected for the detailed design.	114	25.2 Volume sensitivity.	122
23.2 Detailed power budget.	115	25.3 Power consumption sensitivity.	122
24.1 Compliance matrix	120	25.4 Power Consumption Sensitivity of Thermal Subsystem.	123
		26.1 Cost Breakdown Structure.	124
		26.1 Cost Breakdown Structure.	125
		26.2 Cost breakdown per subsystem.	125

1. Introduction

Over recent decades the concentration of aerosols in the atmosphere has increased substantially. This is particularly significant in regions such as North Africa, South-East Asia and the Amazon suffering from elevated pollution levels due to the increased presence of such aerosols. This is believed to have a contribution to global warming, however, due to lack of data, current research is insufficient to determine whether aerosols contribute to warming or cooling of the atmosphere¹. Beyond the global warming concerns, there remain environmental considerations resulting from the increased aerosol presence. The effects on ecosystems and communities also sets forth a cause for investigation. Hence, this field's great absence of research-driven data presents an opportunity for a contemporary solution. This Design Synthesis Exercise aims to investigate this further by designing the observation platform and analyzing the available instruments needed to perform such measurements [1].

This report aims to provide a final design of the spacecraft upon which the instrumentation will be hosted [1]. This is a decisive stage of the design process, where a final concept has already been selected, and is subjected to an in-depth analysis regarding its subsystems, configuration, and compliance with requirements. Employing a top-down approach, each subsystem can be elaborated upon to provide a finer level of detail. With these details it is possible to accurately assess the final design's configuration and ability to adhere to the stakeholder requirements. Hereafter, the final budgets can be discussed, addressing mass, volume, power, and cost. For the inquisitive financial stakeholders, the cost budget is elaborated upon with a profitability assessment obtained from a market analysis. On a final note, the report delivers on the processes required to continue the CASE mission to completion.

The report will assume the following structure, beginning with a chapter discussing the project objectives in Chapter 2, followed by the user requirements as established in previous reports in Chapter 3, adjusted where necessary. Then a market analysis is performed to estimate the marketability of a venture such as the CASE mission, Chapter 4. Next, a recap is provided of results from previous reports in Chapter 9. Chapters 5, and 6 assess the technical risks and sustainability of the CASE mission, respectively. The reliability, availability, maintainability and safety characteristics are then outlined in Chapter 7, while verification & validation procedures for the subsequent subsystem designs are outlined in Chapter 8. Chapter 10 then pioneers the subsystem designs, and is followed by the payload (PL, Chapter 11), propulsion (PROP, Chapter 12), command & data handling (CDH, Chapter 13), thermal control (TC, Chapter 14), telemetry, tracking & command (TT&C, Chapter 15), attitude determination & control (ADCS, Chapter 16), guidance, navigation & control (GNC, Chapter 17), electrical power system (EPS, Chapter 18), and structural subsystems (STR, Chapter 19). Finally, launch vehicle (LV) selection and ground station (GS) design are outlined in Chapters 20 and 21, respectively. The configuration of the final design and its layout are documented in Chapter 22; a final design overview is provided in Chapter 23. The results are then corroborated by Chapters 24 and 25. A final cost breakdown is provided in Chapter 26. Finally, the report is concluded in Chapter 27. Supporting diagrams, moment of area calculations, and task distributions are provided in Appendices A, B, and ??, respectively.

¹<https://earthobservatory.nasa.gov/features/Aerosols>, [Retrieved on May 19, 2021]

2. Project Objectives

The aim of this project is to design a mission that enables the gathering of valuable data about aerosols in different parts of the world. The stakeholders, Herman Russchenberg and Hans Kuiper, have stated their needs in terms of filling in the science gap. The mission aims to have higher temporal resolution than many other existing missions for detecting aerosols. Furthermore, the payload alternatives that are considered are state of the art technologies. So, this mission also aims to be competitive in terms of spatial resolution. It is the group's aim to design a mission that enables high-performance aerosol detection with low cost and good sustainability using system engineering methods. The project objectives are [1]:

“Provide a solution to enhance atmospheric aerosol detection and monitoring with industry-leading spatial resolution.”

Mission Need Statement (MNS)

“Design an aerosol Earth-observation system with industry-leading spectro-polarimetric sensors.”

Project Objective Statement (POS)

This is a large scale project that enables the monitoring of various locations on Earth. Therefore, several stakeholders are present from all over the globe. Aerosol data is valuable for the science community and is highly demanded. It can be correlated to public health and well being. Furthermore, the effect of aerosol levels on climate can be examined. The relationship between storms, hurricane formations and aerosol levels can provide valuable knowledge. Lastly, the effect of aerosol concentrations on agriculture in developing countries can also provide very valuable data. The data gathered by this mission can serve as a validation tool for data that has already been gathered, and can help predictive models become more accurate [1].

The Dutch government and TU Delft are stakeholders in this mission. The Dutch government has been increasing their efforts to be a part of the growing space industry. They have been able to breach the market with their industry-leading spectro-polarimeter. Their combined efforts with the Netherlands Institute for Space Research (SRON) provided them with a chance to be a part of a very large scale National Aeronautics and Space Administration (NASA) mission. Now with a newer chip being developed by the Netherlands Organisation for Applied Scientific Research (TNO), the Dutch government will most likely want to stay as the industry leader in this niche field. Consequently, TNO and SRON are also stakeholders since the choice of payload helps validate their design. Lastly, as this mission is covering different areas, it will also create jobs and opportunities in multiple nations, such as Kenya, Uganda, and Ecuador.

In conclusion, the mission aims to provide industry-leading aerosol monitoring system with high-performance resolution, low cost and good sustainability. It will provide valuable data for fields such as agriculture and health, in addition to increasing knowledge about aerosol effects on weather and climate. Due to these reasons, it is worthwhile to design this mission and gain more information about aerosols.

3. User Requirements & Constraints

In this chapter, the requirements and constraints for the CASE mission are presented. Firstly, the requirements set out by the stakeholders are detailed. Following this, the top-level mission requirements, as well as the system requirements for both the space and ground segment are specified. Finally, the requirements for each subsystem on the spacecraft are given. Once the design iteration is completed, a compliance matrix and feasibility analysis is provided, which can be consulted in Chapter 24.

Some of the requirements were altered during the design process in consultation with the stakeholders. The changes made to a requirement are depicted using color: red text indicates the initial status and black text indicates the current status. Additionally, an altered requirement is indicated with roman numerals in the unique identifier (ID). In Table 3.1, the abbreviations used for the requirements can be found.

Table 3.1: Abbreviations used in the requirement IDs.

Abbreviation	Meaning
ADCS	Attitude Determination & Control
CDH	Command & Data Handling
GNC	Guidance, Navigation & Control
MIS	Mission
PL	Payload
EPS	Electrical Power System
PROP	Propulsion
ST	Stakeholder
STR	Structures
SYS	System
TBD	To Be Defined
TC	Thermal Control
TTC	Tracking, Telemetry & Command
Requirement - A	Performance based requirement
Requirement - B	Sustainability based requirement
Requirement - C	Cost based requirement
Requirement - D	Safety based requirement
Requirement - E	Logistics & operations based requirement

3.1. Stakeholder Requirements

The stakeholders have determined several requirements that the mission should adhere to. These were already listed as user requirements in the project plan [2]. They serve as a basis for the mission, system and subsystem requirements that were generated in the baseline report [3]. Note that the requirement ID includes the categories A through E, the meaning of which is given in Table 3.1. The requirement status (unchanged, changed, defined, new, or removed) is also shown, as well as a column dedicated to requirement verification & Validation (V&V). This column outlines through which process the requirements will be verified and/or validated. Finally, there is also a column which indicates the origin of the requirement. The possible options for this column are the following: Stakeholders (SH), Baseline Report (BR), Midterm Report (MR), Functional Analysis (FA), Risk Analysis (RA).

Status	Identifier	Description	V&V	Origin
Changed	CASE-ST-A01-II	The mission shall have a spatial resolution of 100 x 100 1000 x 1000 m ² .	Testing	SH
	CASE-ST-A02	The mission shall have an area coverage of 250 x 250 km ² .	Analysis	SH
	CASE-ST-A03	The mission shall have a visible light (VIS) spectral resolution of 100 nm.	Testing	SH

Changed	CASE-ST-A04-II	The mission shall have a temporal resolution of 30 minutes 2 hours at Points of Interest (POIs).	Analysis	SH
	CASE-ST-A05	The mission shall have a Signal-to-Noise value of at least 100.	Analysis	SH
Defined	CASE-ST-A06	The polarimeter instrument shall have a polarimetric accuracy of 0.003.	Testing	MR
	CASE-ST-A07	The mission shall have a duration of at least 2 years.	Analysis	SH
New	CASE-ST-A08	The mission shall have a swath width at least 40 km.	Analysis	SH
	CASE-ST-B01	The spacecraft shall consist of only non-toxic materials.	Inspection	SH
	CASE-ST-B02	The mission shall use the End of Life (EOL) strategy of burning the satellite.	Analysis	SH
Removed	CASE-ST-C01	The mission shall not exceed 4 M€ total for a constellation of 4 CubeSats and the required ground segment.	Inspection	SH
Defined	CASE-ST-C02	The mission shall not exceed a total cost of 70 M€.	Inspection	MR
	CASE-ST-D01	The spacecraft shall not damage the launcher.	Testing	BR
	CASE-ST-D02	The spacecraft shall not damage other payload inside the launcher.	Testing	BR
	CASE-ST-D03	The mission shall have a reliability of at least 98%.	Testing	BR

3.2. Mission Requirements

From the stakeholder requirements, several top-level requirements were derived. These requirements affect the mission as a whole and are thus called mission requirements. These are listed below for the CASE mission, along with unique identifiers for later referencing.

Status	Identifier	Description	V&V	Origin
	CASE-MIS-A01	The CASE mission shall observe aerosol particles in the troposphere of Earth.	Analysis	BR
	CASE-MIS-A02	The spacecraft shall be brought into orbit in one launch.	Analysis	BR
	CASE-MIS-A03	The spacecraft shall autonomously orient itself to a safe attitude after separation from the launcher.	Analysis	BR
	CASE-MIS-A04	The spacecraft shall complete initialization procedures at most 1 orbital period after launcher separation.	Analysis	BR
Defined	CASE-MIS-A05	The orbit altitude shall be 500 km.	Analysis	MR
Defined	CASE-MIS-A06	The orbit inclination shall be $0^\circ \pm 0.2^\circ$.	Analysis	MR
	CASE-MIS-A07	The orbit eccentricity shall be 0.	Analysis	BR
	CASE-MIS-A08	The spacecraft shall be in view of Ground Stations (GSs) for at least 10% of one orbit.	Testing	BR
	CASE-MIS-A09	The spacecraft shall re-enter the atmosphere at EOL.	Analysis	BR
Defined	CASE-MIS-C01	The development cost of the mission shall not exceed 30 M€.	Inspection	FA
Changed	CASE-MIS-C02-II	The production cost shall not exceed 200000 20 M€ per spacecraft.	Inspection	MR
	CASE-MIS-C03	The operation cost shall not exceed 250,000 € per year for the entire constellation.	Inspection	BR
	CASE-MIS-D01	The spacecraft shall not incur mission failure resulting from the failure of one subsystem component.	Analysis	BR
	CASE-MIS-D02	The space segment shall remain operational during all maintenance activities (planned/unplanned/ground segment maintenance).	Testing	BR
	CASE-MIS-E01	The final CASE mission design shall be completed before the first of July 2021.	Inspection	BR
Changed	CASE-MIS-E02-II	The launch of the CASE mission shall nominally occur before January 2024 2027.	Inspection	MR
Changed	CASE-MIS-E03-II	The CASE mission shall be compatible with launch opportunities in 2024 and 2025 (after nominal launch window) two years after the nominal launch window.	Inspection	MR

CASE-MIS-E04	SI units shall be used throughout the mission timeline; with respect to angular units, radians, degrees and arcseconds are accepted.	<i>Inspection</i>	<i>BR</i>
CASE-MIS-E05	The CASE mission shall have a total mission duration of at least 2 years.	<i>Analysis</i>	<i>SH</i>

3.3. System Requirements

From these mission requirements, several more detailed requirements were generated. These requirements apply to the entire system, which consists of a constellation of spacecraft and a corresponding ground segment. The requirements for both are listed below.

Space Segment

Status	Identifier	Description	V&V	Origin
Changed	CASE-SYS-SS-A01-II	The spacecraft dry mass shall not exceed 50 150 kg per spacecraft.	<i>Inspection</i>	<i>MR</i>
	CASE-SYS-SS-A02	The spacecraft wet mass shall not exceed 175 kg per spacecraft.	<i>Inspection</i>	<i>BR</i>
	CASE-SYS-SS-A03	The spacecraft shall be able to stay in the intended orbit for its lifetime.	<i>Analysis</i>	<i>BR</i>
	CASE-SYS-SS-A04	The spacecraft structure shall withstand launch loads as specified in the launch vehicle catalogue.	<i>Testing</i>	<i>BR</i>
	CASE-SYS-SS-A05	The spacecraft shall be compatible with the launcher integration procedures.	<i>Testing</i>	<i>BR</i>
	CASE-SYS-SS-A06	The spacecraft shall be able to withstand impact of small meteorites and space debris with a probability of 0.998.	<i>Analysis</i>	<i>BR</i>
	CASE-SYS-SS-A07	The spacecraft lifetime for pre-launch ground activities shall be at least 2 years.	<i>Analysis</i>	<i>BR</i>
	CASE-SYS-SS-A08	The spacecraft shall withstand the radiation environment over its entire lifetime.	<i>Analysis</i>	<i>BR</i>
	CASE-SYS-SS-A09	The spacecraft shall accommodate the payload and all subsystems with the mass and volume margins of 5%.	<i>Demonstration</i>	<i>BR</i>
	CASE-SYS-SS-A10	The spacecraft shall have an operational mode in which all subsystems are operational and the payload can take measurements.	<i>Demonstration</i>	<i>BR</i>
	CASE-SYS-SS-A11	The spacecraft shall have a power saving mode in which only critical subsystems are active, which includes EPS, ADCS, TC, and CDH.	<i>Demonstration</i>	<i>BR</i>
	CASE-SYS-SS-A12	The spacecraft shall have a safe mode in which spacecraft and instrument safety are prioritized.	<i>Demonstration</i>	<i>BR</i>
	CASE-SYS-SS-A13	The spacecraft shall autonomously detect separation from the launch vehicle.	<i>Analysis</i>	<i>BR</i>
	CASE-SYS-SS-A14	The spacecraft system shall adhere to Coordinated Universal Time with an accuracy of 100 ms.	<i>Demonstration</i>	<i>BR</i>
	CASE-SYS-SS-A15	The spacecraft shall support changes in the mission timeline by ground command.	<i>Analysis</i>	<i>BR</i>
	CASE-SYS-SS-A16	The spacecraft shall be able to reboot after a critical system failure.	<i>Analysis</i>	<i>BR</i>
	CASE-SYS-SS-A17	In case of cessation of communications between ground and space segment, the spacecraft shall continue its operations autonomously for up to 7 days.	<i>Demonstration/Analysis</i>	<i>BR</i>
	CASE-SYS-SS-A18	The spacecraft shall support remote software updates.	<i>Testing</i>	<i>FA</i>
	CASE-SYS-SS-D01	The spacecraft shall enter safe mode when anomalies prevent autonomous recovery.	<i>Analysis</i>	<i>BR</i>
	CASE-SYS-SS-D02	The spacecraft shall not enter safe mode when a redundant subsystem ceases to function.	<i>Analysis</i>	<i>BR</i>
	CASE-SYS-SS-E01	A right-handed coordinate system shall be used for the spacecraft and mission design: X-axis is the body axis, Z-axis is pointing nadir, Y-axis completes the system.	<i>Inspection</i>	<i>BR</i>

CASE-SYS-SS-E02	The space segment shall use operational software.	<i>Demonstration</i>	<i>FA</i>
------------------------	---	----------------------	-----------

Ground Segment

Status	Identifier	Description	V&V	Origin
	CASE-SYS-GS-A01	The ground segment shall be able to restore functionality in less than 2 hours after system failure.	<i>Demonstration</i>	<i>BR</i>
	CASE-SYS-GS-A02	The ground segment shall be able to monitor probable collision with space debris larger than 3 cm in size.	<i>Testing</i>	<i>BR</i>
	CASE-SYS-GS-A03	The ground segment shall be able to send evasive commands at least 15 minutes in advance of probable collision.	<i>Testing</i>	<i>BR</i>
	CASE-SYS-GS-A04	The ground segment shall collect and report maintenance data of the spacecraft.	<i>Testing</i>	<i>BR</i>
	CASE-SYS-GS-A05	The ground segment shall monitor the quality of the communication link with the space segment.	<i>Testing</i>	<i>BR</i>
	CASE-SYS-GS-A06	The ground segment shall support the maximum uplink data rate as specified in CASE-SYS-TTC-A01 .	<i>Testing</i>	<i>BR</i>
	CASE-SYS-GS-A07	The ground segment shall support the maximum downlink data rate as specified in CASE-SYS-TTC-A02 .	<i>Testing</i>	<i>BR</i>
	CASE-SYS-GS-E01	The ground segment shall archive all received data for future reference.	<i>Demonstration</i>	<i>BR</i>
Removed	CASE-SYS-GS-E02	The ground segment shall have a primary ground segment at <i>TBD</i> .	<i>Inspection</i>	<i>BR</i>
Removed	CASE-SYS-GS-E03	The ground segment shall have a back-up ground segment at <i>TBD</i> .	<i>Inspection</i>	<i>BR</i>
	CASE-SYS-GS-E04	The ground segment shall use operational software.	<i>Demonstration</i>	<i>BR</i>
Added	CASE-SYS-GS-E05	The ground segment shall have sufficient GSs to ensure downlink for at least 90% of the mission.	<i>Inspection</i>	<i>RA</i>

3.4. Subsystem Requirements

Finally, more detailed requirements were generated, specific to each subsystem that the system will consist of. Nine subsystems were considered, which are listed below.

- Payload (PL)
- Electrical Power System (EPS)
- Tracking, Telemetry & Command (TTC)
- Thermal Control (TC)
- Attitude Determination & Control (ADCS)
- Command & Data Handling (CDH)
- Guidance, Navigation & Control (GNC)
- Propulsion (PROP)
- Structure (STR)

The requirements for each of these subsystems are listed separately in a dedicated subsection below. The unique identifiers also include an abbreviation for the relevant subsystem, the meaning of which is given in Table 3.1.

Payload

Status	Identifier	Description	V&V	Origin
Changed	CASE-SYS-PL-A01-II	The field of view of the polarimetry instrument shall comply with CASE-ST-A02 CASE-ST-A08 .	Inspection	MR
	CASE-SYS-PL-A02	The payload subsystem shall only measure at 3 POIs.	Inspection	FA
	CASE-SYS-PL-A03	The payload subsystem shall have a visible light (VIS) spectral resolution of 100 nm.	Testing	SH
Changed	CASE-SYS-PL-A04-II	The payload subsystem shall have a spatial resolution of 100 x 100 1000 x 1000 m ² .	Testing	MR
	CASE-SYS-PL-A05	The payload subsystem shall have an area coverage of 250 x 250 km ² .	Analysis	SH
Changed	CASE-SYS-PL-A06-II	The payload subsystem shall have a temporal resolution of at least 30 minutes 2 hours at POIs.	Analysis	SH
	CASE-SYS-PL-A07	The payload subsystem shall have a polarimetric accuracy of 0.003.	Testing	MR
Defined	CASE-SYS-PL-A08	The payload subsystem shall have a Signal-to-Noise Ratio (SNR) of at least 300.	Analysis	FA
	CASE-SYS-PL-A09	The payload subsystem shall allow for instruments to be calibrated during pre-launch activities.	Testing	BR
	CASE-SYS-PL-A10	The payload subsystem shall allow for instruments to be re-calibrated during the mission.	Analysis	BR
	CASE-SYS-PL-A11	The payload subsystem shall send all data generated to the CDH subsystem.	Testing	FA

EPS

Status	Identifier	Description	V&V	Origin
	CASE-SYS-EPS-A01	The EPS battery shall manage to cope with worst case eclipses.	Testing	BR
	CASE-SYS-EPS-A02	The EPS shall be able to provide the spacecraft's power needs at any stage of the mission.	Analysis	BR
	CASE-SYS-EPS-A03	The EPS shall be sized to account for degradation of the power system during the mission.	Analysis	BR
	CASE-SYS-EPS-A04	The EPS shall store excess generated power when not used and when batteries are not at maximum capacity.	Testing	BR
	CASE-SYS-EPS-A05	The EPS shall be in power saving mode from launch until a Sun acquisition attitude has been reached.	Analysis	BR
	CASE-SYS-EPS-A06	The EPS shall be in power saving mode when the spacecraft is under eclipse conditions.	Testing	BR
	CASE-SYS-EPS-A07	The EPS shall be able to send power data to the CDH subsystem.	Testing	BR
	CASE-SYS-EPS-A08	The EPS shall be made redundant with the implementation of a backup battery.	Analysis	BR

Telemetry, Tracking & Command

Status	Identifier	Description	V&V	Origin
Changed	CASE-SYS-TTC-A01-II	The TT&C subsystem shall be able to receive data at a rate of at least 100 kbit/s.	Testing	MR
Changed	CASE-SYS-TTC-A02-II	The TT&C subsystem shall be able to transmit data at a rate of at most 90 Mbit/s at least 1 Gbit/s.	Testing	MR
Removed	CASE-SYS-TTC-A03	The TTC subsystem shall have a communication link to Earth with a Signal-to-Noise value of at least 100 .	Analysis	BR
	CASE-SYS-TTC-A04	The TTC subsystem shall have a maximum bit error rate (BER) of 10 ⁻³ .	Analysis	BR
	CASE-SYS-TTC-A05	All telemetry data shall be prevented from overwriting until reception (delivery) on Earth is confirmed.	Inspection	BR

Removed	CASE-SYS-TTC-A06	The TT&C subsystem shall operate on the S frequency band.	<i>Inspection</i>	<i>MR</i>
Removed	CASE-SYS-TTC-A07	The TT&C subsystem shall utilize a frequency ranging between 1.92 and 2.88 GHz.	<i>Inspection</i>	<i>MR</i>
	CASE-SYS-TTC-A08	The TTC subsystem shall be able to deliver data received from the GS to the CDH subsystem.	<i>Analysis</i>	<i>BR</i>
	CASE-SYS-TTC-A09	The TTC subsystem shall be able to receive data and commands from the CDH subsystem.	<i>Testing</i>	<i>BR</i>
Removed	CASE-SYS-TTC-A10	The signal-to-noise ratio for the downlink shall be at least 10 dB.	<i>Analysis</i>	<i>MR</i>
Removed	CASE-SYS-TTC-A11	The signal-to-noise ratio for the uplink shall be at least 20 dB.	<i>Analysis</i>	<i>MR</i>
New	CASE-SYS-TTC-A12	The TT&C subsystem shall be able to re-calibrate its connections with the CDH subsystem and ground segment.	<i>Testing</i>	<i>FA</i>
	CASE-SYS-TTC-D01	The TTC subsystem shall not interfere with instrument measurements.	<i>Testing</i>	<i>BR</i>
	CASE-SYS-TTC-D02	The TTC subsystem shall not interfere with other spacecraft subsystems.	<i>Testing</i>	<i>BR</i>

Thermal Control

Status	Identifier	Description	V&V	Origin
	CASE-SYS-TC-A01	The thermal control subsystem shall be able to manage the spacecraft's temperature levels at all stages of the mission.	<i>Testing</i>	<i>BR</i>
	CASE-SYS-TC-A02	The spacecraft temperature during the mission shall remain within temperature ranges as required by the various subsystems on the spacecraft.	<i>Testing</i>	<i>BR</i>
	CASE-SYS-TC-A03	The thermal control subsystem shall provide temperature data to the CDH subsystem.	<i>Testing</i>	<i>BR</i>
	CASE-SYS-TC-A04	The temperature of any surfaces directly contacting with propellant shall not exceed the maximum safe storage temperature.	<i>Testing</i>	<i>BR</i>
	CASE-SYS-TC-A05	The temperature of surfaces directly contacting with propellant shall not drop below the freezing temperature of the propellant.	<i>Testing</i>	<i>BR</i>

Attitude Determination & Control

Status	Identifier	Description	V&V	Origin
	CASE-SYS-ADCS-A01	The ADCS subsystem shall dampen residual angular rates after separation from the launch vehicle within 30 min.	<i>Analysis</i>	<i>BR</i>
	CASE-SYS-ADCS-A02	The ADCS subsystem shall be able to determine its orientation in a fixed orthogonal coordinate system.	<i>Analysis</i>	<i>BR</i>
	CASE-SYS-ADCS-A03	The ADCS subsystem shall be able to maintain attitude estimation in case of critical sensor failure.	<i>Analysis</i>	<i>BR</i>
	CASE-SYS-ADCS-A04	The ADCS subsystem shall bring the spacecraft in a power generating attitude during power saving mode.	<i>Analysis</i>	<i>BR</i>
	CASE-SYS-ADCS-A05	The ADCS subsystem shall possess redundancy to allow for continued operation following failure of one ADCS component.	<i>Testing</i>	<i>BR</i>
	CASE-SYS-ADCS-A06	The ADCS subsystem shall be able to correct the spacecraft orientation in response to a disturbance force or torque.	<i>Demonstration</i>	<i>BR</i>
	CASE-SYS-ADCS-A07	The ADCS subsystem shall be able to sense the spacecraft attitude about three axes with an accuracy complying with CASE-SYS-ADCS-A12 .	<i>Demonstration</i>	<i>BR</i>
	CASE-SYS-ADCS-A09	The sensors in the ADCS subsystem shall transmit attitude data to the CDH subsystem.	<i>Testing</i>	<i>BR</i>
	CASE-SYS-ADCS-A10	The actuators in the ADCS subsystem shall be able to execute commands from the CDH subsystem.	<i>Testing</i>	<i>BR</i>
	CASE-SYS-ADCS-A11	The ADCS subsystem shall be able to adhere to commands from the GNC subsystem.	<i>Testing</i>	<i>BR</i>

Changed	CASE-SYS-ADCS-A12-II	The ADCS subsystem shall have a pointing accuracy better than 66.7 26.5 μ rad.	<i>Demonstration</i>	<i>FA</i>
---------	-----------------------------	--	----------------------	-----------

Guidance, Navigation & Control

Status	Identifier	Description	V&V	Origin
	CASE-SYS-GNC-A01	The GNC subsystem shall be able to determine the spacecraft orbital position with an accuracy of 10 m.	<i>Analysis</i>	<i>BR</i>
	CASE-SYS-GNC-A02	The GNC subsystem shall be able to provide the CDH system with periodic orbital position data.	<i>Analysis</i>	<i>BR</i>
	CASE-SYS-GNC-A03	The GNC subsystem shall be able to determine the required orbital manoeuvres for station keeping.	<i>Analysis</i>	<i>BR</i>
	CASE-SYS-GNC-A04	The GNC subsystem shall be able to provide the CDH system with required attitudes for orbital manoeuvres.	<i>Analysis</i>	<i>BR</i>
	CASE-SYS-GNC-A05	The GNC subsystem shall be able to generate an alternative orbit to avoid probable collisions with space debris.	<i>Analysis</i>	<i>BR</i>
	CASE-SYS-GNC-A06	The GNC subsystem shall be able to determine the spacecraft orbital velocity with an accuracy of 0.01 m/s.	<i>Analysis</i>	<i>BR</i>

Command & Data Handling

Status	Identifier	Description	V&V	Origin
	CASE-SYS-CDH-A01	The CDH subsystem shall be able to store the data generated by the payload before transmission.	<i>Testing</i>	<i>BR</i>
	CASE-SYS-CDH-A02	The CDH subsystem shall be able to store the health and status information from other spacecraft subsystems.	<i>Analysis</i>	<i>BR</i>
	CASE-SYS-CDH-A03	The CDH subsystem shall be able to store housekeeping data of the spacecraft every 10 seconds.	<i>Testing</i>	<i>BR</i>
	CASE-SYS-CDH-A04	The CDH subsystem shall be compatible with the maximum data rates of the payload.	<i>Testing</i>	<i>BR</i>
	CASE-SYS-CDH-A05	The CDH subsystem shall be able to command the subsystems and payload of the spacecraft.	<i>Analysis</i>	<i>BR</i>
	CASE-SYS-CDH-A06	The CDH subsystem shall add location and time tags to observations generated by the payload subsystem.	<i>Analysis</i>	<i>BR</i>
	CASE-SYS-CDH-A07	The CDH subsystem shall be able to receive firmware updates from the ground segment.	<i>Inspection</i>	<i>BR</i>
	CASE-SYS-CDH-A08	The CDH subsystem shall be able to send the stored maintenance data to the TTC when in contact.	<i>Testing</i>	<i>BR</i>
Removed	CASE-SYS-CDH-A09	The CDH subsystem shall provide a TBD quantity of data pre-processing.	<i>Analysis</i>	<i>BR</i>
New	CASE-SYS-CDH-A10	The CDH subsystem shall be able to re-calibrate its connections with the ground segment and subsystems.	<i>Testing</i>	<i>RA</i>
	CASE-SYS-CDH-D01	The CDH subsystem shall encrypt data before transmission to the ground segment.	<i>Testing</i>	<i>BR</i>
	CASE-SYS-CDH-D02	The CDH subsystem shall decrypt encrypted commands from the ground segment.	<i>Testing</i>	<i>BR</i>
	CASE-SYS-CDH-D03	The CDH subsystem shall execute commands from the ground segment.	<i>Inspection</i>	<i>BR</i>
	CASE-SYS-CDH-D04	The CDH subsystem shall perform fault detection and correction.	<i>Testing</i>	<i>BR</i>

Propulsion

Status	Identifier	Description	V&V	Origin
Changed	CASE-SYS-PROP-A01	The propulsion subsystem shall be able to desaturate the ADCS subsystem.	<i>Testing</i>	<i>BR</i>
	CASE-SYS-PROP-A02	The propulsion subsystem shall be able to perform the EOL re-entry burn.	<i>Testing</i>	<i>BR</i>
	CASE-SYS-PROP-A03	The propulsion subsystem shall be able to provide the required ΔV for unforeseen manoeuvres.	<i>Testing</i>	<i>BR</i>
	CASE-SYS-PROP-A04	The propulsion subsystem shall be able to operate under any spacecraft attitude.	<i>Testing</i>	<i>BR</i>
	CASE-SYS-PROP-A05	The propulsion subsystem shall be able to provide at most 2.7 37.2 km/s/year of ΔV for orbit keeping.	<i>Analysis</i>	<i>FA</i>
	CASE-SYS-PROP-D01	The propulsion subsystem shall not damage any subsystem of the spacecraft.	<i>Inspection</i>	<i>BR</i>

Structures

Status	Identifier	Description	V&V	Origin
New New	CASE-SYS-STR-A01	The spacecraft structure shall allow for subsystem altering and calibration after installation.	<i>Inspection</i>	<i>BR</i>
	CASE-SYS-STR-A02	The spacecraft structure shall support the subsystems at all stages of the mission.	<i>Analysis</i>	<i>BR</i>
	CASE-SYS-STR-A03	The spacecraft structure shall withstand the launch loads specified in the launcher vehicle catalogue.	<i>Testing</i>	<i>BR</i>
	CASE-SYS-STR-A04	The spacecraft structure shall allow integration with the launch vehicle.	<i>Inspection</i>	<i>BR</i>
	CASE-SYS-STR-A05	The spacecraft structure shall provide a stable platform for payload.	<i>Analysis</i>	<i>FA</i>
	CASE-SYS-STR-A06	The spacecraft structure shall have minimal natural frequencies specified in the launcher vehicle catalogue.	<i>Analysis</i>	<i>FA</i>

In this chapter, the requirements for the CASE mission were presented. These requirements were generated by considering not only the performance but also the operability and the sustainability of the mission. The requirements that were generated went down to the subsystem levels. In the following chapter, the observation platform trade-off that was made in the initial stages of the design is shown, in order to converge on a certain design process. Later, the preliminary design concepts for the CASE mission will be presented.

4. Market Analysis

In this chapter, the market analysis for the CASE mission is discussed. As a satellite mission using state-of-the-art technology, the CASE mission has a high potential to fulfil the market needs. Over the last decades, the potential for Earth observation systems has kept increasing. Furthermore, the importance of sustainability has increased significantly over the last few years. With the effects of climate change and the deteriorating nature of the Earth, the longevity of the human race is under threat. In the last few years, the legislation concerning sustainability has been getting stronger in order to hold countries accountable for their actions that harm the environment. With the sustainable development goals that have been set by the United Nations (UN), developing countries will also have the chance of sustainable growth. Therefore, being able to measure the climate effects in the upcoming years will not only be beneficial in terms of being aware of the well-being of the planet but also be a validation system for the sustainable development goals for countries to be monitored.

The primary target for this mission is the equatorial region of the Amazon rain forest. The secondary targets are Singapore, Nairobi and Kampala. The tertiary target is Libreville. These regions were selected due to the need for climate mitigation solutions, especially for aerosols. The regions are elaborated on in the upcoming sections.

4.1. Earth Observation and Aerosol Detection

In this section, the market analysis of the Earth observation market, targeting aerosol detection will be discussed. The current and prospective look at the small satellite market and the importance of aerosols is briefly discussed in this section.

4.1.1. Small Satellite Market

Looking at the latest studies done on the market for small satellite systems, a large increase in the market size is expected. In 2019, the market cap for small satellite systems was around 3 billion dollars. According to the prospective analysis done by different parties, the market size is expected to reach around 7.73 billion in 2027 with a compound annual growth rate of around 18.99% [4][5]. For the CASE mission, taking the scale of the mission and the small satellite market for Earth observation into account, the target market share of 1.7% will be aimed for in 2027. This results in an achievable market size of around 125 M€. The annual growth rate of the small satellite industry is very high compared to the one for the global space equipment market which is around 4%.

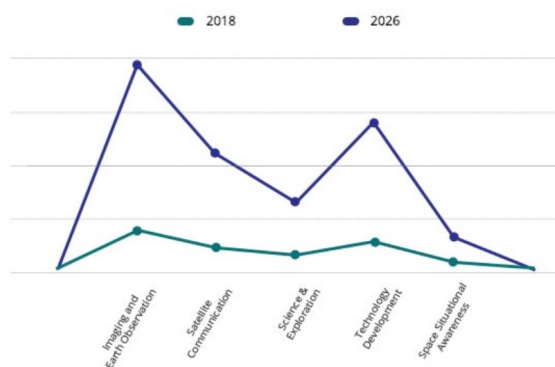


Figure 4.1: Market segmentation for small satellites [5]

There are few factors that were key to the growth of the small satellite market. With the privatization of the space industry by companies, sending small satellites to orbit became much cheaper and accessible. Companies have been emerging in the market and have been increasing the supply for the increasing demand. With the private parties pushing the market by meeting the demands with their cheaper supplies, they have been able to push the prices down. In addition, as the effectiveness and feasibility of Earth-observing systems increase, especially for subjects such as climate observation and 5G systems, the demand has also increased. Consequently, the growth opportunity and the high tech nature of the market has been attracting a lot of investors [4]. Looking at market segmentation in terms of application for the small satellite systems, it can be

stated that this mission falls under the Earth observation segment as a micro-satellite. Expected growth of the global

small satellite market by application is visualized in Figure 4.1 [6]. According to this graph, Earth observation and imaging is going to witness the greatest increase in market share in the forecasted period. This is due to the increased demand for gaining insight on meteorology, climate change, ocean, aerosol and many more subjects [4].

4.1.2. Aerosol Observation

In the last few years, with the technological advancements in imaging and observation, scientist were able to detect aerosol levels with greater accuracy. It is known that 90% of the aerosols in the atmosphere have natural origins. The remaining 10% are human-made and come from various sources². Burnt fossil fuel is one of the biggest contributors to the increased sulfate levels in the atmosphere. Furthermore, biomass burning, such as the burning of crops, release black carbon into the atmosphere. These substances are known to pollute the air. Air pollution can have harmful effects on daily life, where especially in big industrial cities, the air is much more concentrated with aerosols. Also, deforestation and drought are known to contribute to the number of aerosols in the air.

4.2. Target Locations

This section elaborates on all the target locations that will be considered when measuring aerosols over the equator.

4.2.1. Amazon Rain Forest

The Amazon rain forest is the world's largest intact forest. It is 1.4 billion acres of dense forests, which is half of the planet's tropical forests. It is home to more than 24 million people in Brazil alone, including hundreds of thousands of Indigenous Peoples belonging to 180 different groups. The Amazon is home to 10% of all known animal and plant species on Earth. With more than 40,000 species of plants, more than 400 mammals and almost 1,300 different kinds of birds and insects, it is the epitome of the biodiversity of Earth. Furthermore, more than 30 million people, including 350 indigenous and ethnic groups, live in the Amazon and depend on nature for agriculture, clothing, and traditional medicines. Most live in large urban centers, but all residents rely on the Amazon's natural bounty for food, shelter, and livelihoods³. The Amazon spans 8 countries: Brazil, Bolivia, Peru, Ecuador, Colombia, Venezuela, Guyana, Suriname, and French Guiana. These countries are all rapidly developing and their economies highly depend on the Amazon. It contributes to the economy of these countries through agriculture, livestock and manufacturing. The equatorial region of the Amazon will be monitored in the CASE mission. In the last 40 years, the Amazon has lost 18% of its rain forests to illegal logging, soy agriculture and cattle ranching. Forest areas the size of entire cities are cleared in the Brazilian Amazon every year and "burning season" fires have returned at record-breaking levels, putting the forest and the freshwater at risk. Firstly, poorly planned infrastructure destroys the integrity of the forest and cuts the connection between rivers. Secondly, the extensive cattle ranching and agricultural expansion is a vital issue. Currently, 80% of the deforested areas are occupied by cattle pastures. Their waste contaminates the water and the forest fires started to clear the area usually spreads to other areas. In addition, many scientists assert that the Amazon rain forest is the center of the global water cycle, helping propagate rainfall and other climate patterns globally. The Amazon is figuratively known as the lungs of the Earth. It has an essential role in controlling the carbon levels of the atmosphere. The Amazon Basin stores approximately 100 billion tons of carbon, which is more than ten times the annual global emissions from fossil fuel^{3,4}.

The legislation in order to protect the Amazons locally is also insufficient. 90% of the deforestation in the Amazon is illegal⁵. Currently, there are international and local efforts to protect the Amazon. Non-governmental organizations (NGOs) led by the World Wide Fund for Nature (WWF) and Greenpeace have various projects in infrastructure, education and pushing legislation in the region. Furthermore, countries such as France also showed interest in the economy surrounding the Amazon [7]. Furthermore, with increasing carbon pricing schemes and sustainability regulations, the carbon sequestration market has been emerging in the Amazon. The market is

²<https://earthobservatory.nasa.gov/features/Aerosols>, [Retrieved June 6, 2021]

³<https://www.worldwildlife.org/places/amazon>, [Retrieved June 7, 2021]

⁴<https://www.greenpeace.org/usa/issues/brazil-and-the-amazon-forest>, [Retrieved June 7, 2021]

⁵https://rainforests.mongabay.com/amazon/amazon_destruction.html, [Retrieved June 7, 2021]

divided into two: the Compliance markets where carbon rights are traded and the Voluntary market which is funded by goodwill payments from environmentally responsible corporations. In 2019, the Compliance market had an estimated worth of 214 billion dollars. Meanwhile, the Voluntary market was less than 1 billion dollars⁶. Many argue about the ethics of the Compliance market as companies get permission to buy offsetting solutions and instead they should be cut off from unsustainable sources. By monitoring the levels of different particles in the atmosphere above the Amazon, can give valuable data on the rate of deforestation, change in climate and cloud formation. Therefore, given the rate of deforestation and the importance for the global climate, monitoring aerosols in this area can be very useful.

In conclusion, the Amazon rain forest not only contains vast biodiversity and is essential to the climate of the planet, but also has a great value from an economical point of view. There is a clear need for smarter legislation and stronger implementation to save nature and educate people to grow the economy while adhering to environmental sustainability. Detecting aerosols above this region can help science and push legislation to protect the Amazon.

4.2.2. Africa

Various locations in the equatorial region of Africa were examined. Given the markets, Nairobi and Kampala were selected. The details are discussed in this section.

Nairobi, Kenya

Nairobi is the capital of Kenya and one of the busiest cities in Africa. In Kenya, half of the population will be living in cities by 2050. The population of its capital city Nairobi is approaching 4.5 million and the number of vehicles is growing exponentially, generating emissions that are dangerous for the public, especially for vulnerable groups working alongside the roadways. Air quality is deteriorating due to the increasing traffic and inadequate air pollution policy and regulation. The emissions caused by burning industrial waste, rubbish and urban biomass, as well as natural mineral dust, all contribute to this situation. Yet air quality data is often unavailable, and the sparse data that does exist, often omits gaseous air pollution. Also, the unorganized infrastructure that came with the construction boom, substantially contributed to the aerosol levels in the air [8]. According to the data from WHO, the level of fine particulate matter in the city's outdoor air is $17 \mu\text{g}/\text{m}^3$. This is 70% above the recommended maximum level. Furthermore, the monitoring system is quite robust in this area so there is a good chance that this number will be higher [9].

There is a strong need for data and knowledge to improve the air quality in Nairobi. With the expected growth to come in the coming few decades, it is important to take necessary actions to ensure public health and safety. In conclusion, Nairobi is a valuable location to monitor due to its need for such a monitoring system to reduce the extreme air pollution in the city.

Kampala, Uganda

Kampala is the largest city and the capital of Uganda with 6.7 million inhabitants. It is regarded as one of the fastest-growing cities in Africa. With widescale urbanization and industrialization, it has been classed as one of the best cities in East Africa to live in. On the other hand, the air quality is six times worse than global standards. Kampala's air quality index measured at Nsambya (a city suburb) by the air pollution monitor on September 5, 2018 at 10 A.M is six times higher than World Health Organization Air Quality Guidelines [10].

It is thought that air pollution usually results from dust from unpaved roads, exhaust fumes from cars and burning of waste. Jennifer Musisi, a well-acclaimed lawyer and public administrator from Uganda, said: "Kampala Capital City Authority (KCCA) has the mandate to develop regulations and laws that can help mitigate the pollution. This requires the development of an adequate air quality monitoring and management system. KCCA is working with Makerere University Software Development Centre to develop tools, plus the school of Public Health Makerere University to monitor air quality around the city. These efforts are financed under the Kampala Climate Change project supported by the European Union." [10]. In conclusion, as a fast-growing country, Uganda is willing to

⁶<https://www.reuters.com/article/us-carbontrading-turnover>, [Retrieved June 7, 2021]

take initiatives to help sustainable growth. Due to its current needs and for the future, having a state-of-the-art monitoring system for aerosols will be highly suitable.

Libreville, Gabon

Libreville is the capital of Gabon and is one of the fastest-growing cities in Central Africa. It is a tertiary target for the CASE mission and will only be measured upon request and if there is extra data space. Currently, the air pollution levels are not as bad as in Kampala and Kenya but the growing industry there shows that this might change in the upcoming few years. It is a tertiary target of the mission but this area will be monitored very rarely.

4.2.3. Singapore

Singapore is a city-state located 137 kilometres north of the equator. It consists of Singapore Island and some 60 small islets. Singapore also has the largest port in Southeast Asia and is one of the busiest cities in the world. As an island state, Singapore is highly prone to climate change. They aim to reduce emissions intensity by 36% below 2005 levels by 2030 and stabilise with the aim of peaking around 2030. In order to achieve this goal, 100 billion Singapore dollars will be invested from reserves, ministry budgets and loans. Due to the sustainability efforts, Singapore's Carbon Intensity, or carbon dioxide emissions per dollar of economic output, is among the lowest in the world. Singapore ranks 123rd out of 141 countries, placing them among the 20 best-performing countries⁷. On the other hand, the growing manufacturing industry in Singapore, especially for the automotive sector, is a growing problem. Singapore aims to implement their sustainable development goals by improving energy efficiency will be vital for mitigating emissions across the industry, transportation, household, waste and water handling. In addition, they aim to create awareness by educating people, pushing legislation, and building capabilities in order to reduce carbon emissions and waste. Building new technologies that enable sustainable development is also one of their strategies. Lastly, they aim to build a national consensus and culture towards green development and sustainability. In order to achieve this, Singapore is willing to collaborate with agencies, institutions, individuals and businesses locally and internationally [11]. Currently, there are efforts to measure aerosols around Singapore but the data is outdated and low resolution. In conclusion, Singapore will be taking actions to mitigate carbon emissions and adapt to climate change in order to ensure the longevity of the nation. In this process, they will be looking for international collaborations in addition to local efforts.

4.3. Market Positioning

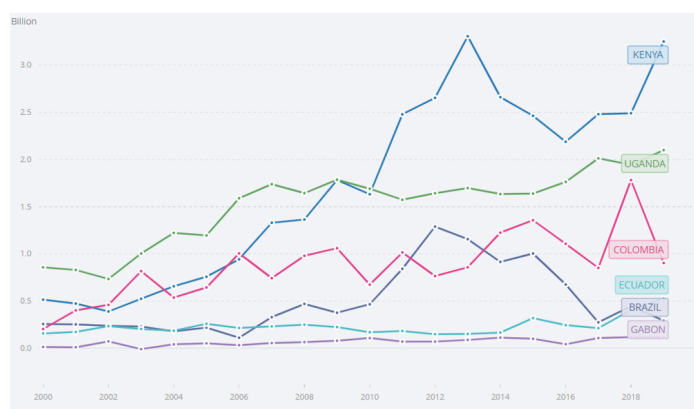


Figure 4.2: Net official development assistance and official aid received (current US dollars)

In Figure 4.2, the net official development and official aid received is presented. According to the data from World Bank, the number of investments in African countries for sustainable development goals are far larger compared to the other countries to be monitored. Kenya received the largest aid of 3.3 billion dollars, followed by Uganda which received 2.1 billion dollars. Then come South American countries which in total received less than 1.8 billion dollars. Therefore, Kampala and Nairobi are more likely to look for projects to invest in the sustainable development aid they have received. Singapore, on the other hand, has not received any aid and is looking to finance its efforts to fight climate change mostly locally. This graphic puts

⁷<https://www.nea.gov.sg/our-services/climate-change-energy-efficiency/climate-change/singapore's-efforts-in-addressing-climate-change>, [Retrieved June 8, 2021]

the African countries Uganda and Kenya in a much more valuable market position. The market analysis had an influence on the areas to be monitored and assigned Kampala and Nairobi higher importance for the mission.

4.3.1. Potential Partners, Competitors and Stakeholders

The potential partners for the CASE mission can be categorized as governments, institutions, NGOs, and businesses. CASE is an international mission, which attracts local and exterior governments. Therefore, governments on the monitoring path and the governments interested in these locations are potential partners. For the primary targets, this involves Brazil, Colombia and Ecuador, for the secondary targets Kenya and Uganda, and for the tertiary targets Singapore and Gabon are selected for the CASE mission. In addition, countries in the UN are also potential partners due to the Paris Agreement and other climate change action legislation. Furthermore, the EU and the Dutch government are potential partners as this mission has influences on scientific merit. Countries from the UN are potential partners considering the aid fund from the World Bank mostly comes from them. The data that CASE will measure will be unique and valuable. This will attract research institutions such as ESA, NASA, the Brazilian Space Agency and other institutions that need the data. In addition, educational institutes such as TU Delft and local institutions are potential partners for this mission. Furthermore, there are many NGOs that can be partners with the CASE mission. For the well-being of the Amazon rain forest, there are many NGOs looking to take action, such as WWF, Greenpeace and Amazon Watch. There are also various NGOs in Africa, such as Advocates Coalition for Development and Environment in Uganda and Climate Network Africa in Kenya. In addition to these local efforts, many international NGOs are willing to take actions such as Care and the Green Belt Movement. Lastly, there are certain groups of businesses that can be partners for the CASE mission. Firstly, the manufacturers that provide parts and other material for the CASE mission can be partnered with. Some components of the mission have a low Technology Readiness Level (TRL), therefore the validation service that CASE will provide is valuable to those companies such as TNO and Tethers Unlimited, Inc. (TUI). In addition, businesses and investors looking to invest in the sustainable development of these regions are also potential partners.

In the last few years, more satellite missions to observe aerosols have been launched. With the decreasing cost and the increasing performance of the imaging technologies, satellites missions are becoming more viable for aerosol detection. There are several large competitors emerging in the market, the first one being the NASA PACE mission, which will be launched in 2022-2023. Along with other observation instruments, this spacecraft also carries the spectro-polarimeter SPEXone on-board. The PACE mission has a fixed budget cap of 805 million dollars [12]. The second biggest competitor is the EarthCare mission operated by ESA and Japan. The launch for this mission is also scheduled for 2023. The objective of the EarthCare mission is to observe clouds and aerosols while measuring the reflected radiation from Earth's surface to the atmosphere. ESA signed a 260 million euro contract in 2008 for this mission. The cost has doubled in almost 8 years to 500 million euros and has been persistently increasing thereafter⁸ [13]. Lastly, the Terra and Aqua satellites, carrying the MODIS instrument, also measure aerosol levels in different parts of the world once every 1 or 2 days. For the Amazon region, the satellite of the Brazilian Space Agency monitors several areas but has a low spatial and temporal resolution. For the monitoring locations in Africa, there is no specific satellite system assigned to monitor those cities. The current solution is to have air quality monitors around the city to measure the air pollution levels.

The biggest advantage of the CASE mission against its competitors is the high temporal resolution. Currently, there is no other mission that can measure aerosols with a temporal resolution of 33 minutes. Most of the current missions for aerosol detection have temporal resolution of days. The change in aerosol levels in time for various locations will be measured in much quicker intervals, which will reveal local trends for the aerosol levels. For example, the difference in aerosols for the peak hours versus other times can be measured. Furthermore, the high spatial resolution of the CASE mission compared to missions like PACE and MAIA, creates unique opportunities to monitor aerosols at a much higher accuracy. Lastly, even though the current cost of the mission is high, which will be elaborated on in Chapter 26, it is still lower than the current missions available that detects aerosols in different parts of the world, from space. In a more general sense, the current aerosol monitoring solutions from space are larger scale missions with very high cost, low resolution and global coverage. The CASE mission, on the other hand, has less areas to monitor, but has higher temporal resolution and spatial resolution with lower cost. Therefore, the CASE mission will not only provide valuable and unique data, but also will be more economic and sustainable compared to its competitors.

⁸<https://www.bbc.com/news/science-environment-12506847>, [retrieved June 21, 2021]

The stakeholders for the CASE mission are as follows. Firstly, our TU Delft Faculty of Aerospace Engineering, the DSE management and Group 16 are the main stakeholders. Furthermore, the partners and the clients are stakeholders since the data generated is in their interest. These include the countries that will be monitored and the countries that have an interest, local and international NGOs, educational and research institutes and companies and businesses who provide material for the mission or who are interested in the data. The data generated by the CASE mission will not only reveal the aerosol behaviour around the selected locations but also be a pioneering system for aerosol observation in LEO. This data can be related to climate change, health and well-being, agriculture and weather forecasting. The mission data can be used to validate existing climate prediction models and monitoring industrialization effects on climate. Furthermore, the deforestation rate. This makes the scientific community also a stakeholder for the mission. Furthermore, since the Amazon has a great impact on the climate of the globe, the people and the wildlife can also be considered as stakeholders.

4.3.2. Strengths, Weaknesses, Opportunities, Threats

Strengths

1. The CASE mission, compared to the other existing missions, offers a very competitive temporal and spatial resolution. Especially, the 33 minutes temporal resolution is very valuable because the areas that are monitored do not have any system that can deliver a temporal resolution close to 30 minutes.
2. The CASE mission not only will benefit sustainable development in the monitored areas but also values sustainability in the mission process. Aspects such as the use of non-toxic material are taken into account in this mission. More details can be found in Chapter 6.
3. The equatorial region is highly concentrated with aerosols. In the selected locations, there is an undeniable demand for aerosol observation technologies.
4. The CASE mission will specifically measure aerosols. This means that the performance of the mission will be solely dedicated to gathering accurate and valuable aerosol data. This niche approach puts the CASE mission in competitive advantage.
5. Although the CASE mission is still in its design phase, companies such as TNO and NEEDRONIX have already shown interest in being partners because they believe in the benefits of this mission.

Table 4.1: Strengths, Weaknesses, Opportunities, Threats (SWOT) Analysis

Strengths	Weaknesses
1. Temporal and spatial resolution	1. High cost
2. Sustainability	2. Low TRL
3. Location selection	3. Low resources
4. Specific to aerosols	4. Low experience
5. Collaborations with the industry	
Opportunities	Threats
1. Growing private interest in industry	1. Competition from other missions
2. Growing need for climate monitoring systems	2. Unsatisfied investors/partners backing offs
3. Collaboration with governments	

Weaknesses

1. The CASE mission requires state-of-the-art technology to be operational. Therefore, the material and parts needed to execute the mission are quite expensive. The cost-breakdown will be explained in Chapter 26.
2. As mentioned before, the TRL of some of the parts and components to be used for this mission is still low, for example, TRL 3 for the TNO chip. Therefore, there is higher uncertainty and so, higher risk.
3. As a student group, currently, there are very few resources to be able to bring this mission to life.
4. A project on this scale is something that the group does not have a lot of prior experience with. Therefore, it is still an ongoing learning process.

Opportunities

1. In the last few years, there has been substantial interest in Earth observation applications and small satellites by the private industry. This might open new opportunities for the mission.
2. In the last decade, the importance of climate change actions and sustainable development has grown exponentially. Therefore, a monitoring system that is able to detect the climate change effects is in growing need
3. The countries to be monitored are in need of a system like the CASE mission. Furthermore, this can be an inspiration for other countries to implement a monitoring system like CASE.

Threats

1. It is expected that by the time the CASE mission is launched, there will be more competitive missions with better technologies. This might decrease the market share of the CASE mission if CASE does not remain competitive enough.
2. The CASE mission does not yield direct profit for the investors even though it contributes to the economy. This might discourage some investors to backing off from giving funds.

In conclusion, the CASE mission is offering an aerosol observation system that is highly in demand. Due to the market needs in South America, Africa and Asia, certain hot spots on the equator were deemed highly attractive. Furthermore, there are international and local initiatives to achieve sustainable growth in these areas. In the later chapters, the cost of the mission are presented and are related to the achievable market share.

5. Technical Risk Assessment

This chapter concerns itself with the risks that could be faced by the CASE mission during its timeline. The risks span any operation that occurs between the launch and decommissioning of the satellite. Naturally, this includes a wide range of operations in which many risks can be faced. Furthermore, risks could also be present during the production, manufacturing and transporting of the spacecraft components. As such, this chapter touches on both facets of the spacecraft lifetime during which risks can occur. After identifying the most likely or impactful risks, a risk map is produced to visualize the distribution of risks along a likelihood-impact scale. A section is then dedicated to risk mitigation strategies alongside a mitigated risk map [3]. Finally, the chapter concludes with a section commenting on the risks associated with each subsystem.

5.1. System-level Technical Risk Analysis

To identify the most system-level risk-prone processes, one must analyze the timeline of the spacecraft. Beginning with production and manufacturing, there are several ways in which delays and impediments can occur. Examples are unforeseen unavailability of resources, unsuitable or inefficient production methods and obstructions in manufacturing or transportation. Therefore, a sufficiently robust production plan must be produced to take into account these areas of failure, and mitigate them once they occur. Such mitigation strategies, include identifying a substitute for each member contributing to the production process. For instance, finding a backup supplier could alleviate delays from resource shortages. In similar fashion, a backup manufacturing or transportation provider could eliminate any manufacturing or transportation-related delays. Thus, managing contingency at this stage in development is an exercise in foresight and communication: establishing sufficient dependencies to share and minimize risk [3].

With regards to the CASE mission itself, a great number of risks can be identified, however, only those of significant likelihood of occurring, or with noticeable impacts on the mission performance are accounted for. Each risk will be given an impact:likelihood (x:y) rating, with each value scoring between 1-5 (5 indicating high impact or likelihood). This will be assessed holistically and uniquely for each risk, with the goal of assisting the placement of risks on the risk map. There exist two ways in which risks can lead to mission failure [3]:

- Failure to produce mission deliverables.
- Failure to adhere to mission budget.

The following risks have been identified to have a substantial contribution to the aforementioned conditions across all design concepts [3]:

- **RSK-G1 - Unsuitable weather & other launch site inconveniences (1:5)** : Rough weather conditions at the launch site can often adversely affect the launch and operations of the spacecraft. Unexpected weather changes can lead to launch delays, as the weather conditions for a safe launch are specific. In terms of operations, weather can interfere with communications between the ground and space segments. This must be sufficiently catered for so as not to hinder the spacecraft from achieving its objectives [3].
- **RSK-G2 - Power shortages at the ground segment location (2:2)** : The mission can be negatively impacted if the ground segments lose power and, thus, disconnect with the satellites. This is closely tied to the previous risk and varies per geographical location and can be made contingent by a redundant power supply [3].
- **RSK-G3 - Failure to deploy satellites from launch vehicle (5:1)** : Separation from launcher processes can severely affect the mission success if executed incorrectly. This can not only be of danger to the CASE spacecraft, but also to the launch vehicle. Thus, not only could an error put the CASE mission at risk, but the team could also be liable for the launch company's losses, as well as any other spacecraft on-board the launcher [3].

- **RSK-G4 - Space debris (5:1)** : Space debris is a risk any spacecraft faces during its operational lifetime. Due to the high velocity at which space debris travels, even low-mass projectiles can prove to be large threats to the spacecraft's survivability. Thus, it is an important risk to appropriately manage as it can single-handedly lead to catastrophic mission failure [3].
- **RSK-G5 - Software malfunctions and errors (5:3)** : The reliance on software for space endeavors has increased rapidly over recent decades. For this reason, malfunctions of the software can be incredibly detrimental to the mission timeline. Thus, sufficient testing must be performed to ensure that no mission-critical errors present themselves in the software. See Chapter 7 for more information.
- **RSK-G6 - Increased radiation from solar storms (3:1)** : Solar storms also present a noteworthy risk to the mission success. When solar storms occur in the direction of Earth, much of the electronics not shielded by the Earth atmosphere can be temporarily or permanently damaged. This can lead to communication interference between the space and ground segments. Furthermore, solar storms can also lead to increased levels of electromagnetic radiation which could disorient and damage the spacecraft [3].
- **RSK-G7 - Subsystem malfunctions (5:4)** : The direct failure of any subsystem will almost certainly guarantee mission failure. Therefore, subsystems must be made redundant, or sufficiently reliable that their failure is highly unlikely. As there are multiple subsystems, each with its own avenues of failure, they will be provided with their own sections to address their risks (see Section 5.3).
- **RSK-G8 - Incorrect orbit insertion (3:2)** : Upon separation from the launch vehicle, three orbital parameters must be achieved: altitude, eccentricity and inclination. If any of these are met to an insufficient degree of accuracy, the orbit insertion will be unsuccessful and the mission at risk.

Two additional aspects are worth noting which do not inherently cause mission failure if not satisfied but must be catered for nonetheless. This excludes any stakeholder requirements mentioned in the baseline report [3], as those are leading. Any conflict with stakeholder requirements will be resolved with the prioritization of the stakeholder. Nevertheless, failures of secondary goals include [3]:

- Failure to adhere to mission production, manufacturing and launch timeline.
- Failure to meet sustainability goals.

The following risks have been identified as threats to the aforementioned timeline and sustainability goals [1]:

- **RSK-S1 - Production, manufacturing, testing & transportation delays or inefficiencies (1:5)** : A delay in any of these components could lead to difficulties in adhering to the mission timeline. Furthermore, due to the large number of suppliers involved in this process, delays can easily occur due to miscommunication, scheduling difficulties, and scarcity/unavailability of resources [3]. Furthermore, inefficiency in these stages will also lead to the wasting of resources, thus violating the sustainability requirements [1].
- **RSK-S2 - Inaccurate profitability, budget & market share analysis (3:3)** : If the market analysis is inaccurate by too large of a degree, it may be that the mission will struggle to be profitable. If the profitability is overestimated, the mission may struggle to generate the revenue and cash flow that it was designed for; if underestimated, the spacecraft may be under-designed and a sub-optimal level of profit could be generated. Similar concerns exist for an overestimation/underestimation of the cost budget [1].
- **RSK-S3 - Lack of lean manufacturing and design philosophies (2:3)** : If the design and manufacturing/production stages are not performed with a lean philosophy, then it is possible for the spacecraft to be over-designed. This would delay the timeline and increase the costs unnecessarily, leading to wasting of resources. Furthermore, this would not align with the mission's sustainability goals [1].
- **RSK-S4 - Wasteful budget management & distribution (2:3)** : A budget that is not used optimally will result in an inefficiently designed mission. This can result from an extravagant budget that exceeds the needs of the mission, or an inappropriate distribution of the budget amongst the various systems that comprise the design [1].

5.2. Risk Maps & Mitigation Strategies

This section will discuss the aforementioned risks and their impacts and likelihoods on the mission success. Risk can often be considered to comprise of the product of impact and likelihood. Thus, it makes sense to plot the

various risks on impact and likelihood axes: a risk map. A preliminary risk map is shown in Figure 5.1, taking into account the risks as they stand; global and sustainability-related risks are shown code and color separated [1].

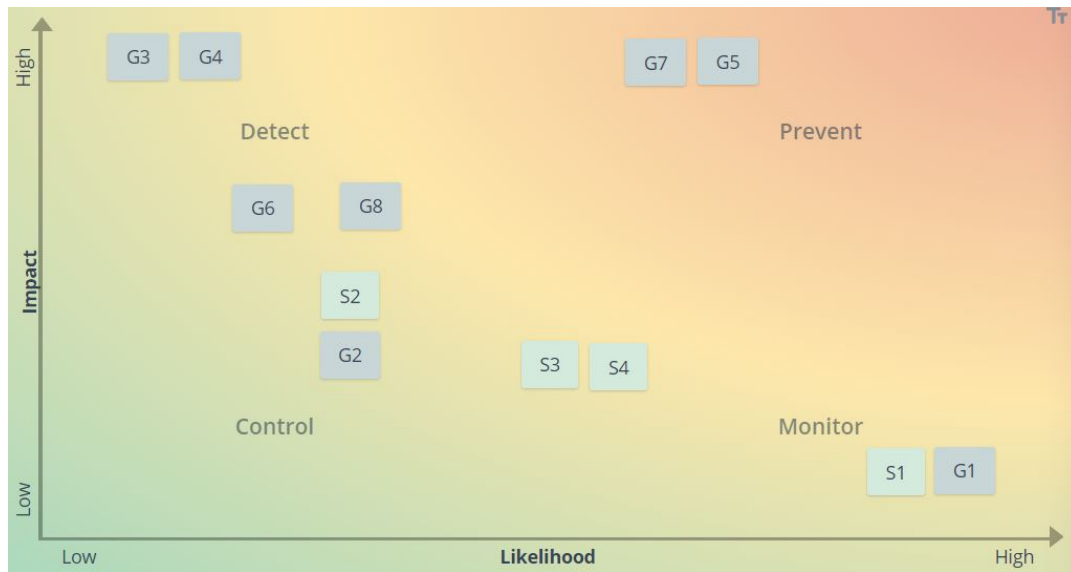


Figure 5.1: Risk map before mitigation.

As can be seen, the most impactful risks (in ascending likelihood) are **RSK-G3**, **RSK-G4**, **RSK-G7** and **RSK-G5**. Thus, these shall be the most important to prevent and mitigate early on. Risks **RSK-G3**, and **RSK-G4** are difficult to mitigate as they involve factors (space environment and launch vehicle related) beyond the grasp of the CASE mission's capabilities. Risks **RSK-G7** and **RSK-G5** can, however, be mitigated. **RSK-G7** is important to mitigate since as will be discussed in Chapter 7, software issues result in a large fraction of CubeSat mission failures. This can be reduced in likelihood, but not impact, with sufficient software testing and simulation. **RSK-G5** can then be mitigated with sufficient subsystem contingency management. This assists in both impact and likelihood mitigation. **RSK-G6** can also be reduced in impact by sufficiently equipping vulnerable subsystems with the means of withstanding high radiation doses; no mitigation can be provided in the likelihood of occurrence. **RSK-G8** can be made less likely with sufficient testing, and less impactful with the implementation of redundancy. This is elaborated upon in Chapter 10, alongside **RSK-G4** & **RSK-G6**.

Equally important to address are the sustainability risks. Several of these risks can also be mitigated by taking appropriate countermeasures. For instance, risk **RSK-S1** can be decreased in likelihood by maximizing communication channels between all parties involved in production, manufacturing, testing and transportation. In a similar fashion, risk **RSK-S2** can also be decreased in likelihood by bolstering the profitability analysis. Performing valuable verification procedures on the profitability calculations can lessen the likelihood of inaccuracies in the results. This will be further elaborated upon in Chapter 8. Risks **RSK-S3** & **RSK-S4** are already being mitigated by virtue of the lean manufacturing philosophy that the CASE mission embodies. The updated risk map with risk mitigation strategies taken into account is shown in Figure 5.2 [1].

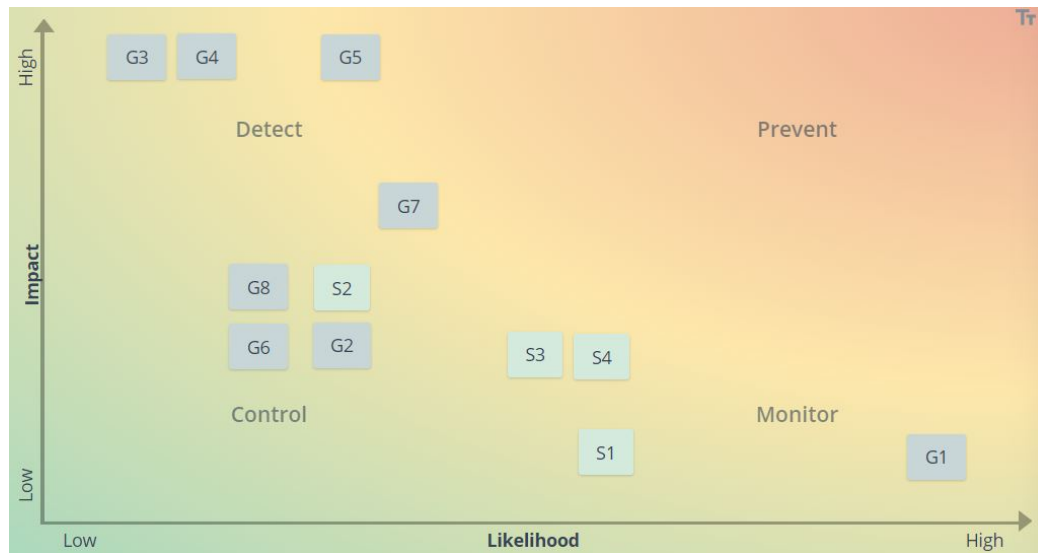


Figure 5.2: Risk map after mitigation.

5.3. Subsystem-level Technical Risk Analysis

The critical failure of any subsystem will lead to eventual mission failure, thus posing a great risk to the mission success (**RSK-G7**). However, the avenues by which subsystem failure can occur are multiple and vary per subsystem. Furthermore, an advanced level of design detail is required to adequately assess the risks of each subsystem. For this reason, this section is dedicated to listing the various subsystems' risks, while in-depth descriptions and mitigation strategies/considerations are then elaborated upon in their respective chapters.

5.3.1. Payload Subsystem Risks (see Section 11.5)

- **RSK-PL1** - De-calibration of payload instrument
- **RSK-PL2** - Data transmission failure (to CDH)
- **RSK-PL3** - Insufficient TRL

5.3.2. Propulsion Subsystem Risks (see Section 12.4)

- **RSK-PROP1** - Leakage of fuel
- **RSK-PROP2** - Breaking/jamming of valves
- **RSK-PROP3** - Ignition/combustion failures
- **RSK-PROP4** - Toxic properties of fuel
- **RSK-PROP5** - Corrosive properties of fuel

5.3.3. CDH Subsystem Risks (see Section 13.6)

- **RSK-CDH1** - Data corruption
- **RSK-CDH2** - Data transmission failure
- **RSK-CDH3** - Data reception failure
- **RSK-CDH4** - Data storage failure
- **RSK-CDH5** - Data pre-processing failure/errors
- **RSK-CDH6** - Software failure/errors

5.3.4. Thermal Subsystem Risks (see Section 14.5)

- **RSK-TC1** - Payload overheating
- **RSK-TC2** - Temperature mis-calibration
- **RSK-TC3** - Temperature correction failure

5.3.5. TTC Subsystem Risks (see Section 15.5)

- **RSK-TTC1** - Electronic failure
- **RSK-TTC2** - Insufficient uplink pointing accuracy
- **RSK-TTC3** - Insufficient downlink pointing accuracy
- **RSK-TTC4** - Failure of rotating mirror mechanism
- **RSK-TTC5** - Mirror rotation algorithm failure
- **RSK-TTC6** - Software failure
- **RSK-TTC7** - Cloud coverage

5.3.6. ADCS/AOCS Subsystem Risks (see Section 16.5)

- **RSK-ADC1** - Attitude determination (sensor) failure
- **RSK-ADC2** - Attitude orientation (actuator) failure
- **RSK-ADC3** - Mis-calibration or de-calibration
- **RSK-ADC4** - Obstruction of view

5.3.7. GNC Subsystem Risks (see Section 17.4)

- **RSK-GNC1** - Exposure to space environment
- **RSK-GNC2** - Occlusion of antenna's line of sight
- **RSK-GNC3** - Receiver malfunction

5.3.8. EPS Subsystem Risks (see Section 18.3)

- **RSK-EPS1** - Power supply failure
- **RSK-EPS2** - Power storage failure
- **RSK-EPS3** - Failure of the solar array deployment mechanism
- **RSK-EPS4** - Power Conditioning and Distribution Unit (PCDU) incorrect application of switch configuration
- **RSK-EPS5** - PCDU connections are done incorrectly

5.3.9. Structural Subsystem Risks (see Section 19.5)

- **RSK-STR1** - Primary structure failure
- **RSK-STR2** - Secondary structure failure
- **RSK-STR3** - Subsystems attachment failure
- **RSK-STR4** - Deformation of the structure
- **RSK-STR5** - The payload platform failure
- **RSK-STR6** - Material flaws made during manufacturing process

5.3.10. Launcher risks (see Section 20.7)

- **RSK-LNCH1** - Launch vehicle failure (DOA))
- **RSK-LNCH2** - CASE damaged during launch
- **RSK-LNCH3** - CASE or launcher damaged during separation (CASE arrives Dead On Arrival)
- **RSK-LNCH4** - Delay of launch date
- **RSK-LNCH5** - Launcher communication loss

5.3.11. GS Risks (see Section 21.5)

- **RSK-GS1** - Loss of communication with CASE
- **RSK-GS2** - Data retrieval issues
- **RSK-GS3** - Software failure
- **RSK-GS4** - Power failure/outage
- **RSK-GS5** - Labour disputes/strikes
- **RSK-GS6** - Human error in operations

This chapter has outlined the various risks that the CASE mission has been envisioned to possibly encounter during its design and lifetime. Several countermeasures have also been proposed, which will be elaborated upon where they apply to the design. The greater implications on the final design have not been elaborated upon in this chapter as it requires a higher-level design. As such, they will be mindfully present during the subsequent design iterations of the CASE spacecraft. Details such as the reliability and redundancy of the spacecraft and launcher are further detailed in Chapter 7.

6. Sustainable Development Strategy

At an early stage of the design process, the Life Cycle Assessment (LCA) method was chosen to be the most suitable tool to assess the sustainability of the CASE mission [1, 2, 3]. The LCA method is an internationally standardized tool (ISO 14044:2006⁹, ISO 14040:2006¹⁰) that assesses the environmental impact of each phase in the entire life cycle of the mission, the product and its components. Both ESA and NASA have used this method in space missions, as these missions are unique in terms of low production rates, long development cycles and special materials needs. The expanded LCA methods are described in the ESA and NASA handbooks which are used as a guideline to assess the sustainability of the project [14, 15]. In Section 6.1 how sustainability is defined. In Section 6.2 the LCA method is used to discuss the impact of each of the mission phases on the three sustainability aspects: environmental, social and economic sustainability. On top of this, a thorough analysis has been performed for each of the subsystems using the LCA method to assess the subsystems sustainability in each of the subsystem chapters from Chapter 10 to Chapter 21.

6.1. Sustainability Definition

The definition of sustainability is given in the widely accepted Brundtland report [16] as: *"Sustainable development is development that meets the needs of the present without compromising the ability of future generations to meet their own needs."* The sustainability of a project or product is assessed by looking at the three aspects: environmental, social and economic sustainability. In order to maximise the sustainability of a mission, a process or a product, the negative impact on these three aforementioned aspects needs to be minimised over the entire life cycle of the mission, process or product. For the CASE mission, the environmental aspect is mainly related to five aspects. First are the emissions from manufacturing and transport processes, followed by resource consumption and depletion. Additionally, there are the emissions directly emitted in the high atmosphere, as well as the use of non-toxic materials. Finally, the disturbance of wildlife on Earth should be considered. The social aspect is more related to job creation, the impact of the mission on society and safety and efficiency during all of the mission processes. The economic aspect is mainly related to the market, profitability and how this project can make a contribution to the current economy. Since the two latter aspects are closely related in some ways, it was chosen to merge those two aspects into the socioeconomic aspect.

6.2. Mission Life Cycle Assessment

In this section the LCA method is performed on the different mission phases that were obtained in the previous reports [1, 3]. This is done by looking at the environmental and socioeconomic impacts of each of the mission phases on its environment. Finally, an assessment on the general mission sustainability is provided.

6.2.1. Design

This phase mainly includes office work that is being done on the feasibility and the design of the mission.

- **Environmental impact:** Since this phase only includes the design processes of the project, this phase has very little to no impact on the environment. The facilities used during the design processes might have a small impact on the environment, considering that heating and electricity were used.
- **Socioeconomic impact:** The design process was executed by a team of nine students for educational purposes. Students are guided by mentors, get in contact with experts and gain insights in space system

⁹<https://www.iso.org/obp/ui/#iso:std:iso:14044:ed-1:v1:en>, [Retrieved on May 28, 2021]

¹⁰<https://www.iso.org/obp/ui/#iso:std:iso:14040:ed-2:v1:en>, [Retrieved on May 28, 2021]

design. For this reason, no jobs were created but the project itself is economically very sustainable since no money was spent during the design phase.

6.2.2. Manufacturing, verification & testing

This phase concerns all the manufacturing, assembly, integration and testing processes. Also, the obtainment of resources and the transportation of components are included in this phase. In this phase, it should be noted that the use of toxic materials should be minimised since this is given as a stakeholder requirement.

- **Environmental impact:** This phase has a large environmental impact since the product and its components need to be manufactured from raw materials to the final product. These processes require a lot of resources, electricity and a lot of emissions are produced during these processes. For this project, most of the satellite subsystems are made from commercial off-the-shelf (COTS) components. A drawback of using COTS components is that it is hard to trace the origin of the raw materials and their transportation. It is also hard to identify the exact manufacturing processes used. On the other hand, COTS components are already certified and tested, which greatly decreases the costs and resources required for research and development (R&D). The assembly and integration of all the components are done in their respective facilities and for this, transportation of the components to these facilities can be taken into account. Therefore, it is beneficial to have all of the assembly, integration and testing facilities close to each other. For these processes, existing facilities can be used to minimise the environmental impact.
- **Socioeconomic impact:** In this phase, a lot of jobs are created directly and indirectly since the processes are very labor-intensive. These processes are indirectly created for the manufacturers of the COTS components because they will need enough people to transform raw materials into the product that will be transported to the assembly facilities. Jobs are directly created for the team of people that will assemble, integrate and test all of the different components and subsystems. In these labor-intensive processes, it is necessary to have safety regulations for the health and safety of the employees. It is important that inefficiencies in these processes are minimised as they lead to delays, which can also lead to a waste of resources or unreliability on the market. A lack of lean manufacturing is often seen as a way of inefficient working. This can be improved by employing a team of engineers who manage all of these processes and check whether the lean manufacturing methodologies are performed correctly.

6.2.3. Utilisation

This phase mainly consists of the transportation to the launch site, the preparation for the launch, the launch event itself, mission control & operations and finally also the facilities used for these tasks.

- **Environmental impact:** The impact on the environment of the rocket launch could be greatly decreased by ride-sharing, an already existing launcher and a planned launch. This means that no launcher or fairing needs to be developed for this mission. This will be further explained in Section 20.1. It should be noted that the transportation of the satellites and the rocket to the launch station will provide emissions. The part of the launching phase that has the most impact on the environment is a large amount of expulsion of emissions into the atmosphere during the burning of a propellant. It should also be noted that the control centers and GSs used for control, operations and data handling of the mission will require the use of electricity and gas, but this is negligible compared to the impact of the launch itself on the environment. On top of these aspects, it is important to take into account the propellant on-board of the satellite and a ΔV for space debris mitigation. For the on-board propellant, it was chosen to use a hydrogen-based propulsion system that minimises the use of toxic materials. The space debris mitigation strategy is considered such that a very small ΔV is kept for potentially mitigating space debris as stated by the United Nations Space Debris Mitigation Guidelines [17].
- **Socioeconomic impact:** The mission control and operations will also create a large number of jobs, mainly in the field of research and mission maintenance and control. The countries and regions that will benefit from this are elaborated upon in Chapter 4.

6.2.4. Disposal

This final mission phase includes the End-of-Life (EOL) strategy of the spacecraft, the post-processing of the obtained data and finally also the reuse possibilities for the facilities.

- **Environmental impact:** For the disposal phase of this mission, the EOL strategy is determined. The satellites used in the mission will do a de-orbit maneuver from their 500 km altitude and burn up in the atmosphere within 25 years without requiring an additional ΔV [18]. It is crucial that any leftover propellant is burned up before the burn-up, so if there would be leftover propellant, this can be used to speed up the de-orbiting process. The facilities that are used for the post-processing of data will still require some electricity and gas consumption but the impact of this on the environment will be negligible. It can also be mentioned that the facilities used throughout the whole mission can be reused for the design, production, control and data processing of other missions, as this would greatly improve the sustainability of the project.
- **Socioeconomic impact:** Again, jobs are created for post-processing the data. The EOL strategy will not have a huge impact on the socioeconomic aspects since the CubeSats are seen as very small satellites which fully burn up during the re-entry for all initial conditions [18]. Therefore no care has to be taken to avoid debris reaching Earth's surface.

6.2.5. General mission

Finally, the environmental and socioeconomic aspects of the entire mission are discussed here.

- **Environmental impact:** The entire mission is based around the retrieval of information on aerosols. Therefore, this mission is able to provide valuable information that can be used in further research on the effect of aerosols on the environment, people's health and agriculture. In general, this mission has some processes such as the production of components and the launch, which can still be greatly improved in terms of environmental sustainability, but the information obtained from the mission and its effects in the future are promising and helpful to solve certain environmental problems such as air pollution, deforestation and weather changes.
- **Socioeconomic impact:** The data and information obtained from this mission will be used in research and some media coverage on this can spark interest in the retrieval of aerosols and the importance of it or more generally it can even spark an interest in science and space missions increasing the number of future engineers and scientists. On top of that, this mission has created a lot of jobs and cooperation between different countries as measurements are done above the equator.

6.3. Subsystem Life Cycle Assessment

The sustainability of each subsystem is assessed by using the LCA method to look at their impact on the environment. The considerations that are mainly taken into account are the materials used for their components, the processes that are used to obtain them, the transportation needed to its assembly and integration location and their EOL considerations. These aspects are all discussed in the respective subsystem chapters.

7. RAMS Characteristics

This chapter shall outline the RAMS characteristics of the CASE mission design. Previously, a preliminary assessment of the Reliability, Availability, Maintainability and Safety (RAMS) characteristics has been performed. However, with increased detail of relevant systems and subsystems, the RAMS characteristics can be revisited. As done previously, the chapter is divided into each of the four RAMS characteristics and assessed individually.

7.1. Reliability

The reliability assessments used in aerospace applications range drastically in methods and results. The infancy of the space industry, combined with the privacy of many agencies results in a lack of information regarding the failures of many spacecraft [19]. For this reason, the applicability of statistics and literature is limited in its ability to assess the reliability of a spacecraft mission. Alternative methods would include the individual assessment of each subsystem's reliability, however, privacy policies prevent access to such details at this stage in development. Additionally, simply analyzing the product of all of the reliabilities of the subsystem parts does not necessarily lead to accurate reliability estimation. Modern components boast high reliability, and the CubeSat's small size implies a relatively low number of components, low levels of integration, and thus less room for error [19]. Commonly flight heritage is also used to estimate reliability, however, given that this will be the CASE mission's maiden flight, no such heritage data is available. For this reason, statistical estimation based on literature will be the primary way in which the mission reliability will be assessed.

The unique nature of the CASE mission makes it an unconventional exercise in reliability estimation. One could assess the reliability by comparison with other CubeSats, however, the large mass makes it a notable outlier. Conversely, one could make a comparison with low mass satellites (<500 kg), however, CASE lies on the lower bound of that and would again present itself as an outsider. In this exercise, comparisons will be made with CubeSats due to the similarities in design processes. On the assessment of CubeSats, their failure is commonly dominated by DOA cases [20]. This entails the spacecraft being non-functional from the moment it separates from the launcher. The difficulty in addressing this is that often the cause of the failure remains unknown [21]. This can be visualized in Figure 7.1:

As Figure 7.1 shows, 33% of DOA cases result from an unknown cause. The subsequent subsystems responsible for the most failures include EPS, on-board computing (OBC) and communication systems. In total, these 4 remain the most dominant causes for failure throughout the mission lifetime. This is evidenced in the progression

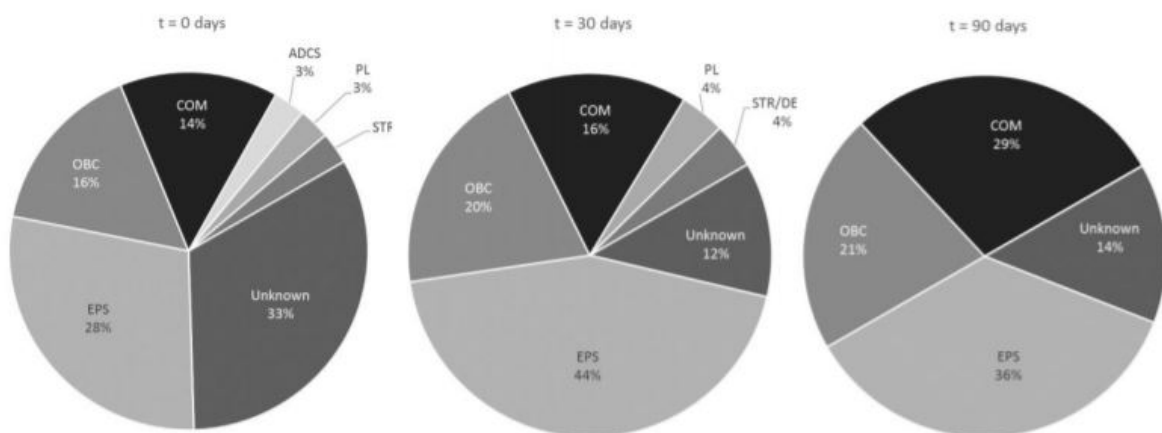


Figure 7.1: CubeSat failure by subsystem after injection [20].

of the figure, as the leftmost figure ($t = 0$ days) depicts the state of affairs immediately after initialization. The two remaining pie charts then display 30 and 90 days after BOL, respectively. While the unknown element cannot be accounted for, it is worth noting that the remaining subsystems share a commonality in their reliance on software. Over the past years, software has played an increasingly pivotal role in the operation of spacecraft and has accompanied with it new opportunities for failure. In the years spanning from 1998 and 2000 more than half of all reported spacecraft failures resulted from software issues [22]. The referenced article continues to elaborate that software errors nearly always result from errors in code design, and are thus exempt from the benefits that redundancies provide. Furthermore, human errors are even more prevalent in software than hardware, and are not statistically independent in practice [23]. As the same mistakes are likely to be repeated by different groups independently, redundancies in software are often obsolete. The article concludes that for CubeSats, significant time should be dedicated to proactive testing of software with careful attention to design [19]. This also follows the logic one can interpret from the Pareto distribution of code error, where 20% of the code contains 80% of the errors [24].

The sensitivity to errors in code is of particular interest to the CASE mission due to the use of cutting-edge payload. Verbal communication determined that novel algorithms would be necessary for the processing of measured data [B]. Therefore, such algorithms should be sufficiently tested, especially if they are to be deployed on-board the spacecraft. However, the testing of the EPS, OBC and COM subsystems should not be neglected, since Figure 7.1 shows that after 90 days of operations, most CubeSats fail due to one of these subsystems. Details on how these subsystems can be tested will be presented in the sections that follow.

Investigating beyond the DOA cases, one discovers that CubeSats are also notorious for their infant mortality rates. A study among 178 CubeSats confirmed the high rates of infant mortality with a reliability rate of 81.5% and a 2 standard deviation (95%) confidence interval ranging between 87% and 76.5% [19]. The full range of these results can be visualized in Figure 7.2, where the data was obtained using a Kaplan-Meier estimator [19].

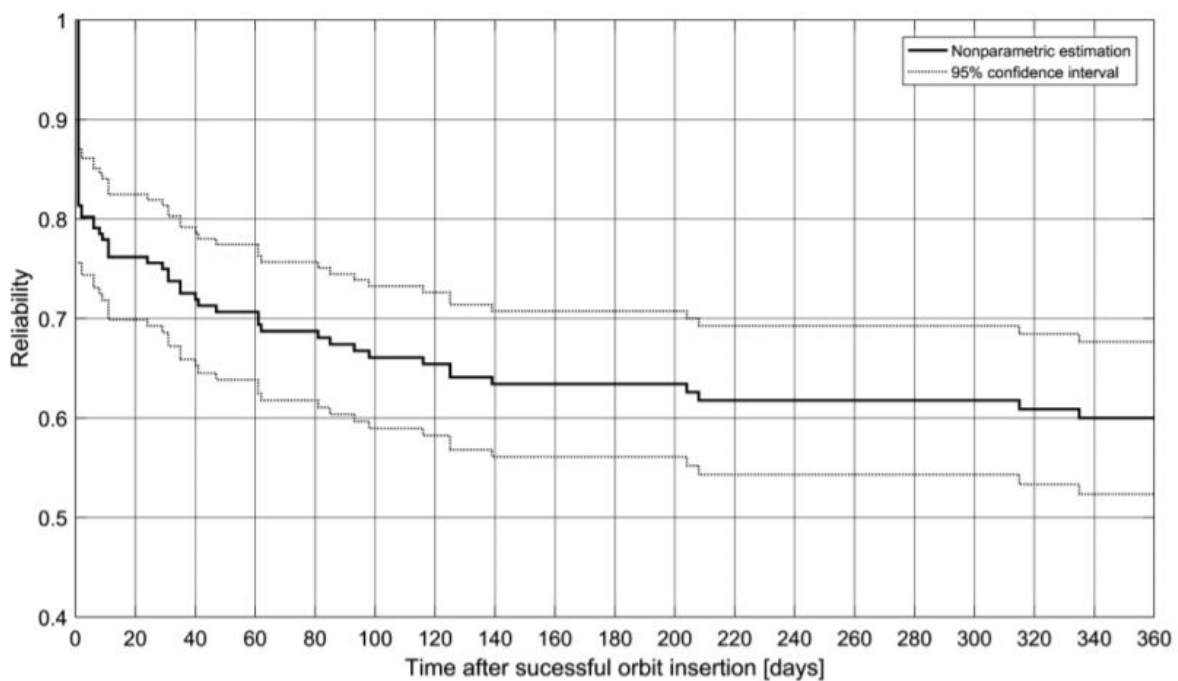


Figure 7.2: Reliability estimation of CubeSats over one year [19].

Furthermore, after one year the reliability reaches a low of 60%. The author does note, however, that the data suggests CubeSats are currently not as prone to wear-out failure as larger spacecraft. The author continues to state that if the spacecraft survives its first year, its likelihood of surviving an additional year (and years thereafter) are increased.

Similar findings were presented by NASA, also employing a Kaplan-Meier estimation, shown in Figure 7.3. The article accompanies the figure by claiming the median life of 110 days [25]. This is a reliability estimate even lower than that of M. Langer et. al, but was also performed on a smaller sample size (62 CubeSats). Further, with the use of a Weibull distribution, parametrized with $\alpha = 200.25$ days and $\beta = 0.54$, an even lower reliability estimation was determined, with a reliability of 0.2165 after 90 days. For the CASE mission with a projected lifetime of 2 years, this proves troublesome; the Kaplan-Meier reliability estimation for 2 years is 0.2258, while that of the Weibull distribution is 0.

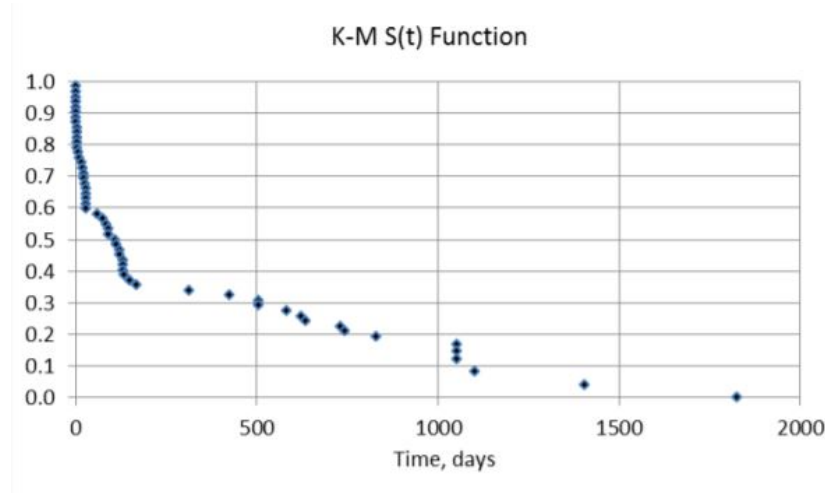


Figure 7.3: NASA reliability estimate obtained using Kaplan-Meier estimation [25].

It should be noted that in the aforementioned studies, the vast majority of CubeSats had a mass between 1 and 5 kg. A few outliers had masses nearing 10 kg, however, none approached CASE's mass of 25 kg. While more massive CubeSats typically have a lower reliability, it is likely that they may also have been designed with a smaller lifespan in mind, which should not be neglected.

A possible conclusion from the aforementioned data (and prevalence of infant mortality) is that a large majority of CubeSats are simply not "flight ready" by the time they are launched. There are various factors that could contribute to and corroborate this theory. For instance, CubeSats often rideshare as secondary payloads on launchers, and as such may accelerate design & manufacturing in order to meet pressing deadlines; this may also result in insufficient time for necessary testing [26]. Other reasons include the lack of heritage and restricted resources since CubeSat missions often result from limited budgets [19].

Due to the generally low reliability of CubeSats, one might question the team's decision to opt for a CubeSat over larger and more reliable structures. While the low reliability presents sufficient reason for concern, it is noteworthy that smaller spacecraft are also more reliable due to the diminished part quantity and overall complexity. Further, they suffer from lower rates of human error during the design and manufacturing phases [19]. Additionally, many CubeSats are launched as pioneers to test newly developed systems and instruments, and should for this reason be expected to have a higher than average failure rate. This applies directly to the CASE mission with its TRL 3 payload system [D].

Beyond this, there are several countermeasures that can be taken to improve the reliability of the CASE mission. It has been established that one of the most effective methods of improving reliability is by thorough system and subsystem-level testing. A study suggests several system-level tests that should be considered [19]. For instance, satellite testing over the entire chain of communication from ground control to the satellite, through all interfaces and subsystems it would employ under mission circumstances. The deployment system, hardware and software can all be tested under various environments that simulate the mission. Hardware-in-the-loop & software-in-the-loop environments can also be used to model and test the system's functionalities [19]. Further elaboration will be provided in the remaining sections and in Chapter 8. To conclude with a quick note that the launch vehicle reliability is quantified and elaborated upon in Chapter 20.

7.2. Availability

The CASE mission is merely one of many aerosol observation missions launched in the past several decades. That is not to say that it is not unique in its goals and design. Nevertheless, many of its subsystems and by extension, components and sub-components can be inherited from previously successful aerosol (or general) observation missions. This bodes well when performing the analysis concerning the availability of necessary products, as one can rely on historical usage. Furthermore, availability is also a strong component in Chapter 9's trade-offs (also referred to as Technology Readiness Level (TRL)) due to the importance of adherence to the mission timeline. Fortunately, most components used on-board the CASE spacecraft boast a high TRL, and are easily obtained through their vendors.

A few noteworthy exceptions include the polarimeter-on-a-chip instrument in development by TNO. This payload does not benefit from being technologically ready (TRL 3 [D]), and may prove burdensome to the final mission timeline. The cutting-edge technology employed on the TNO chip also presents availability issues beyond its own technological readiness constraints. For instance, due to the unusually large quantity of data output by the instrument, novel technologies must also be employed to obtain a sufficient data rate. For this reason, Hyperion Technologies' CubeCat lasercom module has been selected for the TT&C subsystem. However, this module also suffers from a limited TRL of 7-8 ¹¹. Finally, the propulsion subsystem also suffers from a low TRL of 6 ¹².

7.3. Maintainability

Few Low Earth Orbit (LEO) missions benefit from being free of maintenance and the CASE mission is no exception. The spacecraft is expected to allow for maintenance activities during its life cycle to maximize its longevity and performance. Requirements have been established to facilitate the implementation of maintenance activities with minimal hindrance to the mission performance. Requirement **CASE-MIS-D02** dictates that the spacecraft should be capable of continuing all operational activities while undergoing scheduled and unscheduled maintenance [3]. Several maintenance activities have been foreseen, while any unscheduled maintenance activities must be catered to as well, as they present the largest risks [1]. Thus, it follows that this section is divided into the addressing of foreseen and unforeseen maintenance activities.

7.3.1. Scheduled Maintenance Activities

Planned maintenance activities include actions that are necessary to maintain the robustness of the spacecraft. Due to the limited resources of this mission, the maintenance is performed remotely, as a physical maintenance/repair mission would be too costly in all regards. Maintenance tasks of this nature include the remote upkeep of anything that could deteriorate in quality over time. For instance, any software updates will be a form of scheduled maintenance activity. Either due to the discovery of errors or compatibility requirements, a software update is likely to be required at some points during the mission; the exact time, however, is difficult to predict at this stage.

Re-calibration efforts will also be an expected form of maintenance that will be required during the mission. The payload instrument will need to undergo re-calibration several times during its lifetime due to the altitude variations. It may also require additional re-calibration depending on its performance. Other subsystems will also be prone to re-calibration requirements. This includes, for instance, the ADCS subsystem, whose sensors will undoubtedly require several acts of re-calibration to maintain their pointing accuracy. The TT&C and CDH subsystems will likely also require re-calibrations in their communication channels. These considerations derive from requirements **CASE-SYS-TTC-A12** & **CASE-SYS-CDH-A10**, respectively. These re-calibrations may occur routinely as a form of quality control, or may also be implemented as a preliminary countermeasure in response to subsystem failure (**RSK-PL1**).

Further, the GS with which the spacecraft communicates may need to undergo necessary maintenance. This may be physical maintenance (hardware related), or software-related maintenance. Consequences of such maintenance could be downtime in the connection between the ground and space segments. Following such downtime, the

¹¹<https://hyperiontechnologies.nl/products/cubecat/?cn-reloaded=1>, [Retrieved on June 07, 2021]

¹²<https://www.tethers.com/wp-content/uploads/2019/09/2019-HYDROS.pdf>, [Retrieved on June 07, 2021]

aforementioned re-calibrations may be necessary again.

A final set of scheduled maintenance activities include those dedicated to risk mitigation. Risks **RSK-G4**, **RSK-G6**, and **RSK-G8** deal with dangers the spacecraft can encounter during its orbit. For instance, **RSK-G4** deals with space debris, a risk that is preventable with sufficient foresight in collision detection and avoidance. The same can be said for the remaining two risks, which deal with solar radiation and orbital insertion. An in-depth breakdown is provided in Section 10.4 of Chapter 10.

7.3.2. Unscheduled Maintenance Activities

Unscheduled maintenance activities will likely originate from unexpected obstructions to the mission. Ideally, this would be resulting from a risk that has been previously identified in Chapter 5, and for which sufficient countermeasures have been provided. In such cases, the following unscheduled maintenance activities have been devised. Segueing from the scheduled GS maintenance activities, there may also arise unscheduled maintenance activities. Causes of this could include an unexpected power outage, labour disputes, and human error in operations, (**RSK-G2**, **RSK-GS4**, **RSK-GS5** & **RSK-GS6**).

Another risk from which notable maintenance would be required is the cessation/failure of certain subsystems (**RSK-G7**). In these cases, maintenance would be required to bring their contingencies online. In some subsystems, this would consist of engaging their redundancies, while other subsystems may require remote repairs (if possible). Following from this, software malfunctions and errors (**RSK-G5**) would also result in unscheduled maintenance activities, and would probably necessitate an impromptu software update or reset.

7.4. Safety

Finally, the safety concerns of the CASE mission shall be addressed. Not only is the safety of CASE itself a primary concern, but the safety of stakeholders and other space missions must be considered as well. The safety considerations have already been alluded to and elaborated upon in Chapter 3. Specific requirement labels exist to discern those dedicated to ensuring the safety of the mission and will be referenced extensively in this section. Beyond general safety considerations (e.g. **CASE-ST-D01**, and **CASE-ST-D02**) several functionalities have been implemented to allow optimal safety management.

Firstly, the spacecraft has been designed to support several modes of operation, depending on the level of safety. Requirements **CASE-SYS-SS-A10**, **CASE-SYS-SS-A11**, and **CASE-SYS-SS-A12** detail operational, power-saving and safe mode, respectively. These system-level design choices serve to protect the spacecraft in dire situations. A system-level safe mode does not provide a sufficiently accurate description, so the contributions of each subsystem to the spacecraft's safety will be elaborated upon next.

7.5. Conclusion

This chapter has discussed the various efforts implemented to ensure a reliable, available, maintainable and safe mission. Beginning with the reliability, it has been discussed that assessing each individual subsystem's reliability is unfeasible either due to privacy constraints or other lack of information. Furthermore, this has little bearing on the final mission reliability due to an uneven distribution of failure amongst subsystems, and the existence of infant mortality and DOA cases in CubeSats. A statistical estimation of 81.5% mission reliability has been obtained in accordance with a meta-analysis of many CubeSat missions [19]. The availability of components has been discussed, with several components suffering from low TRL conditions. This is not assumed to be a hindrance due to the payload readiness already driving the mission timeline. The activities facilitating maintainability have been outlined, with reference to the requirements where they were initially conceived. This was split into the scheduled and unscheduled maintenance activities, both of which the spacecraft must be prepared for. Finally, a similar procedure has been applied to the safety of the mission, predominantly led by the preconceived safety requirements.

8. Verification & Validation

In designing the final design of the CASE mission, it is imperative that the methods, models and calculations used thus far are credible, robust and relevant. For this reason, appropriate verification & validation (V&V) procedures must be applied. The V&V will be implemented in two forms for this project. Firstly, all requirements will be subjected to verification/validation. This has already been displayed in Chapter 3. For each requirement, it is shown how it shall be verified/validated, with the options ranging between inspection, demonstration, analysis, and testing. For the second aspect of the project's V&V, all models used in designing and sizing require sufficient corroboration that they comply with the function they are tasked to perform (validation). Furthermore, it must also be confirmed that they perform this function to the desired degree of success (verification). This latter form of V&V shall be the main focus of this chapter, discussing the various models used and how they have been successfully verified/validated. The structure of this chapter will first address system-level testing and V&V procedures, followed by subsystem-level V&V.

8.1. System-level V&V

Below, several miscellaneous models are discussed that do not fit within a specific subsystem, but still warrant V&V analysis. One such model that must be verified is the cost analysis tool used recurrently during the project and described in Chapter 26. This has been produced by the team's business manager [2], but due to its complexity could benefit from verification. For this reason, access has been requested and granted to NASA's Mission Operations Cost Estimation Tool (MOCET) tool for cost estimation. The combined implementation of these tools has resulted in an initially accurate cost estimation for the CASE mission. The accuracy was corroborated by personal communications with representatives from SRON [D]. However, the MOCET tool no longer applies to the final design due to the choice of a laser communications system, which the MOCET tool is not configured for (Chapter 15). Nevertheless, the initial verification corroborates the fact that the analytical tool served as an accurate estimator.

Additionally, the trade-off that was performed leading up to this final design stage was also subjected to verification. Since the AHP method was selected for use, it was possible to verify that it was used impartially. One suitable method is by use of the CR. This method has also been used in the Midterm Report [1]. The consistency ratio is an assessment of the randomness of the chosen importance factors. As a general principle, if the CR exceeds a value of 0.1 (meaning the weights are more than 10% randomly chosen), the resulting weights are deemed untrustworthy since the importance scalars are too randomly distributed [27]. First, the Consistency Index (CI) is calculated using Equation 8.1.

$$CI = \frac{\lambda - n}{n - 1} \quad (8.1)$$

Here, λ is a weighted parameter based on the grading criteria and the relative importance factors that results from the AHP process, and n is the number of grading criteria used. Then, the consistency ratio can be calculated using Equation 8.2.

$$CR = \frac{CI}{RI} \quad (8.2)$$

This value for CR is then calculated for every instance in which the AHP method is employed. This has been necessary in several subsystems in this report, namely, Chapter 11 and Chapter 20.

Finally, system-level testing will also be performed in an experimental setting. Beyond the verification and

validation of individual subsystems (which will be addressed shortly), the spacecraft must be certified to function as the sum of its constituents. This will mainly test the interactions between related subsystems and the means by which they are connected. Furthermore, tests should be performed to assess the health of the software upon which the spacecraft will activate and run. This will serve to significantly reduce the risk of a DOA mission failure. Additionally, a simulated test of all performance capabilities to be facilitated during one orbit would identify a large fraction of remaining errors. This is of particular interest due to the high likelihood for CubeSat missions to experience infant mortality (see Chapter 7).

8.2. Subsystem-level V&V

Due to the diversity and varying complexity of each subsystem, they will be subjected to different forms of V&V. Naturally, not all subsystems will benefit from this due to their lack of complex calculations. That is not to say that their calculations have not been subjected to V&V, however, it will mainly consist of visual inspection and demonstration. For this reason, only the more complex subsystems benefiting from thorough V&V procedures will be outlined in detail. These detailed descriptions will follow each subsystem in its respective chapters. Below, Table 8.1 is displayed with proposed V&V strategies. Among these methods, some may exceed the capabilities of the DSE, however, still warrant mentioning.

Table 8.1: Verification & validation strategies shown for each subsystem.

Subsystem	Verification strategies	Validation strategies
PL	<ul style="list-style-type: none"> • Integration testing • Model testing 	<ul style="list-style-type: none"> • Radiation tolerance test • Comparison with similar missions • Temperature tolerance test • Load tolerance test
STR & TC	<ul style="list-style-type: none"> • Structural model analysis • Structural analysis with Computer-aided Design (CAD) render • Kinematic simulation with CAD render • Thermal control simulation 	<ul style="list-style-type: none"> • Non-destructive tests • Thermal conductivity test • Qualification testing (QT) and acceptance testing (AT) performed by ISISpace
EPS	<ul style="list-style-type: none"> • Signal verification with VHDL software (e.g. ModelSim) 	<ul style="list-style-type: none"> • Voltage/current magnitude & duration test
ADCS	<ul style="list-style-type: none"> • Software verification • Kinematic simulation with CAD render • Dynamic attitude test bed • Software simulation 	<ul style="list-style-type: none"> • Flight heritage
CDH, TT&C & GNC	<ul style="list-style-type: none"> • Software verification • Flight simulation 	<ul style="list-style-type: none"> • Radiation tolerance test • Thermal cycling test
PROP	<ul style="list-style-type: none"> • Fill & drain valve inspection • Verification with Pathfinder Technology Demonstration 1 (PTD-1) mission results 	<ul style="list-style-type: none"> • Engine sizing test • Leakage test • Sizing calculations verification

As can be seen, not all subsystems are subjected to the same level of verification and validation. This follows from the inherent differences between each subsystem. As stated previously, for the relevant subsystems, the V&V strategies will be outlined in greater detail in their respective chapters. In the following chapters, the design of the subsystems will be put forth.

9. Preliminary Design Overview

This chapter provides a short description of the results that were generated in previous reports. First, the trade-off between observation platforms is discussed in Section 9.1. Next, the three preliminary design concepts that were generated are summarized in Section 9.2. The trade-off between these is presented in Section 9.3. The resulting final concept and a preliminary configuration is then given in Section 9.4.

9.1. Observation Platform

The first trade-off that was performed was between the various observation platforms that have been considered for this mission. Such a trade-off was performed at an early stage [3] to allow for a greater level of depth in the final design. It was determined that a sufficient level of understanding of the mission requirements existed to justify an early trade-off of the observation platform. Aircraft and drones were immediately discarded due to their altitude and endurance constraints. This left for a trade-off to be performed between balloons and spacecrafts. The results favoring a spacecraft concept are displayed in Table 9.1.

Table 9.1: Trade-off between a stratospheric balloon and satellite constellation [3].

Exceeds requirements, Meets requirements, Correctable deficiencies, Unacceptable deficiencies

	Stratospheric balloon	Satellite constellation
Spatial resolution	Due to low altitude of the balloon the required spatial resolution is easily achievable with SPEXone	Due to the payload restrictions the spatial resolution is only met by flying at low altitudes.
Area coverage	At the maximum altitude of 20-25 km a viewing angle of 78.7-80.9° is needed to meet the area coverage requirement. The balloon can only measure one place on Earth from a static location.	For an area coverage of 250 x 250 km at an altitude of 230 km a viewing angle of 28.5° is needed. A satellite constellation could provide measurements on different places in the world.
Temporal resolution	Continuous measurements.	For a temporal resolution of 2 hours multiple Low Earth Orbit (LEO) satellites are needed.
Regulations	Can not be near crowded areas, needs to avoid certain locations for geopolitical reasons, very few locations available for monitoring.	More possibilities of areas to monitor. A lot of regulations for satellite.
Risk	Low development and mission risk.	High mission risk, moderate development risk but both can be mitigated.
Sustainability	Re-usable, minimal fuel use.	End of life burn, higher carbon footprint compared to balloons due to rocket launch.
Mission duration	Difficult to reach 2 years, current balloon missions last 2-6 weeks. Multiple balloons could be used.	Typical missions reach 2 years.
Maintenance	Simple maintenance. Can have touch down and re-launch quickly.	Very difficult maintenance. Payload, TT&C, or other problems can be devastating.
Revenue	Low revenue possibility, low market capital	Very high revenue possibility, driven by growing private industry. Market value expected to increase highly in the coming few years.
Cost	Low development and operations cost. The cost of a balloon flight can be one hundred times less than a rocket launched satellite mission.	High development and operations cost for a constellation of 4 CubeSats.

In conclusion, both systems are viable options to measure aerosols above a city. The stratospheric balloon could provide continuous measurement data, enables high spatial resolution and has a low cost. The satellite constellation system could observe aerosols on a global level, has a higher area coverage and is easier to scale to different

regions, which is harder for the balloon system as regulations prevent balloon observations at many locations. For the sake of future applications and scalability, a satellite constellation was selected for the CASE mission. For more information regarding the observation platform trade-off, the baseline report can be consulted [3].

9.2. Preliminary Design Concepts

This section presents the preliminary design concepts that were generated for the CASE mission. Three design options were selected. These were worked out in more detail in the Midterm Report [1]. Following the selection, the preliminary sizing and budgets were made for the three concepts in order to give an impression of the implications of the design choices on the mission. This was necessary to perform an accurate trade-off. The main difference between the design options was the payload since it drove the imaging performance of the mission. Furthermore, the design concepts differ in coverage and number of satellites. The important outcomes from the preliminary calculations and the main characteristics of the preliminary design options are presented in this chapter. A summary is given in Table 9.2 and the concepts are visualized in Figure 9.1.

Table 9.2: Design option specification.

	Payload	Coverage	Constellation
Design option 1	SPEXone (or an altered version)	South of India/Bangalore	Constellation of 18 small satellites
Design option 2	Polarimeter-on-a-chip	Global	Constellation of 21 CubeSats
Design option 3	Both SPEXone and polarimeter-on-a-chip	Equatorial	Constellation of 3 small satellites

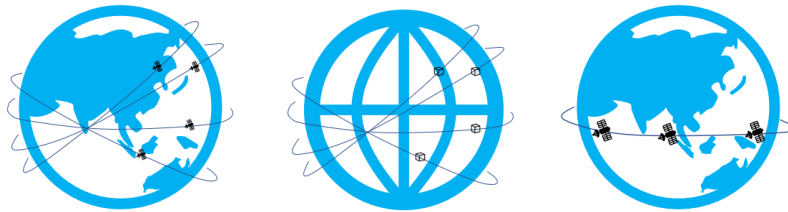


Figure 9.1: Schematic visualisations of the design concepts. Left: concept 1, middle: concept 2, right: concept 3.

Below, Table 9.1 depicts various criteria for each design concept along with their respective values, which were determined in a previous report [1]. The relative scoring of each concept for the criteria was crucial during the concept trade-off, which is summarized in Section 9.3. The justification for the selection of each criteria was detailed in the Midterm Report [1].

Table 9.1: Assessment of grading criteria per design concept for trade-off. Some criteria are assessed using a relative grading scale.

Grading criterion	Design concept 1	Design concept 2	Design concept 3
Spatial resolution [m]	1000	100	100
Area coverage [1-5]	3	5	1
Swath width [km]	40	250	250
Temporal resolution [hrs]	1	3.4	0.5
Polarimetric accuracy [-]	0.002	0.003	0.003
Wet mass [kg]	104	16	109
Volume [dm ³]	46	5	48
Cost [1-5]	5	4	3
Risk [1-5]	2	4	4
TRL [1-5]	4	2	3
Sustainability [1-5]	1	3	4
Return on Investment (ROI) [1-5]	2	5	3

9.3. Trade-off Summary

For this trade-off between design concepts, the Analytic Hierarchy Process (AHP) method was employed to ensure a balanced and consistent weighting system. The inner workings of the AHP method applied to this trade-off can be consulted in the Midterm Report [1]. The results of the AHP method in regards to the calculation of weights can be visualized below in Table 9.2.

Table 9.2: Weights assigned to each criteria, determined by the AHP method.

Area coverage	Spatial resolution	Swath width	Temporal resolution	Polarimetric accuracy	Wet mass	Volume	Cost	Risk	TRL	Sustainability	ROI
3.6%	9.5%	15.5%	13.0%	7.5%	5.3%	5.6%	10.7%	4.1%	6.2%	2.0%	16.9%

The results of the AHP method show that the most significant criteria, according to the team were (in order of importance) ROI, swath width, and temporal resolution. However, to verify that the selection of weights was conducted in a consistent manner, the Consistency Ratio (CR) was calculated. To summarize the process, whose entirety can be consulted in the Midterm Report [1], a CR below 0.1 must be achieved for a consistent AHP method; the trade-off in this chapter yielded a CR of 0.0321. Having established the methodology was consistent, the final outcomes can be discussed.

The results of the trade-off can be seen below in Table 9.3, with each design concept's scoring for each criterion. The results are obtained by multiplying each criterion's results from Table 9.1 with Table 9.2's results. The final row then displays the sum total of each concept.

Table 9.3: Trade-off results, score per criterion.

Criterion	Design concept 1	Design concept 2	Design concept 3
Spatial resolution	0.45%	4.54%	4.54%
Area coverage	1.19%	1.98%	0.40%
Swath width	1.15%	7.17%	7.17%
Temporal resolution	3.95%	1.16%	7.91%
Polarimetric accuracy	3.23%	2.15%	2.15%
Wet mass	0.63%	4.12%	0.60%
Volume	0.46%	4.64%	0.45%
Cost	2.74%	3.42%	4.56%
Risk	2.06%	1.03%	1.03%
TRL	2.76%	1.38%	2.07%
Sustainability	0.25%	0.74%	0.99%
ROI	3.38%	8.46%	5.08%
Total	22.26%	40.80%	36.94%

As can be seen, the victorious concept is concept 2, slightly beating concept 3. It is worth noting that this final result is heavily influenced by the choice of weights for each grading criterion. Therefore, a sensitivity analysis was also performed. The way in which this was done is by iterating through each criterion and observing the difference in final outcome in response to a factor increase in the criterion weight.

Table 9.4: Overview of change in relative importance factors for sensitivity analysis.

Parameter(s)	Change in importance	Effect, in change of percentage points (pp)
Return on investment	x2	Winner: Design option 2 (+2pp)
Return on investment	x0.5	Winner: Design option 2 (-0.9pp)
Sustainability	x2	Winner: Design option 2 (+0.2pp)
Spatial resolution	x2	Winner: Design option 2 (+0.5pp)
Swath width	x2	Winner: Design option 2 (+0.7pp)
Temporal resolution	x2	Winner: Design option 3. Design option 2: -3.6 pp, design option 3: +2.7 pp.
Polarimetric accuracy	x20	Winner: Design option 1 (only 0.12pp higher than option 2)
Polarimetric accuracy & risk	x10	Winner: Design option 2 (Design option 1 is 0.26pp shy of beating design option 2).
All	Equalized	Winner: Design option 2 (+10pp)

As the table shows, most criteria still result in the second concept being the preferred choice. The main exception is with regards to the temporal resolution, where design option 3 becomes dominant if the weight for the temporal resolution is increased. A *reductio ad absurdum* approach was taken to demonstrate the futility of concept 1. Due to its sole victorious criterion being the polarimetric accuracy, the criterion required a 20-fold increase in weight in order for design concept 1 to become the best concept. This appeal to extremes concludes that concept 1 is not a valid option. A final sensitivity test was performed where all criteria were given equal weights; design concept 2 reigns triumphant as well.

9.4. Final Concept

The trade-off detailed in Section 9.3 showed design concept 2 to be the most suitable choice. However, due to the temporal resolution being substantially worse in the second concept than the third concept, a combination of these two concepts was proposed. This combined concept, henceforth referred to as the final design, will take the spacecraft concept from concept 2 and the orbit design of concept 3. This will consist of three CubeSats equipped with TNO's polarimeter-on-a-chip instrument in an equatorial orbit. This exploits the benefits of both concepts 2 and 3 and produces an improved final design. Further rationales and calculations supporting this combination can be found in the Midterm Report [1].

Despite the unanimous favor for the final design option, it was necessary to impartially determine whether it indeed performed better than any of the original three concepts. For this reason, the trade-off of Section 9.3 was repeated, with the final design included. The scoring of each concept after performing the AHP method is shown in Table 9.5. As can be seen, the final design wins by a sufficiently large margin to justify its selection.

Table 9.5: New concept scores after adding the final design, found using the AHP method.

	Concept 1	Concept 2	Concept 3	Final design
Score	15.48%	27.15%	24.25%	33.12%

While at this stage no intricate sizing of the subsystems was possible, a general render was produced for stakeholders. At this stage, the final design consisted of the following subsystem specifications. Note that the numbering is consistent with the render shown in Figure 9.2.

1. **Payload:** TNO Optical Metasurfaces based Spectro-Polarimeter (1)
2. **ADCS:** Magnetorquer (2.1), sun sensors (2.2), star sensors (2.3)
3. **EPS:** Solar array (3.1), battery (3.2), PMAD unit (3.3)
4. **Propulsion:** Fuel tank (4.1), HYDROS-C thruster (4.2)
5. **Thermal:** Insulation (5)
6. **Structure:** 6U CubeSat (6)
7. **TT&C:** Patch antenna (7.1), S-band transceiver (7.2)
8. **CDH:** Microprocessor (8)
9. **GNC:** Galileo receiver (9)

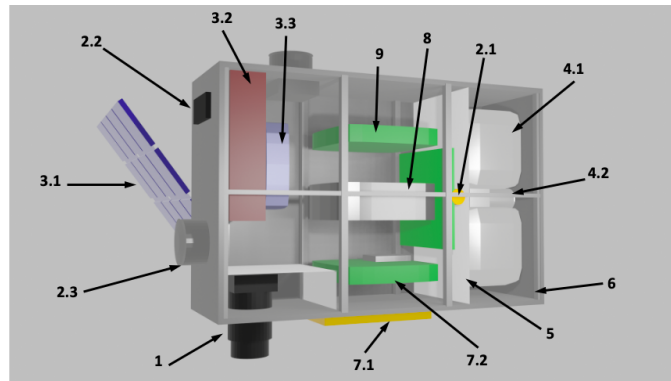


Figure 9.2: Preliminary render of the subsystem layout in the satellite with the components indicated by numbers following from the list of components.

While the configuration is still in its preliminary stages (due to limited subsystem design), an early configuration has been established. Naturally, the payload should align in the nadir direction to allow for measurements, and should be thermally isolated from the other subsystems. For efficient ground communication, the TT&C subsystem faces the same way. The ADCS sensors is located outside of the spacecraft, while the actuators are placed in vicinity of the propulsion system. The EPS consists of a solar panel system, located on the outside of the spacecraft, next to the battery and PMAD system to minimize cable length; the cable length between CDH and TT&C is also minimized.

The previous chapters have endeavoured to inform the reader regarding the progress made over the first three reports [1, 2, 3]. For further detail, the reports themselves can be consulted. The following chapters will continue where the previous report [1] concluded, beginning with the sizing of each subsystem. The payload will be the first subsystem to be sized due to its significant contributions to the overall mission requirements and cost. The remaining subsystems will follow using an iterative approach. It should be mentioned that after the Midterm Review, some of the primary vital criteria were altered. Due to the cost of the payload, which will be elaborated in Chapter 11 and Chapter 26, the CASE mission had to scale down on the number of satellites not drive the mission cost extremely high. Furthermore, more technical knowledge was acquired considering the payload and other subsystems. These will also be discussed in the coming chapters.

10. Astrodynamic Characteristics

In previous reports, the orbital design of the mission was evaluated. This chapter presents the final considerations towards the mission orbit, and creates the foundation for the detailed design of each spacecraft subsystem. First, the characteristics of the final orbit are presented in Section 10.1. Then, the POIs that were identified in consultation with stakeholders are discussed in Section 10.2. Using this information, several considerations for the spacecraft subsystem design were extrapolated. This is presented in Section 10.3. Finally, the risks and sustainability of the astrodynamic design are discussed in Section 10.4 and Section 10.5 respectively.

10.1. Orbit Characteristics & ΔV Budget

The main driving requirement behind CASE's orbit selection was the temporal resolution. To come close to the initially required 30-minute resolution at each of the measurement locations, the orbital characteristics were selected as shown in Table 10.1. The orbit is classified as an Equatorial Low Earth Orbit, and thus only covers the equator. This choice was made in a previous report since an inclined orbit with the same temporal resolution would lead to the number of CubeSats increasing to roughly 18 spacecraft [1]. This would drive up cost and complexity immensely and was therefore decided against. As the satellite is flying in the same direction as the Earth is rotating, the temporal resolution becomes 33.76 min, which proved to be sufficient upon [L].

Table 10.1: Summary of orbital characteristics.

Parameter	Value
Altitude	500 km
Orbital velocity	7.61 km/s
Ground velocity	6.59 km/s
Orbital period	5677 sec (94.6 min)
Inclination	0°
Eccentricity	0 (circular orbit)
Constellation	3 CubeSats
Temporal resolution	33.8 min



Figure 10.1: Visualisation of the final orbit¹³.

For the final selection of the altitude of the constellation, the driving factor was the ΔV budget. In order to minimize the required propellants, the amount of ΔV should also be minimized. To aid in this evaluation, a graph was created showing the ΔV budget at varying altitudes. This is shown in Figure 10.2.

An important observation is the sudden increase in ΔV at the altitude of 500 km. This is due to international regulations involving space debris. These regulations, adopted by ESA, stipulate that spacecraft should de-orbit within 25 years¹⁴. For a typical spacecraft, this is achieved passively due to drag, up to an altitude of 500 km. Above this altitude, active de-orbiting is necessary, where the spacecraft uses its thrusters to decelerate and de-orbit. Therefore, in Figure 10.2, the ΔV necessary for de-orbiting was taken to be zero below this altitude. Above 500 km, the ΔV necessary to lower the periaapsis to 75 km is taken, which was described in a previous report [1].

¹³<https://observablehq.com/@jake-low/satellite-ground-track-visualizer>, [Retrieved June 7, 2021]

¹⁴http://www.esa.int/Safety_Security/Clean_Space/Scuttling_satellites_to_save_space, [Retrieved June 7, 2021]

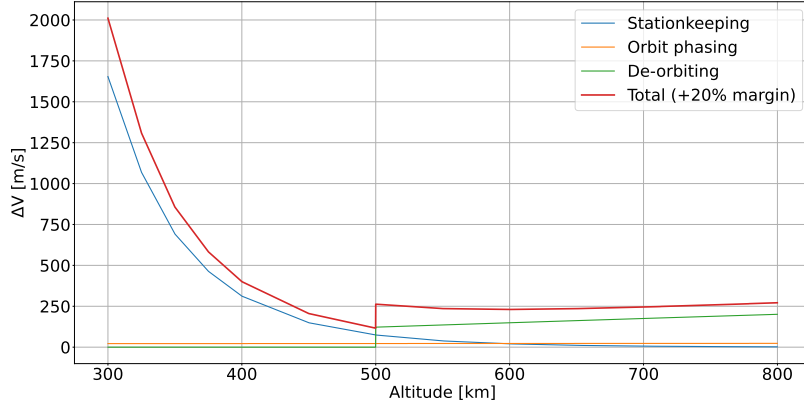


Figure 10.2: ΔV budget at various altitudes. The contributions as well as the total with margin are shown.

Aside from the ΔV for de-orbiting, another main contributor is the ΔV required for stationkeeping. To maintain altitude, drag forces must be counteracted, especially in Low Earth Orbit (LEO). As becomes clear from Figure 10.2, it is preferable to have a high altitude for this contributor to be minimized. The final contribution, orbit phasing, is used to place the spacecraft in the correct phase of the orbit. After launch, the spacecraft are all at the same position in the orbit. However, there needs to be spacing in between them such that the temporal resolution requirement is met. Overall, this contribution is not as influential as the other two contributors.

For the final selection of the altitude, two factors were taken into account. First, the altitude should be as high as possible to reduce the effects of drag on the spacecraft. Second, the altitude should not exceed 500 km, since otherwise ΔV would be necessary for de-orbiting. Combining these two factors leads to an altitude of 500 km, which was also given in Table 10.1. The ΔV requirements for this altitude can be found in Table 10.2. A 20% margin was added for contingency [28].

Table 10.2: ΔV budget of the spacecraft.

Maneuver	ΔV [m/s]	with 20% margin
Station keeping [28]	74.4	89.28
Orbit phasing	22.26	26.71
De-orbiting	0	0
<i>Total</i>	96.66	115.99

From the selected altitude, the other parameters in Table 10.1 could be calculated using previously described methods [3][1]. A final consideration was made for the ground velocity of the spacecraft. The spacecraft could either orbit in the same direction as the rotation of Earth, or opposite to it. While orbiting in the opposite direction would increase the temporal resolution with roughly 4 minutes, it was decided to opt for orbiting in the same direction. This allows for longer contact with GSs and smaller frame rates for the payload instruments. Additionally, this makes the launch trajectory more easily achievable. Thus, the spacecraft orbits from West to East as seen on a map. The ground velocity is then calculated using Equation 10.1, where R_E is the Earth radius, T_E the duration of one Earth day, and h the orbit altitude.

$$V_{\text{ground}} = V \frac{R_E}{R_E + h} - \frac{2\pi R_E}{T_E} \quad (10.1)$$

10.2. Points of Interest

In a previous report it was determined that it would not be possible to measure for the entirety of the orbit, the limiting factor being data downlink. To solve this, one could either process some of the data on-board of the spacecraft, or measure a smaller portion of the orbit. After consulting with the stakeholders, it was found that the latter option was preferred [F].

To comply with this preference, several targets along the equatorial orbit were selected for being the most scientifically valuable, again in close discussion with stakeholders. Furthermore, the different locations on the equator were analyzed to determine their need for such a monitoring system. The details of this analysis are mentioned in Chapter 4. Considering these aspects, it was concluded that the targets to be monitored are the Amazon rain forest in South America, Nairobi, Kampala, and Singapore. Furthermore, since it is possible for the CASE mission to select any location on the equator to measure, some extra locations such as Libreville can also be measured.

The limited downlink capability presented an upper limit on the time that could be measured each orbit. It was determined from this maximum measurement time that with a swath width of 250 km, roughly 1375 km of along-track ground coverage was possible each orbit. Here, the reliability of GSs was taken into account, which is explained in more detail in Chapter 21. Note that the swath width was fixed due to the choice of payload, described in Chapter 11.

The estimated along-track ground coverage of 1375 km can be divided over multiple measurements, taking into account the preferences of the stakeholders and the market needs. The final selection of targets is presented in Table 10.3. Note that this division is flexible. At any point during the mission this selection could be altered, as long as the total measurement length does not exceed 1375 km per orbit. Additionally, it was decided by consulting with the stakeholders that cities should be covered with a sufficiently large area to allow for context in the measurement data [F].

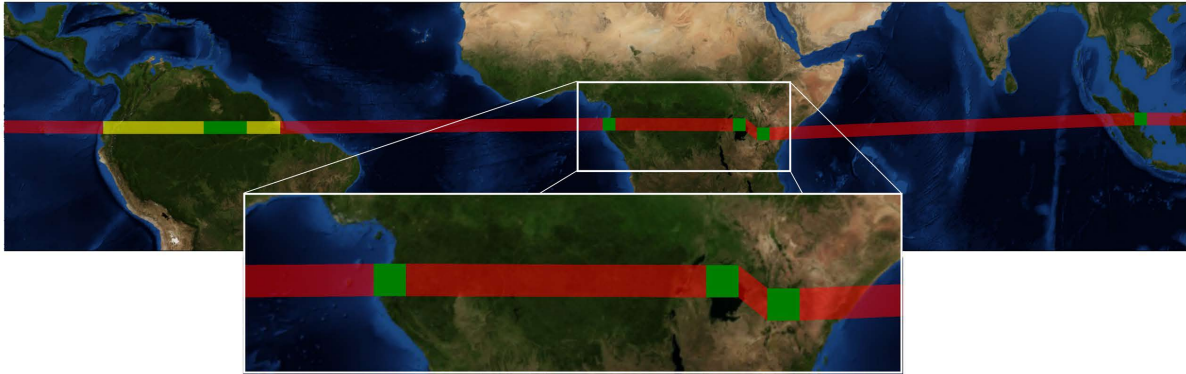
Table 10.3: Specification of the mission targets, divided into three categories based on their priority.

Category	Target	Measurement length
Primary targets	South America	950 km
Secondary targets	Singapore	250 km
	Nairobi/Kampala	175 km
Tertiary targets	Libreville	175 km

The targets have been divided into three categories. The primary targets are of the highest interest and present the largest scientific value to the stakeholders. Then, the secondary targets are of less importance, but are still preferably measured every orbit, since they fit into the measurement budget. Finally, the tertiary targets present the least scientific value, and should only be measured when there is downlink capacity to spare. The coverage of all of these targets is visualised in Figure 10.3, where Figure 10.3a shows the primary and secondary targets, and Figure 10.3b additionally shows the tertiary targets. Note that the length of the 950 km attributed to South America in Table 10.3 is indicated in green, where the yellow bar represents the possible range in which this measurement could be taken.



(a) Swath coverage when measuring primary and secondary targets in a single orbit.



(b) Swath coverage when measuring primary, secondary and tertiary targets in a single orbit.

Figure 10.3: Differences in swath coverage depending on measurements at tertiary targets.
Note that the spacecraft orbits from West to East.

An important observation from this figure is the fact that the targets lie at different latitudes. Since the spacecraft is in an equatorial orbit, it needs to angle the payload instruments in order to obtain a view of the target areas. This is called off-nadir pointing, which influences the design of subsystems such as the ADCS. These considerations are discussed in more detail in the next section.

10.3. Results

While the spacecraft is orbiting above the equator with a latitude of 0° , the mission targets lie slightly above and below this latitude. Thus, the spacecraft needs to point the instruments towards these targets, creating an off-nadir angle in the across-track direction. This is visualised in Figure 10.4. For each of the mission targets, the required pointing angle was calculated, which is summarized in Table 10.4.

Table 10.4: Properties of the measurements during the orbit. Note that positive off-nadir pointing indicates a measurement above the equator, while negative pointing is a measurement below the equator.

Category	Target	Measurement length	Measurement time	Latitude	Off-nadir pointing
Primary targets	South America	950 km	144.1 s	-0.18°	-2.3°
Secondary targets	Singapore	250 km	37.9 s	1.35°	$+16.7^\circ$
	Nairobi/Kampala	175 km	26.5 s	$-1.29/0.32^\circ$	$-16.0/+4.0^\circ$
Tertiary targets	Libreville	175 km	26.5 s	0.41°	$+5.2^\circ$

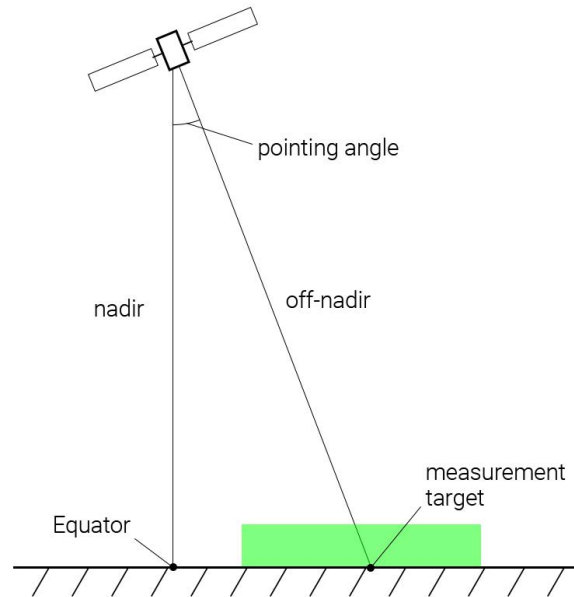


Figure 10.4: Off-nadir pointing to allow the payload to view the target area. Note that the flight direction is out-of-plane.

Combining these numbers with Figure 10.3b, a problem becomes apparent. After the measurement in Nairobi, the spacecraft needs to angle from -16.0° off-nadir pointing to $+4.0^\circ$ in a short time frame to view Kampala. This is visible in the figure as a kink in the swath coverage track. This greatly influences the design of the ADCS subsystem, which would need to be able to generate larger torques. To give an impression of the required angle changes between measurements, Table 10.5 details the average angular velocity between measurements. Note that this is not entirely accurate since the spacecraft needs to first accelerate and then decelerate. It only serves to indicate the order of magnitude of the rotation.

Table 10.5: Time between measurements and the required pointing change.

Ending measurement	Starting measurement	Inoperative time	Pointing change	Average angular velocity
Nairobi	Singapore	1098.9 s	32.7°	0.0298 deg/s
Kampala	Nairobi	45.3 s	20.0°	0.4415 deg/s
Libreville	Kampala	363.6 s	1.2°	0.0033 deg/s
South America	Libreville	972.4 s	7.5°	0.0077 deg/s
Singapore	South America	2948.9 s	19.0°	0.0064 deg/s

From these values, it becomes clear that the pointing change between Nairobi and Kampala would require a significantly higher torque than the other changes. During the detailed design of the ADCS subsystem in Chapter 16, it was found that these targets cannot be measured in the same orbit. Since they are both of high importance, they will be measured in consecutive orbits separately, thus providing a 1 hour temporal resolution for both. This was confirmed with stakeholders [L]. Following this, it was decided that the best coverage scheme in terms of performance would be, in each orbit covering Amazon and Singapore, and either Nairobi or Kampala. This will lead to measurements in the Amazon and Singapore to have 30 minutes temporal resolution, and Nairobi and Kenya to have 1 hour temporal resolution in the span of the mission duration. The tertiary locations such as Libreville can be measured upon request.

Finally, from Table 10.4 it follows that the spacecraft is taking measurements for 208.5 s each orbit, when excluding the tertiary targets and considering that Kampala and Nairobi are measured in alternating orbits. With the orbital period found in Section 10.1, this is roughly 3.67% of the orbit. All of the results discussed in this chapter could now be taken into account for the detailed subsystem design.

10.4. Risk

As with any space mission, there are a number of risks that need to be mitigated to maximise the chances of a successful mission. Some of these risks include high radiation doses, space debris and incorrect orbit insertion.

10.4.1. Radiation

As for radiation, at higher altitudes the atmosphere offers less protection against ionizing particles¹⁵. Thus, the risk of radiation damaging or interfering with the spacecraft must be considered. Generally, the dose of radiation depends on the altitude and the solar cycle¹⁶. This latter variable was already considered in a previous report [1], where the worst-case scenario was assumed; solar maximum. The solar cosmic rays emitted by the Sun can cause damage to electronics and data lines, which is considered in the respective chapters.

As for the altitude, an important source of radiation are the Van Allen belts surrounding Earth. These consist of an inner and an outer belt, the inner belt starting at an altitude of roughly 640 km¹⁷. Thus, for the CASE mission orbiting at 500 km, this does not present a serious risk.

Solar storms and solar winds, however, do have the potential to pose a serious risk to the spacecraft **RSK-G6**. While the occurrence of such solar storms is difficult to predict, especially when the launch date is still a variable, however countermeasures must still be considered. One such countermeasure would be to bolster the structure of the CASE CubeSat to sufficiently withstand high radiation doses. Alternatively, the propulsion system could be fitted with sufficient fuel to perform an emergency change of orbit. These countermeasures are detailed in their respective chapters, Chapter 12 and Chapter 19.

10.4.2. Space Debris

Space debris, also known as space junk, are pieces of human-made objects in an Earth orbit that no longer support any useful function. NASA tracks and monitors more than 27000 pieces of space debris as small as 5 cm in diameter in LEO. Space debris can be very harmful and threatening to a satellite's mission success due to the potential for collisions (**RSK-G4**)¹⁸.

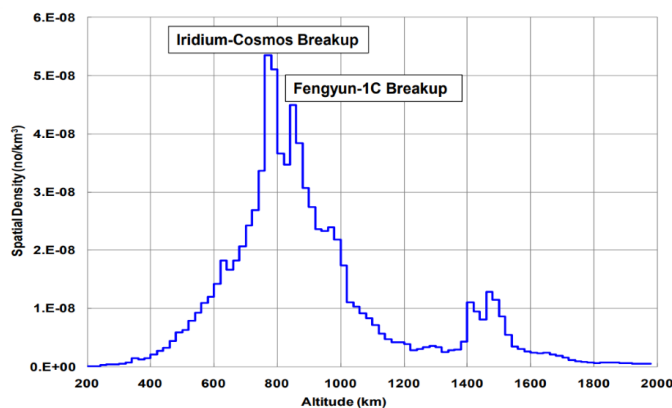


Figure 10.5: Spatial density of LEO space debris by altitude from 2011¹⁹.

As shown in Figure 10.5, the spatial density of space debris is highest at altitudes of 750 and 850 km, caused by the collision of a Russian satellite with a French satellite in 2009 and the deliberate destruction of a Chinese satellite in 2007, respectively. Luckily for the CASE mission, both of these orbits have a higher altitude than the 500 km LEO orbit that CASE will fly at. The spatial density of space debris is significantly lower in this orbit. At the altitudes of 750 and 850 km, respectively, the orbital decay time of the space debris is measured in a number of decades²⁰. Since CASE is projected to launch in 2027 with a 2-year mission lifespan, these higher concentrations of space debris should yield no significant increase in collision risk throughout CASE's mission life.

¹⁵<https://www.spaceflight.nasa.gov/spaceneeds/factsheets/pdfs/radiation.pdf>, [Retrieved June 7, 2021]

¹⁶<https://www.nasa.gov/analogs/nsrl/why-space-radiation-matters>, [Retrieved June 8, 2021]

¹⁷<https://www.nasa.gov/content/goddard/van-allen-probes-spot-impenetrable-barrier-in-space>, [Retrieved June 8, 2021]

¹⁸https://www.nasa.gov/mission_pages/station/news/orbital_debris.html, [Retrieved on June 8, 2021]

¹⁹<http://www.unoosa.org/pdf/pres/stsc2011/tech-31.pdf>, [Retrieved on June 8, 2021]

²⁰https://www.nasa.gov/news/debris_faq.html, [Retrieved on June 8, 2021]

There are two ways to mitigate the risk of space debris for a satellite mission:

1. **Angle the spacecraft in flight such that it has the smallest frontal surface area:** This reduces the chance of being hit by space debris since the spacecraft's target area is as small as possible.
2. **Size the ΔV budget to include space debris avoidance:** If enough fuel is taken on-board of the spacecraft, it can be used to slightly change its orbit long before the potential impact of space debris occurs. This active avoidance can be facilitated using NASA's and ESA's tracking information on space debris.

Both of these risk-reducing measures will be applied in the CASE mission to minimize the hazard of a space debris collision, as will be shown in Chapter 22 and Chapter 12, respectively.

10.4.3. Incorrect Orbit Insertion

The launch vehicle failing to bring the spacecraft into the planned orbit can significantly hinder the spacecraft to fulfill its mission objectives (**RSK-G8**). Three possible deviations were considered; incorrect altitude, eccentricity, and inclination. In the case of an incorrect altitude, it could be impossible for the payload instruments to take measurements of Earth. The sensors and lenses were designed and calibrated for the planned altitude, and might suffer performance loss or total disability to take measurements.

Another hindrance to the payload could be an incorrect eccentricity. If the final orbit is not circular, the altitude variations throughout the orbit would be difficult or impossible for the payload to handle, thus failing to generate mission deliverables. A spacecraft in the selected orbit would naturally circularize its orbit, thus limiting the impact of this risk. At the lowest point of the orbit, the spacecraft would experience more drag, lowering the apoapsis and thus decreasing the eccentricity towards the desired value of zero.

Finally, if the inclination of the final orbit is incorrect, the requirement on the temporal resolution can likely not be met. Additionally, some of the mission targets identified in this chapter might not be covered. Since the mission already uses active pointing of the spacecraft to target areas, this could possibly be partially mitigated, given that the inclination does not differ excessively.

10.5. Sustainability

One of the most important factors regarding the sustainability of the astrodynamics design is the EOL strategy. As mentioned in Section 10.1, an altitude of 500 km was selected where active de-orbiting is not required [18]. This reduces the amount of fuel required for the mission, reducing fuel usage of the CASE mission. Instead, the spacecraft will lose altitude due to drag, eventually burning up in the Earth's atmosphere. This is expected to take at most 25 years²¹, conforming to international regulations. Even though burning up a satellite in the Earth's atmosphere seems unsustainable, it is the most sustainable way to dispose old satellites. If they were to remain in orbit, they would pose a larger threat to other satellites in the form of space debris and make space travel more dangerous. To potentially accelerate the de-orbiting process, the spacecraft could use any remaining propellant to lower the orbit periapsis. The spacecraft would then experience more drag, leading to earlier atmospheric re-entry.

To limit the amount of propellant that is used for station keeping, it is important to minimize the drag that the spacecraft experiences. The configuration discussed in Chapter 22 shows that the spacecraft body is angled such that it produces the smallest possible frontal surface area, thus reducing drag.

²¹http://www.esa.int/Safety_Security/Clean_Space/Scuttling_satellites_to_save_space, [Retrieved June 7, 2021]

11. Payload Subsystem

CASE's payload system is the instrument that will perform the aerosol measurements. In the previous report, a trade-off was performed between the SPEXone instrument from SRON, and the Optical Metasurfaces Based Spectro-Polarimeter from TNO [1]. The TNO instrument was selected due to its capability to meet the payload requirements with more suitable instrument characteristics. In this chapter, the payload subsystem is further detailed and analysed. First, the requirements of the instrument are shown as given by the developer. Second, the configuration trade-off is performed and the viewing angles are determined. Next, the final characteristics of the payload instrument are defined. Finally, the risk and sustainability is assessed.

11.1. Optical Metasurfaces Based Spectro-Polarimeter

The Optical Metasurfaces Based Spectro-Polarimeter is a promising concept. As the metasurfaces allow for direct integration of the spectro-polarimeter on the detector chip, the instrument will have a low volume and mass while providing accurate spectro-polarimetric measurements²². The main goal of TNO with this instrument design study was to determine if they could usefully incorporate the meta-surface technology in a real instrument and, in doing so, reduce the size of the instrument and add performance beyond the currently available instruments, e.g. SPEX, 3MI [D].

The instrument will fly at an altitude of 500 km and cover 6 polarized bands ranging from 443 - 870 nm. With its swath width of 250 km, the payload must be pointed towards the target areas, this is discussed in Chapter 16. The requirements for each unit of the instrument as given by Andrew Bell from TNO are shown in Table 11.1.

Table 11.1: Requirements Optical Metasurfaces based Spectro-Polarimeter from TNO [D].

Property	Value
Spatial resolution	151 m
Swath width	250 km
Field of view	14° across-track x 7° along-track
Spectral coverage	443nm, 490nm, 550nm, 620nm, 670nm, 870nm. Full width at half maximum (FWHM) ranging from [2-6] nm
Polarimetric accuracy	<0.01 for calibrated optics, <0.005 for the first 5 polarized bands
Radiometric SNR	280-780
Pixel size	>10 μm
Resolution	2000 x 1000 pixels
Digitization	12 bit
Dimensions	\varnothing 50 mm x 150 mm

The pixel size needs to be bigger than 10 μm to meet the necessary accuracy for making the meta-surface elements. The instrument needs 4 pixels to reconstruct the full characterization of the aerosols in the measured ground sample²³.

Measurements can also be done at night as the instruments measures at 870 nm, which is inside the infra-red spectrum. However, as the aerosols are only measured in one spectral band the retrieval will be less accurate. The measurements of the smaller wavelengths during night above the sea will be used to reduce the noise of the instrument, e.g. subtract dead pixels from the measurements.

²²<http://resolver.tudelft.nl/uuid:95dc5d23-3589-4043-b816-34dcb88fb32e>, [Retrieved on May 17, 2021]

²³<http://resolver.tudelft.nl/uuid:95dc5d23-3589-4043-b816-34dcb88fb32e>, [Retrieved on May 17, 2021]

11.2. Configuration Trade-Off

In this section, a more detailed examination of the configuration of the instrument is performed. The focus is placed on the selection of the number of viewing angles.

11.2.1. Number of viewing angles

Multi-angular measurements are preferred for the retrieval of aerosol properties from the measurements, as these make it easier to distinguish between the underlying reflective surface (oceans, glaciers, forests, etc.) and the aerosols [29]. The comparison of MODIS (single viewing angles) and MISR (9 viewing angles) on-board of the TERRA mission with the measurement of AERONET, an aerosol detection network on Earth²⁴, showed that errors on the retrieved parameters are significantly decreased when including multiple viewing geometries [30]. However, this improvement stagnates when more than five viewing angles are included in the retrieval [31]. The mean absolute errors of aerosol optical depth (AOD) and single scattering albedo (SSA) over the number of measurement angles are shown in Figure 11.1.

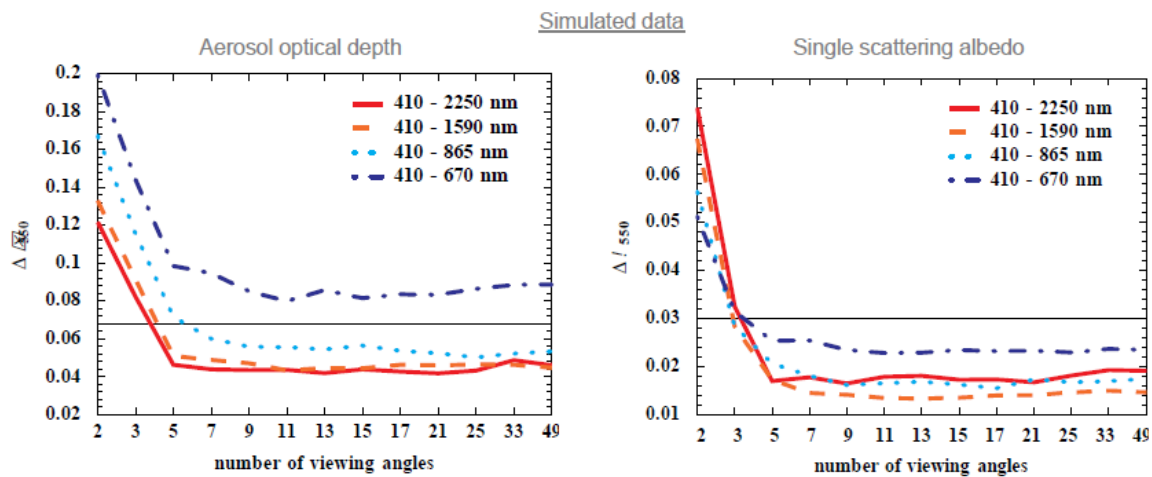


Figure 11.1: The results of mean absolute errors of aerosol optical depth (left), single scattering albedo (right) as a function of the number of viewing angles between retrieved and true values for four different polarimetric measurement configurations. The black line indicates the target accuracy on aerosol parameters. For the target accuracy of AOD, 10% of the mean AOD is used and for the SSA the accuracy formulated by Mishchenko et al. [32] is used.

As the instrument measures from 443nm - 870nm, the light blue dotted line shows its accuracy. As shown in the figure, the target accuracy on aerosol parameters formulated in [31] is met with 5 viewing angles for the AOD and with 3 for the SSA. However, both angles are taken into account, as they both meet the stakeholder accuracy requirements [F]. The option of a single and double viewing angle was discarded, due to the high slope in mean absolute errors at a small number of viewing angles.

Thus, the number of viewing angles is an important variable for the payload subsystem. Two methods were identified which could provide a multi-angle system; multiple instruments could be used to create multiple viewing angles, or an instrument could be rotated after measuring to provide another viewing angle. To decide on the best solution, eight options were conceived, providing various combinations of these methods. These are summarized in Table 11.2.

²⁴<https://aeronet.gsfc.nasa.gov/>, [Retrieved on June 17, 2021]

Table 11.2: Options considered for the payload instrument configuration.

Option	Number of instruments	Number of viewing angles	Rotation methods
Option 1	3	3	Static
Option 2	5	5	Static
Option 3	1	5	Full spacecraft rotation
Option 4	1	3	Full spacecraft rotation
Option 5	1	5	Independent instrument rotation
Option 6	1	3	Independent instrument rotation
Option 7	3	5	Full spacecraft rotation
Option 8	2	5	1 spacecraft rotation & 1 independent instrument rotation

The first two options only consider static instruments, where option 1 provides three viewing angles, and option 2 provides five. Next, two options consider rotating the full spacecraft to point a single instrument to either three or five viewing angles. The following two options considered the same configuration, but rotate the instruments independently from the spacecraft, using a hinge or gimbal system. Option 8 combines multiple instruments and spacecraft rotation, by utilizing three instruments that are rotated to cover five viewing angles. This relaxes requirements on the ADCS, which would need to quickly and accurately rotate the instruments. The final option uses two instruments to cover five viewing angles. One instrument is angled by rotating the full spacecraft, while the other is simultaneously rotated by a hinge or gimbal system to cover a different viewing angle.

Note that the options using spacecraft and gimbal rotation would limit the maximum measurement time. If a measurement is too long, the spacecraft does not have time to angle the instrument to the next viewing angle, and would thus miss part of the ground coverage. Nevertheless, these options are taken into consideration since measurements could be made in smaller intervals, resulting in the same total measurement time as with other options.

To select the best option from Table 11.3, the AHP method was used. This method was also used in a previous report to select the most suitable design concept [1], which was discussed in Chapter 9.

The different payload configurations were scored based on 7 different criteria. These criteria are scientific value, area coverage, cost, risk, complexity, volume, and mass. These criteria were chosen for their influence on the final design and their importance. In Table 11.3 the scores given to each option for the criteria are listed. Below, an explanation is given for the scores.

First of all, the scientific value is directly related to the number of viewing angles. As mentioned before, 5 viewing angles minimize the error on the retrieved parameters [31], therefore the scientific value is 10 for these options. The value of 3 viewing angles is 6, as the associated accuracy was found to be sufficient [F].

Secondly, area coverage is determined mostly by the data rate, which is also partly dependent on the number of viewing angles. For the TNO-chip the data rate was given to be about 1.3 Gbit/s, which for 3 or 5 viewing angles is multiplied by 3 and 5 respectively. Using 7 GSs and a downlink data rate of 1 Gbit/s (more information on this in Chapter 15 & Chapter 21), calculations were performed to find the percentage of orbit the payload could be active. For 3 viewing angles, the payload can be active for 3.4% of the orbit, while 5 angles allows for 2%.

Furthermore, the cost increases as more instruments are needed. Every viewing angle was estimated to cost 10 M€ After contact with TNO, it was determined that the cost would not increase linearly with the number of instruments, but would slightly decrease with more instruments purchased. Additionally, costs for ADCS systems and algorithms for angling the spacecraft or instrument are increased for options 4-8. Making a gimbal construction will be more costly because it adds another construction to the spacecraft while simply angling it only affects the ADCS. The same can be said for the volume and mass, although they do increase linearly with the amount of instruments. Therefore, the cost for the options with the static 3 detector option and the spacecraft-pointed-instrument has a rating of 3 and the cost for the more expensive 5 detector and complex ADCS systems are rated 4. The volume of the of the system is ranked based on the amount of detectors (2 points per detector and/or gimbal added to the system), the mass is ranked in the same way, but the gimbal of option 5 and 6

are ranked with 3 points as they are considered to have a higher mass than volume.

The risk increases when fewer instruments are used, simply because the failure of one instrument has a higher impact. The option with 3 static detectors is ranked to be 1 and the option with 5 static detectors to have the lowest risk of 1. Additionally, adding a more complicated ADCS system or an entire gimbal construction to the spacecraft will also add risk. Making a separate moving spacecraft combined with a moving payload will even further increase risk.

Lastly, the complexity is the same low value for 3 or 5 static viewing angles because it does not add anything to the spacecraft. The spacecraft does not need to rotate along track or need additional constructions. When considering dynamic viewing angles, however, rotating along track for 5 viewing angles is more complex than for only 3 viewing angles due to the available time between rotations. Additionally adding a gimbal to the spacecraft further increases complexity. The most complex option is option 8 because it has a double separately rotating instrument which means multiple ADCS systems are needed to coordinate them.

In Table 11.3, the criteria with which the different options are compared, together with the scores that were given for the different option are shown.

Table 11.3: Assessment of the criteria for each of the payload configuration options.

Grading criterion		Option 1	Option 2	Option 3	Option 4	Option 5	Option 6	Option 7	Option 8
Scientific value	[1-10]	6	10	10	6	10	6	10	10
Area coverage	[%]	3.4	2	2	3.4	2	3.4	2	2
Cost	[1-10]	3	4	3	3	4	4	4	4
Risk	[1-10]	2	1	6	5	8	7	3	8
Complexity	[1-10]	1	1	7	5	8	6	4	8
Volume	[1-10]	6	10	3	3	5	5	8	7
Mass	[1-10]	6	10	3	3	6	6	8	7

After the importance of each criterion relative to the other criteria was determined, the resulting weights were listed in Table 11.4.

Table 11.4: Weights assigned to each criteria, based on the AHP method.

	Scientific value	Area coverage	Cost	Risk	Complexity	Volume	Mass
Weight	21.1%	32.8%	12.8%	10.3%	10.5%	6.3%	6.3%

Applying these to the values listed in Table 11.3 yields the scores for each configuration option. These are summarized in Table 11.5, which shows that option 1 was found to be the best option, followed by option 2 with a small margin.

Table 11.5: Scores for each of the payload configuration options, based on the AHP method

	Option 1	Option 2	Option 3	Option 4	Option 5	Option 6	Option 7	Option 8
Score	15.8%	15.4%	12.3%	13.7%	10.3%	11.6%	10.8%	10.0%

11.2.2. Sensitivity analysis

To ensure that option 1 was indeed the most suitable option, a sensitivity analysis was performed. For each option, some combination of weights was altered until the option would yield the highest score. This analysis is summarized in Table 11.6.

It was already stated that option 2 was a close contender, only differing 0.4 percentage points compared to option 1. This close match was also found in the sensitivity analysis, where a 1.5x increase of the scientific value criterion

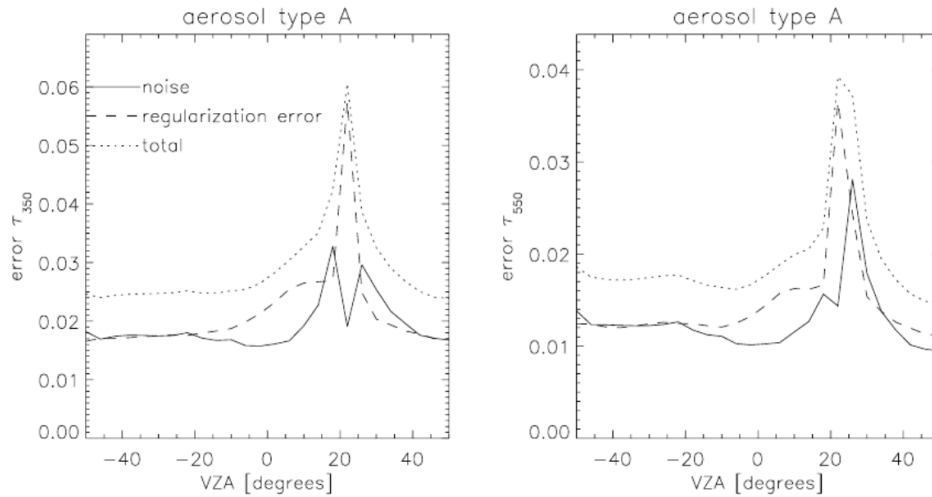


Figure 11.2: Retrieval noise and regularization error on the retrieved optical thickness of aerosols due to biomass burning at 350 nm and 550 nm, as a function of viewing zenith angle [33].

resulted in option 2 winning. Then, for option 3 to win, a larger change was necessary, for example increasing the scientific value by a factor of five. Option 4 is the most volume and mass efficient option, shared with option 5. Thus, if the volume and mass criteria are increased threefold, option 4 wins. It was found that option 5 could not win the trade-off with any combination of factors, since it can only win from option 4 on scientific value, but then other options would be more suitable. Options 6 and 8 would never win for similar reasons, while, option 7 required factors in the order of thousands, and was thus deemed unfeasible.

Table 11.6: Payload configuration sensitivity analysis. Values are the weight increase needed for each option to win. Note that some options could never win the trade-off, or required unfeasibly large factors to win.

	Option 1	Option 2	Option 3	Option 4	Option 5	Option 6	Option 7	Option 8
Scientific value		1.5x	5x	1x				
Cost	Original	1x	3x	1x	Never	Never	Unfeasible	Never
Volume	winner	1x	2x	3x				
Mass		1x	2x	3x				

As option 1 and 2 were both found to be suitable, these two were presented to stakeholders. These preferred the increased area coverage achieved with 3 viewing angles over the higher accuracy of measurements achieved with 5 viewing angles [F]. Hence, option 1 was chosen.

11.2.3. Viewing Angles

The viewing angles can range from $\pm 60.14^\circ$ and TNO uses $\pm 60^\circ$, $\pm 25^\circ$ and nadir (0°) as their nominal concept. However, these angles could be set to different values. The chosen viewing angles for the CASE payload are $\pm 45^\circ$ and nadir because the error on the AOD is relatively small at these viewing angles as shown in Figure 11.2 and the two angles of the same magnitude allow for easier configuration.

11.3. Instrument Characteristics

After the payload configuration was determined, the characteristics of the final product could be estimated. In this section the detector, lens and final properties are discussed.

As the instrument is still in the breadboard stage, the type of detector is still unknown. The Gpixel GSENSE400BSI Cooled Back illuminated USB3 camera from XIMEA was chosen to estimate the properties. This camera exceeds

the required pixel size for the accuracy to make the meta-surface elements, as well as low noise and the high dynamic range needed to make the distinction between clouds and aerosols [L]. The required frame rate for a spatial resolution of 151 m was found to be 44 fps, as it follows from the inverse of the dwell time. The dwell time has been calculated by Equation 11.1 to be 0.023 seconds.

$$\text{Dwell time} = \frac{\text{GSD}}{\text{Ground velocity}} \quad (11.1)$$

Where GSD is the ground sampling distance and the ground velocity is given in Table 10.1.

However, the required frame rate of 54 fps provided by TNO [D] is higher than the default frame rate of the camera, meaning that the frame rate of the camera should be increased. This frame rate can be achieved by reducing the vertical resolution. The gains are linear, hence halving the vertical pixels would result in a frame rate of 96 fps [G]. The properties of the camera are shown in Table 11.7.

For the estimations on supply voltage and operating current, the properties of the CMOS Space Camera from 3D-plus were considered.²⁵ This interface was proposed by Andrew Bell from TNO [E].

Table 11.7: Properties Gpixel GSENSE400BSI Cooled Back illuminated USB3 camera²⁶.

Property	Value
Mass	170 g
Power consumption	3.5 W
Pixel size	11 μm
Resolution	2048 x 2048 pixels
Digitization	12 bit
Dynamic range	90 dB
Frame rate	48 fps
Lens Mount	M42
Operating temperature range	10 - 25 $^{\circ}\text{C}$
Cost	8,525 €

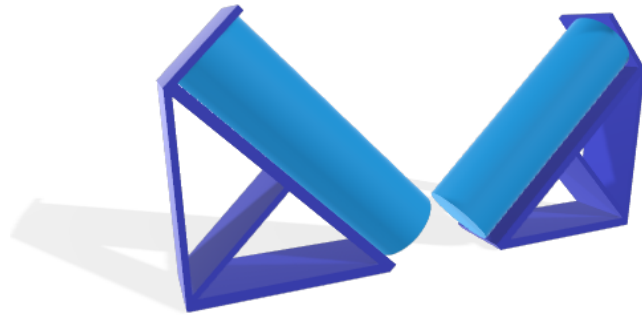


Figure 11.3: Schematic 3D render of payload structure for the 2 angled detectors.

The LM35VM42 lens from Kowa was chosen, as this lens is M42 mount and has a focal length of 35 mm²⁷. Hence, this provides a good estimation of the mass (375 g) of the to-be-developed lens as the required focal length is 33 mm. This focal length was calculated using Equation 11.2.

$$F = Px \cdot \frac{h}{\text{GSD}} \quad (11.2)$$

Here, F is the focal length, Px the pixel size and h the altitude.

The properties of the final instrument are summarized in Table 11.8, the detector unit properties are given in Table 11.1 and the schematic structure is visualized in Figure 11.3. The thermal control of the payload will be described in Chapter 14. The mass of the metasurfaces was discarded, as it was estimated to be in the order of 10^{-14} g.

11.4. Verification and Validation

The verification of the detector will be mostly done by TNO. Such testing can be assumed to include assessments of radiation, temperature and load-bearing capabilities. Testing will also be performed through models of the final

²⁵https://www.3d-plus.com/data/doc/products/references/shortform_space_camera_2018.pdf, [Retrieved on June 6, 2021]

²⁶<https://www.ximea.com/en/products/cameras-filtered-by-resolution-and-sensors>, [Retrieved on June 7, 2021]

²⁷<https://www.kowa-lenses.com/en/lm35vm42-50mp-industrial-lens-m42-mount?c=51>, [Retrieved on June 6, 2021]

Table 11.8: Payload instrument properties.

Property	Value
Mass	1.635 kg
Power consumption	10.5 W
Supply voltage	4.5 - 9 V
Operating current @ 5V	0.4 A
Volume	< 3U
Data rate	3.89 Gbit/s
Cost	30 M€

instrument. In 2021 a representative meta-surface for polarimeter in TNO labs (3 spectral bands) will be built and tested. In 2022, a scaled-up version covering the targeted 6 spectral bands matched to a real detector format (pixel size and area of the array) will be built and tested. Then, in 2023 the full instrument will be built and tested in the lab and finally, the science will be verified in 2024 by an airborne demo with multiple angles. The finalized calibrated instrument is expected in 2025.[I] If the instrument flies on the CASE mission, the measurements will be validated by comparing the gathered data to other aerosol detection missions, e.g. PACE, TERRA and MAIA.

One aspect where verification could be performed by the team was regarding the AHP method, as used in the payload trade-off. This method, which entails the use of the trade-off's CR parameter, is described in detail in Chapter 8, where it has also been used in other trade-offs. Essentially, it is a measure of whether the trade-off has been performed in a consistent and unbiased manner. The CR parameter for this trade-off has been calculated to equal 0.0184 (Equation 8.2). Since this value is less than 0.1, the trade-off method can be concluded as verified.

11.5. Risk

Several risks regarding the payload were identified in Chapter 5. Firstly, the de-calibration of the payload instrument is a risk that must be possible to address in-flight (**RSK-PL1**). For this reason, remote calibration of the payload must be tested before certifying it as flight-ready. In the next step of the communications chain, the data transmission to the CDH subsystem must be bolstered (**RSK-PL2**). This will require significant testing on the connection between these two subsystems. Lastly, the TRL of the system will be 3 before 2022 [D] and hence the risk of using this product is high (**RSK-PL3**), as the feasibility of this product for this mission is still uncertain. However, the promising technical performance of this instrument exceeds the requirements which allow for a mission design of great scientific value. The stakeholder requirements could not be met without this detector and the use is therefore considered a necessity. The absence of moving parts simplifies the instrument and makes it more robust and reliable [34]. Therefore, the reliability of the instrument should be sufficient.

11.6. Sustainability

TNO strives to have a positive impact on solving major societal challenges and provides sustainable development. TNO signed the United Nations Global Compact, a world-wide network of more than 9500 companies and 3000 non-business participants that want to help to build a sustainable future.²⁸ The CMOS from XIMEA is built according to the Restriction of Hazardous Substances guidelines [M]. No data from Kowa regarding the sustainability of their lenses is available [N].

In conclusion, the aerosols will be monitored at 3 different viewing angles with 3 optical metasurfaces based spectro-polarimeters provided by TNO. The properties derived in this chapter will be the foundation for the design of the subsystems in the following chapters.

²⁸<https://www.tno.nl/nl/onze-impact/>, [Retrieved on June 10, 2021]

12. Propulsion Subsystem

After calculating the required ΔV for the mission in Chapter 10, the selection of a propulsion subsystem was deemed necessary. In this chapter, the propulsion subsystem for the CASE mission is discussed. Firstly, the selection procedure is shortly mentioned. Afterwards, the sizing and the characteristics of the propulsion subsystem are put forth. The verification and validation strategies, sustainability and risk are also discussed. The propulsion system to be used for the CASE mission is the HYDROS-C engine developed by Tethers Unlimited, Inc. (TUI). This engine works by using water electrolysis to create its own fuel in space. The engine has an internal system that can separate water by means of an electric current into hydrogen and oxygen for combustion. This engine combines high performance and sustainability with low cost. This is an engine that is currently in development and has not been approved for flight. On the other hand, it is highly promising considering its properties that are elaborated in this chapter.

12.1. Subsystem Selection

In this section, the reasons for selecting HYDROS-C will be discussed. Firstly, the trade-off made in the previous design stages for the propulsion subsystem will be briefly discussed. Following this, the specifications and characteristics of the engine will be presented.

12.1.1. Engine Selection

In the previous design phase, a trade-off was made between different propulsion subsystem options such as bi-propellant, monopropellant and electric propulsion [3][1]. In general, electric propulsion options were eliminated due to their low thrust/mass ratios. Due to their lower TRL, compared to the mono-propellant and bi-propellant options, electric propulsion systems are still rather bulky. Even though there are options for very high specific impulse, overall they do not meet the station-keeping requirements for the CASE mission. Furthermore, the bi-propellant options were more massive compared to the monopropellants when the total impulse is less than 45000 Ns [35]. Thus, in terms of performance, monopropellant propulsion system options deemed the most promising.

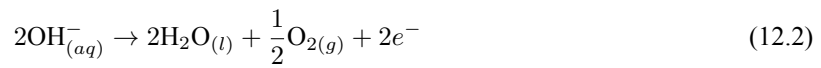
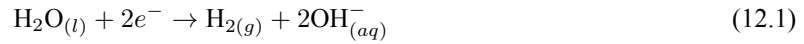
During the trade-off, another criteria to be considered was sustainability. To comply with the requirements for sustainability (**CASE-ST-B01**), the use of toxic materials was not allowed for the propulsion subsystem. So, the options that used green fuel alternatives were favoured heavily. In addition, using non-toxic fuel is not only better for sustainability, but also decreases the overall mission risk substantially. Most conventional monopropellant subsystems use hydrazine, which is highly toxic. Furthermore, most bi-propellant and electric propulsion options also use toxic fuel in order to attain high performance. With this in mind, propulsion systems with green fuels were examined. From the different options, the HYDROS-C engine developed by TUI was found to be the most viable solution. HYDROS-C is a propulsion system that uses water electrolysis to generate thrust. In the coming subsection the operating principles of the HYDROS-C engine will be briefly discussed. Later, the detailed design surrounding the HYDROS-C engine will be put forth.

12.1.2. Water Electrolysis

Electrolysis is the decomposition of an electrolyte by an electric current. Water electrolysis is the chemical reaction of separating water into its constituents, hydrogen and oxygen. This way it is possible to use hydrogen as fuel and oxygen as the oxidizer for combustion. The simple block diagram of a water electrolysis is given in Figure 12.1 [36].

In the process of water electrolysis, there are multiple components. Firstly, electrolyzers are placed in the water

to conduct an electric current to the water. The electrolyzers are composed of two electrodes, the anode and the cathode. Furthermore, the water tank also contains compounds such as potassium hydroxide (KOH), sodium chloride ($NaCl$) or sulphuric acid (H_2SO_4) to help ionize the water. Sulphuric acid is not preferred for space applications since it is very corrosive, so overall it increases the mission risk (**RSK-PROP5**) [37]. The electric power needed to generate enough current for water electrolysis is provided by a battery. In the CASE mission, the DC current will be supplied by the photovoltaic cells. After the current is applied, the hydrogen will appear at the cathode and oxygen will appear at the anode. The cathode reaction is shown in Equation 12.1 and the anode reaction is shown in Equation 12.2 [38].



12.1.3. HYDROS-C

HYDROS engines are hybrid chemical/electric propulsion systems that use water to separate it into hydrogen and oxygen for bi-propellant combustion. They provide green, safe, high-thrust and high fuel economy propulsion [39]. HYDROS-C is the engine that is sized for CubeSats and the HYDROS-M is sized for micro-satellites. Therefore, HYDROS-C is more applicable since CASE is a CubeSat mission. A simple block diagram of water electrolysis is given in Figure 12.1.

When in orbit, the HYDROS-C engine uses an electrolysis system designed to operate in zero-G. The electrolysis and pressure systems to ensure propellant flow, only start working when the spacecraft is in orbit and photovoltaic cells have available power. When power is fed to the engine using DC current, the electrolysis process starts. For HYDROS-C, it takes 825 seconds to fill the hydrogen and oxygen tanks to the desired amount for combustion [40]. When there is enough propellant, the valves feed them into the combustion chamber for ignition. The hydrogen and oxygen molecules form water vapour and get propelled through the nozzle. The hydrogen and oxygen resulting from these reactions are collected in separate tanks.

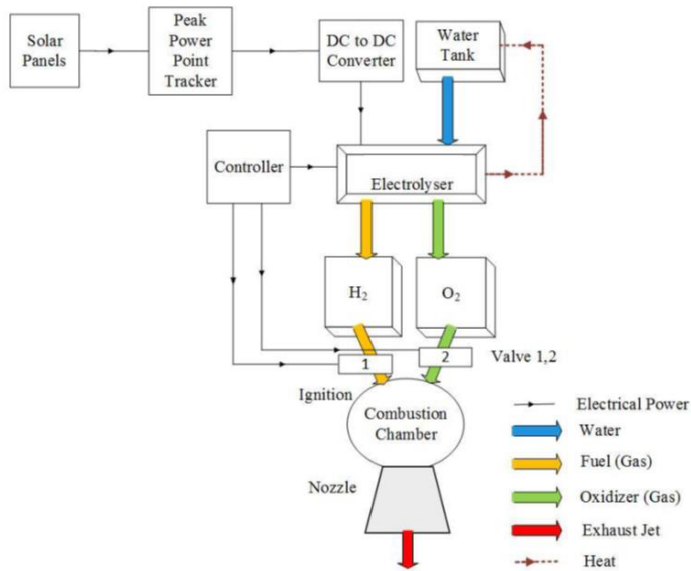


Figure 12.1: Water electrolysis rocket propulsion diagram [36].

Compared to electrical propulsion options, the HYDROS-C offers a higher thrust efficiency while requiring lower power input than electric propulsion systems and a higher specific impulse than monopropellant propulsion systems. The HYDROS-C engine is flight-approved and has a TRL of 6+ [39]. The engine will be tested in the PTD-1 mission by NASA, where the engine will be validated for spaceflight [41]. It is expected that by the launch of the CASE mission, the TRL for HYDROS-C will come close to 8 or 9. Therefore, it is possible that in the future steps for the mission, a more reliable and higher performance version of HYDROS-C will be available. To prevent the water from freezing in eclipse conditions, the engine is designed to be freeze-tolerant. In addition, HYDROS-C supports straightforward integration with the structure using deck or rail mount systems and has built-in avionics which simplifies integration to the host satellite. Since

water is used as fuel, the risk during production is quite low, especially for the personnel during integration (**RSK-PROP4**). Also, water does not pose any risk towards the primary loads during launch [42]. Furthermore, the engine has a lifetime of 3 years in LEO which satisfies the CASE mission's 2-year duration. There was no

information available on the cost of the engine and TUI was unresponsive to any inquiries on the matter. To continue with the calculations, it is estimated that the cost of the HYDROS-C engine to be around 100,000 €. This is estimated by looking at other existing propulsion subsystems, combined with the engine's low TRL level and high complexity. Lastly, the HYDROS-C engine has customizable fuel capacity and tank size [39]. The water tanks and the engine can be sized to fit different mission needs. For the CASE mission, the already existing configuration was sufficient enough to fulfil the propulsion subsystem requirements. The sizing and performance will be elaborated upon in the coming section. In conclusion, the HYDROS-C engine is selected due to its high performance, sustainability, low cost and ease of operation. In the next section, the sizing of the propulsion subsystem and the important properties can be found.

12.2. Sizing

To start sizing the propulsion subsystem, certain system parameters had to be acquired. These values were gathered from the datasheet on TUI's website²⁹, the data sheet acquired from SatSearch and various online articles. Following this, an Excel sheet was made with the equations relevant for the sizing, such as the rocket equation. This tool was used to iterate on the values for the propellant mass and thrust. The rationale behind the calculations will be presented. It should be noted that TUI was not able to share some of the information needed to perform a more detailed design due to their proprietary knowledge. Due to its low TRL and groundbreaking capabilities in propulsion and sustainability performance, the details of the internal systems of the HYDROS-C engine is under discretion. To avoid diplomacy and bureaucracy, which would greatly delay the design process, the sizing was done with the information available. It is expected that by the time the production of this mission starts, the HYDROS-C engine will have more reliable data available for more accurate sizing.

There are two different options for the tank sizes in the HYDROS-C engine: one tank that fits in 1U and one in 2U. The one used in the CASE mission will be the 2U configuration due to its ability to take more propellant on board. Furthermore, HYDROS-C, the size of the tanks are adjustable to meet the mission needs. Currently, there are two versions of the 2U configuration: the 0.5 kg propellant mass and the 0.74 kg propellant mass using the "saddle bag" formation [40]. It was later found that the 2U version is sufficient for the CASE mission due to its higher performance in terms of specific impulse and thrust. The specification of the HYDROS-C engine with the saddle bag formation is presented in Table 12.1.

Table 12.1: Properties of the HYDROS-C water propulsion unit [39][40].

Parameter	Value	Parameter	Value
Specific Impulse	>310 s	Total Impulse Delivered	>2151 s
Thrust	>1.2 N	TRL	6+
Power	5-25 W	Total # of Thrust Events	1230
Size	190x120x92 mm	Impulse per Thrust Event	>1.75 Ns
Dry Mass	1.87 kg	Thrust Efficiency	0.13 MN/W
Water Capacity	0.5 kg	Orbit-Averaged Thrust	2.2mN
Lifetime	3 years in LEO	Time to Refill Gas Plenums	825 s

12.2.1. Propulsion Performance

The required ΔV for the CASE mission at 500 km altitude is presented in Chapter 10. ΔV was found to be needed for both station-keeping and orbit correction. The orbit insertion ΔV will be provided by the launcher, which will be explained in Chapter 20. The ΔV needed for station-keeping was found to be 89.28 m/s and 26.71 m/s for orbit phasing. Thus, the total ΔV needed for the mission is 115.99 m/s. During the sizing of the engine, it was seen that extra propellant mass is left from the initial 0.5 kg. So, the remaining mass will be allocated to space debris avoidance and unexpected manoeuvres. These calculations will be further elaborated upon in this section.

In the specifications sheet, the specific impulse is higher than 310 s. Using the HYDROS engine sizing graph from the TUI website, taking 310 s for the specific impulse value was found to be sufficient. The sizing started

²⁹<https://www.tethers.com>, [retrieved June 21, 2021]

with using the Tsiolkovsky rocket equation given in Equation 12.3:

$$\Delta V = I_{sp} g_0 \ln \frac{m_i}{m_f} \quad (12.3)$$

In the equation, I_{sp} is the specific impulse, g_0 is the gravitational acceleration and m represents the initial and final mass of the system. In this engine, hydrogen is used as fuel and oxygen is used as the oxidizer. According to the study done by Pothamsetti, the maximum specific impulse is found to be 482.22 s for the system [36]. This value is found by using the enthalpy values for the combustion process consisting of water vapour and the condensation of the water due to the extreme temperature change when exiting the nozzle. This is the theoretical specific impulse of a rocket operating at steady state. For a very short pulse, this can be lower than 50 %, and with pulses of 0.45 s, it can be around 75 to 88 %. Assuming this maximum specific impulse is the same for the HYDROS-C engine, it is possible to find the pulse duration for the HYDROS-C engine using extrapolation. Thus, a pulse duration of around 0.7 seconds was determined [36]. This approximation for the pulse duration will be later used to calculate the thrust values.

The ΔV budget for different mission stages is calculated separately due to the nature of the mission. After detumbling and the solar panel deployment, the spacecraft will have to perform the orbital phasing manoeuvres. These manoeuvres will be performed consecutively in order to configure the satellites in the right formation in the orbit. With the current formation, only 2 satellites out of 3 will have to perform orbital phasing. This because one of the satellites will be leading, the other will be trailing the one in the middle. This required different positioning in the orbit, hence different ΔV . Assuming the initial mass of 0.5 kg, the total propellant mass needed to perform the orbital phasing was found using Equation 12.3. The propellant mass for this phase was calculated. The HYDROS-C engine has the capability of delivering a total of 1230 thrust events in its lifetime. For the CASE mission, it is assumed that 300 of those events will be reserved for orbital phasing and will be done consecutively since the orbital phasing must initiate the mission. From this, the propellant mass burned per event is found. Then, the number of events allocated to each phase was also subject to iteration and the finalized number will be presented later in this chapter. Assuming a pulse width of 0.7 from before, the thrust generated can be calculated using Equation 12.4.

$$I_{sp} = \frac{F}{\dot{m}g_0} \quad (12.4)$$

F represents the force and \dot{m} represents the mass flow. In order to be compliant with the engine, this value has to be higher than 1.2 N. The final value after iteration was close to 1.7 N. Therefore, taking into account contingency, the maximum thrust required was taken to be 1.8 N with a contingency of 5% [28]. The tank refill time is known to be 825 seconds, and so, for the orbit phasing for every 0.7 seconds of burn time, 825 seconds needs to pass to fill the tanks. Since the orbit phasing is done at once, these events occur continuously. The duration of this phase was calculated to take around 2.9 days by taking into account a certain number of thrust events associated with the orbital insertion and the refill time.

The same methodology was used for the station-keeping phase. The initial mass in this phase is equal to the final mass of the previous. The final mass for this phase is taken as the dry mass of the satellite. Also, from the 1230 total events, some of the events will be saved for space debris avoidance and unexpected events. The rest will be assigned to station-keeping events. It is assumed that the station-keeping events will be synchronized. The number of thrust events for the station-keeping is the same for all satellites, which is 920 events. Dividing this number of events by the total mission duration left, it is expected that in every 19 days, or 912 orbits, the satellites will perform a station-keeping manoeuvre. Firstly, the total propellant mass needed is calculated. Then, just like before, the propellant mass per event and the thrust generated per event is calculated. Adding the propellant mass needed for each phase yields the total propellant mass burnt to reach the required ΔV . This number is supplemented with a 5% contingency factor [28]. Subtracting from the total propellant mass, the amount of fuel reserved for space debris avoidance and other unexpected events is found. With this propellant mass, it is possible to calculate the extra ΔV available for unexpected events. Furthermore, in satellite 2, there is less propellant mass needed since it only has to perform station-keeping manoeuvres. Using the same equations and values for the specific impulse and pulse width, it was found that the propellant mass required for satellite 2 was 0.4 kg. For simplicity

in production, all satellites will be equipped with the same engine but satellite 2 will have a lower propellant mass. Lastly, HYDROS-C engine has a high thrust efficiency. Given the power required to operate the engine, the achievable thrust is quite high. The engine uses 2 W for active standby, 5 W for survival heating and 5 W for operations [40]. Since this is the case, the operational power will only be necessary for a short amount of time once in a few orbits. This also saves on the overall power consumption of the engine.

12.2.2. Dimensions

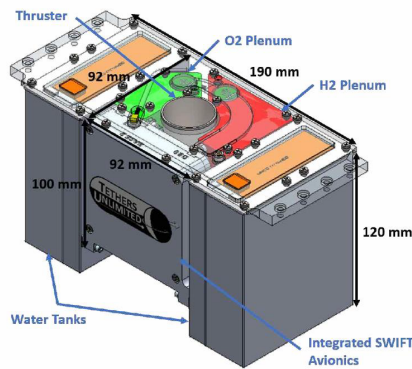


Figure 12.2: HYDROS-C engine dimensions.

In Figure 12.2, the dimensions of the engine can be seen. The total volume of the engine fits almost in a 2U size. The dimensions of the engine with 0.74 kg of water is $190 \times 120 \times 92 \text{ mm}^3$. The base thruster is $92 \times 92 \times 92 \text{ mm}^3$ [40]. The hydrogen and oxygen tanks are situated inside the base thruster. It should be noted that the tank size for the hydrogen should be double the size for the oxygen due to the mole fractions of the chemical reaction. For this combustion, two hydrogen molecules are needed for every oxygen. Therefore, the tank sizes are different. The green tank indicates the oxygen and the red tank indicates the hydrogen tank. The built-in avionics and the combustion chamber is located inside the base thruster as well. The water tanks are on the side in the saddle bag formation and are scalable. The tanks that are sized for 0.74 kg of water is $120 \times 92 \times 49 \text{ mm}^3$ [40]. Downsizing the tanks

linearly, the new dimensions of the water tanks become $82 \times 92 \times 49 \text{ mm}^3$. Consequently, the volume of the engine, including the new tanks, becomes $190 \times 82 \times 92 \text{ mm}^3$. The volume of the engine will be the same in each engine to ease production. On the other hand, sloshing on the tank with less propellant will be higher than the ones without as much water.

Table 12.2: HYDROS-C Sizing for the CASE mission.

Parameter	HYDROS-C for CubeSats 1 & 3	HYDROS-C for CubeSat 2
Specific impulse (I_{sp})	310 s	310 s
ΔV	26.71 m/s (orbit phasing), 89.28 m/s (station-keeping), 2.59 m/s (debris avoidance, etc.)	(-) (orbit phasing), 89.28 m/s (station-keeping), 6.12 m/s (debris avoidance, etc.)
Max. thrust required	1.8 N	1.8 N
Propellant mass	0.5 kg total; 0.114 kg for orbit phasing; 0.375 kg for station-keeping; 0.01 kg for debris avoidance and etc.	0.4 kg total; 0 kg for orbit phasing; 0.376 kg for station-keeping; 0.024 kg for debris avoidance and etc.
Size	$190 \times 82 \times 92 \text{ mm}^3$	$190 \times 82 \times 92 \text{ mm}^3$
Dry mass	1.87 kg	1.87 kg
Number of events	1230 total; 280 for orbit phasing; 920 for station-keeping; 30 for debris avoidance and etc.	1230 total; 0 for orbit phasing; 920 for station-keeping; 60 for debris avoidance and etc. 250 will be unused
Burn time/Pulse width	2 years in 500 km altitude	2 years in 500 km altitude
Power	2W active standby, 5W operational power, 5W survival heater	2W active standby, 5W operational power, 5W survival heater

12.3. Verification and Validation

The Excel sheet to size the HYDROS-C engine was verified by inspection and testing. The sheet has been created multiple times with the equations used during sizing to decrease the risk of human errors. Furthermore, different propulsion subsystems were used as input to verify the equations. For the verification and validation of HYDROS-C, a collaborative effort with TUI will be necessary to conduct the tests correctly. To verify the propulsion, comparing the sizing methodologies and the equations is a necessary start. The sizing for the HYDROS-C engine was already done for the PTD-1 mission which is flight approved. Therefore, it is logical to use those calculations to verify the propulsion subsystem. When the system is verified, the validation can be started. Firstly, the mass and the volume of the system shall be measured in order to validate that the engine can fit in the spacecraft and is not too heavy. Water is a difficult substance to handle in space. The system surrounding the water could be prone to leaks. Therefore, leakage tests shall be done. Furthermore, firing tests are also necessary to validate whether the propulsion system will be able to complete the electrolysis process successfully in space conditions. Furthermore, the timing of the combustion and how much time it takes to collect the required amount of hydrogen and oxygen shall be validated. This can be done by doing scenario tests of different expected situations.

12.4. Risk

In terms of risk, HYDROS-C engine is highly advantageous. Firstly, the use of water as a propellant decreases the production and operation risks significantly (**RSK-PROP3**) [42]. The safety of the employees and the integrity of the equipment will be much safer with the use of water compared to toxic fuels such as hydrazine (**RSK-PROP4**) [42]. Since the engine only starts separating the fuel in orbit, the transportation of the engine to the launch location and the launch itself is substantially less risky. The biggest risk of using water in the system is its corrosive properties (**RSK-PROP5**), which is still less than the risk that occurs due to the corrosive properties of hydrogen-oxygen and superheated steam. In the design of the HYDROS-C engine, there is very little redundancy in the system. Except for the valving to prevent leakage (**RSK-PROP1**, **RSK-PROP2**), the design overall is a single string. This is done to have better performance in terms of size, weight and power [H]. So, the safety is traded-off for the performance of the mechanisms. In order to increase the redundancy, while not exceeding the mass budget, the extra mass resulting from the propellant calculations can be assigned to having stronger valving, cabling or other internal systems. This will decrease the failure risk of the engine substantially. Also, sloshing of water inside the tanks can also result in some disturbance torques on the spacecraft. In addition, the unused manoeuvres from the engine can be used in case of wrong orbit insertion to make sure the satellite can still be operational (**RSK-G8**). So, there are risk mitigation strategies available to ensure there is low risk for the propulsion subsystem.

12.5. Sustainability

Water is one of the greenest fuels available in rocket propulsion. It is quite abundant on Earth and it does not need production or any type of process to acquire. Given the accessibility advantages and the safe nature of water, it provides financial and operational sustainability. Furthermore, the burst that comes out of the nozzle is water steam. This means that there is no toxic material on-board, but also no toxic material is produced after the combustion. Sustainability was one of the biggest reasons why the water electrolysis engine was chosen over other alternatives. Besides its high-performance properties, it is also one of the most eco-friendly propulsion modules available. As sustainability is becoming more important in the space industry, using a state-of-the-art technology that uses green fuel is more desirable. At the EOL of the satellite, all the fuel needs to be used before the burn-up of the satellite.

To conclude, the HYDROS-C engine will be used as the propulsion subsystem for CASE mission. With water electrolysis, it is possible to get high specific impulse and thrust values while using green fuel. Furthermore, the use of non-toxic material not only decreases the mission risk but also decreases the cost of the mission. With a TRL level of 6+, it is expected that by the time the HYDROS-C engine is acquired for the mission, it would have flown in few missions and would be validated for commercial use. In Chapter 22, the integration of the engine to the CubeSat structure will be visualized.

13. Command & Data Handling Subsystem

With the payload and other subsystems defined in more detail, a final revision was made on the CDH subsystem, leading to its final design. A global overview was created to serve as a basis for the design work, showing all sources of data on the spacecraft in a data handling block diagram which is discussed in Section 13.1. Then, the required performance of the processing unit is determined in Section 13.2. Based on the outcome, processing and storage components are selected in Section 13.3. Next, the spacecraft data bus is discussed in Section 13.4. Finally, verification & validation, risk and sustainability are discussed in Section 13.5, Section 13.6 and Section 13.7 respectively.

13.1. Data Handling Block Diagram

Before any detailed design work could be performed, a global overview of all data sources and flows within the spacecraft was necessary. A block diagram was created showing all the connections and interactions with the CDH subsystem. This diagram is presented in Figure 13.1. Note that for some connections, data is flowing both ways, while for others a one-way connection is sufficient. This is indicated by separate lines, for example between the processing unit and mass storage. For each connection, the type of data as well as their speed or size is indicated.

From the diagram, it becomes apparent that the processing unit is a key component of the spacecraft, with at least one connection to every subsystem. In a previous report, it was stated that the storage component of the CDH subsystem is typically part of the processing unit [1]. While this is still the case, the mass storage component is indicated separately from the processing unit in the diagram to better indicate the connections.

The first connection of interest is the data flow between the ADCS and the CDH subsystem. Two types of sensors deliver attitude data to the processing unit. This new sensor data is then combined with the previous state, allowing the processing unit to estimate the new attitude. This is then compared to the desired attitude, for example for payload pointing, which generates a command for the ADCS actuators. This ties into the GNC subsystem, which keeps track of the spacecraft position, indicating which measurements or manoeuvres are approaching.

For the payload subsystem, two main connections can be identified. First are the commands generated by the processing unit, such as the initiation of a measurement. These are sent to each of the three instruments, which then start generating data. This data then flows into mass data storage. This component then periodically outputs all stored data to the TT&C subsystem, which uses optical communication to downlink the data to Earth. This subsystem also receives uplink data, which is fed to the processing unit. Finally, the remaining subsystems deliver State of Health (SoH) data, which is checked by the processing unit for anomalies, and is subsequently sent to mass data storage to await downlink.

After the data has been downlinked, it is stored in a central database. The measurement data is then refined, and the received SoH data is verified again. From this, as well as any other factors that influence the direction of the mission, spacecraft commands are generated. These are transmitted to the spacecraft from a GS. The refined data is then provided to end users.

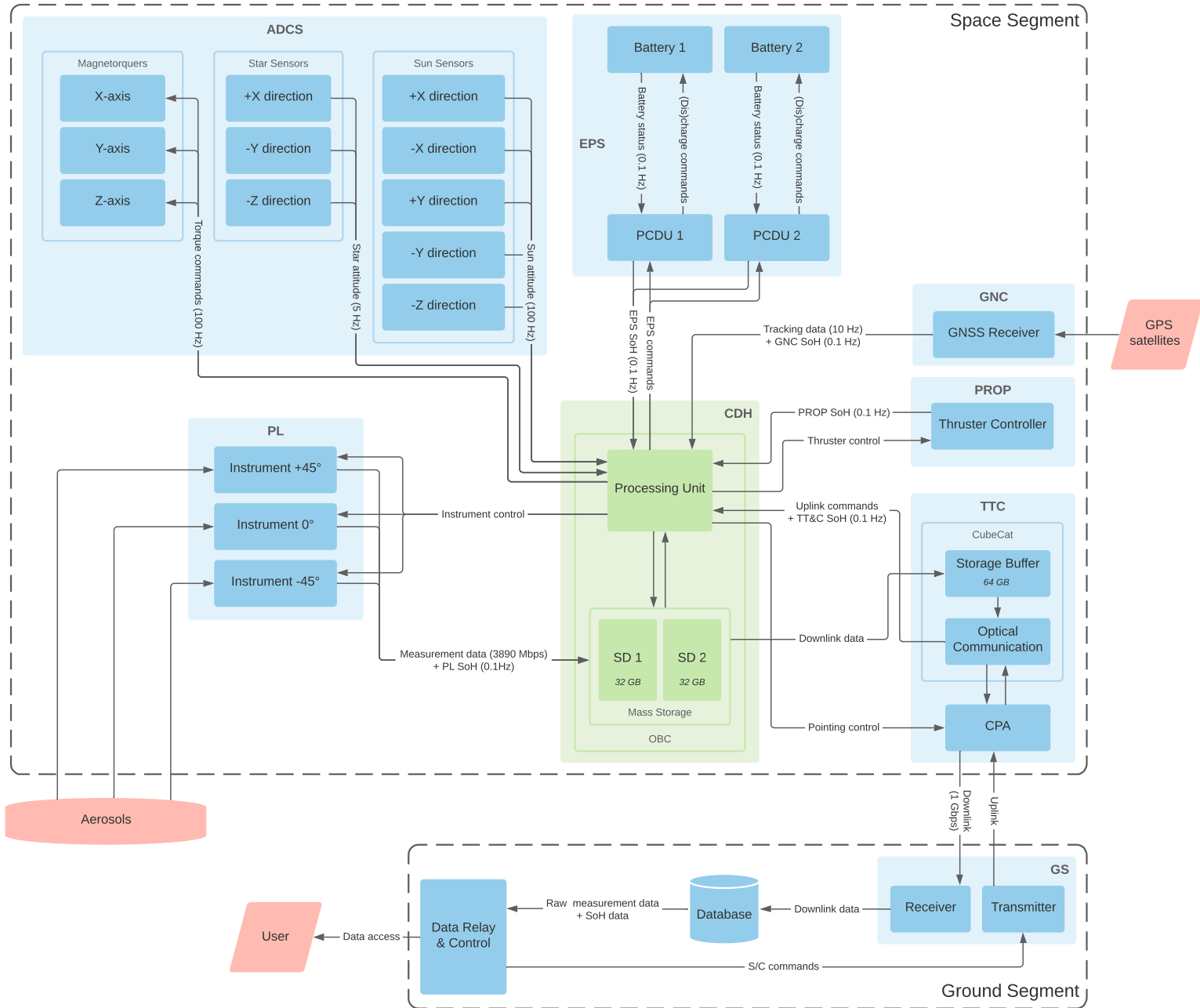


Figure 13.1: Diagram showing the flow of data between subsystems in the space and ground segments, combined with external data sources.

13.2. Processing Requirements

After the subsystem trade-off in midterm report, it was determined that it would be preferable to minimize the amount of pre-processing of data [1]. With a more detailed design of the TT&C subsystem, it was found that it was possible to downlink all mission target data generated by the payload without pre-processing. This was also discussed with stakeholders, which indicated that they preferred shorter measurements with raw data over longer measurements with pre-processed data [F].

With this in mind, the processing unit does not need excessive processing power, and only needs to handle standard spacecraft functions such as attitude processing and SoH data verification. An analysis was performed to determine

the required throughput of the processing unit, following the method described in [28]. The throughput is a typical measure used to determine the required computing power, ensuring that hardware limits are not exceeded. A summary of the analysis is given in Table 13.1, which details all contributions to the processor throughput requirement. Note that the values for the required throughput were estimated using the principle of similarity, based on factors such as update rates and spacecraft characteristics [28]. The values should be refined after generating the software for the spacecraft, however, in this design stage, a margin is used to prevent any capacity limitations in the future.

Table 13.1: Contributions to the required throughput of the processing unit, based on the method described in [28].
Note that throughput is measured in thousand Instructions Per Second (kIPS).

Component	Data source	Required throughput [kIPS]	Note
ADCS			
Sun Sensors	5x, 100 Hz	500	Data flow from 5 Sun sensors
Star Sensors	3x, 5 Hz	3000	Data flow from 3 star sensors
Magnetic Control	3x, 100 Hz	150	Data flow to magnetorquer unit
Kinematic Integration	100 Hz	150	Integrate angular rates to attitude
Error Determination	100 Hz	120	Difference with desired state
Ephemeris Propagation	10 Hz	20	Prediction of future attitudes
<i>Subtotal</i>		3940	
Payload			
Sensor Control	3 sensors	3	Control the payload instruments
Data Movement	3900 Mbit/s total	3.9	Data flow from 3 instruments
Metadata Application	3 events per orbit	0.3	Add location and time info to data
<i>Subtotal</i>		7.2	
Communications			
Command Processing	10 Hz [28]	7	Process uplink commands
Telemetry Processing	10 Hz [28]	100	Data flow to TT&C subsystem
<i>Subtotal</i>		107	
Other Functions			
Power Management	5 Hz [28]	25	Monitor power, command battery
Autonomy	1 Hz [28]	1	Autonomy without ground contact
Fault Monitoring	5 Hz [28]	15	Monitor data & subsystem faults
Fault Correction	5 Hz [28]	5	(Attempt to) correct detected faults
<i>Subtotal</i>		46	
Operating System (OS)			
Executive	$n = 5464$	1639.2	Task scheduler and manager
Runtime Kernel (COTS)		-	Support for higher-order languages
I/O Handlers	10 interfaces, $m = 5700$	285	Data movement to and from OBC
Test and Diagnostics	0.1 Hz [28]	0.5	Testing computer systems
Utilities		-	Routine software functions
<i>Subtotal</i>		1924.7	
Margins			
<i>Total before margins</i>		6024.9	
Requirement uncertainty	100% of non-COTS [28]	6024.9	Capacity for pre-launch alteration
On-orbit spare	100% spare [28]	12049.8	Capacity for on-orbit alteration
Total after margins		24099.6	

The contributions are divided into five main sections, being: ADCS, payload, communications, OS, and miscellaneous functions. First, as was mentioned previously, the CDH subsystem needs to handle the data generated by the ADCS sensors, and use them to determine the current and future attitude of the spacecraft. This is compared to the desired attitude, leading to a command for the ADCS actuators. These functions make up roughly half of the required processor throughput, and depend heavily on the update rate of the ADCS components.

For the payload, the CDH subsystem sends commands to the instruments, which then returns measurement data. The processing unit appends metadata such as location and time, and subsequently sends it to the mass storage component. Overall, the payload requires little computing power, and is insignificant compared to other

requirements. Periodically, the TT&C subsystem is able to downlink data to Earth, requiring the processing unit to offload data from mass storage to the communication unit. Additionally, the TT&C subsystem periodically receives commands through uplink, which need to be processed as well.

After considering the functions required for these three subsystems, some miscellaneous tasks were identified for the processing unit. The first is managing the thermal control system. As is described in Chapter 14, the spacecraft uses passive thermal control. Thus, there are no active components for the CDH subsystem to interface with, only the spacecraft temperature levels should be monitored. Next, the processing unit needs to monitor the power bus on the spacecraft, as well as command the battery unit in conjunction with the PCDU. Furthermore, the spacecraft needs some level of autonomy, since it cannot be in contact with GSs continuously. More specifically, the spacecraft needs to ensure that the spacecraft is pointed correctly for each measurement, collects the scientific data, and prepares for the next downlink opportunity. The final two miscellaneous functions are dedicated to fault monitoring and correction. This encompasses the verification of the SoH data from various subsystems, as well as other problems on the spacecraft or in data flow.

The final contributor to the processing throughput is the OS of the CDH subsystem. This system controls and manages the hardware, allocating computer resources to the specified functions. The first component of the OS is the executive, which schedules and manages the tasks of the processing unit, allocating memory access and detecting memory faults. For the estimation of the throughput of this component, the number of scheduled tasks per second n was estimated using Equation 13.1. It is the sum of each frequency f_i multiplied by the number of functions running at that frequency n_i .

$$n = \sum f_i \cdot n_i \quad (13.1)$$

The next component is the runtime kernel, which is typically a COTS component. This software provides a platform for the use of higher-order languages, and allows interaction between devices using different languages [28]. Then, the input/output (I/O) handlers control the movement and reformatting of data to and from the processing unit. Eight connections are used by the ADCS sensors, then two more are considered for external commanding and telemetry [28]. Using this, the number of words per second m was estimated, which is presented in Table 13.2. It is important to note that a word in this case does not refer to a part of a sentence, but rather a unit of data of a fixed size. The number of bits in a word is a characteristic of the processor, and typically ranges between 8 and 64 bits³⁰.

Table 13.2: Estimation of the number of words per second m [28].

Component	Connections	Words [28]	Frequency	Words per second
Sun Sensor	5x	10	100 Hz	5000
Star Sensor	3x	10	5 Hz	150
Telemetry	1x	-	-	500
Command	1x	-	-	50
Total	10x	-	-	5700

Another function that was considered for the OS is testing and diagnostics, which keeps track of and isolates any faults in the CDH subsystem. Finally, the OS also contains several standard utilities which are routinely used by software. Since this software is yet to be written or selected, and the expected throughput is not impactful, no value was assigned at this point in the design process.

After identifying all of these contributions to the processor throughput, two margins were applied. The first margin counteracts the uncertainty in the determination of the processing requirements, since the necessary computing power could grow before deployment. This ensures that any changes in the software do not require a redesign of the hardware. The second margin provides on-orbit spare throughput. This is used to correct for any anomalies that occur during flight, or a required increase of performance after calibration [28]. Adding these margins to the total leads to a required throughput of roughly 24.1 MIPS. This is used in Section 13.3, where a suitable processing unit is selected.

³⁰<https://learn.saylor.org/mod/page/view.php?id=18960>, [Retrieved on June 3, 2021]

13.3. Component Selection

With the required computing power determined, a commercially available system was selected for the CDH subsystem. Many of these systems exist for CubeSats, so the selection was first narrowed down. Components with incompatible or insufficient connectors, excessive volume, mass or power usage were all neglected. Furthermore, some smaller systems could not handle the required throughput that was found in Section 13.2.

The payload data rate, discussed in Chapter 11, was larger than previously estimated, and necessitated a revision of the required storage capacity from a previous report [1]. The results from this analysis are shown in Table 13.3. Here, the data rate of the payload was presented in Table 11.8, which was determined to be active for a total of 208.5 seconds every orbit in Chapter 10. The data rate of the SoH data was estimated using the frequency of subsystems sending SoH data, which is 0.1 Hz as defined in requirement **CASE-SYS-CDH-A03**. A 10 kbit package is sent every update cycle by each of the six subsystems, which excludes the structure and thermal control subsystems that produce no SoH data. This leads to a data rate of 6 kbit/s, which is constant throughout the orbit. This leads to a total required storage capacity of 101.3 GB per orbit. The communication system selected in Chapter 15 has 64 GB of storage buffer available, which could thus store a majority of the data before downlink. This leaves 37.3 GB of capacity to be provided by the CDH subsystem. Note that the storage capacity is likely not fully used, since data from the start of an orbit will have been downlinked before the end of that orbit.

Table 13.3: Contributions to the required data storage capacity.

Data source	Data rate	Activity	Data per orbit
Payload	3.89 Gbit/s	3.67% of orbit	101.3 GB
SoH	7 kbit/s	100% of orbit	0.004 GB
<i>Total</i>	-	-	101.3 GB
Stored by TT&C	-	-	64 GB
Stored by CDH	-	-	37.3 GB

The system that was selected is the on-board computer offered by ISISpace³¹. Some of its properties can be found in Table 13.4. The unit boasts high performance compared to other options, while still being one of the most lightweight and compact systems. Additionally, this unit was the only option that could provide the required storage capacity. The system accepts two regular-sized SD cards, up to 32 GB in capacity each, thus easily meeting the capacity requirement. Most of the other options did not meet the 37.3 GB requirement, typically reaching 16 GB at most. An additional component dedicated solely to data storage would need to be selected, increasing volume, mass, and cost significantly. Therefore, the selected unit provides the best solution.

Table 13.4: Properties of the selected processing unit [43].

ISISpace on-board computer (iOBC)	
Processor performance	400MHz 32-bit ARM9 processor (~440 MIPS)
Mass data storage	2x high-reliability SD cards, up to 32 GB
Mass	94 g
Volume	96 x 90 x 12.4 mm (~0.15U)
Power consumption	400 mW average
Operating temperature	-25 °C to +65 °C
Data storage capacity	64 GB
Cost	6,150 €

The processing unit has flight heritage since 2014³¹, and contains several measures to improve reliability. This is discussed in greater detail in Section 13.6, where the risks of the CDH subsystem are assessed. First, in Section 13.4, the interfacing to other subsystems is discussed.

³¹<https://www.isispace.nl/product/on-board-computer/>, [Retrieved on June 3, 2021]

13.4. Spacecraft Data Bus

In order for the processing unit to exchange data with components in other subsystems, a spacecraft data bus is necessary. The processing unit provides various connectors and support many bus architectures, such as Inter Integrated Circuit (I²C) and Serial Peripheral Interface (SPI). The components that require connections are listed in Table 13.5, detailing the type of interface specified by their manufacturers, as well as cabling that supports the respective connections. Note that the specified cabling could be altered at a later stage depending on factors such as availability. The interface protocols were obtained from the specifications of the selected components of the respective subsystem chapters.

The final weight of the cabling harness is determined in Chapter 22, which details the location of all subsystem components, thus allowing an assessment of the cable lengths. All of the interfaces specified in Table 13.5 are supported by the processing unit [43]. The unit can be supplied with a daughter board, complementing the main board without exceeding the outer dimensions of the component. The extra board serves to fan out the I/O connections, and provides flexible and customizable interfacing. The daughter board can be configured to accept specific connectors, thus providing each component with a dedicated data line³¹. Additionally, the processing unit provides USB and Joint Test Action Group ports for programming and debugging during the development phase. Overall, the required connections to and from the CDH subsystem are supported and can be customized if alterations are necessary.

Table 13.5: Connections between various subsystem components and the CDH subsystem.

Subsystem	Component	Interface protocol	Weight	Cabling		Note
				Diameter	Operating temperature	
Payload	3x TNO instrument	SpaceWire	10.5 g/m	3.28 mm	-100 °C to +150 °C	[44] 1 cable for all
ADCS	8x NXSS3V00 sun sensor	I ² C or SPI	11.8 g/m	2.24 mm	-150 °C to +165 °C	[45]
	3x PST-1 OCE star sensor	RS-422 or CAN	4.32 g/m	1.92 mm	-100 °C to +200 °C	[46]
	3x magnetorquer	I ² C	11.8 g/m	2.24 mm	-150 °C to +165 °C	[45]
EPS	2x STARBUCK-NANO-PLUS PCDU	I ² C	11.8 g/m	2.24 mm	-150 °C to +165 °C	[45]
Propulsion	HYDROS-C water propulsion system	RS-422	4.32 g/m	1.92 mm	-100 °C to +200 °C	[46]
TT&C	CubeCat lasercom module	I ² C or USB3.0	11.8 g/m	2.24 mm	-150 °C to +165 °C	[45]
GNC	GNSS200 navigation receiver	UART	3.4 g/m	1.4 mm	-200 °C to +200 °C	[47]

13.5. Verification and Validation

In Chapter 5, it was found that a large portion of space missions fail due to faults related to software. Since this ties in heavily with the CDH subsystem, it is of high importance to verify and validate the hardware and software of the CDH subsystem, ensuring that a reliable system can be created.

The manufacturer of the processing unit provides several testing procedures before shipment. The qualification model was tested for vibration, mechanical shock, and thermal vacuum resistance. Additionally, the unit that is to be shipped and placed in the CASE spacecraft is tested functionally, and is put through a thermal cycling test³². Aside from these procedures, the unit also has flight heritage since 2014, and has thus proven its flight worthiness.

Next to the testing of the processing unit, the software in the CASE spacecraft should be verified and validated thoroughly. This should be performed by first using smaller unit tests, which test specific functions or components of the software. Then, gradually larger systems should be tested, ultimately concluding in a full flight simulation. Here, as many of the conditions that would affect the CDH subsystem throughout the mission should be emulated. All possible states and operations of the spacecraft should be simulated, and it should be verified that the system acts as expected. To reduce the amount of new software that should be developed, optional software libraries are available during the purchase of the processing unit. Any subsystems on the spacecraft made by the same manufacturer can be provided with flight proven software³².

³²<https://www.isispace.nl/product/on-board-computer/>, [Retrieved on June 7, 2021]

13.6. Risk

Long duration LEO missions require careful consideration of the risk of radiation affecting the CDH subsystem³³. This radiation can interfere with operations either through radiation accumulated over the long term, or through Single Event Effects (SEEs). This first factor can cause the performance of the processor to decrease as the dose of radiation increases. The second factor can affect memory, flipping one or multiple bits and thus potentially corrupting data. These risks pertain to **RSK-CDH1**, **RSK-CDH2** and **RSK-CDH4**, identified in Chapter 5. To avoid mission-critical failure of the CDH subsystem, strategies have to be developed and maintained to mitigate such problems.

The selected processing unit contains several measures to increase the reliability of the system. First is the use of Ferroelectric Random Access Memory for critical data, which is less likely to be influenced by the two factors described above [48]. Typically, this is used for critical software, which should under no circumstance be compromised. The unit also contains a redundant Real-Time Clock, allowing the subsystem to continue operations if one fails. Additionally, a watchdog is used to detect malfunctions and initiate correction procedures. This external component contains a timer, which needs to be reset periodically. If the processing unit fails to do so, the watchdog generates a signal to indicate that a malfunction was detected. Finally, to avoid errors in data streams, the processing unit uses checksumming to detect errors, specifically using three types of Cyclic Redundancy Checks.

Another set of risks identified in Chapter 5, include **RSK-CDH5** & **RSK-CDH6**. These relate to the software executing the CDH subsystem's commands and the ensuing pre-processing of data. The underlying software of the CDH will need to be thoroughly tested, since Chapter 7 identified that a large majority of mission failures originate from software errors. Sufficient testing will also ensure that **RSK-CDH3** is satisfied and inter-connectivity with the remaining subsystems is robust. This will prevent any failure to receive, process or transmit data.

13.7. Sustainability

Overall, the CDH subsystem does not present any issues regarding sustainability. No toxic materials are used in any components, and the system does not require large amounts of raw materials. However, some of the materials used in computer parts could prove to be scarce, leading to limited availability. The CDH components are also made of electronic components which require some chemical processes when being manufactured. This is not expected to affect the CASE mission however, since only a single unit needs to be produced.

During the development phase of the mission, large amounts of software have to be written and tested, as was described in Section 13.5. This provides numerous job opportunities, leading to a positive socioeconomic impact. During this process, no raw materials are being processed, although the testing procedures could inflate energy usage.

³³<https://www.nasa.gov/smallsat-institute/sst-soa-2020/command-and-data-handling>, [Retrieved June 4, 2021]

14. Thermal Subsystem

The satellite will experience temperature fluctuations as it orbits around Earth. To keep the temperature as constant as possible and ensure every subsystem stays inside its operating temperature, a thermal control system (TC) is needed. In this chapter a detailed description of the TC is given. First, all the temperature ranges for the components of the satellite are analysed in Section 14.1. Then, the active thermal control is listed in Section 14.2 and in Section 14.3 the passive thermal control is explained. In Section 14.5 the risk is evaluated and lastly the sustainability of the system is assessed in Section 14.6.

14.1. Temperature Requirements

Every component of the spacecraft has its own temperature range in which it can operate and survive. In Table 14.1 the operating temperature of the components of the satellite are given.

Table 14.1: Operating temperatures of the spacecraft components.

Component	Temperature range [°C]
Payload	15 ± 0.5 [D]
Sun sensors	-40 to 85 [49]
Star sensors	-30 to 60 [50]
Magnetorquers	-35 to 75 [51]
Solar array	-150 to 110 [28]
Battery	-10 to 50 ³⁴
PCDU	-25 to 65 ³⁵
HYDROS-C engine	0 to 100
CubeCAT	-20 to 40 [52]
GNSS receiver	-40 to 85 ³⁶
Patch antenna	-30 to 70 ³⁷
Spacecraft structure	-40 to 80 ³⁸

As shown in the table, the payload is the most temperature sensitive component as the optic set-up is calibrated at room temperature and will therefore be thermally isolated from the rest of the spacecraft. However, TNO communicated the instrument was not super sensitive to temperature and therefore no failure is assumed if the requirement in Table 14.1 is not met [D]. The CubeCAT (see Chapter 15) has the volume of 1 U and is therefore hard to isolate from the rest of the satellite, as the multi-layer insulation cannot fit between the instrument and the structure. Therefore, this temperature range is most critical, as the battery and propulsion subsystem have a build-in cooling system.

The thermal control system will ensure the internal temperature of the satellite stays within the operating temperature change of the CubeCat. As the efficiency of the solar panels improves with decreasing temperature, the temperature of the panels will be kept as low as possible with passive control. The panels on the top (zenith) and front (+ram) will be isolated from the rest of the spacecraft, to ensure minimal heat transfer from the spacecraft to the panels.

³⁸[cubesatshop.com/wp-content/uploads/2016/06/iOBC-Brochure-v1.pdf](https://www.cubesatshop.com/wp-content/uploads/2016/06/iOBC-Brochure-v1.pdf), [Retrieved on June 11, 2021]

³⁸https://www.aac-clyde.space/assets/000/000/180/AAC_DataSheet_Optimus_original.pdf?1614275732, [Retrieved on June 11, 2021]

³⁸https://hyperiontechnologies.nl/wp-content/uploads/2015/07/HT_GNSS200_v2.1-flyer.pdf, [Retrieved on June 21, 2021]

³⁸https://www.isispace.nl/wp-content/uploads/2021/01/ISIS-GAPA-DSH-0001-GNSS_Antenna_Datasheet-02_00.pdf, [Retrieved on June 21, 2021]

³⁸<https://www.isispace.nl/product/12-unit-cubesat-structure/>, [Retrieved on June 21, 2021]

14.2. Active Control

The temperature regulation of the OPTIMUS-40 batteries will be an active system that requires < 0.1 W per battery. As the optimal temperature of the battery is < 10 °C.³⁹ The batteries will dissipate around 0.2 W of heat [Q].

The HYDROS-C engine has an active thermal control systems which ensures the water does not freeze, or vaporize. The survival heater of the engine requires 5 W of power. However, as the temperature of the spacecraft will be around 7 °C this heater will be rarely used.

14.3. Passive Control

The passive thermal control system ensures smooth heat transfer inside the spacecraft and proper heat exchange with the environment. The system will keep the temperature of the spacecraft within the required range without the use of electrical power.

14.3.1. Radiating Surfaces

To keep enough of the heat produced by the subsystems inside the spacecraft without the system overheating, the right ratio between the emissivity and absorptivity must be found. This will be done by selecting the right surface finishes which will be applied to the outside surfaces of the spacecraft fit for radiating.

To start the selection of the surface finishes, an assessment was made of the solar, albedo and Earth infrared radiation received by each of the sides based on the values in Table 22-11 of [28] and linear integration between these values. The 22 types of surface finishes, all the white paints from AZ Technology and the Paladin black lacquer were considered.

First, the minimal radiating area for the payload system was calculated based on Equation 14.1.

$$Q_{in} = Q_{out} \quad (14.1a)$$

$$Q_{in} = Flux \cdot A_p \cdot \alpha + P \quad (14.1b)$$

$$Q_{out} = A_r \cdot \epsilon \cdot \sigma \cdot T^4 \quad (14.1c)$$

Where A_p is the projected area and A_r the radiating area, which are equal in case of the payload. P is the dissipated power of the instrument, σ the Stefan–Boltzmann constant, ϵ the emissivity and α the absorptivity of the surface finish, T the equilibrium temperature of the instrument and $Flux$ all the incoming radiation on the radiating surface.

The radiating area was optimized when the white paint AZ-2100-IECW was chosen, because of its high emissivity ($\epsilon = 0.9$) and low toxicity, and found to be 6.5 cm^2 per payload instrument. These radiating areas will be placed on the sides of the spacecraft (sun & anti-sun) as these sides receive minimal solar radiation, because these surfaces are in the shadow of the deployable solar panels. The paint will ordered from AZ Technology Inc.⁴⁰ and applied in the Netherlands. The paint was estimated to cost 300 €, which is a general prize for cooling paints.⁴¹ However, this prize might be higher as AZ Technology Inc. is specialized in aerospace paints.

Based on the dissipated power and the temperature tolerance of the instruments, the available area on the back (-ram) and bottom (nadir) of the spacecraft need to be covered in the black lacquer of Paladin.⁴² This finishing, with an absorptivity of 0.95 and a emissivity of 0.75⁴³, allows for a temperature range of 259.87 K in the case the

³⁹https://www.aac-clyde.space/assets/000/000/180/AAC_DataSheet_Optimus_original.pdf, [Retrieved on June 13, 2021]

⁴⁰<http://www.aztechnology.com/products/paints/az-2100-iecw.html>, [Retrieved on June 13, 2021]

⁴¹<https://www.bergerpaints.com/resources/pdf/gst/mrp-dec18.pdf>, [Retrieved on June 18, 2021]

⁴²<http://paladinchemicals.com/markets/coatings/industrial-transportation.html>, [Retrieved on June 16, 2021]

⁴³<http://web.archive.org/web/20001209172600/http://fridge.arch.uwa.edu.au/materials/SolarAbsorption.html>, [Retrieved on June 16, 2021]

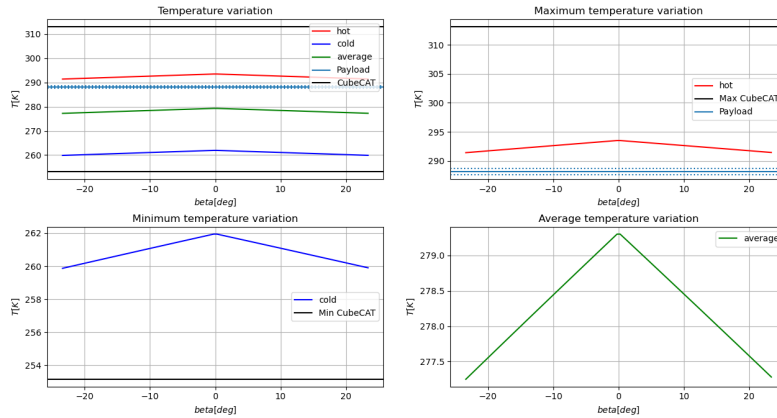


Figure 14.1: Temperature range over β -angle

satellite is on standby and when the incoming heat flux is lowest, to 293.51 K when all systems, excluding the thermally isolated payload, are running and the incoming heat flux is at its maximum. During the 'cold' case, the heater of the engine is on and during the 'hot' case the battery is actively cooled. A more updated assessment on the lacquer properties is needed as the values used in the current analysis are outdated. However, the sensitivity analysis showed that if either the absorptivity of the lacquer decreased to 0.83 or the emissivity increased to 0.83 the temperature requirement of the CubeCAT system would still be met. The cost of the lacquer was estimated to be 4,000 €, as this is the price of a high-end car paint job.⁴⁴ The real properties will be provided by Paladin in the next mission phase.

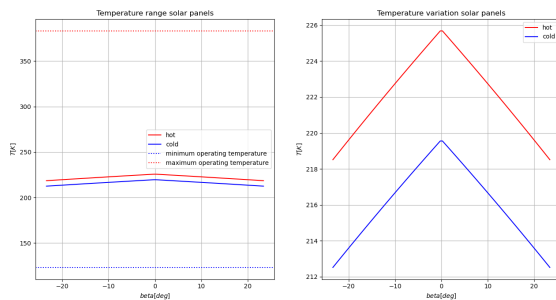


Figure 14.2: Temperature range of solar panels over β -angle.

The internal temperature of the satellite for different β -angles, ranging from -23.4° to 23.4° as the satellite flies in a circular orbit around the equator, is shown in Figure 14.1. The red line indicates the temperature during the 'hot' case, and the blue line indicates temperature during the 'cold' case. The green line shows the temperature during the average power consumption of the spacecraft. The light blue line shows the operating temperature of the payload and the black line the operating temperature of the CubeCAT.

The back of the solar panels will be painted with the white paint AZ-2100-IECW, The back of the 2 deployable solar panels will be used to radiate the heat away from all 5 of the solar panels. Using the AZ-2100-IECW paint the average temperature of the solar panels will be 219.12 K, or -54.03°C , which falls within the operating temperature of the solar cells. Figure 14.2 shows the temperature variation of the solar panels over the β -angle. The real temperature of the solar panels will be higher as not all radiation from the spacecraft will be blocked by the insulation.

14.3.2. Multi-Layer Insulation

To isolate the solar panels and the payload system from the rest of the spacecraft, multi-layer insulation (MLI) is used. The solar panels will be isolated by a MLI made of aluminum foil and chemical fiber spacer (ELK/EL), this MLI was chosen because of the low thickness of the aluminum sheet layers (0.0065 mm) used in the insulation, resulting in a lower mass. The solar panel insulation will consist of 40 layers as this is a standard amount, which

⁴⁴<https://www.thepricer.org/cost-to-paint-a-car>, [Retrieved on June 18, 2021]

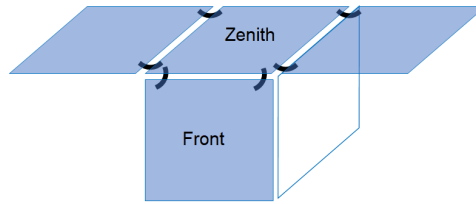


Figure 14.3: Schematic of GFTS configuration. The black lines show the location of the GFTS.

will result in sufficient blockage of the spacecraft radiation.⁴⁵ More than 329 W of heat radiation would be needed to exceed the maximal operational temperature of the panels, this insulation is deemed sufficient.

The payload will be isolated with a MLI made of aluminized polyester and chemical fiber spacer (EDLK/EDL), this MLI was chosen because this highly flexible and tensile insulation allows for ease of handling and assembly, which is needed to wrap it around the payload instrument. The payload insulation will be made of 25 layers, which is usually sufficient to obtain a minimum overall conductance value [28], which results in a thin insulation. The lower performance due to the lower layer count, is expected to be minimal as the average temperature of the spacecraft is 278.3 K, which is close to the operating temperature of the payload itself. Hence, the heat transfer between the spacecraft and the instrument will be slow by default.

Both of the sheets will be provided by Frako-Term, which ensures high purity of the insulation material. The properties of both insulation types are given in Table 14.2. The cost of insulation was estimated to be around a 1,000 €, but the real price needs to be provided by Frako-Term in the next design phase.

Table 14.2: Multi-layer insulation properties.

Component	ELK/EL	EDLK/EDL
Density	1.2 kg/m ²	0.8 kg/m ²
Layers	40	25
Thickness	20 mm	19 mm

Table 14.3: Properties Graphite Fiber Thermal Straps⁴⁷.

Component	Value
Mass	10 - 30 g
Thermal conductivity	800 - 1000 W/m-K
Width	38.1 mm
Thickness	12.7 mm
Volume	22 cm ³
Cost	1,000 - 5,000 € ⁴⁶

14.3.3. Graphite Fiber Thermal Straps

To ensure proper heat distribution, graphite fiber thermal straps (GFTS) are used. This light-weight link has a thermal conductivity of 800 - 1000 W/m-K and will therefore enable smooth heat transfer from components to the radiating areas of the spacecraft. The GFTS have a lower labor and material cost and mass compared to comparable thermal straps e.g. Pyrolytic graphite film or Graphene-based products⁴⁷ and have a lower mass than the HiPeR straps from Airbus⁴⁸. Each payload unit will need a strap which connects the detector and the radiating areas as the sides of the spacecraft. The CubeCAT will need thermal straps as will be demonstrated on the CubeSat mission.⁴⁹ The solar panels will need 6 thermal straps as shown in Figure 14.3, to connect the top and front panel to the radiating backs of the deployable solar panels. The GFTS will be provided by Technology Applications, Inc. and its properties are shown in Table 14.3.

⁴⁵<https://frakoterm.com/cryogenics/multi-layer-insulation-ml/>, [Retrieved on June 14, 2021]

⁴⁶https://www.techapps.com/hubfs/documents/Thermal_Straps_-_Performance,_Price_and_Product_Options-1.pdf, [Retrieved on June 17, 2021]

⁴⁷<https://www.techapps.com/graphite-fiber-thermal-straps>, [Retrieved on June 14, 2021]

⁴⁸<https://www.airbusdefenceandspacenerlands.nl/products/hiper-flexlinks/>, [Retrieved on June 16, 2021]

⁴⁹<https://www.techapps.com/blog/tno-uses-graphite-fiber-thermal-straps-on-cubesat>, [Retrieved on June 14, 2021]

14.4. Verification and Validation

The verification and validation of the thermal control system is crucial, as the overheating or undercooling of a system could lead to mission failure. Both the software and the hardware need to be tested.

The code written to perform the surface finishing trade-off and calculate the payload radiator area was verified by unit tests applied to all functions in the program. The active control of the battery and the engine are validated by the manufacturer and the GFTS have been extensively tested by industry. The complete thermal control system will first be verified by simulation, before a thermal balance test will be used to validate the TC, which will be done in the Large Space Simulator of ESTEC in Noordwijk.

14.5. Risk

As the thermal control system will be mostly passive, the risk of malfunction of this system will be low after the validation. The risk of the absorptivity of the AZ-2100-IECW paint increasing to unfeasible level is low, as this paint has been thoroughly tested in space, having been flown on the Optical Properties Monitor, the MIR MEEP POSA-I experiment and the Materials International Space Station Experiment⁴⁰. Furthermore, the increase in payload temperature would probably not result in mission failure, as the payload does not have a high sensitivity to temperature [D] (**RSK-TC1**). The risk of the GFTS is low as it has an extensive spaceflight heritage and is qualified by NASA⁴⁷. The largest risks present themselves in the active thermal control systems, such as the one used in the propulsion subsystem. In this case, instrument mis-calibration for temperature measurement and correction poses a substantial risk (**RSK-TC2 & RSK-TC3**, respectively). These will be mitigated with sufficient testing schemes.

14.6. Sustainability

To ensure the sustainability of the thermal control system the toxicity of the surface finishes need to be addressed. For the sustainability analysis of the black lacquer the properties of the PALADIN SATIN BLACK LACQUER 12412 were assumed.⁵⁰ This paint is toxic to humans and therefore protection must be used during handling, to prevent inhalation and skin contact with the lacquer. Paladin strives to 'strike a harmonious balance between industrial development and ecological well-being'⁵¹.

The AZ-93 paint would result in a smaller payload radiator and a lower solar panel temperature. However, it has a hazard classification of H400 and H410 and therefore very toxic to aquatic life.⁵² As the paint would enter the environment after the end of life burn, the AZ-2100-IECW paint was selected. This paint has a hazard classification of H302 and H312, which means it causes health damage when swallowed or when it comes in contact with skin.⁵³ Hence, during the handling of the paint, protection must be used.

No data on the sustainability of the GFTS or MLI could be found on the websites of Technology Applications, Inc. and Frakto-term. For the MLI the toxicity is assumed to be within acceptable bounds as it consists of aluminum sheets, which is only toxic in high amounts and will not significantly pollute the environment after the end-of-life burn. As the GFTS mostly consists of carbon, this non-toxic product will have almost no impact on the environment when burned in the atmosphere, as the amount of CO₂ is too small to significantly contribute to the greenhouse effect.

In conclusion, the thermal control of the satellite will be mainly passive, except for the built-in temperature control of the batteries and the engine. In Chapter 25 the allowable increase/decrease in power usage of the satellite will be derived, for which this TC maintains the desired temperature range.

⁵⁰http://www.chemcas.com/msds112/cas/3971/64-17-5_71-36-3_1330-20-7_100-41-4_50-00-0.asp, [Retrieved on June 16, 2021]

⁵¹<http://paladinchemicals.com/research-and-development.html#green>, [Retrieved on June 16, 2021]

⁵²<http://www.aztechnology.com/wp-content/uploads/SDS/SDS-AZ-93.pdf>, [Retrieved on June 14, 2021]

⁵³<http://www.aztechnology.com/wp-content/uploads/SDS/SDS-AZ-2100-IECW.pdf>, [Retrieved on June 14, 2021]

15. Tracking, Telemetry & Command Subsystem

In this chapter, the design of the TT&C subsystem is explained. In Section 15.1, the possibility of using optical LEO-to-Ground communication is considered. Then, Section 15.2 presents an overview of different available laser communication systems. After that, the mechanisms which can be used for precise laser pointing are explained in Section 15.3. In Section 15.4, the Verification and Validation procedures for TT&C subsystems are discussed. The technical risks involved are described in Section 15.5. Finally, the sustainability concerns are discussed in Section 15.6.

15.1. Data Generation and Transmission

In the previous design phase, a trade-off was made between different antenna systems. A patch antenna operating in the S-band was determined to be the optimal choice, providing up to 10 Mbit/s downlink data rate [1]. However, as the rate at which the payload generates data was determined to be significantly higher than the initial estimate, an even higher downlink data rate is required and the S-band downlink turned out to no longer be the best option. Higher downlink data rates enable more data to be sent during GS contact, allowing the payload sensors more time to perform measurements. One way to significantly increase the data rate is to use a laser communication system. Under the right circumstances, lasercom systems can provide data rates in the order of several gigabits per second, which can not be achieved with radio frequency (RF) communication⁵⁴. Table 15.1 demonstrates the increase in the amount of collected data, measurement time and measurement length, in case a 1 Gbit/s lasercom downlink is used compared to 10 Mbit/s RF downlink. The values presented in the table are for one GS contact (414 seconds, see Section 15.3).

Table 15.1: Payload measurement time vs downlink data rate.

Property	10 Mbit/s	1 Gbit/s
Max. data that can be sent to Earth	0.518 GB	51.8 GB
Max. measurement duration	1.06 s	106.44 s
Max. measured distance on land	7.02 km	701.87 km

It can be seen that a 10 Mbit/s connection only allows measuring over a strip of land with a total length of 7.02 km, which is insufficient to meet the area coverage requirement even if several GSs would be used.

15.2. Selection of a Laser Communication System

The high data rates of CASE's instruments do not allow for conventional radio frequency communication methods. To ensure that all the data that is gathered per orbit can still be sent to Earth, a laser communication system was selected for its high downlink data rate capabilities.. The existing satellite laser terminals are generally larger and have more mass than RF antennas. Also, only a few existing terminals can support both downlink and uplink connection. Selection of only downlink laser communication must be avoided as it would require an additional antenna and a receiver on-board, as well as additional GSs that operate in radio frequencies. In Table 15.2 an overview of four existing lasercom systems is presented.

⁵⁴<https://blog.satsearch.co/2020-01-22-optical-communications-for-small-satellites-and-cubesats-product-roundup>, [Retrieved on May 31, 2021]

Table 15.2: Various optical communication systems⁵⁵.

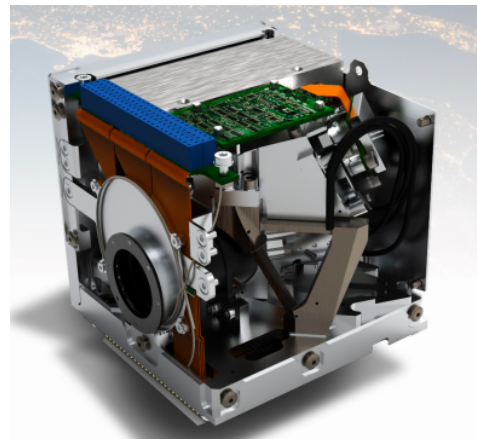
Component	Manufacturer	Mass [kg]	Size [mm]	Data Rate	Communication type
CubeCat	Hyperion Technologies	1.33	96x96x96	1 Gbit/s	LEO to ground. Uplink + Downlink
SmartLCT	Tesat-Spacecom	30	350x350x200	1.8 Gbit/s	LEO to GEO satellites
Laser Downlink + Star Tracker	Sinclair Interplanetary	0.335	79x68x68	1 Gbit/s	LEO to ground. Downlink only
TOSIRIS	Tesat-Spacecom	9	150x20x550	1.25 to 10 Gbit/s	LEO to ground. Uplink + Downlink

From the comparison above, it can be seen that the CubeCat laser terminal developed by TNO and Hyperion Technologies is the most suitable option, as it is relatively compact (fits inside 1U) and it supports both downlink and uplink. Other options are either too massive or do not provide uplink. Figure 15.1 shows a render of the CubeCat laser terminal.

The CubeCat can provide up to 1 Gbit/s downlink and 200 Mbit/s uplink connection. It consumes 12 W of power when transmitting and 1 W in standby. It also has an on-board buffer, where at least 64 GB of data can be stored before sending it to Earth. The maximum slant range of the CubeCat that is given by Hyperion Technologies is 1000 km, however, as TNO is working on increasing the efficiency and the laser power of the CubeCat, it can be assumed that the maximum slant range will be increased to 1500 km by the time the CASE mission flies [P]. The cost estimation for the CubeCat that is used in the total mission cost calculations has been provided by TNO, however, the design team was asked to limit the distribution of this information. The main characteristics of the CubeCat are summarized in Table 15.3

Table 15.3: Properties of the CubeCat [52].

CubeCat	
Downlink data rate	1 Gbit/s
Uplink data rate	200 Mbit/s
Max. slant range	1500 km
On-board buffer size	64 GB
Mass	1.33 kg
Size	96 x 96 x 96 mm
Power consumption	12 W (Tx), 1 W (average)
Operating temperature	-20 °C to +40 °C

**Figure 15.1:** CubeCat by Hyperion Technologies [52].

15.2.1. Link Budget

Hyperion Technologies ensures the laser communication terminal will meet the signal-to-noise ratio (SNR) requirements at the maximum slant range (1500 km). Thus, it is assumed that the link performance has been already assessed by Hyperion Technologies. It should be noted that there are mission-specific factors such as atmospheric conditions around the equator that can heavily influence optical communication performance. For example, the presence of fog/rain/clouds above a GS may result in signal attenuation of 10 to 100 dB/km [53]. Although the link budget calculation has probably accounted for various atmospheric conditions, the mission-specific link performance should be further verified with Hyperion.

15.3. Coarse Pointing Assembly

The maximum slant range of 1500 km means that communication is only possible when a satellite and a GS are no more than 1500 km apart. This imposes a limit on the contact duration and the latitudes at which the GSs can be

⁵⁵<https://satsearch.co/>, [Retrieved on June 2, 2021]

placed and built (see Chapter 21). For the 500 km orbit, the maximum contact time to one GS was calculated to be 413.8 seconds, assuming the GSs are all located exactly on the equator. The angle to rotate the beam is calculated with Equation 15.1:

$$\theta = 2 \cdot \cos^{-1} \frac{h}{R_{\max}} \quad (15.1)$$

In the above equation, h is the height of the orbit and R_{\max} is the maximum slant range. In this way the full angle to rotate the beam is 141° . This can be achieved by either rotating the entire spacecraft or just steering the laser beam itself with a so-called Coarse Pointing Assembly (CPA). There are multiple ways in which a CPA can be designed; it can involve mirror or prism assemblies.

15.3.1. Mirror System CPA

It is possible to achieve 2-axis control of the laser beam with the use of two rotating mirrors. One mirror is placed at a 45° angle above the laser beam coming out of the laser terminal. This mirror changes the beam direction by 90° . Another mirror is placed with an offset, parallel to the first mirror. This second mirror also changes the beam direction by 90° . The working principle of a mirror-based CPA is shown in Figure 15.2.

A mirror-based CPA for CubeSat LEO-to-Ground communication is currently being developed by TNO. This CPA will be highly integratable with the CubeCat structure, which will allow to significantly reduce its size. The TRL of the CPA is already higher than that of the payload, which means that it will be available by the time the mission flies. [54]

15.3.2. Risley Prisms CPA

An alternative CPA design involves two or three rotating Risley prisms. Prisms are placed above each other and can rotate around the same axis. By rotating the prisms, control over the refraction angle is achieved, in this way the laser beam can be steered. An example of the Risley prism CPA is shown in Figure 15.3. One major disadvantage of the Risley configuration is that the refracted laser beam has a smaller cross-section area which is effectively equivalent to having a smaller aperture size. This reduces the laser power by about 40%. In addition to that, the Risley prism configuration has a limited Field Of Regard [P]. This makes the mirror-based CPA the best option, which is, therefore, selected as the CPA for the CASE spacecraft.

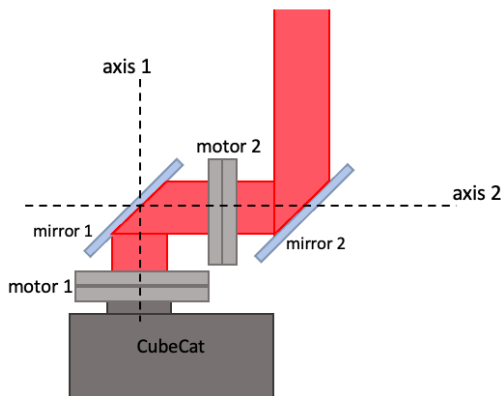


Figure 15.2: Mirror based CPA.

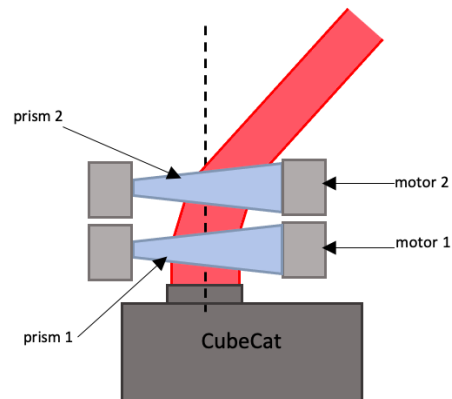


Figure 15.3: Risley prism CPA.

15.4. Verification and Validation

The V&V strategies employed for the TT&C subsystem will run in parallel to those performed for the CDH and GNC subsystems. The individual components (the CubeCat and CPA units) which comprise the TT&C subsystem are assumed to be tested by their respective manufacturers. However, their integrated function must still be tested in the environment of the entire spacecraft. Furthermore, their integration with the remaining subsystems must also be sufficiently tested. This includes communication streams with the CDH subsystem, but also communications with the GSs. The latter will be difficult to test, and will likely only be possible to simulate. Ideally, a full flight simulation will be performed in which the capabilities of the TT&C subsystem will be realized.

Simulation will be one of the most effective ways for testing the underlying software as well, and ensuring it is not prone to errors in flight. However, it would be prudent to also subject the software itself to verification such as unit tests to find any human errors in code design. Once again, in modern space ventures software seems to be the Achilles' heel of many CubeSats, and so the amount of verification and validation dedicated to that aspect will be biased. The rationale for this is provided in Chapter 7.

The benefit of laser communication is the lack of any antennas. For this reason, the majority of the TT&C subsystem will be integrated with the interior of the spacecraft. Nevertheless, the mirror pointing mechanism will suffer exposure to the harsh environment of space. As such, thermal testing will be necessary to ensure that the components can function adequately. The pointing mechanism will also need to be subjected to mechanical testing to ensure it does not fail under the torques and rotational velocities it needs to induce.

15.5. Risk

Chapter 7 has shown that the communications subsystems are often to blame for CubeSat failure. This becomes increasingly true as mission time increases, and therefore presents sufficient motivation to accurately assess the risks of the TT&C subsystem. The first risk that has been identified pertaining to the TT&C subsystem (though it is not unique to it) is the failure of underlying electronics (**RSK-TTC1**). Fortunately, this presents a minute risk and can be mitigated with sufficient testing.

The next risk concerns the pointing accuracy required to facilitate the uplink and downlink of data (**RSK-TTC2 & RSK-TTC3**). This will be achieved by the CPA, however, the software will be needed to determine the required pointing angles. As one can surmise, there are several avenues through which this can fail: mechanical error, software-based error, or algorithmic error. For instance, if the CPA were to fail (**RSK-TTC4**), the required pointing will no longer be controllable and communication will fail. Similarly, if the underlying software or algorithm which controls the mirror's mobility were to fail, the same outcome will be suffered (**RSK-TTC5 & RSK-TTC6**). Furthermore, the required software updates to fix such a problem would become impossible due to the communications being inhibited.

Finally, cloud cover is an issue that plagues the TT&C subsystem (**RSK-TTC7**). Since laser communication cannot penetrate cloud formations, countermeasures must be implemented. This currently includes the use of several GSs as redundancies for when one or several are occulted. Nevertheless, if the misfortune of total equatorial cloud cover were to occur, the TT&C subsystem will not be able to communicate. The possibility for data storage exists, and this will be a possible countermeasure until the storage unit is filled. At this point, however, either data measuring will need to be halted or previously obtained data will be deleted. Both of these outcomes are undesirable, but a necessary consequence of choosing laser over radio-frequency communication

15.6. Sustainability

The TT&C subsystem consists of the CubeCat laser communication system and the mirror system CPA. Both of these components are made of non-toxic materials. Since these laser communication systems need to be extremely precise, their manufacturing process also requires a lot of precision and time. The mirrors in the laser as well as for the CPA also require high precision and are made from aluminium or silver. The rest of these systems are electronics that require certain chemical processes and materials. These components are purchased as COTS

components from TNO and Hyperion Technologies which makes that the materials and manufacturing processes used in the COTS options give little insight on their sustainability impact, and hence no distinction can be made in the use of resources from each of the COTS components. On the other hand, the use of COTS components eliminates the need for an R&D phase and reduces the amount of component testing required. This has a positive influence on the sustainability of the components.

In conclusion, in this chapter, the design of the laser communication system was discussed. Because of the high data rate, an optical communication system is the only option with which the coverage requirements can be met. The CubeCat laser terminal and a mirror-based Coarse Pointing Assembly were selected as the main components of the TT&C subsystem.

16. Attitude Determination & Control Subsystem

The ADCS subsystem is vital for the CASE mission as it makes sure the satellite is pointing in the right direction accurately. Additionally, the ADCS is needed to stop the satellite from tumbling after launcher separation. Lastly, the ADCS should counteract any unwanted external and internal torque experienced by the satellite. Therefore, the ADCS system includes star sensors, sun sensors and magnetorquers. In this chapter a detailed explanation is given of the ADCS. Firstly, the sensors are described in Section 16.1 followed by the actuators in Section 16.2. An overview of the selected ADCS components can be found in Section 16.3. Finally, the verification and validation, the risk and the sustainability of the ADCS are discussed in Section 16.4, Section 16.5 and Section 16.6 respectively.

16.1. Sensors

The first part of attitude determination is done by making use of sensors. In the previous report preliminary calculations were made to find the accuracy needed of the sensors. They are shortly repeated and justified in further detail.

16.1.1. ADCS Sensor Requirements

The accuracy of the sensor has to be great enough to sense small deviations in the attitude during measurements. The pointing stability can be calculated using Equation 16.1 [55].

$$PA = k \cdot \frac{GSD}{h} \quad (16.1)$$

GSD has been defined in Chapter 11 and h was defined in Chapter 10. k, the stability margin, is the percentage of the pixel that can have overlap. It was difficult to determine due to the payload still being in the development stage. Looking at other mission also yielded varying results between 15% and 40% [55][56][57]. To be on the safe side, the lowest value of 15% was taken for our mission. This resulted in a required pointing stability of 11 arcseconds. Furthermore, the pointing accuracy of the satellite has to be at least 11 arcseconds. Additionally, the ADCS needs to detect a minimum turn rate. This is determined by dividing the pointing accuracy by the dwell time of the spacecraft. The dwell time was calculated in Chapter 11 and was found to be 0.023 seconds. This results in a minimum angular velocity determination accuracy of 0.136 °/s

16.1.2. Star Tracker

In the last report it was found that star trackers are the only sensors that can meet the 11" accuracy requirement. The properties of multiple off-the-shelf star sensors were assessed and can be found in Table 16.1. Any star tracker that was either too over designed or not compatible with the others listed below was not included in the table.

Table 16.1: List of star trackers and their most important parameters⁵⁶.

Company	Product	Pointing-Rolling accuracy [arcsec]	Mass [g]	Volume [cm ³]	Power [mW]	Update rate [Hz]
Hyperion	ST-400 [58]	10-120	280	5.38x5.38x9.05	700	5
Hyperion	ST200 [59]	10-70	106	5x5x8.3	670	5
arcsec	Sagitta Star Tracker [60]	2-10	270	4.5x5x9.5	1300	5
Blue Canyon Technologies	NST star tracker [61]	6-40	350	10x5.5x5	1500	-
Nano avionics	ST-1 [62]	8-10	108	4x4.2x8.3	1200	5
OCE technologies	NST-2 [50]	3-25	130	5x5x5.2	1000	10
OCE technologies	PST-1 [50]	6-40	50	3.2x3.2x4.5	500	5
Kairospace	star tracker [63]	5-60	197	5.6x6x9.3	700	10

PST-1 from OCE technologies, is the best star tracker for the CASE mission. It has the lowest mass, volume and power consumption of all star trackers while meeting the accuracy requirement. In order to have 11" accuracy throughout the mission in pitch, yaw and roll a minimum of 3 star trackers are needed. No star tracker should be placed in positive z direction since the Earth will be there, obstructing the Field of View (FOV). One should point in negative or positive y-direction since the Earth and sun will not enter its FOV. The second one should be orthogonal to the first one. A third star tracker is necessary, for operations when the second is blinded by the sun, since the sun will be in its FOV for part of the orbit. This one should be orthogonal to the first and second star tracker. The only problem star trackers have is detecting and working during fast rotations because the shift in stars can become too large for the star tracker to track them. The PST-1 works up until a slew rate of 1.5 °/s. This does not a problem during normal operations, but might be a problem during detumbling. In the next section, this will be more elaborated.

16.1.3. Sun Sensors

For detumbling the spacecraft, it is beneficial to have a sun sensor on every side of the spacecraft. This allows for quick initial attitude determination, after which corrections can be made. Initially, 6 sun sensors would be needed, but since one of those would constantly face the Earth it can be omitted. Hence, 5 sun sensors are used. Sun sensors can be for either one or 2 axis. They are generally very small and consume little power but are also less accurate compared to star sensors. They have a high FOV, mostly around 100 ° and a medium to high update rate. This allows them to work during and detect high slew rates and are thus perfect for detumbling the spacecraft or during power saving mode and safe mode.

Sun sensors come in different styles: coarse analog, fine analog and digital⁵⁷. Coarse sun sensors purely give the angle the spacecraft makes with the sun. So, 2 sensors are needed for 2 axis spacecraft attitude information. Fine sun sensors can give 2 axis attitude information by creating a sun spot over 4 quadrants. Digital sun sensors also give 2 axis spacecraft attitude information, but are also able to distinguish reflected sunlight from actual sunlight. Coarse sun sensors are not assessed since they require more sensors and more bulky constructions and digital sun sensors are not commonly used. Therefore, multiple fine analog sun sensors were assessed to find the best option. These sun sensors and their performance parameters can be found in Table 16.2.

⁵⁶<https://satsearch.co/>, [Retrieved on June 3, 2021]

⁵⁷<https://blog.satsearch.co/2020-02-12-sun-sensors-an-overview-of-systems-available-on-the-global-marketplace-for-space>, [Retrieved on June 3 2021]

Table 16.2: List of sun sensors and their most important parameters⁵⁸.

Company	Product	Accuracy [°]	Mass [g]	Volume [cm ³]	Power [mW]	Update rate [Hz]	Cost [€]
SolarMEMS	Nano-SSOC [64]	0.5	4	2.74x1.4x0.59	10	-	2200
SolarMEMS	SSOC [65]	0.3	25	3x3x1.2	36	-	7200
NewSpace systems	NFSS [66]	0.1	35	3.4x4x2	150	5	12000
Bradford Space	Mini FSS [67]	0.2	50	5x4.6x1.7	0	-	-
Hyperion	SS200 [68]	1	3	2.466x1.5x0.35	40	1-100	-
NEEDRONIX	NXSS2v01 [69]	1	5	1.9x1.9x0.9	26	1-100	-
NEEDRONIX	NXSS3v00 [49]	1	3	1.55x1.5x0.47	7.2	1-100	1800

Since the spacecraft uses the star tracker for accurate pointing, accuracy of the sun sensors is not of great importance. Thus the sun sensor was chosen for its low mass, volume and power usage. According to Table 16.2, the NXSS3v00 of NEEDRONIX is chosen. The company also expressed interest in entering a sponsorship deal, if an actual satellite would be constructed, further decreasing the price of the product which would be beneficial for both parties.

16.2. Actuators

The second part of the ADCS, Attitude Control, is done with actuators, they control the attitude of the spacecraft. This can be done in a couple different ways: reaction wheels, thrusters and magnetorquers. In the last report it was found that the magnetorquers would be the best option for the spacecraft [1]. In the Section 16.2.1 the different requirements for the actuators are determined. This is followed by describing the actuators that will be used as well as its accuracy in Section 16.2.2.

16.2.1. ADCS Actuator Requirements

The requirements on the ADCS actuator depend on a couple factors. Firstly, the accuracy of the actuator needs to be sufficiently high to meet the pointing stability as calculated in Section 16.1. Secondly, the slew rates that are required between measurements to angle the spacecraft to the right direction need to be met. Lastly, to counteract disturbance torques, internal and external, acting on the spacecraft.

Slew Rate Requirement

The slew rates that need to be met depend on the areas where measurements will take place, which can be found in Chapter 10. The biggest difference in measurement latitude is between Nairobi and Singapore, additionally the distance between these places is also the shortest. It should be mentioned that, the satellite does not need to turn for ground station contact, this will be taken into account in the pointing assembly. In Table 16.3 the latitude, pointing angle, longitude and the difference between the last two is shown. The pointing angle is the angle the spacecraft needs to have across track with nadir to ensure the city is in the center of the measurements.

Table 16.3: Latitude, longitude and their difference between Nairobi and Singapore⁵⁹.

City	Latitude [°]	Pointing Angle [°]	Longitude [°]
Nairobi	-1.292066	-15.93	36.82
Singapore	1.352083	15.98	103.85
Difference	2.644149	31.91	67.03

⁵⁸<https://satsearch.co/>, [Retrieved on June 3, 2021]

⁵⁹<https://www.latlong.net/>, [Retrieved on June 1 2021]

As can be seen in Table 16.3 the spacecraft needs to rotate around the x-axis by approximately 32 degrees between Nairobi and Singapore. The distance between measurements on the ground is found using Equation 16.2, where $\Delta\lambda$ is the difference in longitude and D_m is the distance where measurements are still being taken.

$$D = 2\pi R_e \frac{\Delta\lambda}{360} - D_m \quad (16.2)$$

This results in a distance between measurements of 6212 km. The time to rotate between measurements would then be this distance divided by the ground velocity of the satellite and is 942 seconds. This means the spacecraft needs to rotate 32 degrees in 942 seconds. The angular acceleration needed for this can be calculated using Equation 16.3 [28]. Keep in mind that for half the time the angular acceleration is positive and the second half the angular acceleration is negative, such that the final angular velocity is 0. Therefore, half the angle is achieved in half the time. $\Delta\theta$ is the change in angle the spacecraft needs and t the time between measurements.

$$\alpha = \frac{\Delta\theta}{\frac{t^2}{2}} \quad (16.3)$$

Resulting in a required angular acceleration of $0.14 \text{ m}^\circ/\text{s}^2$. The torque required for this angular acceleration is found by multiplying it with the mass moment of inertia (MMOI) around the x-axis. The MMOI of the spacecraft is explained in more detail in Chapter 19 and was determined to be 0.11 kgm^2 around the x-axis. And leads to a required torque of $0.27 \mu\text{Nm}$.

Disturbance Torques

The pointing stability of the spacecraft is threatened by different disturbance torques. The following different phenomena that generate disturbance torques are distinguished: solar radiation, aerodynamic drag, magnetic field, gravity-gradient & internal torques. Aerodynamic drag is always in the direction of the flight. In order to calculate the worst case scenario for the total disturbance torque, all torques are calculated for the same direction as the aerodynamic drag torque. The first one, solar radiation, is active on the side of the spacecraft that is facing the sun. It can be calculated using Equation 16.4 [28].

$$T_s = \frac{\Phi}{c} A_s (1 + q) (cp_s - cm) \cos \phi \quad (16.4)$$

In this equation Φ is the solar constant which is 1367 W/m^2 at Earth, c is the speed of light, A_s is the surface area which is 0.04 m^2 for the front, q the reflectance factor which for the solar panels is 0.09, cp_s is the center of solar pressure, cm the center of mass and lastly ϕ is the sun incidence angle which in worst case is 0 degrees. For now the center of mass is assumed to be in the absolute center of the spacecraft and the center of pressure is assumed to be at worst 75% of the center of mass to the furthest side which would be 0.075 meters. This all results in a solar radiation torque of 14.9 nNm around the y or z axis. Since slew maneuver calculated in the previous part is a rolling maneuver, the solar radiation torque is also estimated around the x axis. For this Φ , c , q and cm remain the same, while A_s increases to 0.18 m^2 due to deployed solar panels and cp_s increases to 0.2 m since the center of pressure could shift due to the solar panels. Resulting in a torque of 179 nNm around the x axis.

The torque induced by the aerodynamic drag is can be calculated using Equation 16.5 [28]. In this equation ρ is the density of the air, C_d is the drag coefficient of the spacecraft assumed to be 2.5 [28], A_r is the front surface of the satellite which is 0.04 m^2 and cp_a the center of aerodynamic pressure which is assumed to be the same as cp_s . Plugging these all into the equation results in an aerodynamic torque of $0.44 \mu\text{Nm}$.

$$T_a = \frac{1}{2} \rho C_d A_r V^2 (cp_a - cm) \quad (16.5)$$

The magnetic field induced torque can be calculated using Equation 16.6 [28]. Where D is the residual dipole moment of the spacecraft which was assumed to be 1 mAm^2 [12] and B is the magnetic field strength, also shown in Figure 16.1⁶⁰.

$$T_m = D \times B \quad (16.6)$$

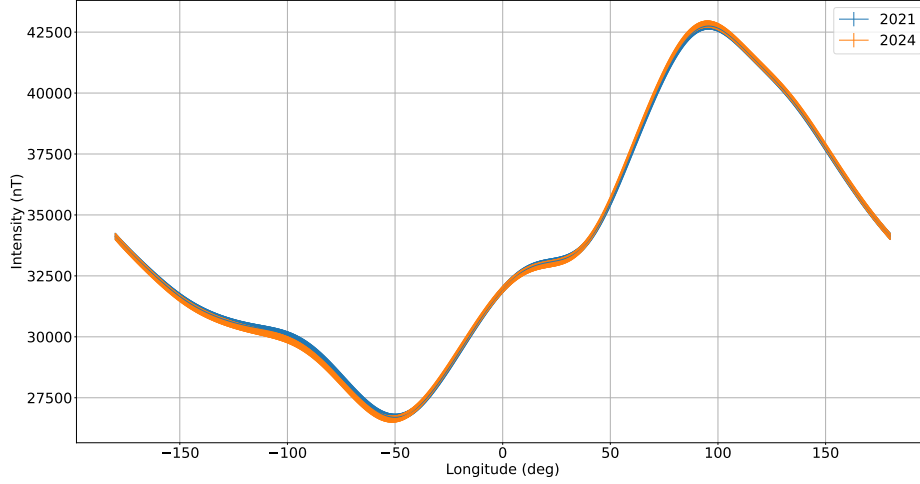


Figure 16.1: Magnetic field around the equator at 500 km altitude in June 2021 and 2024.

The models for the magnetic field only go up to 3 years after the current date in order to stay accurate, up until 2024 the magnetic field deviates slightly. In Figure 16.1 the magnetic field at 500 km altitude around the equator is shown for 2021 and 2024, the line thickness is dependent on the uncertainty in the model. As can be seen there is only a very minor difference in the magnetic field strength between 2021 and 2024. There is a large difference in the longitude though. For the disturbance torque the worst case is when the magnetic field is strongest and orthogonal to the spacecraft, in this case $32.94 \mu\text{T}$ at a longitude of 90° . Resulting in a magnetic field induced torque of $0.33 \mu\text{Nm}$.

The last disturbance torque not coming from the satellite itself is the gravity gradient induced torque. This disturbance torque is calculated using Equation 16.7 [28]. Where μ is the gravity constant of the Earth, R the distance between satellite and Earth center, I_z and I_y the MMOI around their respective axis and θ the angle between the local vertical and Z principal axis. The MMOI is calculated in Chapter 19 and was found to be 0.179 around the y -axis and 0.151 around the z -axis. The angle in a worst case scenario would be 90 degrees (while in a stabilized scenario it would be small). Resulting in a gravity gradient induced torque of $0.050 \mu\text{Nm}$.

$$T_g = \frac{3\mu}{2R^3} |I_z - I_y| \sin 2\theta \quad (16.7)$$

The internal torque generated by the spacecraft can be generated by two things. First of all would be the deploying of the solar panels. Since the solar panels are deployed symmetrically the internal torque generated by the deploy mechanisms should be equal and in opposite direction, as long as the time they take to deploy and the MMOI of the solar panels are equal. The deviations in these will be so small the resulting torque is assumed to be 0. The second internal torque could come from the propulsion subsystem. If the thrust vector has a slight off-set from the center of mass it will produce a torque. Therefore the layout was made in such a way that the thrust vector would be as close as possible to the x -axis.

⁶⁰<https://www.ngdc.noaa.gov/geomag/calculators/magcalc.shtml#igrfwmm>, [Retrieved on May 31, 2021]

16.2.2. Actuators

The torques calculated in the previous subsection have to be generated by the actuators. In the last report it was found that magnetorquers would be the best option if they are strong enough [1]. Magnetorquers control the attitude by creating a magnetic dipole moment. This magnetic dipole moment is dependant on the physical properties of the magnetorquer as well as on the current going through the magnetorquer. The dipole moment that is needed for the magnetorquer is calculated using Equation 16.8 [28].

$$m = \frac{\tau}{B \sin \beta} \quad (16.8)$$

Here τ is the required torque, for the worst case scenario torque it is assumed that all disturbance torques work in the same direction, creating a pitching or yawing moment. Resulting in a total disturbance torque of $1.29\mu\text{Nm}$. B is the strength of the Earth magnetic field, shown in Figure 16.1. Here in a worst case scenario the magnetic field is the lowest as possible, therefore the magnetic field is assumed to be $23.97\mu\text{T}$. And β was added to account for the angle between the magnetorquer and the magnetic field, it was assumed to be 30 degrees. This would mean a dipole moment of 0.11 Am^2 . This is purely for the disturbance torque around the y and z axes. For the slew maneuver around the x axis the drag does not play a role, but there is more solar radiation pressure. The rest of the disturbance torques are assumed to be similar. Adding these torques to each other results in a total required rolling torque of $0.83\mu\text{Nm}$. Using Equation 16.8, a minimum required dipole moment of 0.07 Am^2 is found.

The above calculations have multiple assumptions in them, therefore a 20% margin is added for contingency [28]. This results in the final magnetic dipole required for pitch, yaw and roll as presented in Table 16.4.

Table 16.4: Magnetic dipole moment required for the magnetorquer for pitch yaw and rolling motion.

Rotation	Magnetic Dipole [Am^2]	with margin [Am^2]
Pitch	0.11	0.13
Yaw	0.11	0.13
Roll	0.07	0.08

As the table shows the minimum magnetic dipole moment for the magnetorquer is required to be 0.13 Am^2 . With this information some magnetorquers were assessed, including the MTQ400 and MTQ200.20, the CubeTorquer from CubeSpace⁶¹ and the NCTR-M002 from cubesatshop⁶², and it was found that the MTQ200.20 of Hyperion fits the exact requirements. It has low power consumption, low mass and low volume while also having a nominal dipole moment of 0.2 Am^2 . Furthermore, it also has a boost mode in which the dipole moment can be boosted up to 1 Am^2 . A more detailed list of the properties of the magnetorquer can be found in Table 16.5. 3 of them will be used to achieve three-axis control and they will be placed orthogonal to each other [70]. The accuracy of the magnetorquer is dependant on how accurate the magnetic dipole of the magnetorquer can be controlled. For the MTQ200.20 of Hyperion the magnetic dipole can be changed by increments of 1 mAm^2 . This would result in a change in torque of 24.0 nNm , meaning the torque acting on the spacecraft can be changed with increments of 24.0 nNm . Additionally, a small magnetorquer control board is needed to interpret the commands from the CDH subsystem and accurately control the magnetorquers. These are included with the MTQ200.20 magnetorquer from Hyperion.

This only leaves one problem. So far the actuator has only been assessed for nominal operation. However, this is not the only mode the spacecraft will operate in. Directly after launcher separation the spacecraft is tumbling and needs to be stabilized. This is usually done with the B-dot algorithm. This is an algorithm that controls the magnetorquers to reduce the angular velocity of the satellite. The downside of the B-dot algorithm is that it might increase the spin if the sensing or actuation cycle is not small enough [71]. Additionally, if the sensors can not detect the actual angular velocity of the satellite it will also no longer work, as was the case for the SwissCube satellite [72]. This is quite dangerous as it could quickly result in mission failure. Luckily, the sun sensors that were chosen in Section 16.1 have an update rate of up to 100 Hz which means they are able to detect very high

⁶⁰<https://hyperiontechnologies.nl/products/>, [accessed on June 3, 2021]

⁶¹<https://www.cubesatshop.com/product/cubetorquer-and-cubecoil/>, [accessed on June 3, 2021]

⁶²<https://www.cubesatshop.com/product/nctr-m002-magnetorquer-rod/>, [accessed on June 3, 2021]

angular rates, meaning the sensing will not be the problem. This only leaves the actuation cycle. This depends on the computer and electronics involved with the actuation cycle, which is beyond the scope of this project. In case the actuation cycle is too long an altered B-dot algorithm can be used. This algorithm is a weighted B-dot algorithm and it works for fast spinning satellites. This algorithm has shown to be capable to detumble satellites with an initial angular velocity of over 200 °/s in one day. This shows that detumbling of CubeSats with high angular velocities is possible with magnetorquers [73]. Additionally the MTQ200.20 magnetorquer come with a passive detumbling mode that could be used in case of software failure.

16.3. ADCS Overview

As explained in Section 16.1 the spacecraft will have 3 star trackers, which are used during operational mode. Additionally 5 sun sensors will be placed to be active during detumbling of the spacecraft and during power saving mode. These will be used to determine the attitude of the spacecraft, their properties are listed in Table 16.5. In Section 16.2 the requirements for the magnetorquers were determined and a magnetorquer was chosen of which 3 are needed to have three-axis attitude control. The properties of the magnetorquer are listed in Table 16.5. The costs for the sun sensors are the actual costs [J], but for the magnetorquers and star trackers they were estimated by looking at the prices of comparable star trackers and magnetorquers ⁶³.

Table 16.5: Properties of the different ADCS parts, all properties are given for a single instrument.

Property	Star tracker	Sun sensor	Magnetorquer
Company	OCE technologies [50]	NEEDRONIX [49]	Hyperion [51]
Instrument	PST-1	NXSS3v00	MTQ200.20
Amount used	3	5	3
Accuracy	6"	1°	1 mAm ²
Field of View [deg]	15 x 12	100	-
Mass [g]	50	3	39.6
Dimensions [mm]	32 x 32 x 45	15.5 x 15 x 4.7	10.7 x 10.7 x 80
Power [mW]	500	7.2	90
Temperature range [°C]	-30 to +60	-40 to +85	-40 to +70
Update rate [Hz]	5	1-100	-
Cost [€]	1790	4500	2200

16.4. Verification and Validation

In this section the methods with which the ADCS can be verified and validated will be discussed. In Chapter 8 some ADCS verification and validation methods were already mentioned and here they will be explained in more detail. Since all components of the ADCS are verified and validated by the manufacturer and also all have flight heritage the components do need to be verified and validated themselves. Additionally, the calculations done for the ADCS are all from the new Space Mission Engineering & Design book [28] and have been extensively checked for mistakes. This only leaves the software and the system as a whole to be verified and validated.

First of all software verification, this is done by simulating the CubeSat, the different disturbance torques and the initial condition. This requires an extensive code but will prove useful as it can verify the working of the ADCS as well as providing information on the limits of the system and show its weaknesses. Additionally some of the algorithms used, such as the weighted B-dot algorithm have already been extensively verified and also have flight heritage [71]. Secondly, a kinematic simulation with a CAD render can be made to verify the field of view is not obstructed. Additionally rotation around the axes can be demonstrated. Lastly the ADCS can be validated in a dynamic attitude test bed. These test beds can simulate the different disturbance torques on the satellite and see how the ADCS reacts to those disturbance torques [74]. Such test beds already exist such as in the ADCS test Facility of Hawaii Space Flight Laboratory, or in the ADCS test facility at Surrey Space Center for something closer. These facilities rented to validate the entire ADCS system as a whole.

⁶³<https://www.cubesatshop.com/products>, [retrieved June 1, 2021]

16.5. Risk

Due to the large quantity and complexity of moving parts in the ADCS subsystem, there are significant risks involved. Sensors and actuators, each consist of moving components and are therefore more susceptible to failure than non-mobile components. For this reason, two risks have been identified **RSK-ADC1** & **RSK-ADC2** which warn of sensor and actuator failure, respectively. While these dynamic components portray a higher likelihood of occurring than static components, Chapter 7 discussed the unlikelihood of spacecraft failure to originate from the ADCS. For this reason, an industry-wide redundancy philosophy has been implemented and all sensor and actuator subsystems are accompanied by a contingent component. For instance a third star tracker is added for when the sun blinds the other, this one also operates as a back-up star tracker in case one of the others fail.

Another avenue by which the ADCS can be hindered is by mis-calibration of the star and sun sensors, as described in **RSK-ADC3**. This can result in the pointing accuracy being diminished severely and must therefore be accounted for. This can be ensured by the scheduled maintenance activities detailed in Chapter 7, wherein it has been established sensors will be routinely re-calibrated during the mission. Finally, obstruction of view of the sensors is also a risk that must be considered. This will feed into the configuration of the spacecraft in Chapter 22, where it will be guaranteed that ADCS sensors constantly have unobstructed views of their targets.

16.6. Sustainability

From a sustainability perspective the ADCS performs very well. No thrusters and thus also no toxic gasses are used. Additionally, the star trackers, sun sensors and magnetorquers are made of non-toxic materials. They are made from electronic components which require some chemical processes and specific materials. These are all COTS components and therefore it is hard to trace back the exact materials and processes that were used to manufacture these components. Because of that, the R&D and testing is already performed by the manufacturers. Therefore, the ADCS has a negligible impact on sustainability.

17. Guidance, Navigation & Control Subsystem

In this chapter the design of the GNC subsystem is discussed. As mentioned in the previous report, a Global Navigation Satellite System (GNSS) was chosen for the CASE mission. This means the spacecraft should be able to receive and process signals from GNSS satellites, such as Global Positioning System (GPS), GLObalnaya NAVigatsionnaya Sputnikovaya Sistema (GLONASS) or Galileo satellites. In order to achieve this, the satellite must be equipped with the two components: a GNSS receiver and a GNSS antenna. In Section 17.1 the selection of the navigation receiver is explained. Then, in Section 17.2 the design of the navigation antenna is discussed.

17.1. GNSS Receiver

GNSS receivers for CubeSats are usually quite compact, low cost and are able to operate with different navigation systems (different frequency bands). The main criteria based on which a receiver is selected are mass, size, power consumption, accuracy of the position determination, and the operating frequency range. A comparison between various GNSS receivers is shown in Table 17.1.

Table 17.1: Various GNSS receivers⁶⁴.

Component	Mass [g]	Size [mm]	Power consumption [W]	Accuracy	Navigation System
Hyperion Technologies GNSS200	3	20x15x3	0.15	8 m	Multi-constellation
Spacemanic SM-GNSS-MSP430-SKTRQ	25	67x42x15	0.1	2.5 m	GPS/GLONASS/Beidou
DLR Phoenix-S	20	70x47x15	0.85	10 m	GPS
NewSpace Systems GPS Receiver	110	96x91x18	1	<10 m	GPS

From the above comparison it is concluded that the optimal choice for the navigation receiver is GNSS200 by Hyperion Technologies. It has the lowest power consumption, mass and size. Furthermore, it is able to calculate the solution for the satellite position with 8 m accuracy. GNSS200 is a multi-constellation receiver, hence it can receive signals from GPS, GLONASS, Beidou and Galileo satellites.

17.2. GNSS Antenna

For CubeSats, patch antennas are normally selected as the main navigation antennas, as these are very compact, simple and reliable. The GNSS antenna is selected based on mass, size, power required (in addition to that consumed by the receiver), signal power gain and frequency range in which it can operate. In Table 17.2 a comparison between various GNSS antennas is presented.

⁶⁴<https://satsearch.co/>, [Retrieved on June 1, 2021]

Table 17.2: Various GNSS antennas⁶⁵.

Component	Mass [g]	Size [mm]	Power consumption [W]	Gain [dBi]	Navigation System
ISIS GNSS Patch Antenna	<20	70x70x15	0.05	5.5	GPS-L1 / GALILEO-E1
ANYWAVES GNSS L1/E1 Antenna	86.5	68x70x12.1	0	5.5	GPS-L1 / GALILEO-E1
SkyFox Labs miniPATCH-L1	50	75x75x12.5	0.066	1.5	GPS L1
SkyFox Labs piPATCH-L1E1	50	98x98x13	0.066	1.5	GPS-L1 / GALILEO-E1

The comparison above shows the GNSS Patch Antenna by ISISpace is the optimal choice, mainly because of its mass. The GNSS Patch Antenna operates in L1 and E1 frequency bands which means it is compatible with both GPS and Galileo systems. This antenna can be connected directly to the GNSS receiver. The connector is for both radio signal and supply power.

17.3. Verification and Validation

The V&V procedures for the GNC subsystem mainly relate to its components and their integration. As it only consists of two low-complexity components, this will result in a relatively simple description of V&V procedures. The main procedure will be testing. As the components are obtained from a third party, they will be verified and validated. This leaves for the subsystem integration to be the main source of testing. Ensuring that the antenna has an unobstructed line of communication with the receiver is of primary importance. Then, the same conclusion must be observed in the receiver's connection to the CDH subsystem. Eventually, a system level test and simulation will need to be performed analyzing the entire GNC subsystem's competence amongst its counterparts.

17.4. Risk

The risks identified for the GNC subsystem stem from the two components of which it comprises. These include the patch antenna, and the navigation receiver. If either of these were to fail or be occluded in fulfilling their functions, the mission would face significant communication errors. For this reason, several areas of failure for the patch antenna have been identified. One such failure would be the harsh environment of space to which the patch antenna must be exposed (**RSK-GNC1**). The radiation and temperature gradient pose significant threats to any components exposed to the exterior of the spacecraft. Additionally, the remaining external components (solar arrays) could obscure the antenna's direct line of sight and inhibit its function (**RSK-GNC2**). These risks have been taken into account in the design phase, and will be mitigated as necessary. Regarding the receiver, its connectivity with the patch antennae and TT&C subsystem must be made sufficiently robust (**RSK-GNC3**). The risks of this component's failure will primarily be sought to be mitigated by adequate testing. Furthermore, subsystem wide testing will also ensure proper functionality.

17.5. Sustainability

For the GNC subsystem only two main components are considered, the GNSS receiver and the GNSS antenna. Both components are made of electronic components which require certain chemical processes and materials. Since they are COTS components, it is hard to trace back the sustainability impact of these processes and materials used. It is known that Hyperion Technologies and ISISpace take sustainability into account in their designs and therefore it is assumed that these components have a negligible impact on the sustainability of the mission. Both the receiver and the antenna make use of the transmission of electromagnetic waves which are harmless to the environment.

⁶⁵<https://satsearch.co/>, [Retrieved on June 5, 2021]

18. Electrical Power Subsystem

The EPS subsystem concerns the power generation, storage, conditioning and distribution to the other subsystems. It should be able to supply all the subsystems with enough power for them to operate when necessary. The power needs to be regulated to avoid the occurrence of one subsystem consuming the power of others. The EPS should also generate and store the right amount of power, which is done with solar arrays and batteries. In the Midterm Report [1], a trade-off was performed for the different design options for the three EPS subsystems: power generation, power storage and power conditioning and distribution. In this final phase of the project, the components for the subsystem are sized and selected in Section 18.1. After that, the calculations of the sizing are verified and validated in Section 18.2 and finally, an analysis on the risk and sustainability of the subsystem and its components is performed in Section 18.3 and Section 18.4, respectively. The results of the sizing and component selection of the EPS subsystem are summarized in Chapter 23 and also the electrical block diagram is explained there.

18.1. Subsystem Selection

For the EPS, a trade-off was performed in the Midterm Review for which the optimal design option for power generation was chosen to be solar power [1]. For power storage, the use of secondary batteries was chosen, and for power conditioning and distribution a PCDU would be used. In this section, the sizing and selection of these components are done. The sizing of both the solar array and the battery are performed based on the computations that were given in a paper about the design of the EPS systems for satellites [75].

Before any sizing can be done, the subsystems' total power requirements were determined. This is a driving factor in the sizing of the solar array. The solar array power can be obtained with Equation 18.1. Here, P_d and P_e represent the power consumed by the subsystems during daylight and eclipse, respectively. Also, T_d and T_e represent the duration of day and eclipse and finally, η_d and η_e are efficiencies related to the day and eclipse time, respectively. This equation is a preliminary estimation and is not optimised for this specific mission. Therefore, the previous equation was expanded to account for the active and non-active times of the different subsystems. This is shown in Equation 18.1.

$$P_{SA} = \frac{\frac{P_d T_d}{\eta_d} + \frac{P_e T_e}{\eta_e}}{T_d} = \frac{\sum P_{\text{subsystem}} T_{\text{active}}}{\eta_d} + \frac{\sum P_{\text{subsystem}} T_{\text{non-active}}}{\eta_e} = 33.37 \text{ [W]} \quad (18.1)$$

Knowing this, the sizing of the solar array and the battery can easily be performed. The parameters that are used and the intermediate results that are obtained in the sizing of the solar array and the battery, are given in Table 18.1 and Table 18.3, respectively.

18.1.1. Solar Array

This section explains the process for obtaining the solar array by first sizing the solar array and after that, selecting the most optimal solar cell. It should be noted that for the sizing of the solar array, some iterations were done starting with assumptions for certain solar cell parameters, which were later substituted for the selected solar cell parameters.

Sizing

The solar power that needs to be generated by the solar arrays was obtained in Equation 18.1. The next step in the sizing process is that the Begin Of Life (BOL) and EOL power need to be obtained, which is done using Equation 18.2 and Equation 18.3. Note that all the values of the used parameters in the following equations are given in Table 18.1.

$$P_{\text{BOL}} = P_o \cdot \eta_{\text{cell}} \cdot I_d \cdot \cos \theta \quad (18.2)$$

$$P_{\text{EOL}} = P_{\text{BOL}} \cdot (1 - \text{degradation per year})^{\text{lifetime}} \quad (18.3)$$

The solar intensity P_o is known to be roughly 1360 W/m^2 , η_{cell} is the efficiency of the solar cell, I_d is the inherent degradation, and θ is the incidence angle the cells make with the sunlight. This is taken into consideration by taking the average incidence efficiency over the whole orbit. The maximum incidence angle of 90 degrees is reached two times every orbit and in the middle of those an incidence angle of 0 degrees is reached. This results in an average incidence efficiency of $\cos \theta = \frac{2}{\pi}$. Now that P_{EOL} is known, the solar array area and the array mass can be found using Equation 18.4.

$$A_{\text{SA}} = \frac{P_{\text{SA}}}{P_{\text{EOL}}} \quad M_{\text{SA}} = \frac{P_{\text{SA}}}{\delta_p} \quad (18.4)$$

In this last equation, δ_p represents the power density of the solar array. Lastly, the number of cells that are necessary to supply enough power to the satellite should be calculated. This was done by dividing the estimation of the solar array area by the area of a single solar cell as seen in Equation 18.5.

$$N = \frac{A_{\text{SA}}}{A_{\text{cell}}} = 49 \quad (18.5)$$

From this equation, the maximum amount of cells is chosen. The values obtained by this derivation are just estimates since some parameters, such as the inherent degradation, the incidence angle and the degradation per year, were based on estimated values obtained by other examples using this same procedure. It needs to be noted that redundant solar cells will be included in the design to account for failing solar cells. This will be elaborated upon in Chapter 22.

The solar arrays will consist of two deployable panels, one on each of the sides (2U by 3U) of the spacecraft, with two static arrays placed on the front side (2U by 2U) and the top side (2U by 3U). The general layout of the solar arrays is explained in more detail in Chapter 22.

Table 18.1: Parameters and intermediate results used for solar array sizing.

Parameter	Symbol	Unit	Value	Parameter	Symbol	Unit	Value
Power per unit area solar cell	P_o	$[\frac{\text{W}}{\text{m}^2}]$	435.52	Average incident angle	θ_{avg}	[rad]	$\frac{2}{\pi}$
Solar cell efficiency	η_{cell}	[-]	0.32	Solar cell degradation per year	δ	[-]	0.04
Solar constant	G_s	$[\frac{\text{W}}{\text{m}^2}]$	1361	Satellite lifetime	N	[year]	2
Orbital period (at 500 km)	T_{tot}	[min]	94.62	Life degradation factor	L_d	[-]	0.9216
Eclipse time	T_e	[min]	35.75	Power density	δ_p	$[\frac{\text{W}}{\text{kg}}]$	30
Day time	T_d	[min]	58.87	Beginning of life power	P_{BOL}	$[\frac{\text{W}}{\text{m}^2}]$	213.5
Path efficiency day	η_d	[-]	0.85	End of life power	P_{EOL}	$[\frac{\text{W}}{\text{m}^2}]$	196.75
Path efficiency eclipse	η_e	[-]	0.65	Solar array area	A_{SA}	$[\text{m}^2]$	0.156
Solar Array power	P_{SA}	[W]	30.73	Solar array mass	M_{SA}	[kg]	1.024
Inherent degradation	I_d	[-]	0.77	Number of cells	N	[-]	49

Component selection

During the design of the solar arrays it was chosen not to go for a COTS solar array as it is hard to find them with the correct dimensions, the correct deploying mechanism or the right power requirements. For this reason, the solar array will be created from COTS solar cells. For the solar cell, efficiency is the most important and defining parameter for the design of the solar array. When looking into the different options for solar cells, it became clear that the *QJ Solar Cell 4G32C* from Azur Space had the best performance with an solar cell efficiency of 32% meaning that this solar cell can convert 32% of the the incoming solar energy into electrical power. The other properties of this cell can be found in Table 18.2.

Table 18.2: Properties of the selected solar cell⁶⁶.

QJ Solar Cell 4G32C - Azur Space	
Efficiency	32%
Base material	AlInGaP/AlInGaAs/InGaAs/Ge on Ge
Dimensions	40 x 80 mm ± 0.1 mm
Weight	≤ 1780 mg
Voltage at max. Power V_{mp}	3025 mV
Current at max. Power I_{mp}	433.5 mA
Price (62 cells)	17,500 €

Having dimensions as given in Table 18.2, it is possible to meet the power requirements with three panels with an area of 2U by 3U each and one panel of 2U by 2U. If another solar cell with the same dimensions and lower efficiency would be used, the number of cells and the number of panels would both increase. On top of that, some margin is needed for when the solar cells start degrading. Therefore, some spare solar cells are implemented as back-up. The *QJ Solar Cell 4G32C* was chosen to be the most optimal since it meets all the requirements while offering high efficiency.

18.1.2. Battery

In this section the battery of the EPS subsystem is first sized and then a COTS battery is chosen. The battery needs to be able to store enough power to supply all the subsystems with power during eclipse times.

Sizing

The sizing of the battery is done to estimate its mass and volume. The methods and equations used for this are again obtained from the paper on electrical power system design for satellites [75]. First of all, the amount of energy the battery must be able to store (capacitance) is calculated by Equation 18.6. With that, it is possible to calculate the EOL and the BOL capacitance of the battery which can also be found in Equation 18.6.

$$C_{\text{req}} = P_e \cdot T_e \quad C_{\text{EOL}} = \frac{C_{\text{req}}}{\text{DOD} \cdot \eta_{\text{bat}}} \quad C_{\text{BOL}} = \frac{C_{\text{EOL}}}{1 - F_{\text{fading}} N} \quad (18.6)$$

In these equations, P_e and T_e represent the eclipse power and time. The parameters DOD, η_{bat} , F_{fading} and N are the Depth of Discharge, the battery efficiency, a fading factor and the lifetime of the satellite, respectively. The final step is to estimate the mass and volume of the battery by using the specific mass (m_{sp}) and the energy density (e_{density}) of the battery in Equation 18.7.

$$M_{\text{battery}} = \frac{C_{\text{BOL}}}{m_{sp}} \quad V_{\text{battery}} = \frac{C_{\text{BOL}}}{e_{\text{density}}} \quad (18.7)$$

⁶⁶http://www.azurspace.com/images/0005979-01-01_DB_4G32C_Advanced.pdf, [Retrieved on June 7, 2021]

Finally, the estimated values for the mass and volume are found for the final design of the battery. All of the parameters used for the battery sizing, including the final mass and volume of the battery, can be found in Table 18.3.

Table 18.3: Parameters and intermediate results used for battery sizing.

Parameter	Symbol	Unit	Value	Parameter	Symbol	Unit	Value
State of charge	SoS	[-]	0.7	Capacity at beginning of life	C_{BOL}	[Wh]	64.45
Depth of discharge	DoD	[-]	0.3	Specific mass	m_{sp}	$[\frac{Wh}{kg}]$	200
Required capacitance	C_{req}	[Wh]	17.05	Energy density	e_{dens}	$[\frac{Wh}{L}]$	400
Battery efficiency	η_{bat}	[-]	0.9	Battery mass	M_{bat}	[kg]	0.322
Fading factor	F_{fading}	[-]	0.01	Battery volume	V_{bat}	[L]	0.161
Capacity at end of life	C_{EOL}	[Wh]	63.16				

Component selection

The most important parameter to take into account when choosing a battery is the capacity of the battery. It can be seen in Table 18.3 that the BOL capacitance is given to be 64.45 Wh. From this it can be determined that the battery needs to have a capacitance that is higher than this previously mentioned number.

The battery also needs to be easily integratable with the other components of the EPS subsystem. For this reason, it was preferred to choose a battery pack that is easily compatible with the PCDU. The main two options that fitted this requirement were the ISISpace battery of their modular EPS (90 Wh)⁶⁷ and the *OPTIMUS-80* battery from AAC Clyde Space (80 Wh)⁶⁸. From these two options, the *OPTIMUS-80* battery was chosen to be the most optimal one because it is lighter than the ISISpace battery and it fits the required capacitance better as it has 80 Wh of capacitance compared to 90 Wh for the ISISpace battery. Because of space constraints in the structure of the satellite, it was chosen to use two lower capacitance batteries in parallel as this doubles the total capacitance. For this, two 40-Wh *OPTIMUS-40* batteries by AAC Clyde Space are used, resulting in a total capacitance of 80 Wh. These *OPTIMUS-40* batteries have the same specifications as the *OPTIMUS-80* battery but they are smaller. Important properties of the *OPTIMUS-40* battery are given in Table 18.4.

Table 18.4: Properties of the selected battery⁶⁸.

OPTIMUS-40 - AAC Clyde Space	
Capacity	40 Wh
Material	Lithium Polymer
Mass	335 g
Dimensions	95.89 x 90.17 x 27.35 mm
Charge/discharge current	2.6 A
Power consumption	< 0.1 W
Power buses	3.3V and 5V
Price (2 units)	€16000

18.1.3. Power Conditioning and Distribution Unit (PCDU)

In this section, the PCDU is obtained. This component consists of two main modules: a Power Conditioning Unit (PCU) and a Power Distribution Unit (PDU). The solar arrays generate power at unstable high voltages. These solar arrays are connected to the PCU, which converts the solar array voltage down to a lower stable voltage level of the PDU with step down buck Battery Charge Regulators (BCR). These BCRs are Maximum Power Point Tracking- (MPPT-) based. This is the most efficient and the reason for this is that the unstable voltages can be converted to lower stable voltages while operating the solar arrays at their maximum power point. The PDU is responsible for the conversion of the PCU voltages to three lower voltage levels, 3.3 V, 5 V and 12 V, used for the different subsystems. These modules of the PCDU are often offered together as COTS PCDU components. For this reason no sizing was needed. [76]

⁶⁷https://www.isispace.nl/wp-content/uploads/2019/12/ISIS-iMEPSv2-DS-00001-iEPS_Datasheet_v0.2-.pdf, [Retrieved on June 7, 2021]

⁶⁸https://www.aac-clyde.space/assets/000/000/180/AAC_DataSheet_Optimus_original.pdf, [Retrieved on June 7, 2021]

Component selection

For the selection of a PCDU, the amount of outputs the module has, plays an important role. Outputs of this system are regulated buses of 3.3V, 5V and 12V and also unregulated buses such as the battery. The amount of outputs needed for the satellite components turns out to be around 19. The two options that were considered are the *STARBUCK-NANO-PLUS* from AAC Clyde Space and the modular EPS PCDU from ISISpace. Only these options were considered because they are nicely integratable with the rest of the EPS components and they already include MPPT, Battery Charge Regulators and other protection circuits. Both of these options have similar performance, but there are more system specifics given about the *STARBUCK-NANO-PLUS*. On top of that, the AAC Clyde Space *OPTIMUS-40* batteries were chosen to be the most optimal batteries for the EPS. Therefore, the best option for a PCDU would be the *STARBUCK-NANO-PLUS* since it satisfies all the requirements better than the ISISpace PCDU and is better integratable with the other EPS components than the ISISpace PCDU. This PCDU only has 10 power outputs, meaning that two of these PCDU's will be needed. In Table 18.5, the most important parameters of the *STARBUCK-NANO-PLUS* are given.

Table 18.5: Properties of the selected PCDU⁶⁹.

STARBUCK-NANO-PLUS - AAC Clyde Space	
Mass	148 g
Dimensions	95.89 x 90.17 x 20.82 mm
Regulated power buses	3.3V, 5V and 12V
Interfaces	I2C
Number of outputs	10
Power consumption	0.5 W
Price (2 units)	€18000

18.2. Verification and Validation

For the EPS subsystem, there are extensive procedures for verification and validation. In the scope of this project, only the calculations for the sizing of the EPS modules were verified by checking the calculations manually. In further design phases more extensive verification and validation can be performed. This can be done with the following methods.

The EPS consists of different modules that are all interconnected. These modules, such as the solar panels, battery and PCDU all consist of electronic components which make up smaller modules such as controllers, opamps, multiplexers, pulse width modulators (PWM), registers, input buffers, etc. These smaller modules send and receive digital signals at a speed in the order of nanoseconds. Therefore, the correct signals must be sent at the correct times. This can be analysed by using a VHDL software (e.g. ModelSim). With this software, the digital signals can be analysed in depth within the modules themselves and also between the different modules.

The EPS subsystem can be validated by measuring the voltages and currents at all the components in the circuit. This can be done using specialized software in which the electronic circuits can be simulated and checked for their voltage and current levels in different situations. An example of such a software is the freely available LTspice. Once the electronic circuits are manufactured and validated by the software, the same analysis can also be performed on the hardware components with an oscilloscope to see if it has the same results as the software.

18.3. Risk

Addressing the risks related to the EPS subsystem is of utmost importance. As established in Chapter 7, the EPS system can be responsible for mission failure in anywhere from 28% to 44% of CubeSat missions. Thus, it is incredibly important to identify and mitigate the risks of this subsystem as effectively as possible. The first such risk involves the failure of the power supply. If this would occur, it would likely occur due to a failure in the

⁶⁹https://www.aac-clyde.space/assets/000/000/188/AAC_DataSheet_Starbuck-Nano_original.pdf, [Retrieved on June 7, 2021]

photo-voltaic cells of the solar arrays (**RSK-EPS1**). These are highly fragile, and thus several redundant cells are included in the design to factor in their potential failure.

Similarly, the power storage unit must also be sufficiently tested. The batteries which serve to store the power will suffer from degradation over time. In addition to this, battery leakage could occur which would severely threaten the mission (**RSK-EPS2**). For this reason, the batteries will be sufficiently tested to ensure their reliability. When one of the batteries would fail, there is still a chance to keep the mission going with taking less measurements since there are two 40 Wh batteries available in the satellite. Also, subject to testing will be the hinge upon which the solar arrays will be deployed (**RSK-EPS3**). Since it will only be deployed once, fatigue testing will likely not be necessary as the residual torque on the hinge was calculated to be 29.8 nNm (Equation 16.4). Nevertheless, stress and load testing will be vital to ensure that the torque required during the deployment phase will not cause structural failure.

Finally, the risks accompanying the PCDU must also be addressed. A few risks are stated in the user manual [76] and can be discussed. If the switch configuration is incorrect while power is applied, the output of the BCR can be blown, which results in a failure of the EPS (**RSK-EPS4**). Furthermore, exceeding maximum ratings (such as exceeding temperature ranges, vibration and radiation levels) should be avoided. Additionally, the connections to the batteries, solar panels and various subsystems must be tested as they can thermally expand, causing temperature problems. The appropriate level of power must be supplied to each subsystem (**RSK-EPS5**). Furthermore, the CDH bus must not be overloaded in power, as this risk goes hand-in-hand with the CDH subsystem. More details can be found in Chapter 13.

18.4. Sustainability

The EPS consists of multiple components, which should all be considered regarding sustainability. First of all, there are the solar arrays with solar cells. The solar cells used for the mission are quadruple junction gallium arsenide-based. Using this material gives two main drawbacks when it comes to sustainability. Firstly, gallium is a material that is rarer than gold and is very costly. Therefore, the long term use of this material is not so environmentally sustainable. The second drawback is that arsenide is poisonous, creating safety issues in the manufacturing process of these solar cells. This can be accounted for by taking safety precautions.

The lithium in the lithium-based battery used in the satellite is considered a hazardous material. Safety precautions must be made in the manufacturing process. It was stated in the Midterm Review that safety mechanisms should be built for for the battery not to explode [1]. The PCDU module incorporates battery charge and discharge regulator systems, which accounts for this safety and includes these mechanisms [76]. It should also be noted that batteries will be fully discharged at EOL. In general, the EPS consists of electronic components which need to be manufactured from raw materials, using plastics, metals and chemicals. This is not the most sustainable subsystem, but sustainability considerations can be taken into account to minimize the impact on its environment.

To conclude, the EPS has been designed, sized and a choice of the different components has been made in this chapter. It is designed in such a way that it is able to satisfy the power generation and storage requirements. The power is generated by 62 *QJ Solar Cells 4G32C* from Azur Space that are placed on 4 solar arrays of which two panels are deployable. The power is stored by using 2 *OPTIMUS-40* (40 Wh) batteries from AAC Clyde Space which are very compatible with the 2 PCDU's, *STARBUCK-NANO-PLUS* from AAC Clyde Space, which take care of the power conditioning and distribution to the different subsystems.

19. Structural & Material Characteristics

In this chapter the structural and material characteristics of the CASE CubeSat are presented. Firstly, the primary structure selection is discussed using a structural analysis of the CubeSat. This is followed by the design of a platform for the TNO Optical Metasurfaces Based Spectro-Polarimeter payload. Then, the model verification and validation is presented. Finally, the chapter is concluded with risk and sustainability analysis in Section 19.5 and Section 19.6 respectively.

19.1. Primary Structure Selection

In this section, the primary structure selection is explained. Firstly, the components that were selected is discussed in. Then, the structural analysis is presented. The section ends with a depressurization compatibility.

19.1.1. Component Selection

The trade-off for the shape of the structure has been performed in the midterm report [1]. Three conceptual load-carrying structures were considered: a CubeSat, cuboid, and cylinder. The criteria for the trade-off included space efficiency, lateral and axial natural frequencies, mass, production cost, and volume. Each criteria was assigned a weight based on the importance of this factor for the structure effectiveness. Using the AHP method resulted in a CubeSat structure being chosen.

In order to reduce costs and development time, a COTS structure was chosen. Before selecting the product, the required dimensions of the spacecraft had to be known. Initially, the preliminary design resulted in a 6U CubeSat. However, after detailed design of each subsystem, 6U turned out to provide too little space. The main contributor to the size increase is the payload. Firstly, the number of detectors was raised from one to three. Secondly, it has to be fully covered by the structure and cannot protrude out of the spacecraft, which was initially thought not to be the case. This resulted in 12U being the necessary option for the CASE mission.

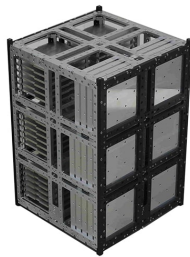


Figure 19.1: 12-Unit CubeSat structure from ISISpace.

The market of 12U CubeSats is not as sizable as those for smaller satellites like 1U, 2U or 3U. It was found that three companies sell COTS structures: ISISpace, NPC Spacemind and Hyperion Technologies. Due to the fact that most components are manufactured in the Netherlands, the NPC Spacemind option is dismissed in order to reduce transportation costs⁷⁰. The bus option from ISISpace mentions compatibility with GomSpace, ClydeSpace and the most of the CubeSatShop products⁷¹, whereas Hyperion offers only compatibility with their own components⁷². Additionally, the ISISpace structure is lighter by 200 g. Therefore, the 12-Unit CubeSat structure from ISISpace was chosen. It can be seen in Figure 19.1⁷¹.

The structure offers detachable side panels for maximum accessibility during assembly. The side frames and ribs act as a primary structure and secondary structural elements are shear panels and printed circuit board (PCB) mounting elements. The structural characteristics are shown in Table 19.1.

⁷⁰<https://www.npcspacemind.com/store/#!/SM12/p/172169670/category=43807390>, [Retrieved on June 1, 2021]

⁷¹<https://www.isispace.nl/product/12-unit-cubesat-structure/>, [Retrieved on June 1, 2021]

⁷²<https://hyperiontechnologies.nl/products/sat12u/>, [Retrieved on June 1, 2021]

Table 19.1: Properties of the selected 12U structure from ISISpace⁷¹.

12-Unit CubeSat structure	
Primary structure mass	1.5 kg
Primary + secondary structure mass	2 kg
Outside envelope (l x w x h)	226.3 x 226.3 x 340.5 mm ³
Inside 1U envelope (l x w x h)	98.4 x 98.4 x 98.4 mm ³
Thermal range	-40 °C to +80 °C
Cost	11,950 €

The ISISpace website does not provide any information about the material used for the structure. According to NASA⁷³, most primary structures are machined from Aluminum alloy 7075 for which the properties at 25 °C are listed in Table 19.2.

Table 19.2: Properties of the Aluminum 7075-T6⁷⁴.

Property	Value	Unit
Density	2810	kg/m ³
Yield strength	572	MPa
Elastic modulus	71.7	GPa
Poisson ratio	0.33	-

19.1.2. Structural Analysis

The selected 12U structure from ISISpace needs to meet the subsystem requirements indicated in Chapter 3. Starting with **CASE-SYS-STR-A01**, the structure allows for subsystem altering and calibration after installation as the side shear panel can be detached and all components are easily accessible. Next, regarding **CASE-SYS-STR-A02**, the structure is designed to support all the subsystems for the duration of the CASE mission. It includes dynamic loads during launch, 0g loads, and micro-meteorites/debris [77]. The main focus of the structural analysis is on requirements **CASE-SYS-STR-A03** and **CASE-SYS-STR-A06**, which specify launch loads and natural frequencies of the CubeSat. The selected launcher, which will be elaborated upon in Chapter 20, provides a user guide which specifies the launch loads. However, the information on the fundamental frequencies is missing and therefore needed to be estimated. For instance, the Ariane 4 and Ariane 5 requirements are 10 Hz lateral and 31 Hz axial for small satellites [78][79], and the Falcon 9⁷⁵ requires 35 Hz of natural frequency. However, looking into mission planning guide from Spaceflight, the minimal fundamental frequencies for CubeSats are much higher⁷⁶. Therefore, it was decided to use 150 Hz in both directions as a requirement.

There are many dynamic loads that the spacecraft undergoes during the launch. Starting with the acceleration loads which are caused by decreasing launcher propellant mass, which is most significant in the later phase of the launch. Then, the shock loads are created by separation of stages and the separation of the spacecraft. The acoustic loads are generated by the working engines as well as the airflow separation (aerodynamic noise). Finally, there are random loads which are usually covered by acoustic loads [77].

Additionally, the transportation loads were included into the analysis. The loads experienced by the satellite are summarized in Table 19.3. As can be seen, the most intense loads are generated by shock loads in magnitude of 700 g. However, it is a peak value and it mainly occurs close to the source. The period in which it is caused is also small, in the range of microseconds, thus it is not the most critical load as it reduces in magnitude along the load path [80]. The most critical loads are acceleration loads, so 7 g compressive load in axial direction and 2 g load applied laterally.

⁷³<https://www.nasa.gov/smallsat-institute/sst-soa-2020/structures-materials-and-mechanisms>, [Retrieved on June 3, 2021]

⁷⁴<http://www.matweb.com/search/DataSheet.aspx?MatGUID=4f19a42be94546b686bbf43f79c51b7d&ckck=1>, [Retrieved on 3 June, 2021]

⁷⁵<https://www.spacex.com/vehicles/falcon-9/>, [Retrieved on May 31, 2021]

⁷⁶<http://spaceflight.com/wp-content/uploads/2019/02/Spaceflight-Mission-Planning-Guide-Rev-G.pdf>, [Retrieved on June 18, 2021]

Table 19.3: Loads experienced by the spacecraft during CASE mission⁷⁷.

Type	Axial	Lateral	Unit
Launch loads			
Acceleration loads	7.5	2	g
Shock loads	700	700	g
Acoustic loads(100-160 Hz)	112	112	dB
Transportation loads			
Water	0.5	2.5	g
Air	3	1.5	g
Truck	3.5	2	g

In order to find the stresses within the structure, some geometrical properties had to be calculated. These characteristics can be seen in Table 19.4. The method is presented in Appendix B.

Table 19.4: Geometrical properties of the 12U CubeSat.

Property	Value	Unit
Axial cross section		
Area	1021.92	mm ²
Second moment of area x	15,670,046.91	mm ⁴
Second moment of area z	4,622,092.82	mm ⁴
Lateral cross section		
Area	484.48	mm ²

The structural analysis starts with establishing the safety factor. It was decided that the structure shall not yield under critical conditions so a yield safety factor of 1.25 was selected [77].

The lateral load is fairly easy to calculate as it is lateral acceleration multiplied by the mass of the spacecraft. Axial load is a combination of axial acceleration and the bending moment due to lateral load acting at the center of gravity of the satellite. The latter can be transformed into axial force as follows [81]:

$$P_{eq} = P_{axial} + \frac{2M}{R} \quad (19.1)$$

Here, P_{axial} is the initial axial load, M is the bending moment and R is the distance between the center of gravity and the side wall.

The natural frequencies can be estimated based on the assumption that the spacecraft is a uniform beam. Considering only the first fundamental frequencies, the structure might be idealized as a single-degree-of-freedom spring-mass system. It follows that natural frequencies equal [81]:

$$f_{lateral} = 0.56 \sqrt{\frac{EI}{mL^3}} \quad (19.2)$$

$$f_{axial} = 0.25 \sqrt{\frac{AE}{mL}} \quad (19.3)$$

Here, E is the elastic modulus, I is a cross-section's second moment of area, m is the mass of satellite, L is the height of satellite and A is a cross-sectional area. The first fundamental frequencies must be larger than the requirements in order to avoid interaction with launch vehicle.

Finally, the Margin of Safety (MS) is calculated with:

$$MS = \frac{\sigma_{allowable}}{\sigma_{design}} - 1 \quad (19.4)$$

⁷⁷<https://www.rocketlabusa.com/assets/Uploads/Payload-User-Guide-LAUNCH-V6.6.pdf>, [Retrieved on 2 June, 2021]

where $\sigma_{\text{allowable}}$ is the yield stress of the material and σ_{design} is calculated with the safety factor. The MS has to be larger than 0. The results of the structural analysis are shown in Table 19.5. The most critical loading scenarios are the acceleration loads as they are experienced for the whole last phase of the launch. The shock loads are much higher in intensity but due to small duration and small probability of transferring the peak loads.

Table 19.5: Structural analysis results of the primary structure.

Type	Axial	MS	Lateral	MS
Launch stresses				
Acceleration loads	1.72 MPa	331.95	0.63 MPa	906.62
Shock loads	313.72 MPa	0.82	220.58 MPa	1.59
Transportation stresses				
Water	0.82 MPa	695.16	0.79 MPa	725.09
Air	0.90 MPa	637.15	0.47 MPa	1209.16
Truck	1.12 MPa	509.52	0.63 MPa	906.62
Natural frequencies				
	1356.17 Hz	8.04	1021.56 Hz	5.81

19.1.3. Depressurization Compatibility

Another important factor of the CubeSat structure is the depressurization compatibility. Depressurization occurs when the launch vehicle ascends at high velocity through the atmosphere, and can cause damage to the CubeSat if the rate of depressurization is too high. The structure should be verified to comply with the depressurization requirements.

Literature stipulates two average depressurization rates during ascent:

1. **Sustained depressurization:** of 2.8 kPa/sec, while ascending through the atmosphere
2. **Transient depressurization:** of 4.8 kPa/sec, while the launch vehicle breaks the sound barrier

CubeSat structures are deemed sufficiently resistant to depressurization when⁷⁸:

$$\frac{\text{Volume to be vented}}{\text{Venting area}} < 50.8m$$

For CASE, the volume to be vented is the volume of all components subtracted from the total CubeSat volume, which is $0.0114 - 0.00787 = 0.00353 \text{ m}^3$. To meet the maximum ratio requirement, the minimum venting area is 0.69 cm^2 . Since the holes in the CubeSat structure for the payload cameras alone already have a total venting area of 47.4 cm^2 , the ratio is much lower than 50.8, meaning that the depressurization requirement is met.

19.2. Payload Platform

The requirement **CASE-SYS-STR-A05** states that structure needs to provide a stable platform for the payload. For the vertical detector this does not introduce any problems as it can easily be mounted to the structure using secondary structural elements like 94 x 94 mm PCBs. However, for the two detectors at $+45^\circ$ and -45° , a special platform had to be designed.

Due to the size of the detectors, it cannot be mounted in a 6U CubeSat without sticking out of the satellite. Therefore the decision to increase the size to 12U was made. There were several options considered for the configuration of the payload and the final concept is shown in Figure 19.2. The cameras are facing into each other as otherwise the 12U structure would obstruct the view of the detectors. The payload is mounted at A(A') and C(C') to the

⁷⁸<https://static1.squarespace.com/static/5418c831e4b0fa4ecac1bacd/t/5f24997b6b6dea10cc52bb016/1596234122437/CDS+REV14+2020-07-31+DRAFT.pdf>, [Retrieved on June 21, 2021]

platform with the weight assumed to be distributed evenly. Then the platform is connected to the primary structure at points A(A') and B(B') via bolts/fasteners.

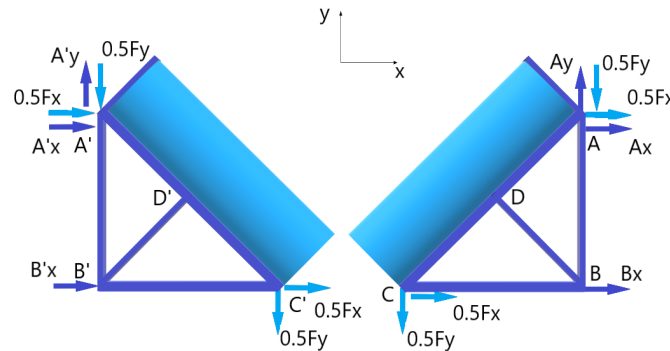


Figure 19.2: Free body diagram of the payload platform.

The platform was analyzed as a truss-like structure. This means that the trusses only transfer axial loads. In the beginning, the vertical reaction forces at B and B' were considered. However, it leads to a statically indeterminate system so they were assumed to be 0 N. Three static equilibrium equations were set up to determine the reaction forces. Then, the stresses inside of each truss were estimated using the method of joints. The chosen material was Aluminum 2014-T6 as indicated by a trade-off made in the midterm report [1]. Its properties are shown in Table 19.6.

Table 19.6: Properties of the Aluminum 2014-T6⁷⁹.

Property	Value	Unit
Density	2800	kg/m ³
Yield strength	395	MPa
Elastic modulus	73.1	GPa
Poisson ratio	0.33	-

The results of the truss-structure analysis are presented in Table 19.7. The mass of the TNO chip instrument was estimated to be 0.57225 kg (with 5% margin) in Chapter 11. For the most critical loading case the acceleration loads are considered and values in Table 19.7 are representative of this scenario. Although it is unlikely that shock loads would propagate to the payload structure, it is still able to withstand the peak shock acceleration of 700 g. The total mass of two stable platforms turned out to be around 0.110 kg.

Table 19.7: Structural analysis results of the payload platform.

Truss	Axial load	Thickness	Stress	MS
AB	0	0.5 mm	0	-
AC	29.77 N	1 mm	0.60 MPa	662.39
CB	-26.67 N	1 mm	0.53 MPa	739.66
DB	0	0.5 mm	0	-
A'B'	0	0.5 mm	0	-
A'C'	29.77 N	1 mm	0.60 MPa	662.39
C'B'	-15.44 N	1 mm	0.31 MPa	1278.32
D'B'	0	0.5 mm	0	-

⁷⁹<http://www.matweb.com/search/DataSheet.aspx?MatGUID=6ad3b196925241c29bb0ac4a4c9d1dc2>, [Retrieved on 8 June, 2021]

19.3. Launcher Integration

One of the requirements that is to be met is **CASE-SYS-STR-A04**. It stipulates that the CubeSat structure shall be properly integrated with the launch vehicle. This means that the CubeSats are attached easily and safely to the payload adapter. The schematic for the payload layout in the launch vehicle can be seen in Figure 19.3. In total, CASE consists of three 12U CubeSats. They will be connected with each other and then the whole payload is linked to the Electron launcher via a connection with the Kick Stage (optional third stage for orbit insertion)⁷⁷. Further information about launcher deployers are presented in Section 20.5.

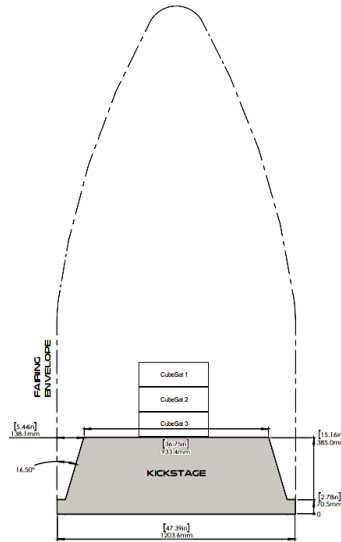


Figure 19.3: Payload integration into the launch vehicle [82]

19.4. Verification and Validation

For the structural model several tests were performed in order to confirm the calculation and check for possible mistakes. They are shown in Table 19.8. Firstly, the centroid calculations were verified. This was done by doubling all the lengths of the cross section geometries. It resulted in centroid values twice as high which means that their positions remain the same w.r.t. the larger shapes. In the table, one of the shapes is shown (Area A) but the result was consistent among the others as well. Next, the total inertia (excluding Steiner terms) was checked. The respective length values were doubled to see if the second moment of area increases by a factor of 3 as the formula $I_x = \int y^2 dA$ suggests. This check was performed for inertia around the x and z axes. Then, doubling lateral and axial loads resulted in stress increasing by a factor of 2 as expected. For the payload platform the signs of the loads were changed. As expected, the negative lateral load would cause lower compressive stress in beam CB and no change in beam AC. The negative axial load changed the loading in beam AC (from tension to compression) and also impacted the beam CB by magnitude and sign. The loading is symmetric to the negative lateral load change so the values for axial loads are the same but with different signs. These tests ensure that the model works as it was intended to do.

Table 19.8: Verification tests on structural model.

Test	Initial value	Outcome value	Change
Doubling all lengths	10.78 mm x 3.18 mm	21.57 mm x 6.36 mm	x2
Doubling x direction lengths	8475 mm ⁴	67799 mm ⁴	x8
Doubling z direction lengths	3838 mm ⁴	30708 mm ⁴	x8
Doubling lateral and axial loads	1.72 MPa & 0.63 MPa	3.47 MPa & 1.27 MPa	x2
Changing sign of lateral load	AC: 29.77 N, CB: -26.67 N	AC: 29.77 N, CB: -15.44 N	x1, x0.58
Changing sign of axial load	AC: 29.77 N, CB: -26.67 N	AC: -29.77 N, CB: 15.44 N	x-1, x-0.58

The selected component, the 12U CubeSat structure from ISISpace, is also validated. Several QT and AT are performed. The QT involve functional, vibration, mechanical shock, thermal cycling, and thermal vacuum tests. The AT focuses on functional performance⁷¹. QT is performed on the design/qualification model and AT is performed on the unit to be shipped. For all of these tests, the hardware is qualified against NASA's general environment verification standard⁸⁰ [O] .

19.5. Risk

The risks of the structural system have a significant impact on the success of the mission. The structure is a system that links all other subsystems together while also supporting and transferring loads. On the scale of Risk Priority Number, the structure system scores the highest 100 [83]. It means that any failure of this subsystem would have a catastrophic consequences for the CASE mission.

The first risk involves **RSK-STR1**, primary structure failure. It has the highest impact of all structural risks. The probability of this is relatively small. In the worst case scenario, if the acceleration load would propagate into the CubeSat (7.5 g and 2 g), the MS is still 331.95 and 906.62 for axial and lateral stress respectively. Therefore, the maximally allowable stress is about 300 times more than the designed stress. Then, **RSK-STR2** discusses secondary structure failure which are the shear panels covering the spacecraft and the PCB panels which mount subsystems to the structure. This also involves **RSK-STR3** - subsystem attachment failure. These will be ensured by performing proper verification tests. Next, the deformation of the structure (**RSK-STR4**) means that the structure could deform plastically (permanently). The design uses the yield stress as an allowable stress with proper MS which makes sure that the structure does not yield under most critical loads. Then, **RSK-STR5** discusses the payload platform failure. Similarly to other failures, it is ensured by margins of failure and a safety factor which equals 1.25 for yield stress. Finally, there could be material flaws created during the manufacturing process (**RSK-STR6**) which cannot be prevented but can be minimized by selecting proper manufacturing techniques with certain materials.

19.6. Sustainability

For the structure, two main components are considered: 12U structure and payload platform. For both, aluminum alloys were used so no toxic materials are present. They do require some energy and labor during the manufacturing phase. The 12U structure comes from ISISpace. Buying off-the-shelf components improves the sustainability of the mission compared to the designed parts. Additionally, the components are manufactured in the Netherlands which reduces the transportation needs of the parts. Using a COTS option decreases the amount of resources spent on R&D and testing, which has a positive influence on the sustainability of the project.

⁸⁰<https://standards.nasa.gov/standard/gsfc/gsfc-std-7000>, [Retrieved on 14 June, 2021]

20. Launch Vehicle Selection

To ensure the design of the CASE mission encapsulates every mission phase, it is crucial to select a suitable rocket launch vehicle to facilitate the launch of the mission. Firstly, to select the rocket best suited for the mission, multiple rockets from different manufacturers are selected and a trade-off is performed. After a sensitivity analysis is presented, the optimal deployers for the CubeSats are chosen.

20.1. Launch Vehicle Data & Justification

Table 20.1 shows the different grading criteria and the launch vehicles that were considered to perform the trade-off. The first three grading criteria (payload mass, payload volume and orbit capabilities) were not used in the trade-off since all launchers met these requirements for the CASE mission and, therefore, the launch vehicle choice should not depend on these criteria.

Six launch vehicles were considered during the trade-off. Two launchers, the Ariane 5[79] and the Soyuz FG⁸¹ are from ESA. They were selected for their high reliability [28]. The Falcon 9⁷⁵ from SpaceX has shown very high reliability in the past decade. Finally, a few smaller launch vehicle suppliers were chosen for trade-off: Rocket Lab's Electron⁷⁷, Relativity's Terran 1⁸² and Firefly's Alpha rocket⁸³.

Table 20.1: Assessment of the criteria for launcher selection.

Not used in trade-off, Predicted value

Grading criterion	Ariane 5 (ESA, EU)	Soyuz (Energia, Russia)	Falcon 9 (SpaceX, US)	Electron (Rocket Lab, US)	Terran 1 (Relativ- ity, US)	Firefly Alpha (Firefly, US)
Maximum payload mass [t, LEO]	20	7.42	22.8	0.3	1.33	0.85
Payload volume	5.4 m diameter, 17 m tall	3.7 m diameter, 7.7 m tall	5.2 m diameter, 13 m tall	1.2 m diameter, 2.5 tall m	2.5 m diameter, 3.2 m tall	2.2 m diameter, 5.2 m tall
Orbit capabilities	LEO, GTO, GEO	LEO, GTO, GEO	LEO, GTO	LEO, SSO	LEO, SSO	LEO, SSO
Total launch cost [M€]	147	67.2	52.1	6.3	10.1	12.6
Success rate [%]	94.5	94.4	98.2	89.5	90	90
Axial loads [g]	4.4	5	8.5	7.5	6.5	7.7
Lateral loads [g]	2	1.8	3	2	1.75	2.4
Apogee accuracy [km]	2.5	12	10	15	15	15
Inclination accuracy [deg]	0.04	0.12	0.1	0.15	0.1	0.1
Launches per year	3	3	27	7	4	4
Re-usability [no = 1, yes = 10]	1	1	10	10	10	10

Currently, the Terran 1 and Firefly Alpha launch vehicles are still in their development phase and have not launched yet. With the Terran 1 rocket aiming to be operational by the end of 2021⁸⁴ and the Firefly Alpha set for launch

⁸¹<https://www.arianespace.com/wp-content/uploads/2015/09/Soyuz-Users-Manual-March-2012.pdf>, [Retrieved on May 31, 2021]

⁸²<https://www.relativityspace.com/terran/>, [Retrieved on May 31, 2021]

⁸³<https://firefly.com/launch-alpha/>, [Retrieved on May 31, 2021]

⁸⁴<https://spaceflightnow.com/2020/06/24/relativity-books-up-to-six-launches-for-iridium-announces-plans-for-vandenberg-pad>, [Retrieved June 12, 2021]

by the end of June 2021⁸⁵, both of these rocket were included into the launch vehicle trade-off since the CASE mission is planned for launch in 2027[1].

20.2. Dedicated Launch Justification

When planning to launch a satellite, companies can choose to share the launch with satellites from other companies (known as ridesharing) or launch only their own satellite(s) (dedicated launch). Ridesharing thus consists of sharing the available space on a rocket with multiple customers, decreasing the overall costs. Even though the number of companies offering ridesharing options has been growing over the past few years, dedicated launches remain more common. For the CASE mission, the decision was made to opt for a dedicated launch. The justifications for choosing a dedicated launch and rejecting ridesharing are given below:

1. **Flexibility in launch date:** With the low TRL levels of both CASE's payload and TT&C system, there is a large amount of uncertainty regarding the launch date of the mission. This makes scheduling for a rideshare mission complicated and uncertain. Delays in development and manufacturing can thus cause delays to the entire rideshare launch. This problem is solved by choosing a dedicated launch instead.
2. **Restrictions to orbital choice:** Ridesharing inherently limits the flexibility of orbit selection since all satellites are forced to be launched into the same orbit. Most CubeSats are launched to sun-synchronous or geostationary orbits (GEO), so CASE's equatorial orbit (0° inclination) is an uncommon option. This means the demand for ridesharing to this orbit will be low, which might delay the launch after a date has been planned.
3. **Larger offer of launch vehicles:** Not all manufacturers offer ridesharing options with their launch vehicles. Therefore, choosing a dedicated launch increases the number of available launch vehicle options.

Note that the decision to opt for a dedicated launch was made based on current knowledge of the launch date, (the absence of) potential rideshare customers and launch costs. These parameters might change significantly in 6 years time, when the CASE mission is planned for launch. For lightweight CubeSat launches, ridesharing remains a very attractive option due to its lower costs and higher sustainability. Based on the growing demand for ridesharing launches and increasing number of CubeSat launches, it is likely that a ridesharing launch will be more favorable than a dedicated launch in 6 years time. This also means that the launch costs may still decrease significantly, from the order of millions of euros to hundreds of thousands. However, based on current information, the dedicated launch is still the most realistic option.

20.3. Launcher Trade-off

To select the best option from Table 20.1, the AHP was used. This method was also used in a previous report to select the most suitable design concept [1]. After the importance of each criterion relative to the other criteria was determined, resulting in the weights listed in Table 20.2.

Table 20.2: Weights assigned to each criteria, based on the AHP method.

	Total cost	Success rate	Axial loads	Lateral loads	Apogee accuracy	Inclination accuracy	Launches per year	Re-usability
Weight	27.8%	23.0%	10.6%	10.6%	5.8%	9.3%	3.5%	9.4 %

The weights from Table 20.2 were then used to determine the scores for each launcher. These scores are shown in Table 20.3.

⁸⁵<https://www.cnn.com/2021/05/04/firefly-aerospace-raises-75-million-to-become-a-space-unicorn.html>, [Retrieved June 12, 2021]

Table 20.3: Scores for each launcher, based on the AHP method.

	Ariane 5	Soyuz	Falcon 9	Electron	Terran 1	Firefly Alpha
Score	15.5%	11.4%	14.3%	22.8%	19.1%	16.9%

From Table 20.3, it is clear that Rocket Lab's Electron Rocket is the best candidate and thus wins the trade-off.

20.4. Sensitivity Analysis

To ensure that the launch vehicle trade-off yields reliable results, a sensitivity analysis was performed. For each option, some combination of weights was altered until the option would yield the highest score. This analysis is summarized in Table 20.4. The criteria which were not altered during the sensitivity analysis are not included in the table.

Table 20.4: Launch vehicle sensitivity analysis. Values are the weight increase needed for each option to win. Note that some options could never win the trade-off.

	Ariane 5	Soyuz	Falcon 9	Electron	Terran 1	Firefly Alpha
Success rate	2x	50x	5x		1x	
Axial loads	2x	5x	1x		1x	
Lateral loads	2x	50x	1x	Original winner	16x	Never
Apogee accuracy	2x	1x	1x		1x	
Inclination accuracy	3x	1x	1x		1x	
Launches per year	1x	1x	5x		1x	

The Ariane 5 is a close competitor to the Electron rocket as only a few parameters need to be doubled. Ariane 5 is a very large launcher with high performance, but it is not suitable for the CASE mission due to exorbitant costs. For the Soyuz launch vehicle, the criteria need to be altered by factor 50 so it is unlikely (almost impossible) to win the trade-off. Falcon 9 presents promising results with only success rate and launches per year weights being increased. However, it is not an option since the ride sharing was dismissed. For the Terran 1 to win, the lateral load factor need to be 16 times higher therefore it is not an option as well. Finally, it was found that Firefly Alpha cannot win under any weight distribution. This concludes the sensitivity analysis with Rocket Lab's Electron being the justified winner of the trade-off.

20.5. Deployer Selection

To accommodate the CubeSats on-board of the Electron, suitable payload deployers need to be chosen. A payload deployer is a device that carries and protects CubeSats during launch and deploys them into orbit with a very small ΔV insertion. Since CASE has a 12U size in a 4x3x1U configuration, the 12U QuadPack CubeSat deployer from ISISpace has been selected, as shown in Figure 20.1. This deployer has proven flight performance since 2014, has a redundant spring-deployment mechanism and does not create space debris upon deployment. Each deployer carries one 12U CubeSat, meaning 3 deployers are required. The estimated price of one deployer is 12,000 €, meaning the total deployer cost will be 36,000 € [O]. Their maximum payload mass is 24 kg, compared to CASE's fully-loaded wet mass of 11.38kg (see Section 23.1). The mass of each QuadPack⁸⁶ is about 7.5 kg. This means the total launch mass, consisting of 3 CubeSats and 3 deployers, is 56.6 kg.

Compared to Table 20.1, this represents $\frac{56.64}{300} * 100\% \approx 19\%$ of Electron's maximum payload mass. This low occupancy is one of the reasons it remains very attractive to search for fellow potential customers in the future who are interested in launching to the same equatorial orbit.

⁸⁶<https://www.isispace.nl/product/quadpack-cubesat-deployer>, [Retrieved June 10, 2021]

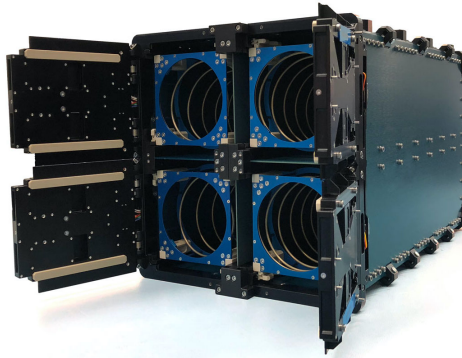


Figure 20.1: 12U QuadPack by ISISpace for CubeSat deployment⁸⁶

20.6. Verification and Validation

To perform the verification of the launcher trade-off, the CR has been employed again. The inner mechanisms of this verification method have been outlined in Chapter 8, and the equations proposed therein will be used again. Using Equation 8.1, the CI was found to equal 0.039 for the launcher trade-off. The value of CR was then found using Equation 8.2, and shown to equal $0.0296 < 0.1$; the calculated value of CR is well below the value of 0.1. Therefore, the importance scalars were not chosen randomly and the resulting weights from the AHP method, as given in Table 20.3, are consistent.

The launch vehicle itself will be validated by the manufacturer in a test-flight and by the vehicle's flight history.

20.7. Risk

As discussed in Section 5.3, the CASE mission faces multiple risks during the launch phase. Like any satellite launch, these risk have to be properly mitigated to maximize the chances of a successful mission. These mitigation strategies are listed below for every risk:

- **RSK-LNCH1 - Launcher explodes:** The risk of a LV explosion can be mitigated by selecting a LV with a high success rate and good flight heritage. In this respect, some of the Electron rocket's early-phase launch failures, combined with its limited flight history, make for a lower success rate than ideally desired. Noting, however, that 17 of the previous 19 Electron launches have been successful⁸⁷, the success rate will very likely increase in the future [84]. This means that the risk of a LV explosion is thus mitigated. Further mitigation of this risk is the responsibility of the engineering teams at Rocket Lab.
- **RSK-LNCH2 - CASE damaged during launch:** The event of sustaining damage to a satellite during launch is extremely low. Satellites are always extensively tested for the launch loads and vibrations they will encounter during launch. The satellite is not deemed suitable for launch if these tests are not successfully completed. Additionally, the chances of a satellite separating or breaking off from the payload adapter during launch are extremely small. As long as the CASE mission is successfully tested for launch loads and vibrations, this risk is mitigated as much as possible.
- **RSK-LNCH3 - CASE or launcher damaged during payload separation:** Before separation of any satellite from the launcher is performed, all systems have to be green. If not, adjustments can first be made to the spacecraft's attitude and roll rate before a safe and efficient separation can be ensured. Damages incurred during separation to either the satellite or launcher are rare. While it is true that a significant number of launch failures can be attributed failed stage separations [84], payload separation failures are not common.
- **RSK-LNCH4 - Delay of launch date:** Rocket launch delays occur often. As with any complex operation with hundreds of suppliers, parties and stakeholders, delays are common and are caused by a wide variety of reasons. These reasons can include transportation delays, manufacturing delays, insufficient funding,

⁸⁷<https://www.rocketlabusa.com/missions/completed-missions/>, [Retrieved on June 9, 2021]

planning delays and unforeseen weather conditions. Even though delays themselves are not critical failures and pose no harm to the mission hardware, mission delays should be minimised for the overall mission planning and schedule. Delays can be minimised with effective oversight, efficient planning and realistic contingency measures.

- **RSK-LNCH5 - Loss of communication with launcher:** Most LVs will have back-up telecommunication systems to prevent a loss of communication being catastrophic for the mission. That said, even without a connection between the launcher and the ground, many LVs will be able to continue their launch and orbit insertion without any interference from the ground and complete their tasks autonomously. Therefore, the loss of communications to the LV is not a critical mission failure. Contingency can be implemented by selecting a LV with proven flight history and back-up communication systems.

20.8. Sustainability

The sustainability of a LV can be assessed by a number of parameters. Three of these parameters are discussed below, and the performance of the LV on those parameters is assessed.

The Electron rocket is the world's only reusable launch vehicle for small satellites. Recent tests have proven the Electron's first stage can return to the Earth's atmosphere under a parachute, where it is caught by a helicopter-suspended tow hook. The flown first stage is then brought to the factory for maintenance and check-ups, after which it is readied to be launched again. This allows Rocket Lab to build fewer Electrons, leading to less material usage. This, in turn, means Electron performs well on a sustainability assessment. At this moment, however, only the Electron's first stage is reusable. The second stage, the Kick Stage and the payload fairings are all discarded and left to burn up in the Earth's atmosphere. This means that the Electron is not yet fully reusable and it is unknown if Rocket Lab is developing the technologies to make the payload fairings and the second and third stages reusable.

Different launch vehicles often use different types of rocket fuels. Depending on the launch vehicles' payload capability, they might use liquid or solid rocket fuel, or both. Being a small launch vehicle with lightweight payload capability, the Electron uses liquid rocket fuel, which is generally less toxic than solid fuel. Specifically, the Electron uses a mixture of Liquid Oxygen and Rocket Propellant-1 (RP-1), also known as Refined Petroleum-1. From a sustainability perspective, this combination is not optimal. RP-1 is a conventional hydrocarbon-based fuel, which releases CO₂, CO, nitrogen oxides and hydrogen pollutants upon combustion, similar to the combustion of gasoline in a car. Liquid Hydrogen (LH₂) could be used instead to yield a higher specific impulse, but the high costs of LH₂ are often prohibitive.

When it comes to manufacturing of the Electron rocket, this process is efficient and optimized. The rocket's body consists of a full carbon composite structure, resulting in enhanced performance⁸⁸. Additionally, Electron's Rutherford rocket engines are additively manufactured in-house to optimize performance and minimize weight. This total control over the manufacturing processes of the Electron rocket's components results in less wasted material, less transportation emissions and improved performance, resulting in a good sustainability assessment.

In conclusion, this section has dealt with selecting the Electron launch vehicle from Rocket Lab in a dedicated launch configuration. Additionally, ISISpace's QuadPack CubeSat Deployers have been selected to carry the CubeSats on ascent and deploy them into their orbit.

⁸⁸<https://www.rocketlabusa.com/rockets/electron/>, [Retrieved on May 31, 2021]

21. Ground Segment

The GS network provides a crucial piece of infrastructure for any space mission. As discussed in Section 15.2, the CubeCat laser terminal was selected for the laser communication system of the CASE mission. This means that the ground segment requires optical GSs to communicate with the satellites, as discussed in Chapter 15. This choice is a driving parameter behind much of the GSs' locations and sizing. In this chapter, the location and sizing of the GS network used in the CASE mission is detailed.

21.1. Ground Station Network

This section will analyse how many GSs are required and the effect of latitude and cloud coverage on GS contact time. Additionally, an availability estimation is made to approximate the contingency required in the number of GSs. After selecting suitable locations for the GSs, verification, validation, risk and sustainability are all discussed.

Number Of Ground Stations

The number of optical laser communication GSs is closely dependent on the data generation of the payload throughout the orbit. As discussed in Section 13.3, the total data storage capacity of CASE is 128GB. To avoid loss of data or limitations on the measurement time, the gathered data should be downlinked throughout the orbit quickly enough that the data storage capacity is never exceeded. To ensure that this is possible, the GSs need to contain enough stations spread around the equator to enable downlink at various locations in the orbit. Under idealized circumstances, the required number of GSs can be calculated using Equation 21.1.

$$\text{Number of GSs} = \frac{\text{Measurement data [GB/orbit]} + \text{SoH data [GB/orbit]}}{\text{Downlink speed [GB/s]} \cdot \text{Contact time per GS [s/GS]}} \quad (21.1)$$

This equation stipulates that the number of GSs should equal the total amount of data (measurement data + SoH data [GB/orbit]) divided by the total data downlink [GB/GS]. Substituting all the numbers into yields that 2 GSs are required to meet the downlink requirement. It is crucial to note that 2 GSs are only enough under the optimal circumstances. As soon as circumstances change and are no longer optimal, the number of GSs will increase. For example, Equation 21.1 assumes a constant contact time per GS of 414 seconds, meaning that each GS should be located precisely on the equator (see Section 21.3). For geographical reasons, this is often not possible. Additionally, it assumes there is no interference or degradation of signal due to atmospheric conditions such as clouds or aerosols (see Section 21.3).

The total number of GSs in real-life circumstances is dictated by requirement **CASE-SYS-GS-E05** as identified in Section 3.3. This requirement says that the ground segment shall have sufficient GSs to ensure downlink for at least 90% of the mission. To identify how many GSs are needed to meet this requirement, real-life circumstances have to be taken into account. Therefore, the effect of latitude on contact time and the effect of clouds on laser communication were both considered when choosing the sufficient number of GSs. Both of these effect are discussed in further detail below.

Latitude effect on contact time

The CASE mission's orbit is equatorial, meaning it flies directly over the equator. As a result, since the Earth is spherical, the contact time between the satellite and the GS will decrease as soon as the GS is located on nonzero latitudes. Additionally, since the maximum slant range of the CubeCat instrument is 1500km, this imposes an

additional constraint to where the GSs can be built. Figure 21.1 shows the decreasing contact time for different latitudes. The contact times were obtained from a simulation in the FreeFlyer software from a.i. solutions⁸⁹.

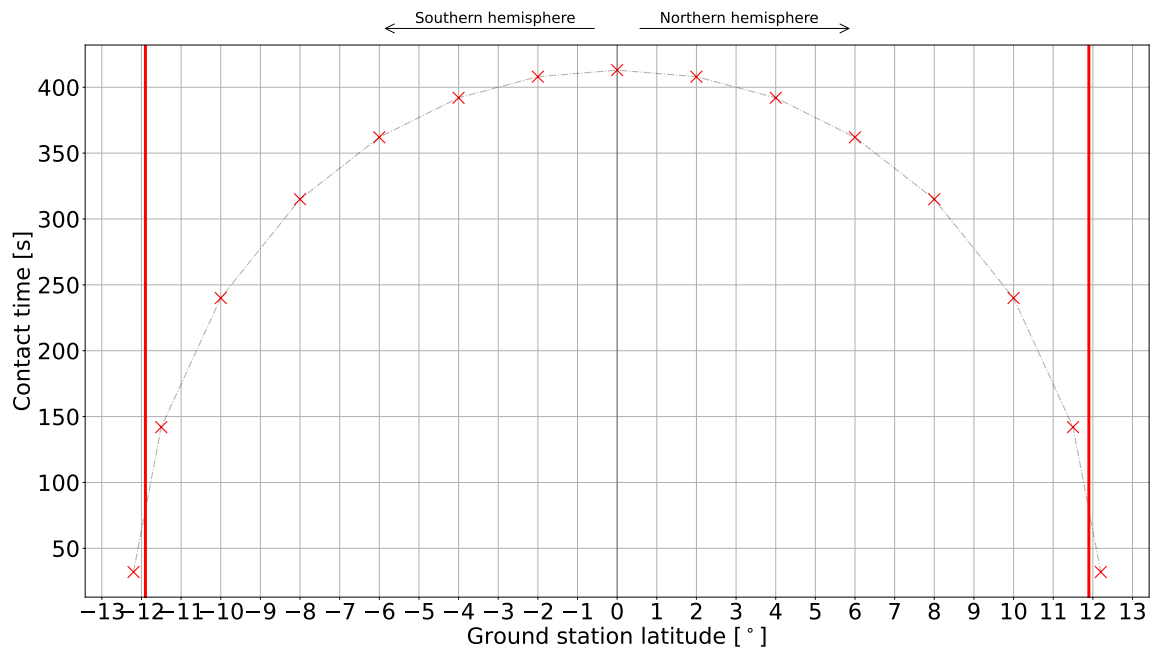


Figure 21.1: Relationship between contact time and different GS latitudes. The vertical red lines indicate the maximum latitudes for possible contact.

Figure 21.1 shows that the maximum GS contact time is 413 seconds for a GS with 0° latitude. Therefore, in order to maximise the contact time with the GSs, they should be placed as close to the equator as possible. Note that for latitudes greater than $\pm 11.8^\circ$, CASE no longer appears within the required slant range of 1500 km for the CubeCat laser terminal, meaning contact can no longer be established. This is indicated by the vertical red lines.

Cloud coverage effect on contact time

Besides latitudes, cloud coverage also has an effect on contact time. The inherent disadvantage of laser communication is that the light is easily distorted and obstructed by clouds and aerosol in the Earth's atmosphere. This means that GSs should be built in locations with very little cloud coverage to minimise the distortion of the laser signal. Compared to conventional radio-frequency communication, this is a much bigger issue and, thus far, it has not been solved by the aerospace and telecommunications industry[K]. Much research is currently being done into laser communication that can pass through clouds without loss of signal. Since no real solution to cloud coverage has been found yet, the only way to mitigate the problem is by having enough contingency.

In order to estimate the effect of cloud coverage on the laser communication, it is imperative to understand which locations on Earth are often covered by clouds. NASA's Aqua weather satellite has been collecting cloud coverage data since 2002 and its results can be used to select suitable GS locations with minimum cloud coverage around the equator. The cloud coverage data is shown in Figure 21.2.

⁸⁹<https://ai-solutions.com/freeflyer-astrodynamic-software/>, [Retrieved on June 16, 2021]

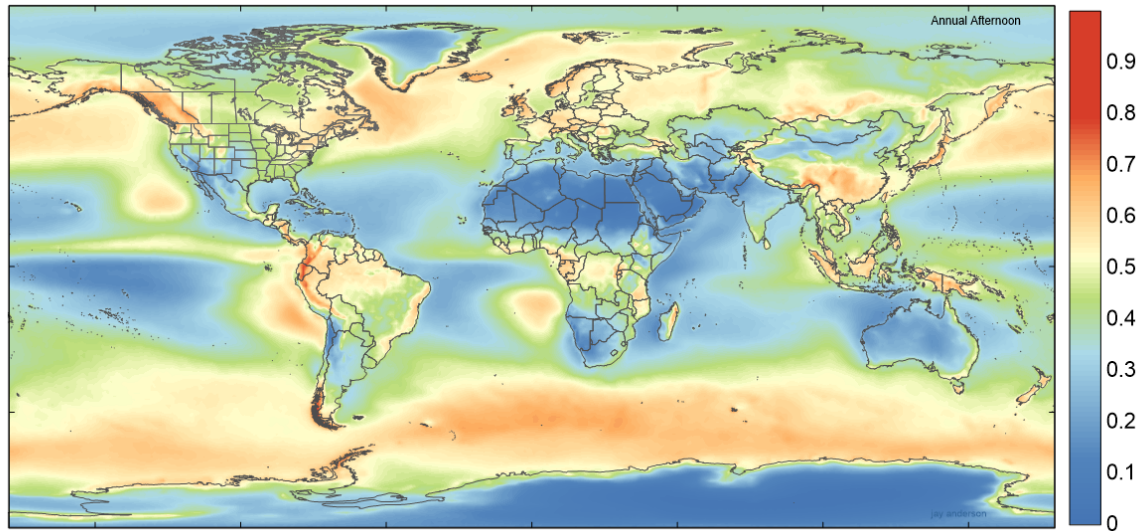


Figure 21.2: Average annual afternoon data of cloud coverage across Earth. Red colours indicate heavy cloud coverage and blue colours indicate low cloud coverage⁹⁰.

The goal of Figure 21.2 is to indicate which locations are suitable for GS locations. Sometimes, however, GS will have to be placed in locations with ample cloud coverage due to the payload's data rate. When this is the case, the preferable option is to select a location with a high altitude. The reason for this is that tall mountains often peek above the clouds and have less atmosphere above them, meaning that cloud coverage poses a smaller issue at high altitudes.

21.2. Availability Estimation

Requirement **CASE-SYS-GS-E05** sets a minimum on the reliability of the GSs. It specifies the availability percentage of the GSs to be at least 90%. The availability percentage is defined as the probability that there is sufficient contact time to downlink the data generated above the primary and secondary targets in a given orbit. A method was created to estimate this reliability for a given configuration of the GS locations (latitude) and their cloud coverage. Here, the data in Figure 21.2 was used to estimate the probability of a location being covered by clouds.

For a given orbit, all possible availability combinations were considered. This is illustrated in Figure 21.3, where an example configuration with five GSs is shown. For each possible scenario, the probability of that scenario occurring is calculated using the cloud coverage probability of each GS. Additionally, the total contact time for that orbit is calculated. If this is not sufficient to downlink the generated data, the probability of this deficient scenario occurring is added to a total. In the end, this results in the probability of a scenario occurring where downlink is not possible. The complement of that probability is the probability of being able to downlink, which is the reliability.

⁹⁰<https://eclipsophile.com/global-cloud-cover/>, [Retrieved on June 15, 2021]











Ground station	1	2	3	4	5	
Contact time	401 s	382 s	411 s	396 s	377 s	
Cloud coverage	0.7	0.2	0.5	0.1	0.6	
Scenario 1						→ $P(\text{scenario 1}) = 0.7 \cdot (1-0.2) \cdot (1-0.5) \cdot 0.1 \cdot (1-0.6) = 1.12\%$ Contact time = $382 + 411 + 377 = 1170$ s
Scenario 2						→ $P(\text{scenario 2}) = (1-0.7) \cdot 0.2 \cdot 0.5 \cdot (1-0.1) \cdot (1-0.6) = 1.08\%$ Contact time = $401 + 396 + 377 = 1174$ s
			⋮			
Scenario n						→ $P(\text{scenario n}) = 0.7 \cdot (1-0.2) \cdot 0.5 \cdot 0.1 \cdot 0.6 = 1.68\%$ Contact time = 382 s

Figure 21.3: Example reliability calculations for a configuration with five GSs, each with their own contact time and cloud coverage probability. The green and red colors indicate that the GS is available or unavailable, respectively.

Several viable GS locations were then selected, which is discussed in more detail in Section 21.3. Using Figure 21.1, the contact time with each GS was found using their latitudes. Additionally, Figure 21.2 was used to find the probability of that location being covered by clouds. Then, using the method described above, the reliability of the configuration was estimated. It was found that a configuration with 7 GSs was necessary to achieve a reliability higher than 90%, as required by **CASE-SYS-GS-E05**. As shown in Table 21.1, the availability will be too low for 6 GSs, and well exceeds the 90% requirement for 8 GSs. Since using an extra GS adds significant cost, it was determined that using 7 GSs was optimal.

Table 21.1: Availability for different numbers of GSs.

 Availability requirement not met,  Availability requirement met,  Availability requirement exceeded

Number of GSs	Availability
6	 84.5%
7	 94.1%
8	 94.3%

To calculate the availability for 6 GSs in Table 21.1, the GS in Macapá, Brazil was removed for the purpose of the calculation. To calculate the availability of 8 GSs, an additional GS was considered on Ascension Island with a latitude of -7.9° and a cloud coverage of 0.2.

21.3. Locations

As discussed in Section 21.2, the total number of GSs required to meet the **CASE-SYS-GS-E05** requirement is 7. The next step is selecting suitable locations for these 7 GSs. These locations have to satisfy the following requirements:

1. Suitable locations should be at latitudes smaller than $\pm 11.8^\circ$.
2. Suitable locations should have a maximum cloud coverage value of 0.5, preferably lower.
3. Suitable locations are situated on land.

A conscious effort was made to avoid cloud coverage by selecting tall mountains for GS locations, as cloud coverage at higher altitudes is often less severe. For this reason, 3 of the 7 chosen GS locations are located on mountains. The 7 required GS locations that were found to match all of the above requirements are given in Table 21.2. Note that the effective contact time was calculated by multiplying the contact time with $(1 - \text{cloud coverage})$, to account for the fact that low cloud coverage yields high effective contact time and vice versa.

Table 21.2: Selected GS locations around the equator.

Location	Lat. [°]	Long. [°]	Contact time [s]	Cloud coverage	Effective contact time
1. Mount Chimborazo, Ecuador	-1.5	-78.8	410	0.5	205
2. Macapá, Brazil	0.1	-51.1	414	0.5	207
3. Mount Kenya, Kenya	-0.2	37.3	414	0.3	289.8
4. Fuvahmulah, Maldives	-0.3	73.4	412	0.4	247.2
5. Mount Kerinci, Indonesia	-1.7	101.3	408	0.5	204
6. Puncak Jaya, Indonesia	-4.1	137.2	392	0.5	196
7. Tarawa, Kiribati	1.5	173.0	410	0.3	287
			Total: 2859		Total: 1636

As can be seen from Table 21.2, the total effective contact time is 1636 seconds. To understand how much contingency this provides, the total required downlink contact time should be calculated. This is tabulated in Table 21.3. With a contingency factor of 2.02, the available contact time is slightly more than twice the required contact time. This increases the likelihood of being able to downlink all the data when cloud coverage is high in certain areas, when a GS fails or when more data is gathered per orbit than initially expected.

Table 21.3: Contingency factor for GS contact.

	Contact time [s]
Total required contact time per orbit	811
Idealized contact time with 7 GSs	2859
Effective contact time incl. cloud coverage	1636
Contingency factor	2.02

Combined with a slant range of 1500km, the selected locations create the coverage as shown in Figure 21.4. Using the method described in Section 21.2, the reliability of this 7-station configuration was found to be 94.1%. With a 6-station configuration, the reliability is only 84.5%, thus failing to meet requirement **CASE-SYS-GS-E05**.

**Figure 21.4:** Overview of 7 GS locations and their 1500km slant range, yielding a 94% availability.

If a GS is situated on or near a mountain, the location on that mountain needs to be decided. From a cloud coverage perspective, the leeward side will be the preferable location. The reason for this is, since the prevailing wind directions around the equator blow from East to West, the leeward side of the mountain will generally be the Western side and thus contain fewer clouds. However, if a GS is placed on the side of a mountain, the signal will be obstructed by it and the contact time will be decreased. Researching this effect requires an analysis of the shape

and size of each mountain to determine the optimum location. This is deemed beyond the scope of this design project, and this effect has thus been ignored.

Since optical laser GSs are still relatively new and very few commercially available stations have been built, it is difficult to find accurate estimations of their costs. However, personal contact with Airbus' Sales, Strategy and Business Developer Daniel Hendrix provided insight. The price of the optical GSs is estimated to be between 500.000 € and 1 M€ per unit [K]. Since the CASE mission will require 7 GSs, the price will be between 3.5 M€ and 7 M€. Some of the costs can be recuperated after the mission life by either selling or renting out the GSs to other commercial parties. More information on this can be found in Chapter 26.

21.4. Verification and Validation

The FreeFlyer software that was used to determine the data in Figure 21.1 has a long performance history since 1997. It has been used by NASA, National Oceanic and Atmospheric Administration (NOAA) and the United States Air Force (USAF) for both commercial and defense missions. It has been independently verified and validated for flight-tested, proven accuracy⁹¹. Because of its flight history and validation, FreeFlyer is a useful tool for the astrodynamic calculations this chapter provides.

Additionally, in Equation 21.1, the FreeFlyer software simulation showed that the maximum contact time for a GS on the equator is 413 seconds. The calculations from Chapter 15 showed that the maximum contact time is 413.8 seconds. This means that the calculated value was only 0.2% higher than the simulated value. For the purposes of the contact time calculations, the calculations from Chapter 15 are shown to be verified by the FreeFlyer software. The difference between the two results may have arisen from the assumption that Earth is perfectly spherical in Chapter 15. FreeFlyer has a more detailed description of Earth's shape, which may have lead to a more accurate result.

21.5. Risk

The risks related to the ground segment are several, and more difficult to address than spacecraft related risks. This is due to the fact that the GS selection is dominated by the orbit that has been selected. This signifies that several GSs will be required along the equatorial orbit. With regards to the risks, this implies that the freedom over which GS is selected is limited, and some risks may not be easily avoidable. For instance, risks **RSK-GS5** and **RSK-GS6** related to personnel, are highly dependent on the level of development in the GS's area or country. For this reason, it is likely that contingent GSs will be necessary, especially in politically or geographically turbulent locations. Human error (**RSK-GS7**) also presents significant hindrances, and could be responsible for several other risks including **RSK-GS1**, **RSK-GS2**, and **RSK-GS3**. However, these latter risks should be lessened with sufficient testing protocols. Testing in this case will not be perfectly indicative of mission performance, since orbital characteristics cannot be simulated in a test environment (due to distance and curvature of Earth's surface, and the use of laser communication). Nevertheless, such testing will be necessary as a baseline for any verification and validation activities to ensure proper performance.

21.6. Sustainability

In this section, the sustainability of the GS is assessed. It is important that GSs are built from non-toxic materials. For the construction of the mirrors and sensors, rare-earth metals might have to be used. These metals are preferably recycled from other previously-used electronics to prevent unnecessary extraction. Alternatively, they should be sustainably sourced under ethical working conditions. To minimize the carbon footprint of the GS manufacturing, all stations should be made of reused or recycled material as much as possible. Another important part of the GS to look at is the operational sustainability. Preferably carbon-free energy sources should be used to generate the GSs' electricity. For the end-of-life of the mission, it should be noted that GSs can be reused for other missions, which benefits the sustainability of the mission.

⁹¹https://ai-solutions.com/_help_Files/freeflyer_features_overview.html, [Retrieved on 17-06-2021]

22. Configuration & Layout

Upon generating the final design of the CASE mission spacecraft, the subsystems were integrated into a coherent structure. The end result is a fully assembled spacecraft containing all of the components selected in the previous chapters. The configuration is then used to iterate, allowing for improvement and optimization of the design. The first step in its design was generating the outer envelope, or outer dimensions, of the spacecraft. This is discussed in Section 22.1 together with the solar array configuration. Next, the inner configuration of the spacecraft is discussed in Section 22.2. Finally, the cabling of the spacecraft components is covered in Section 22.3.

22.1. Outer Envelope

The first factor considered for the outer envelope of the spacecraft was found in the risk analysis of space debris impact presented in Chapter 10. It was determined that the frontal area of the spacecraft should be minimized to minimize the likelihood of a collision. Note that the frontal area faces the direction of flight. Similarly, it is also beneficial for the drag characteristics of the spacecraft if the frontal area is kept to a minimum. More drag could for example affect the ΔV required for station keeping, increasing the wet mass of the spacecraft.

Then, the configuration of the payload influenced the spacecraft configuration to a great extent. Three instruments are taken on-board, each angled differently. One of the instruments is pointing exactly in the nadir direction, while the remaining two are angled positive and negative 45° from this axis respectively. Simultaneously, components protruding out of the main spacecraft structure should be avoided, which was discussed in Chapter 20. Combining these two factors with the size of the lenses on the instruments, it was found that the size of the spacecraft along the nadir direction should be at least two CubeSat units, or 20 cm, to accommodate them. Additionally, since the lenses cannot fit side by side in one CubeSat unit, three Earth-facing units are required.

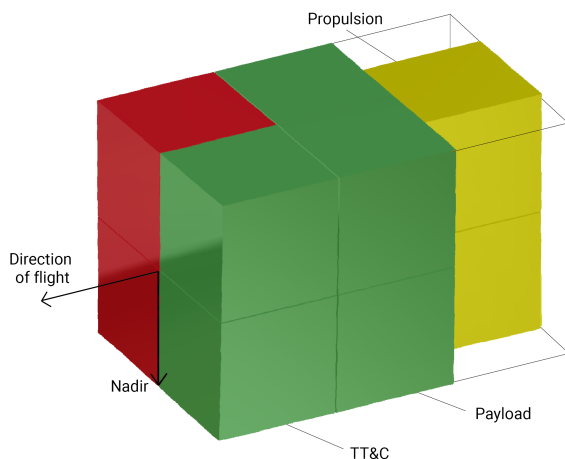


Figure 22.1: Factors contributing to the outer envelope of the CASE spacecraft.

Another component that should face Earth is the CubeCat communication unit in the TT&C subsystem, which takes up a full CubeSat unit. Additionally, a mirror assembly is required, taking up at least part of a CubeSat unit below the communication unit. Combining this with the payload, four Earth-facing units are necessary. The final component that influences the outer envelope of the spacecraft is the HYDROS-C thruster. The engine exhaust should be mounted such that the thrust axis is as close to the center of mass as possible to avoid any undesired torques.

All of these factors were combined, and the result is shown in Figure 22.1, where each cube represents a CubeSat unit taken up by either the TT&C, payload, or propulsion subsystem. It is observed that the spacecraft should consist of 12 CubeSat units, corresponding to an outer envelope of roughly 20 x 20 x 30 cm. Additionally, in the shown configuration, the frontal area of the spacecraft is minimized. Important to note is that

for the cubes indicating the payload and TT&C subsystems, there is still significant space available for other components, which mostly require insignificant volume. However, since these subsystems protrude into these CubeSat units, they are still necessary.

22.1.1. Solar Array Configuration

In Chapter 18, the EPS of the satellite was sized and the different components in that subsystem were obtained. Since solar power was chosen to be the most optimal way to generate power, a configuration of the solar arrays needs to be determined. The sizing of the solar array was done in Section 18.1.1, where it was determined that 49 solar cells would be needed using a fixed (non-sun-tracking) configuration to provide exactly enough power for the subsystems to be powered and the battery to be charged. It would be beneficial to include several redundant solar cells in the case other solar cells fail during the mission (**RSK-EPS S1**).

Several solar array configurations were considered including a deployable sun-tracking solar array, for which the amount of solar cells needed would be about half of the amount of solar cells needed for a fixed configuration. This comes with high risks of the panel not being able to deploy, the rotating mechanism that could malfunction or the structural integrity of the hinge not being high enough which leads to a complete failure of the satellite. Therefore a fixed configuration is chosen. For this, placing solar cells on the sides of the spacecraft need to be minimized in order for the thermal subsystem to perform its thermal control passively. It needs to be taken into consideration that there are star and sun sensors placed on almost all the sides of the satellite.

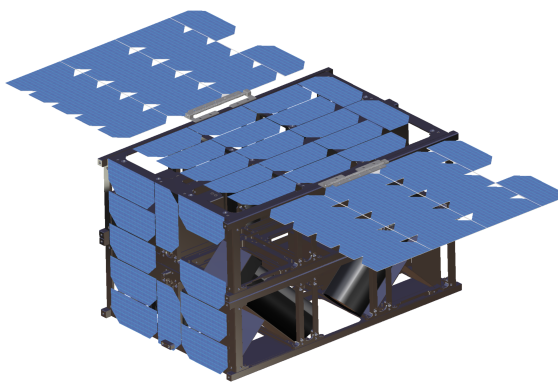


Figure 22.2: Positioning of solar arrays on the spacecraft.

The final configuration of the solar arrays can be seen in Figure 22.2. The solar arrays are composed of two deployable panels, one on each of the sides (2U by 3U) of the satellite and will also be placed on the the top side (2U by 3U) and the front side (2U by 2U). The QJ Solar cell 4G32C has dimensions of 4 cm by 8 cm and with these dimensions the 2U by 3U panels can carry 17 solar cells each and the 2U by 2U panel can carry 12 solar cells. On the top panel and front panel space for a star sensor and sun sensor needs to be considered. For that reason, one solar cell on the top side and one on the front side are taken out of the solar array. This results in a configuration with 62 solar cells in total distributed over two deployable panels and the top panel with each 17 cells and the front panel with 11 cells. From this, it is clear that the 49 solar cells required is reached and 13 redundant solar cells are included to account for failing solar cells.

The deployable panels are deployed after the detumbling of the satellite. It uses spring hinges to deploy the panels passively. This mechanism can also be seen in Figure 22.2. Also a small dampening system is included in order to gently deploy the panels without damaging them.

22.2. Component Configuration

The components discussed in Section 22.1 were placed first since they required the most accurate placement. The thruster had to be placed in the rear of the spacecraft, aligned with the center of the CubeSat. Then, the two diagonal instruments depicted in Figure 19.2 should be placed along the side wall of the spacecraft, fitting into the 6 cm gap that exists on either side of the propulsion unit. Then, the telecommunications system requires an Earth-facing unit of the CubeSat, as well as the one above that. This leaves one Earth-facing unit for the vertical instrument to be placed in, as well as the unit above that. These components and their placement are depicted in Figure 22.3.

Next, before placing any outward facing components such as ADCS sensors, the solar panels were placed since they could potentially block their field of view. As was mentioned in Section 22.1.1, the front and top side of the spacecraft would be covered with solar cells. Additionally, two deployable arrays stowed along the side panels would also be present, with a hinge mechanism attaching them to the top panel. This is shown in Figure 22.2.

Next, the sensors of the ADCS were positioned as was specified in Chapter 16. There is a Sun sensor on each

side, except for the Earth-facing side. Additionally, there are three star sensors facing forward, upward, and to the side respectively. Aside from these sensors, there are two final components that need an outside view. First is the GNSS antenna used for tracking the spacecraft position. Second are the radiating areas described in Chapter 14. The position of these components and the ADCS sensors are shown in Figure 22.4.

For the remaining components, several factors were considered. For the placement of the processing unit, it was decided that it should be as close to the payload and telecommunication subsystems as possible. This reduces the risk of SEEs affecting the measurement data by using shorter cabling, which was discussed in Chapter 13. In Figure 22.5, this location is shown behind the bottom diagonal instrument, next to the CubeCat and below the forward-facing star sensor. Next, the two battery units were positioned. There was only one feasible location for these, which in Figure 22.5 is shown behind the propulsion unit, stacked vertically to take up the available space.

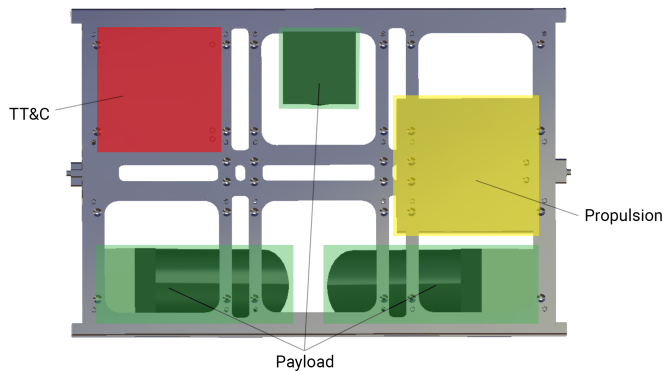


Figure 22.3: Placement of the payload, propulsion, and telecommunications subsystems in the 6U footprint. Note that all of these components extend 2U vertically, out of plane.

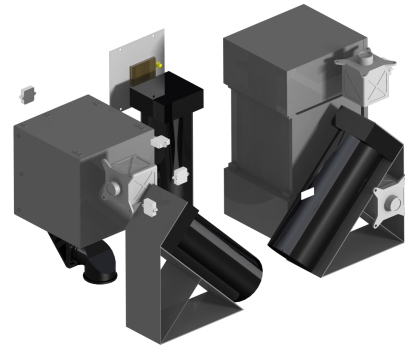


Figure 22.4: Positioning of components with outside view.

Next, the three magnetorquers were positioned, where it was considered that these should point in orthogonal directions. The three components were split into two units, one unit containing two magnetorquers, the other containing a single one. These were then placed above the diagonal instruments, which is indicated in Figure 22.5 as well.

The final components to be placed are the PCDUs and the GNSS receiver. This latter component was placed as close to the GNSS antenna as possible. An available position was found directly on the opposite side of the spacecraft skin, and is thus next to the vertical instrument. For the PCDUs, it was considered that they should preferably be close to the battery units, and have a central location in the spacecraft. It was found that they could be mounted on opposite sides of the vertical instrument, which is indicated in Figure 22.6.

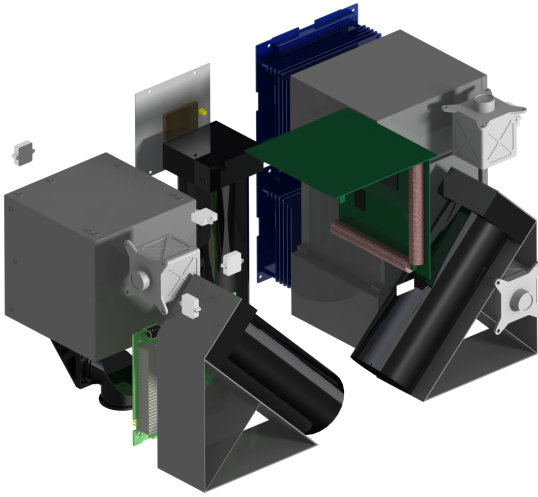


Figure 22.5: Positioning of the processing unit, battery units, and magnetorquers.

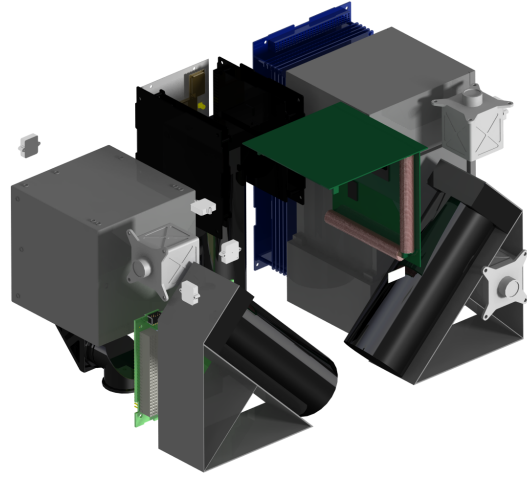
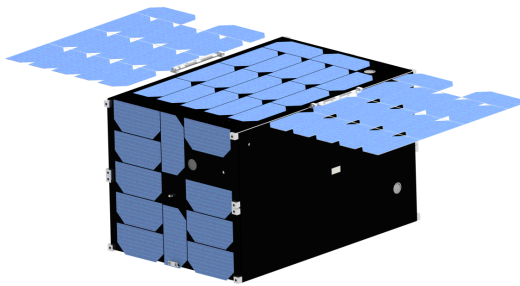
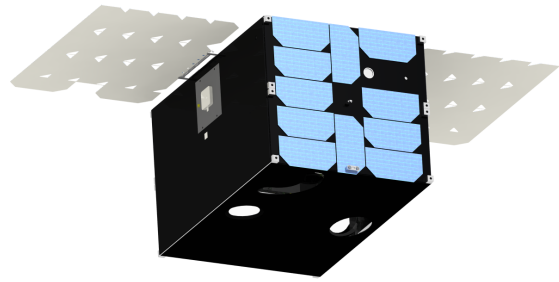


Figure 22.6: Positioning of PCDUs and GNSS receiver.

Finally, the skin panels of the spacecraft were placed, providing cutouts for the ADCS sensors, the payload instruments, and the telecommunications unit. The main panels are painted with black lacquer, aside from the white radiating areas indicated previously. Furthermore, the bottom side of the deployable solar arrays, where no solar cells are present, is covered in a white paint. These final considerations are shown in Figure 22.7.



(a) View showing the top of the spacecraft.



(b) View showing the bottom of the spacecraft.

Figure 22.7: Final configuration of the spacecraft.

22.3. Cabling Harness

As was stated in Chapter 13, the properties of the cabling harness depended on the configuration of the spacecraft. After defining the configuration, the lengths of each connection could be estimated. The cabling was assumed to only follow the orthogonal axes of the spacecraft, indicated in Figure 22.8.

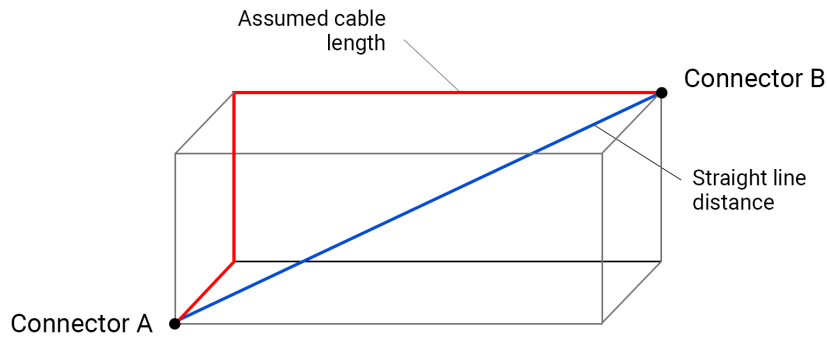


Figure 22.8: Assumed cabling between two connectors compared to the straight line distance.

Then, using the cabling properties given in Table 13.5, the weight of the harness could be estimated. The connections that were identified during the design of the CDH subsystem are presented in Table 22.1, where the estimated length is indicated following from the spacecraft configuration. There is a total of roughly 2.9 m of cabling in the spacecraft, weighing 25.9 g. The longest cable connects the processing unit with the star sensor facing in negative X-direction, which are on opposite sides of the spacecraft.

Table 22.1: Properties of the cabling harness in the spacecraft.

	Component	Cable	Density [g/m]	Length [mm]	Weight [g]
PL	Instrument -45°	28AWG SpaceWire [44]	10.5	50	0.525
	Instrument 0°			70	0.735
	Instrument +45°			100	1.05
ADCS	Sun sensor (+X)	MCJ088D UTiFLEX [45]	11.8	80	0.944
	Sun sensor (-Z)			140	1.652
	Sun sensor (-Y)			270	3.186
	Sun sensor (+Y)			190	2.242
	Sun sensor (-X)			280	3.304
	Star sensor (+X)	Jacketed twisted pairs [46]	4.32	120	0.518
	Star sensor (-Y)			240	1.037
	Star sensor (-Z)			270	1.166
	Magnetorquer (X)	MCJ088D UTiFLEX [45]	11.8	160	1.888
	Magnetorquer (Y&Z)			140	1.652
EPS	PCDU 1	MCJ088D UTiFLEX [45]	11.8	120	1.416
	PCDU 2			200	2.360
PROP	HYDROS C	Jacketed twisted pairs [46]	4.32	200	0.864
TT&C	CubeCat	MCJ088D UTiFLEX [45]	11.8	40	0.472
GNC	GNSS receiver	Space Cable, Type SPLD [47]	3.4	240	0.816
Total				2920	25.87

23. Final Design Overview

In this chapter an overview is given for the final design of the CubeSat. First, the CubeSat design is summarized together with a detailed power budget in Section 23.1. This is followed by the hardware/electrical block diagram of the CubeSat in Section 23.2, as well as the software block diagram in Section 23.3. Lastly, the operations and logistic concept description is defined in Section 23.4.

23.1. Subsystem Design

An overview of the components selected for each subsystem, as well as the main characteristics of these components, such as mass, size and others, is presented in Table 23.1. In this table the power consumption for the different components is left out since that required more detail. The detailed power budget can be found in Table 23.2. Note that some details have been omitted per request of the manufacturer.

Table 23.1: Summary of the components selected for the detailed design. Note that the given properties are for a single component; some values have been omitted or altered per the request of manufacturers.

	Component	Quantity	Mass [kg]	Percentage total mass [%]	Size [mm]	Operating temperature [°C]	Cost [€]	TRL [1-9]
PL	Optical Metasurfaces Based Spectro-Polarimeter	3x	0.545	14.36	∅50 x 150	20 ±0.5	≈10 M	3
ADCS	NXSS3v00 Sun sensor	5x	0.003	0.13	15.5 x 15 x 4.7	-40 to +85	1,790	9
	PST-1 startracker	3x	0.05	1.32	32 x 32 x 4.5	-30 to +60	≈45,000	9
	MTQ200.20 magnetorquer	3x	0.0396	1.04	10.7 x 10.7 x 80	-35 to +75	≈2,200	9
EPS	QJ Solar Cell 4G32C	61x	0.0168	9.00	40 x 80 x 0.11	-150 to +110	17,500	9
	OPTIMUS-40 battery	2x	0.335	5.89	95.89 x 90.17 x 27.35	-10 to +50	8,000	9
	STARBUCK-NANO-PLUS	2x	0.148	2.60	95.89 x 90.17 x 20.82	-40 to +85	≈9000	9
PROP	HYDROS-C	1x	1.87	16.43	190 x 82 x 92	-	≈100000	6
TC	GFTS	10x	0.03	2.64	45 x 12.7 x 38.1	-55 to 240	≈3000	9
	MLI	1x	0.121	1.06	see Chapter 14	-170 to 100	≈1000	9
	White Paint AZ-93	1x	0.045	0.40	see Chapter 14	-180 to 75	≈300	9
	Paladin Satin Black Lacquer	1x	0.108	0.95	see Chapter 14	-180 to 120	≈4000	9
STR	Primary & secondary structure	1x	2	17.57	226.3 x 226.3 x 340.5	-40 to +85	11,950	9
	Payload platform	2x	0.056	0.984	107 x 107 x 50	-40 to +85	≈1000	8
TT&C	CubeCAT lasercom module	1x	1.33	11.69	96 x 96 x 96	-20 to +40	Classified	7/8
	CPA	1x	1.5	13.18	50 x 96 x 96		≈10,000	4
CDH	ISIS iOBC	1x	0.094	0.83	96 x 90 x 12.4	-25 to +65	4,400	9
	Cabling harness	1x	0.033	0.29	-	-100 to +150	≈200	9
GNC	GNSS200 navigation receiver	1x	0.003	0.03	20 x 14.5 x 3.1	-40 to + 85	2,000	9
	ISIS GNSS patch antenna	1x	0.02	0.18	70 x 70 x 15	-30 to +70	1,750	9
Total	CubeSat	3x	11.38	100	224 x 224 x 325	-	32 M	3

From Table 23.1 the total mass of the CubeSat can be determined and was found to be 11.38 kg. In order to account for extra mass due to installation and oversight/assumptions (off-the-shelf components) a margin of 5% [85] was added resulting in a final total dry mass of 11.95 kg. The final wet mass is found by adding the fuel mass of 0.5 kg, resulting in a final CubeSat mass of 12.45 kg. In addition to the mass, the cost is also very interesting.

Some companies did not want to share the cost of their components or did not want them published in this report. Therefore, for some components the cost was estimated by looking at the cost of the same component made by other companies. This is indicated by the tilde symbol (\approx). A more detailed explanation on the cost as well as the cost breakdown structure for the entire mission can be found in Chapter 26.

Power Budget

In Table 23.2 a detailed power budget is presented. This budget shows to power needed by the different components, the time they are active in one orbit and the energy consumed by the component in one orbit. The energy was calculated by multiplying the power usage with the time the component is active, as well as the quantity of components that is active at the same time. This leads to a worst case total energy consumed by the components per orbit, which is equal to 21.36 Wh. For this a contingency factor of 10% [85] was added since the power requirements of some components was estimated, resulting in a final total energy consumption of 23.49 Wh. The power the EPS needs to produce is determined by taking daytime and eclipse time into account. As well as dividing by the daytime path efficiency of 0.85 or eclipse time path efficiency of 0.65 respectively. Taking worst case scenario into account every subsystem that is only active for small amount of the orbit are assumed to be active during eclipse. In Table 23.2 only the power consumed by the components is disclosed, these can also be found in their respective chapters.

As can be seen, the propulsion subsystem uses the most power. This is mostly due to its internal thermal control system and the stand-by power usage, since together they consist of 53% of all energy consumption. The remaining power consumption by the propulsion subsystem is the amount of power needed when it is active. The active time is now the average time per orbit, in reality the propulsion unit is only active once every 27 orbits. The sun sensor has two modes, active and inactive. When the CubeSat is in eclipse the sun sensors are not needed and go into inactive mode, thus lowering the power consumption. For the star trackers only 2 are used simultaneously since the third one is for redundancy. The CubeCat lasercom module has a constant 1 W power consumption and an additional 11 W needed when transmitting. For the mirror system a 2.7 W requirement was estimated. How all the components are connected and receive their power can be found in the next section.

Table 23.2: Detailed power budget.

Component		Quantity active	Power usage [mW]	Time active [s]	Percentage of orbit active [%]	Energy needed [J]	Percentage of total energy [%]
PL	Optical Metasurfaces Based Spectro-Polarimeter	3x	3500	220	4	3850	3.64
ADCS	NXSS3v00 Sun Sensor	5x	7.2	3532	62	127.152	0.055
	PST-1 star tracker	2x	0.072	2145	38	0.772	0.00021
	MTQ400 magnetorquer	2x	500	5677	100	5677	7.61
EPS	OPTIMUS-40 battery	3x	90	5677	100	1533	0.68
	STARBUCK-NANO-PLUS	2x	100	5677	100	1135	1.52
PROP	HYDROS-C	2x	7000	5677	100	39739	53.24
			5000	30.6	1	153	0.20
TT&C	CubeCat lasercom module	1x	1000	5677	100	5677	7.61
			11000	813	14	8943	11.98
CDH	CPA	1x	2700	1626	29	4390	5.88
	ISIS iOBC	1x	400	5677	100	2271	3.04
GNC	GNSS200 navigation receiver	1x	148	5677	100	840	1.13
	ISIS GNSS patch antenna	1x	50	5677	100	284	0.38
Total	-	-	31.69	-	-	76891	100%

23.2. Hardware/Electrical Block Diagram

In this section the hardware block diagram and the electrical block diagram are presented in a merged diagram in Figure 23.1. The hardware block diagram gives an overview of the subsystems with the components and mechanisms they use. It can be seen that only the solar panels and the payload subsystem are thermally isolated from the other subsystems. The dotted lines represent the GFTS connections of the thermal subsystem with different subsystem components. Since this diagram is combined with the electrical block diagram, the electrical connections between EPS and other subsystems are shown. The EPS consists of 4 solar panels of which two are deployable, 2 batteries and 2 PCDUs. The solar panels are each connected to a BCR, which includes multiple MPPTs to allow the solar panels to operate at their maximum power capacity. The BCRs convert the higher voltages of the solar panels to the lower operating voltage of the PCU. Two PCDUs, which include a PCU and a PDU, are used in this design to allow for more connections to the regulated voltage buses. The batteries are connected in parallel to each other such that their total capacity is the sum of their individual capacitance. The batteries are connected to a battery bus, which is connected to the BCRs and the PCUs. The BCRs are connected to the PCUs by first going through undervoltage protectors, which protect the PCUs from damage due to voltages below the design criteria [76]. Before the signal leaves the PCUs there are also overcurrent protectors to protect the circuits from currents that exceed the design criteria. The PCU has four different voltage suppliers, 3.3V, 5V, 12V and an unregulated battery voltage (BATV). The PCU is connected to the PDU which has three 3.3V, three 5V, two 12V and two BATV buses. All of the components of the satellite are connected to these buses. The sun sensors are connected in parallel to each other as well as the star sensors and magnetorquers. All the components are connected to the voltage buses with their own amperages, which are all under the maximum allowable amperage levels. A more extensive explanation on how the PCDU works can be found in the AAC Clyde Space manual [76].

In general it must be noted that this diagram represents all the physical components and mechanisms in the satellite and their electrical connections to the EPS with their respective voltages and amperages while the data flows between the subsystems are represented by the data handling block diagram in Section 23.3.

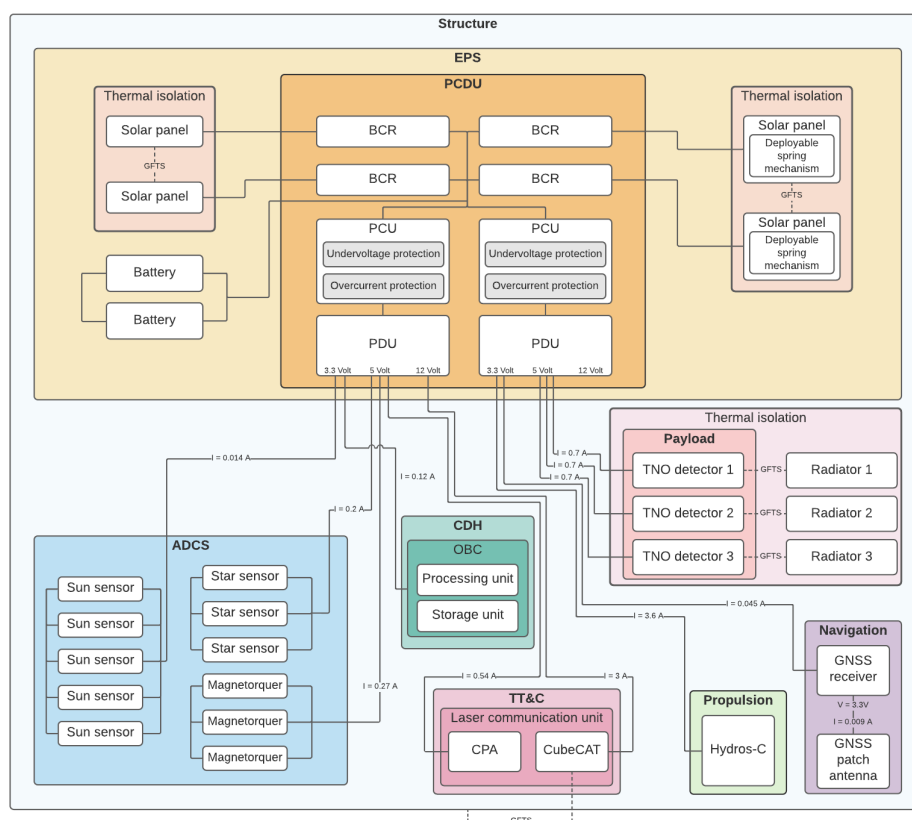


Figure 23.1: Hardware/Electrical Block Diagram.

23.3. Software Diagram

In this section the software diagram of the CubeCat is shown, found in Figure 23.2. It visualizes the different components (shown in blue) together with the inputs they need and the outputs they provide. Additionally the different software programs (shown in green) are shown with a short description what they do, as well as their inputs and outputs and how they are linked to each other. First of all, every subsystem send SoH data to the processing unit that is verified and stored in the storage unit. As can be seen the ADCS has an algorithm which uses the outputs of the sensors to determine the orbit position. Combined with the desired attitude for the CubeSat it determines and sends the appropriate commands to the actuators. The payload also has it's own software, it is used to adjust the measurements for noise and reduce the amount of data it produces by applying a mild form of pre-processing. The resulting data is sent to the data storage unit. The EPS and propulsion have their own thermal control which turns on if the temperature goes over certain thresholds. Furthermore the general subsystem command part in the processing units decides when certain subsystems should be turned on based on ground commands, orbital position and SoH data. The telecommunications software program determines what data should be downlinked, as well as the commands for the CPA of the TT&C subsystem.

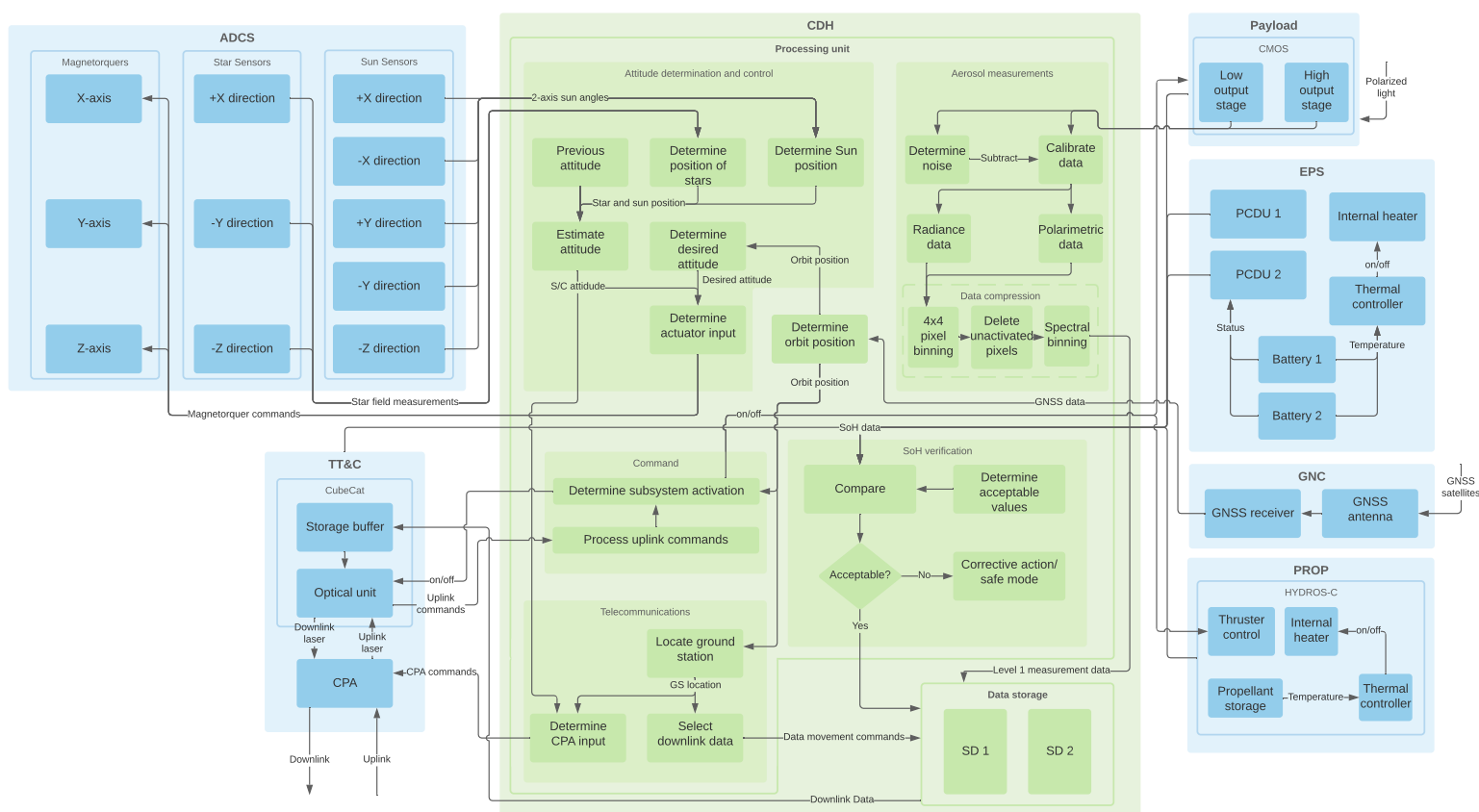


Figure 23.2: Software diagram.

23.4. Operations & Logistic Concept Description

In this section the operations and logistics concept is presented. The Figure 23.3 shows the logistics involved in manufacturing the components and assembling the satellite system. As can be seen, most of the components are made in the Netherlands (especially Delft) and some are also manufactured inside the European Union. It highly decreases the transportation costs as they can be delivered by automotive transport. However, several parts including propulsion from Tether Unlimited, white paint from AZTechnology, black lacquer from Paladin and thermal straps from Technology Applications need to be delivered from the United States. It raises the costs as the

aerial transport remains the most feasible option. Some of the parts will be tested in Noordwijk, NL and then the CubeSats will be assembled there. Then, it will be shipped to the launch site of Rocket Lab, located at Wallops Island, USA.

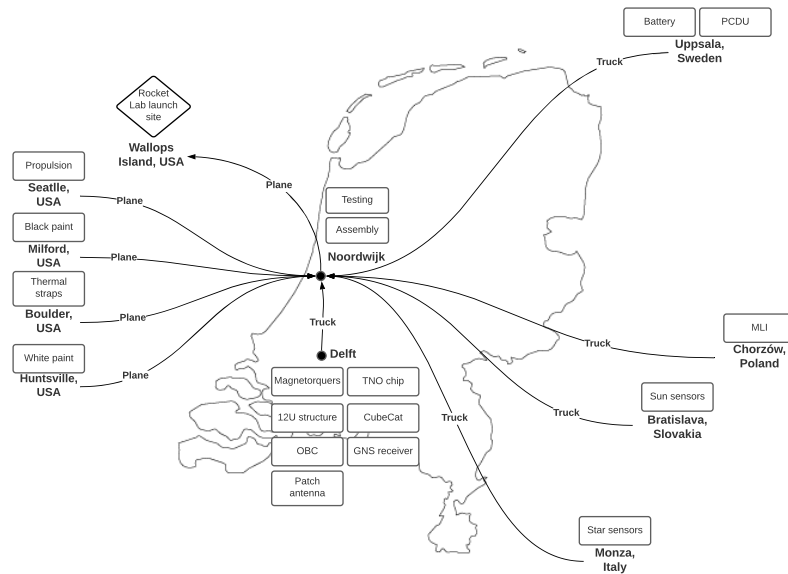


Figure 23.3: Logistic diagram.

The CASE mission will require a total of 26 employees including Group 16 throughout the mission timeline. 14 of those employees will be in the GS locations; hence 2 per GS. Since most GSs will be built on high mountain tops, efficient logistics are necessary. It was decided that using another communication system to relay the data down would be too expensive and complex. In order to save infrastructure and operations costs, the GSs will consist of laser communication, hard drives and a container house to protect the systems. The data will be stored in the hard drives for 2 weeks and every 2 weeks, one of the employees will ascend the mountain and collect the data. This is a laborious but cheap and sustainable solution. The process is shown in Figure 13.1. Furthermore, there will be offices in the near the ground stations for the ground station operations employees. Then data is sent to the nearest data control centers. The ground station employees are tasked to upload the stored data to the website, which offers it to the users. The users can sign up to this website for free. In addition, the weather forecasters, educational institutes and scientists will be especially targeted to give out the data.

The headquarters will be in Delft since the founders of the group are mainly located there. Development, production and testing can be done in various locations in Delft such as the Science Center, Aircraft Hall or the facilities in TNO. Employees will be hired to help during the production, development and testing phase. Lastly, human resources employees will be hired in order to start a mission campaign to start attracting investors as quickly as possible. They will also serve a dual purpose to assess and maintain a healthy and sustainable work environment throughout the remainder of the CASE mission.

24. Compliance Matrix & Feasibility Analysis

This chapter revisits the requirements established in Chapter 3 and determine whether they have been satisfied by the design. This is provided in the compliance matrix, and for every satisfied requirement a green check mark is provided. If not satisfied, the actual parameter value is provided in red. Next, the feasibility analysis is provided, where each unsatisfied requirement is provided an explanation as to why it was not possible or feasible to satisfy. The compliance matrix is detailed below in Table 24.1. For further details on each requirement, Chapter 3 can be consulted.

Since the requirements drive the design, it is the project's intention to ensure all requirements are met. If not, there should be sufficient reasoning to rationalize the decision not to satisfy the requirement. Below the rationale for each requirement left unsatisfied is given.

- **CASE-ST-A06** The polarimetric accuracy of the calibrated optic instrument provided by TNO will be <0.01 , which is lower than the initial requirement of 0.003 . However, the first 5 polarized bands will have an accuracy of <0.005 which approaches the requirement. This polarimetric accuracy is considered to be sufficient to analyse the desired properties of the measured aerosols. Furthermore, this instrument outperforms all currently available instruments in swath width, spatial resolution, mass and volume. Hence, the payload choice is considered justified.
- **CASE-ST-C02** The cost of the mission will be around 120M€, This is above the initial requirement of 70M€, since the cost of the payload alone is already 90M€. After communicating this to the stakeholder it was determined that it was acceptable [A].
- **CASE-ST-D03** The reliability of an average CubeSat is around 75%, conflicting with the 98% requirement. Since the budget for this mission is slightly higher the reliability of this mission can also be made slightly higher.
- **CASE-MIS-A04** The time allocated for de-tumbling the spacecraft after separation from the launch vehicle was originally sought to be less than 30 minutes. After the selection of the ADC subsystem, this was deemed unfeasible, and a de-tumbling time of < 1 day was decided upon.
- **CASE-MIS-C02-II** The cost of a single spacecraft will be above the originally stated 20M€ for the same reason as for **CASE-ST-C02**, the payload alone already costs 40M€.
- **CASE-MIS-C03** Due to the chance of cloud coverage seven GSs were needed. This thus meant more cost for the ground segment, since more ground stations also means more personnel.
- **CASE-SYS-PL-A07** See the feasibility analysis for **CASE-ST-A06** in Section 11.1 of Chapter 11.
- **CASE-SYS-TTC-A04** The BER of the TT&C subsystem remains a subject of great interest for the CASE mission. However, due to privacy concerns of the component distributors, the BER has not been disclosed. Therefore, it cannot be stated whether this requirement is met or not.
- **CASE-SYS-ADC-A01** See the feasibility analysis for **CASE-MIS-A04**.
- **CASE-SYS-PROP-A01** The need for desaturation arose from the consideration of reaction wheels for the ADCS subsystem. Once reaction wheels were no longer considered, it was no longer necessary to provide desaturation protocols, and this requirement was also deemed unnecessary.
- **CASE-SYS-PROP-A02** Through personal communication, it was determined that for altitudes lower than 500 km, a re-entry burn was not necessary [D]. Therefore, this requirement was no longer deemed necessary.

Table 24.1: Compliance matrix. A green checkmark indicates that the requirement is met. Otherwise, the actual value is indicated in red. Additionally, the location where the requirement is considered is indicated.

CASE-ST-A01-II	✓	[1]	CASE-SYS-SS-A15	✓	23.3	CASE-SYS-TC-A02	✓	14.3
CASE-ST-A02	✓	10.2	CASE-SYS-SS-A16	✓	13.3	CASE-SYS-TC-A03	✓	14.2
CASE-ST-A03	✓	11.1	CASE-SYS-SS-A17	✓	13.2	CASE-SYS-TC-A04	✓	14.2
CASE-ST-A04-II	✓	10.2	CASE-SYS-SS-A18	✓	13.2	CASE-SYS-TC-A05	✓	14.2
CASE-ST-A05	✓	15.2.1	CASE-SYS-SS-D01	✓	[1]	CASE-SYS-ADC-A01	<1 day	16.2.2
CASE-ST-A06	<0.01	11.1	CASE-SYS-SS-D02	✓	[1]	CASE-SYS-ADC-A02	✓	16.2
CASE-ST-A07	✓	7.1	CASE-SYS-SS-E01	✓	[1]	CASE-SYS-ADC-A03	✓	16.2.2
CASE-ST-A08	✓	10.1	CASE-SYS-SS-E02	✓	13.1	CASE-SYS-ADC-A04	✓	16.2
CASE-ST-B01	✓	6.2	CASE-SYS-GS-A01	✓	21.1	CASE-SYS-ADC-A05	✓	16.2.2
CASE-ST-B02	✓	10.1	CASE-SYS-GS-A02	✓	10.4	CASE-SYS-ADC-A06	✓	16.2.1
CASE-ST-C02	150Me	26.1	CASE-SYS-GS-A03	✓	21.1	CASE-SYS-ADC-A07	✓	16.2.1
CASE-ST-D01	✓	20.5	CASE-SYS-GS-A04	✓	21.1	CASE-SYS-ADC-A09	✓	13.1
CASE-ST-D02	✓	20.5	CASE-SYS-GS-A05	✓	21.1	CASE-SYS-ADC-A10	✓	13.1
CASE-ST-D03	81%	7.1	CASE-SYS-GS-A06	✓	21.1	CASE-SYS-ADC-A11	✓	13.1
CASE-MIS-A01	✓	11.1	CASE-SYS-GS-A07	✓	21.1	CASE-SYS-ADC-A12-II	✓	16.2.1
CASE-MIS-A02	✓	20.5	CASE-SYS-GS-E01	✓	23.4	CASE-SYS-GNC-A01	✓	17.1
CASE-MIS-A03	✓	16.2.2	CASE-SYS-GS-E04	✓	21.1	CASE-SYS-GNC-A02	✓	17.1
CASE-MIS-A04	<1 day	16.2.2	CASE-SYS-GS-E05	✓	21.2	CASE-SYS-GNC-A03	✓	17.1
CASE-MIS-A05	✓	10.1	CASE-SYS-PL-A01-II	✓	11.1	CASE-SYS-GNC-A04	✓	13.1
CASE-MIS-A06	✓	10.1	CASE-SYS-PL-A02	✓	10.1	CASE-SYS-GNC-A05	✓	10.4
CASE-MIS-A07	✓	10.1	CASE-SYS-PL-A03	✓	11.1	CASE-SYS-GNC-A06	✓	17.2
CASE-MIS-A08	✓	21.3	CASE-SYS-PL-A04-II	✓	11.1	CASE-SYS-CDH-A01	✓	13.3
CASE-MIS-A09	✓	10.1	CASE-SYS-PL-A05	✓	11.1	CASE-SYS-CDH-A02	✓	13.3
CASE-MIS-C01	✓	26.1	CASE-SYS-PL-A06-II	✓	10.1	CASE-SYS-CDH-A03	✓	13.3
CASE-MIS-C02-II	32Me	26.1	CASE-SYS-PL-A07	<0.01	11.1	CASE-SYS-CDH-A04	✓	13.2
CASE-MIS-C03	2Me	26.1	CASE-SYS-PL-A08	✓	11.1	CASE-SYS-CDH-A05	✓	13.1
CASE-MIS-D01	✓	7.1	CASE-SYS-PL-A09	✓	11.4	CASE-SYS-CDH-A06	✓	13.2
CASE-MIS-D02	✓	7.2	CASE-SYS-PL-A10	✓	11.1	CASE-SYS-CDH-A07	✓	13.1
CASE-MIS-E01	✓	A	CASE-SYS-PL-A11	✓	23.2	CASE-SYS-CDH-A08	✓	15.2
CASE-MIS-E02-II	✓	A	CASE-SYS-EPs-A01	✓	18.1.1	CASE-SYS-CDH-A10	✓	13.2
CASE-MIS-E03-II	✓	A	CASE-SYS-EPs-A02	✓	18.1.1	CASE-SYS-CDH-D01	✓	13.2
CASE-MIS-E04	✓	8.1	CASE-SYS-EPs-A03	✓	18.1.1	CASE-SYS-CDH-D02	✓	13.2
CASE-MIS-E05	✓	7.1	CASE-SYS-EPs-A04	✓	18.1.2	CASE-SYS-CDH-D03	✓	13.1
CASE-SYS-SS-A01-II	✓	23.1	CASE-SYS-EPs-A05	✓	18.1.1	CASE-SYS-CDH-D04	✓	13.2
CASE-SYS-SS-A02	✓	23.1	CASE-SYS-EPs-A06	✓	18.1.2	CASE-SYS-PROP-A01	not needed	-
CASE-SYS-SS-A03	✓	12.2.1	CASE-SYS-EPs-A07	✓	13.1	CASE-SYS-PROP-A02	not needed	6.2.4
CASE-SYS-SS-A04	✓	19.1.2	CASE-SYS-EPs-A08	✓	18.1.2	CASE-SYS-PROP-A03	✓	12.2.2
CASE-SYS-SS-A05	✓	19.3	CASE-SYS-TTC-A01-II	✓	15.2	CASE-SYS-PROP-A04	✓	12.2.1
CASE-SYS-SS-A06	✓	19.1.1	CASE-SYS-TTC-A02-II	✓	15.2	CASE-SYS-PROP-A05	✓	12.2.2
CASE-SYS-SS-A07	✓	A	CASE-SYS-TTC-A04	classified	15.2.1	CASE-SYS-PROP-D01	✓	22.2
CASE-SYS-SS-A08	✓	8.1	CASE-SYS-TTC-A05	✓	13.3	CASE-SYS-STR-A01	✓	19.1.1
CASE-SYS-SS-A09	✓	22.2	CASE-SYS-TTC-A08	✓	13.1	CASE-SYS-STR-A02	✓	19.1.2
CASE-SYS-SS-A10	✓	18.1	CASE-SYS-TTC-A09	✓	13.1	CASE-SYS-STR-A03	✓	19.1.2
CASE-SYS-SS-A11	✓	18.1	CASE-SYS-TTC-A12	✓	15.2.1	CASE-SYS-STR-A04	✓	19.3
CASE-SYS-SS-A12	✓	[3]	CASE-SYS-TTC-D01	✓	22.1	CASE-SYS-STR-A05	✓	19.2
CASE-SYS-SS-A13	✓	16.1	CASE-SYS-TTC-D02	✓	15.2	CASE-SYS-STR-A06	✓	19.1.2
CASE-SYS-SS-A14	✓	13.3	CASE-SYS-TC-A01	✓	14.3			

25. Sensitivity Analysis

A sensitivity analysis investigates the sensitivity of a design (solution) to a change in major system parameters. The sensitivity analysis can be an effective tool to identify the critical parameters that the design is sensitive to, and to make a convincing case why the design is a robust solution to a mission. In the Midterm Report, a sensitivity analysis was used to test the robustness of a trade-off. If design parameters, trade criteria or criteria weights change, it is useful to know what the impact will be on the outcome of the trade-off. In this chapter, a sensitivity analysis is used to establish the degree of sensitivity of the final design to changes in mass, volume or power. This analysis shows how a design reacts to a change in parameters and if it still meet the requirements. Section 25.1 aims to assess the sensitivity of the design to variations in dry mass. Then, in Section 25.2 it is shown how the design changes with changing volume. Finally, in Section 25.3 the power consumption sensitivity is discussed.

25.1. Change in Dry Mass

Most of the selected components are off-the-shelf, so no significant fluctuations of the total mass are expected. However, it is important to identify the crucial values which dictate the redesign of certain subsystems. For the changes in values the following steps were chosen: -20%, -10%, -5%, +5%, +10%, +20% and +50%. It has a direct impact on several satellite parameters including: propellant mass, stresses and MMOI. The results of the sensitivity analysis for the mass are presented in Table 25.1.

Table 25.1: Dry mass sensitivity analysis.

Change in mass	Total dry mass [kg]	Propellant mass [kg]	Axial stress [MPa]	MMOI (x, y, z)[kgm ²]
-20%	9.561	0.4	1.37	1.2, 0.142, 0.121
-10%	10.756	0.45	1.55	1.35, 0.160, 0.136
-5%	11.354	0.47	1.63	1.43, 0.169, 0.143
0%	11.951	0.5	1.72	1.5, 0.178, 0.151
+5%	12.549	0.52	1.80	1.58, 0.187, 0.159
+10%	13.146	0.55	1.89	1.65, 0.196, 0.166
+20%	14.342	0.59	2.06	1.8, 0.214, 0.181
+50%	17.927	0.74	2.58	2.25, 0.267, 0.227

As can be seen, the +50% increase in dry mass would rise propellant mass to 0.74 kg which is the limit capacity of the HYDROS-C engine from Tethers Unlimited. Any more mass above that point and new propulsion system needs to be selected. The stresses show a linear relation with the mass as expected and even with +50% dry mass increase they are way below critical 572 MPa yield stress of the Aluminum 7075-T6. So it is fair to say that structural subsystem is not sensitive to small mass increase. This is also a pleasant verification showing that the stress calculations follow the expected linear behavior. Regarding the MMOI, it is assumed that the center of gravity stays the same and MMOI scales linearly with mass. No critical changes were observed during the analysis as current CASE magnetorquers can handle up to 200% increase in MMOI and the largest MMOI due to bigger mass is only approximately 50% higher.

25.2. Change in Volume

In this section, the effects of increasing and decreasing the spacecraft components' volumes are evaluated. The results of changing the volume of all of the spacecraft components' volume are given in Table 25.2.

Table 25.2: Volume sensitivity.

Change in volume	Effect on volume budget	CubeSat structure size	MMOI (x, y, z) [kgm ²]
-20%	6.30 dm ³	8U	0.38, 0.316, 0.268
-10%	7.08 dm ³	10U	0.38, 0.49, 0.42
-5%	7.48 dm ³	10U	0.38, 0.49, 0.42
0%	7.87 dm ³	12U	1.5, 0.178, 0.151
+5%	8.26 dm ³	12U	1.5, 0.178, 0.151
+10%	8.66 dm ³	12U	1.5, 0.178, 0.151
+20%	9.44 dm ³	12U	1.5, 0.178, 0.151
+50%	11.81 dm ³	16U	1.5, 0.316, 0.268

As shown in Table 25.2, the size of the CubeSat structure can change as soon as the volume of components changes. For example, for a 50% increase in the volume of the components, the 12U structure is too small and it should be enlarged to 16U.

Additionally, due to the payload structure that houses the three sensors, the CubeSat will always need at least 4 ground-facing cubes to perform the measurements. This can be achieved by buying off-the-shelf CubeSat structures for all of the sizes by adjusting the configurations. Similarly to the mass sensitivity analysis, the center of gravity stays the same and the MMOI scales quadratically with distance. No critical changes were observed during the analysis as current CASE magnetorquers can handle up to 200% increase in MMOI and maximum increase (16U) shows about 77.8 % larger MMOI.

25.3. Change in Power Consumption

In this section, the effects of increasing and decreasing the total spacecraft power consumption are evaluated.

In case the power consumption of any of the selected components turns out to be higher than the initial estimate, a need for increased power generation arises. This means that the area of the solar panels will need to be increased (more solar cells needed) and a larger battery capacity will be required. The effects of changing power on the battery capacity and the solar cells are summarized in Table 25.3. The table shows the required number of solar cells and the required battery capacity for the power consumption in range from -20% to +50% of the nominal value. The last row also includes the design value, which is actually used in the spacecraft design. The design value is higher than nominal in order to add contingency.

Table 25.3: Power consumption sensitivity.

Power consumption	Solar cells count [-]	BOL battery capacity [Wh]
-20%	40	51.6
-10%	44	58.0
-5%	47	61.2
+0%	49	64.4
+5%	52	67.7
+10%	53	70.9
+20%	59	77.3
+50%	74	96.7
Design value	61	80

To add contingency to the design, the solar panels were designed to consist of 61 solar cells. From the table above it can be seen that that the required number of solar cells increases linearly with increasing power. The selected design is not sensitive to increase/decrease in power up to 20%. However, if the power consumption gets increased by more than about 25%, the solar array would need to be larger. The same can be said about the battery, which can handle power variations of up to $\pm 25\%$, but needs to be redesigned in case of an even higher power increase.

A change in power consumption would also mean that the thermal subsystem might require redesigning. The three

payload instruments are isolated from the rest of the spacecraft and have dedicated radiating surfaces to dissipate heat. The area of these surfaces is strongly linked to the power consumption of the payload and will, therefore, change whenever the payload power changes. However, these design changes can be easily incorporated into the design, as the radiating surfaces area scales linearly with power, and even a tenfold power increase would result in only 65 cm² radiating area.

At the same time, the power dissipated by other subsystems is used to heat up the spacecraft. If the power consumption becomes too low, the temperature might drop below the lower limit (-20°C) which is the lowest temperature at which the CubeCat terminal can operate. The power consumption should not be too high either, in order not to exceed the highest operating temperature of 40°C. Table 25.4 summarizes the effects of changing the power consumption on the thermal balance of the spacecraft.

Table 25.4: Power Consumption Sensitivity of Thermal Subsystem.

Min. power consumption	Temperature margin
-0%	+6.75 °C
-5%	+5.75 °C
-10%	+4.70 °C
-20%	+2.60 °C
-50%	-4.05 °C
Max. power consumption	Temperature margin
+0%	+19.15 °C
+5%	+17.60 °C
+10%	+15.45 °C
+20%	+13.15 °C
+50%	+4.15 °C

From the above table it can be concluded that the power should not be decreased by more than about 30%, otherwise redesign of the thermal system is necessary. At the same time, the system is not that sensitive to increasing the power consumption, and it can be increased by more than 50% without a need for redesign.

In conclusion, the sensitivity of the design to changes in mass, volume and power consumption was assessed in this chapter. The sensitivity analysis has shown that the dry mass can be increased by no more than 50%. The design is also not sensitive to volume increase of up to 20%. The power subsystem components are not sensitive to power variations of up to $\pm 25\%$. For thermal subsystem it is important that the total power consumption of the components does not drop to lower than -20%.

26. Cost Breakdown Structure & Profitability

In this chapter, the cost breakdown structure and the economic value of the CASE mission are discussed. Costs were categorized as production, development, and operational costs. These costs are elaborated upon in Section 26.1. The CASE mission serves the scientific needs of the market rather than generating a profit. Therefore, it was decided that the CASE mission data will be open source to maximize its scale of usage. The funding required would be to conduct the mission for science, not to make a commercial profit. On the other hand, even though there will not be any direct profit from the CASE mission, it adds value to the economy. The added value is discussed further in this chapter. The chapter starts with presenting the cost breakdown structure and then the profitability analysis will be presented.

26.1. Cost Breakdown Structure

In Table 26.1, the cost breakdown structure of the CASE mission is presented. This table consists of the estimations made for the production, development and operational costs of the mission. The values for the cost are given in thousand euros. The data used in this estimation was either gathered from the internet or the cost breakdown of the MARCO POLO mission [86]. In order to have a more accurate cost estimation, the timeline for the post-DSE activities were assumed. The Gantt chart can be found in Appendix A. In order to decrease economical risk, the expenses for the CASE mission are distributed over multiple years. The start date and the end date of the costs are given in the table. The costs where the year does not change indicates that the expense was made only once in that year. For the others, the expenses are made in the span of years between the end and start year. Lastly, a column indicates the number of times the expense has to be made each year.

Table 26.1: Cost Breakdown Structure

Category	Component	Start year	End year	Per year cost [1000 €]	Amount	Total
Development Cost	Research & Development	2022	2029			2954
	<i>Equipment Cost</i>	2022	2029	20	1	140
	<i>Chief Engineer Salary</i>	2022	2029	100	1	700
	<i>Subsystem Lead Engineers Salary</i>	2022	2029	56	5	1974
	<i>Depreciation</i>	2022	2029	20	1	140
	Testing	2025	2026			230
	<i>Testing Equipment Cost</i>	2025	2026	20	1	40
	<i>CubeSat Testing Engineers</i>	2026	2026	50	2	100
	<i>Performance Tests</i>	2025	2026	5	9	90
	Overhead Cost	2022	2029	20	1	140
	Satellite Equipment Cost	2023	2024			96129
	<i>Payload</i>	2024	2024	30000	3	90000
Production Cost	<i>Propulsion</i>	2023	2024	100	3	300
	<i>Other</i>	2023	2023	1943	3	5829
	CubeSat Assembly Employee	2025	2023	75	1	75
	Ground Station Cost	2026	2025			6755
	<i>LaserCom station</i>	2026	2026	750	7	5250
	<i>Infrastructure + Labor Cost</i>	2026	2026	215	7	1505

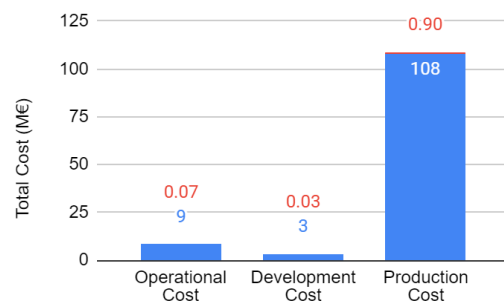
Table 26.1: Cost Breakdown Structure

Production Cost	Overhead Cost	2023	2026	20	1	80
	General & Administrative Cost	2022	2029			4249
	<i>HQ Office Space & Equipment Rent</i>	2022	2029	175	1	1225
	<i>Management Employees</i>	2022	2029	48	9	3024
	Marketing & Advertisement Cost	2022	2029			1085
	<i>Online Marketing</i>	2022	2029	40	1	280
	<i>Seminars & Presentations</i>	2022	2029	5	1	35
	<i>HR Employees</i>	2022	2029	36	3	756
Operational Cost	<i>Other</i>	2022	2029	2	1	14
	Launch Cost	2027	2027	1	1	6200
	Ground Station Cost	2027	2029			2033
	<i>Ground Station Engineer Salary</i>	2027	2029	38	14	1053
	<i>Ground Station Operations Cost</i>	2027	2029	70	7	980
	Legal	2022	2029	20	1	140
	Depreciation	2022	2029	10	7	490
	Overhead Cost	2022	2029	20	1	140
	Operational Cost	2022	2029			8137
Summary	Development Cost	2022	2028			3324
	Production Cost	2023	2026			103039
	Total	2022	2029			114500
	with 5% contingency					120225

The total cost of the mission will be around 120 M€. It was determined that the production cost is the biggest proportion of the costs with 108 M€. This is mainly because of the price of the payload. The costs in terms of M€ and fractions of total cost are depicted in Figure 26.1. The costs in this figure is with a 5% contingency taken into account. The estimated operational cost is around 9 M€ and the estimated development cost is 3 M€. On the other hand, the production cost for the mission is 108 M€. This is because of the very high cost of the payload. After talks with TNO, it was found it that the 1 viewing angle version of the payload would be less than 10 M€. Using the 3 viewing angle version for the CASE mission, the price of the payload is estimated to be 30 M€ to be on the safe side. The breakdown of the remaining subsystems in terms of percentage is given in Table 26.2.

Table 26.2: Cost breakdown per subsystem.

Subsystem	Percentage range for cost	Average percentage
Structure	0.01-0.03	0.02
Thermal	0.04-0.08	0.06
Power	0.05-0.15	0.10
TT&C	0.1-0.5	0.3
Data handling	0.005-0.015	0.01
GNC	0.005-0.015	0.01
ADCS	0.2-0.4	0.3
Propulsion	0.1-0.3	0.2

**Figure 26.1:** Cost Breakdown Structure in M€.

The exact cost estimations of each subsystem will not be presented in this report because the cost information is classified for certain components. Therefore, only the percentage range and the average percentage is presented. From this, it can be seen that the TT&C and the ADCS systems are the most expensive after the payload. This is due to the higher complexity of these subsystems compared to the other subsystems, especially the laser communication used for TT&C. Furthermore, the propulsion subsystem takes a large percentage. The higher cost compared to the remaining subsystems is again due to its complexity since it uses a green initiative. Compared to other satellites, the TT&C and propulsion has a higher share [28]. This is due to the complexity and low TRL of both systems. The payload takes around 98% of the satellite cost. Having 3 satellites, each equipped with this payload leads to a

total of 90 M€ just for the cost of the payload. This means that more than 75% of the cost is due to the payload. In conclusion, the total cost of the mission is 120 M€ taking into account a 5% contingency margin [81]. Decreasing the cost of the payload, the mission cost can be substantially decreased.

26.2. Profitability Analysis

Firstly, the target market share will be explained in this chapter. Then, the market positioning, return on investment and the created economic value will be discussed.

26.2.1. Target Market Share

Looking at the investments and the market opportunities in the selected regions, an achievable market share was determined. The values in this section were determined assuming a launch year of 2027. Firstly, it was decided that the CASE mission shall serve the people and the planet. Therefore, the data generated will be open source such that the data can be used freely. Even though the CASE mission will not be aiming to generate direct profit from operational activities, the data generated will indirectly lead to more profit and sustainable development in sectors such as agriculture. Furthermore, the scientific value the mission creates is very high. As mentioned before, the data can be related to crop quality, public health, weather forecasting and climate change effects.

The preliminary distribution of the funding is given in Figure 26.2. Most of the funds will be from the allocated funds to the sustainable growth and environmental protection from countries in the UN and other countries invested in the areas to be monitored. Furthermore, sponsors and crowdfunding will be another important resource. Since the majority of the cost is due to production costs, making sponsorship contracts with suppliers can greatly decrease mission cost and help find funds. Crowdfunding will be used to recover the funds that have not been able to be acquired from the sponsors. The rest of the funds will aim to be gathered from TU Delft, Dutch Research Council, ESA and the Dutch Government.

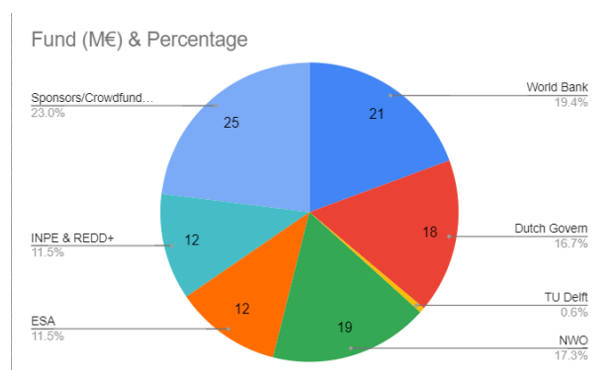


Figure 26.2: Fund Allocation in M€ and percentage.

26.2.2. Return on Investment

It is assumed that the achievable market share is equal to the revenue. Earnings Before Interest and Tax is found by subtracting the total cost from the total revenue. Then, 10% is discounted to take tax and interest into account. This resulted in a net income of 5 M€. Dividing this number by the total cost gives the return on investment value of 0.042. This is very low value, though expected, as the CASE mission does not aim for direct profit. Furthermore, this net income will either be used for the development of the upcoming mission or reinvested into sustainable development.

Even though the profit is not the goal, the economic value the CASE mission brings is important. Studies have shown that the economic benefit of the Amazon rain forest, if conserved, would be 6.2 billion € a year. According to a study done by Script Finance, rain forests give 3 trillion € in value of ecosystem services to the global economy, and over 708 billion € of annual turnover is at risk due to dependency on commodities linked to

deforestation⁹². Considering that the Amazon is almost half of the planet's tropical forests, it also becomes very valuable economically. With the temporal resolution performance of CASE, forest fires can be detected on a large scale and help to stop deforestation. Taking into account the areas to be monitored by the CASE mission as a percentage of the Amazon, around 35 M€ can be saved yearly. Its high temporal resolution allows for an accurate reconstruction of aerosol levels during the day, while the big swath width makes it easier to assess the origin of aerosols in cities and the high spatial resolution allows for exact identification of aerosol sources. With this data, it will be possible to identify the sources of deforestation, illegal logging, burning of waste and the effects of these activities.

Around 4.5 billion € invested in the monitored areas by the World Bank funds are for sustainable development. Therefore, the validation and the climate effects of the investments made will be important indications for the effectiveness of these investments. Last but not least, the CASE mission will span more than 7 countries including the monitored locations and the GS locations. These locations are predominantly in quickly developing countries. This will bring workforce, technical intelligence and infrastructure to these locations and enhance the economic growth. The employees abroad will bring economic value to these developing countries. By bringing money from developed to developing countries, the employees and their families will contribute to the economy. Furthermore, the money invested in this project will create local jobs to help build infrastructure. In addition, the science and the data will create opportunities for universities and scientists to have access to state of the art technology. Providing access to relevant and recent data from Earth observations is critical for the developing countries in question. Scientists will be free to use this data for sustainable growth and climate change detection. In Mozambique, after a GS was built, there were efforts made to educate students and help scientist conduct research with that data⁹³. Similar and even higher scale versions of these educational efforts can be made in the selected locations. This can help governments save money spent on technology investments to be done for their countries. Lastly, the built infrastructure for laser communication will be in very unique locations that can be valuable for future missions. Considering that it is a low TRL system, the GSs to be built will be some of the first ones in use. Therefore, with increasing demand for laser communication, renting out or selling the GSs to other commercial parties after the mission life allows for recuperating some of the early investment costs. Potentially interested parties could be Amazon Web Services or ESA.

In conclusion, the CASE mission will not aim to make a direct profit. The total cost of the mission is determined considering the aspects needed to gather the scientific data needed. When the data is gathered, it will be available for science for free. On the other hand, the data gathered will help these countries fulfill their sustainable development goals while being able to enhance their economic growth by decreasing the risks of pollution. Many countries from around the globe are interested in monitoring climate and help enhance sustainable development in these locations.

⁹²https://rainforests.mongabay.com/amazon/amazon_destruction.html, [Retrieved June 7, 2021]

⁹³<https://hescf.org/projects/satellite-receiving-station-in-mozambique>, [Retrieved June 10, 2021]

27. Conclusion

This report aims to provide a final design of a spacecraft mission that hosts the Optical Metasurfaces Based Spectro-Polarimeter from TNO. This instrument was chosen despite its low TRL of 3, due to its promising technical performance. Based on the specifications and the stakeholder requirements, the subsystems of the satellite were designed taking a systems engineering approach.

The payload, and therefore the satellite, will operate at an altitude of 500 km. To closely approach the initially required temporal resolution of 30 min, a circular orbit around the equator was selected. This orbit allowed for a temporal resolution of 33.76 minutes with 3 satellites, compared to ~ 48 satellites if an inclined orbit was selected.

Each satellite will carry 3 detectors on-board. By measuring the aerosols from 3 different angles, the error on the retrieved properties is decreased compared to one viewing angle, whilst keeping the data rate low enough to keep the area coverage high. With a swath width of 250 km and a frame rate of 54 fps to ensure a ground sampling distance of 151 m, the instrument will gather data at a rate of 3.89 Gbit/s. To ensure the downlink of the gathered data, the CubeCat will be used. This laser communication system designed by TNO and Hyperion Technologies can provide a downlink rate of 1 Gbit/s.

The targets of CASE have been divided into three groups. The primary target, the Amazon rainforest, is of the highest interest since it presents the largest scientific value to the stakeholders and will be measured for 950 km along-track. By measuring the aerosol levels and cloud formation, the relation between aerosols and clouds can be assessed and the effects of deforestation can be studied. The secondary targets, Singapore (250 km) and Nairobi/Kampala (175 km, with a temporal resolution of 60 min), are of less importance but are still preferably measured every orbit since they fit into the measurement budget. Finally, the tertiary target, Libreville (175 km), presents the least scientific value, and should only be measured when there is downlink capacity to spare. However, these cities are interesting to monitor to see the relation between the development of African cities and aerosol levels. During the mission the targets can be changed to any location close to the equator. However, the larger the distance to the equator, the less accurate the measurements will be due to the angling of the spacecraft. Three magnetorquers, allowing for 3-axis control, will be used to point the spacecraft towards its targets.

To send down the data gathered on the primary and secondary targets, 2 ground stations on the equator are necessary. However, as laser communication is unable to send data down through clouds, 7 ground stations will be built to ensure the downlink of data is reliable. By placing the ground stations in relatively dry areas and on elevated mountains, a downlink reliability of 94.0% could be achieved. The communication system will furthermore be used as an indicator of clouds above the location of the ground stations, since a distorted or missing signal can indicate clouds between the satellite and the ground station. As laser communication technology develops, communication through clouds will become more feasible [87]. This option must be assessed when the payload instrument is ready, as it would result in fewer ground stations and therefore a lower mission cost.

The final satellite will be a 12U CubeSat with a wet mass of 12.47 kg and will use 30.73 Wh of energy per orbit, provided by 0.156 m² of solar panels. To provide the necessary 115.99 m/s of ΔV , 0.5 kg of water propellant will be taken on-board. The spacecraft design meets all stakeholder requirements, excluding the polarimetric accuracy. However, as the instrument outperforms the currently available instruments on most other fronts, the polarimetric accuracy of <0.01 (<0.005 for the first 5 polarized bands) was found to be sufficient. The cost of the mission will be 120 M€, largely due to the estimated payload cost of 30 M€ per spacecraft. Due to the high scientific and societal value of this mission, it is expected that enough investors will support this mission.

The CASE mission will reduce the uncertainty in climate models, by measuring aerosols more accurately than was possible before. Its high temporal resolution allows for an accurate reconstruction of aerosol levels throughout the day, the large swath width makes it easier to assess flow of aerosols through cities, and the high spatial resolution allows for exact identification of aerosol sources. These accurate measurements will result in more accurate climate policy and aerosol prevention, which benefits both the planet and human health.

Personal Communication

- [A] (2021-05-06) Dr. ir. J.M. Kuiper, *TU Delft*
- [B] (2021-05-12) Dr. J.M. Smit, *SRON*
- [C] (2021-05-19) Dr. ir. J.M. Kuiper, *TU Delft*
- [D] (2021-05-27) Dr. A. Bell, *TNO*
- [E] (2021-05-31) Dr. A. Bell, *TNO*
- [F] (2021-05-31) Prof. dr. ir. H.W.J. Russchenberg, *TU Delft*
- [G] (2021-06-02) M. Cmok, *XIMEA*
- [H] (2021-06-02) R. Hoyt, *Tethers Unlimited, Inc.*
- [I] (2021-06-04) Dr. A. Bell, *TNO*
- [J] (2021-06-04) R. Laszlo, *Needronix*
- [K] (2021-06-07) D. Hendrix, *Airbus Defense & Space*
- [L] (2021-06-07) Prof. dr. ir. H.W.J. Russchenberg, *TU Delft*
- [M] (2021-06-08) M. Cmok, *XIMEA*
- [N] (2021-06-09) D. van de Sandt, *Kowa*
- [O] (2021-06-09) B. Treacy, *ISISpace*
- [P] (2021-06-14) W.E. Crowcombe, *TNO*
- [Q] (2021-06-14) N. Lonsdale, *AAC Clyde Space*

Bibliography

- [1] J. Jeuken, et al. (2021). *Earth Aerosol Observation Mission: Midterm Report*.
- [2] J. Jeuken, et al. (2021). *Earth Aerosol Observation Mission: Project Plan*.
- [3] J. Jeuken, et al. (2021). *Earth Aerosol Observation Mission: Baseline Report*.
- [4] Fortune Business Insights. (2019). Small Satellite Market Size Share & COVID-19 Impact Analysis, By Type, Components, Application, End-User, and Regional Forecast, 2020-2027.
- [5] A. Narune, E. Prasad. (2019). Small Satellite Market by Mass, Subsystem, Application, N GEO Orbit, End User, Frequency, and Region - Global Forecast to 2025.
- [6] A. Narune, E. Prasad. (2019). Small Satellite Market by Type, Application, and End-User: Global Opportunity Analysis and Industry Forecast, 2019–2026.
- [7] Reuters. (2019). *France's Macron says real 'ecocide' going on in Amazon*.
- [8] M.J. Gichuru, J. Boman, A. Wagner. (2009). *Characterization of aerosol particles at an industrial background site in Nairobi, Kenya*.
- [9] P. DeSouza. (2020). *Air pollution in Kenya: a review*.
- [10] Kampala Capital City Authority. (n.d.). *Kampala's Air Quality Is Six Times Worse Than Global Standards*.
- [11] National Climate Change Secretariat. (2016). *Take Action Today for Carbon-efficient Singapore*.
- [12] H. Kramer. (2018). *PACE (Plankton, Aerosol, Cloud, ocean Ecosystem) Mission*.
- [13] H. Kramer. (2018). *EarthCARE (Earth Clouds, Aerosols and Radiation Explorer)*.
- [14] J. Austin, e. a. (2015). *Developing a standardised methodology for spacespecific Life Cycle Assessment*. CEAS.
- [15] S.R. Hirshorn. (2016). *NASA Systems Engineering Handbook* (2th ed.). NASA.
- [16] G.H. Brundtland. (1987). *Our Common Future*. United Nations.

- [17] United Nations Office for Outer Space Affairs. (2010). Space Debris Mitigation Guidelines of the Committee on the Peaceful Uses of Outer Space.
- [18] R. Janovsky, et al. (2002). *End-Of-Life de-orbiting strategies for satellites*. DGLR Jahrbuch.
- [19] M. Langer. (2018). Reliability Assessment and Reliability Prediction of CubeSats through System Level Testing and Reliability Growth Modelling.
- [20] M. Langer, J. Bouwmeester. (2016). Reliability of CubeSats - Statistical Data, Developers' Beliefs and the Way Forward.
- [21] J.F. Castet, J.H. Saleh. (2009). Satellite and satellite subsystems reliability: Statistical data analysis and modeling.
- [22] P. G. Cheng. (2003). How Software Errors Contribute to Satellite Failures: Challenges Facing the Risk Analysis Community.
- [23] S. Drugalev. (2018). Implementation of a Daemon for Critical Subsystems of the Satellite Mission MOVEII.
- [24] R.S. Pressman. (2010). Software Engineering: A Practitioner's Approach (7th ed.)
- [25] M. Kaminskiy. (2015). CubeSat Data Analysis Revision.
- [26] M. Swartwout. (2013). The First One Hundred CubeSats: A Statistical Look.
- [27] T.L. Saaty. (2004). Decision Making - The Analytic Hierarchy and Network Processes (AHP/ANP).
- [28] James Wertz, et al. (2011). *Space Mission Engineering - The New SMAD-Microcosm Press*. Space Technology Library.
- [29] O. Dubovik, et al. (2019). Polarimetric remote sensing of atmospheric aerosols: Instruments, methodologies, results, and perspectives. *Journal of Quantitative Spectroscopy and Radiative Transfer*, 224, 474–511.
- [30] A. K. Prasad, R. P. Singh. (2007). Comparison of MISR-MODIS aerosol optical depth over the Indo-Gangetic basin during the winter and summer seasons (2000–2005). *Remote Sensing of Environment*, 107(1), 109–119.
- [31] L. Wu, et al. (2015). Aerosol retrieval from multiangle, multispectral photopolarimetric measurements: importance of spectral range and angular resolution. *Atmospheric Measurement Techniques*, 8(6).
- [32] Monitoring of aerosol forcing of climate from space: analysis of measurement requirements. (2004). *Journal of Quantitative Spectroscopy and Radiative Transfer*, 88(1), 149–161.
- [33] O. P. Hasekamp, J. Landgraf. (2005). Retrieval of aerosol properties over the ocean from multispectral single-viewing-angle measurements of intensity and polarization: Retrieval approach, information content, and sensitivity study. *Journal of Geophysical Research: Atmospheres*, 110(D20).
- [34] A. van Amerongen, et al. (2019). *SPEXone: a compact multi-angle polarimeter*. SPIE.
- [35] M. Negri, et al. (2017). New Technologies for Ammonium Dinitramide Based Monopropellant Thrusters – The Project RHEFORM.
- [36] R.K. Pothamsetti. (2015). Electrolysis Propulsion for CubeSat Spacecraft.
- [37] D.V. Mateu. (2011). Electrolysis Propulsion for CubeSat Spacecraft.
- [38] G. Chisholm, L. Cronin. (2017). *Hydrogen from Water Electrolysis*. University of Glasgow.
- [39] Tethers Unlimited. (n.d.). *In-Space Propulsion*.
- [40] Tethers Unlimited. (20202). HYDROS Engine Datasheet.
- [41] NASA. (2021). *NASA CubeSat to Demonstrate Water-Fueled Moves in Space*.
- [42] NASA. (2020). *Water-Powered Engines Offer Satellite Mobility*.
- [43] ISISpace. (2021). On Board Computer (iOBC) Datasheet.
- [44] Axon Interconnectors And Wires Pvt Ltd. (2017). Low Mass 28AWG SpaceWire datasheet.
- [45] Micro-Coax. (2017). MCJ088D UTiFLEX Space Flight cable assemblies datasheet.
- [46] Axon Interconnectors And Wires Pvt Ltd. (2017). Jacketed twisted pairs - ESCC 3901 013 datasheet.
- [47] W. L. Gore & Associates. (2017). Space Cables, Type SPLD datasheet.
- [48] C. Sansoè, M. (2011). Use of FRAM Memories in Spacecrafts.
- [49] NEEDRONIX. (2021). NXSS3v00 datasheet.
- [50] OCE technologies. (2021). St series datasheet.

- [51] Hyperion technologies. (n.d.). MTQ200 datasheet.
- [52] Hyperion technologies. (2019). CubeCat Optical Laser Terminal.
- [53] Ojo, J. (2019). Free space optics atmospheric losses and performance in akure, nigeria. *APTIKOM Journal on Computer Science and Information Technologies*, 4, 35–44.
- [54] Rudolf Saathof, et. al. (2019). Optical satellite communication space terminal technology at TNO. *International Conference on Space Optics — ICSO 2018*, 11180, 213–222.
- [55] H. Kuiper, D. Dolkens. (2020). A cutting edge 6U CubeSat ADCS design for Earth observation with sub-meter spatial resolution at 230–380 km altitude. *CEAS Space Journal*, 12, 613–621.
- [56] N. Nelson, P.S. Barry. (2001). Measurement of Hyperion MTF from on-orbit scenes. *Proceedings of SPIE - The International Society for Optical Engineering*, 7, 2967–2969.
- [57] GeoEye. (2014). GeoEye-1: Instrument/Product Description.
- [58] Hyperion technologies. (2021). ST-400 datasheet.
- [59] Hyperion technologies. (2021). ST-200 datasheet.
- [60] arcsec. (2021). Sagitta star tracker datasheet.
- [61] Blue Canyon Technologies. (2021). NST Star Tracker datasheet.
- [62] Nano avionics. (2021). ST-1 datasheet.
- [63] Kairospace. (2021). Star tracker datasheet.
- [64] SolarMEMS. (2021). Nano-SSOC datasheet.
- [65] SolarMEMS. (2021). SSOC datasheet.
- [66] NewSpace systems. (2021). NFSS datasheet.
- [67] Bradford Space. (2021). Mini FSS datasheet.
- [68] Hyperion technologies. (2021). SS200 datasheet.
- [69] NEEDRONIX. (2021). NXSS2v01 datasheet.
- [70] D.V. Mateu. (n.d.). Three-axes attitude determination and control system based on magnetorquers for small satellites.
- [71] R. Fonod, E. Gill. (2018). Magnetic Detumbling of Fast-tumbling Picosatellites.
- [72] Herbert J. Kramer. (2002). SwissCube.
- [73] W. Lu, L. Duan, Y. Cai. (17-01-2019). De-tumbling Control of a CubeSat.
- [74] Dario Modenini, Anton Bahu, Giacomo Curzi, Andrea Togni. (2020). A Dynamic Testbed for Nanosatellites Attitude Verification.
- [75] Kapoor, A., & Rajak, A. (2020). Design of Electrical Power Systems for Satellites. *Modelling, Simulation and Intelligent Computing*, 659, 307–318.
- [76] Wright, A. (2017). *User Manual: 3rd Generation EPS Range - No Inhibits*. AAC Clyde Space.
- [77] J.J. Wijker. (2010). *Spacecraft structures*. Springer.
- [78] Arianespace. (1999). Ariane 4: user's manual.
- [79] Arianespace. (2000). Ariane 5: user's manual.
- [80] T. Sgobba. (2018). *Space Safety and Human Performance*. Elsevier/Butterworth-Heinemann.
- [81] W.J. Larson, J.R. Wertz. (1999). *Space Mission Analysis and Design*. Kluwer Academic Publishers.
- [82] Rocket Lab. (2020). *Launch: Payload User's Guide*.
- [83] A. Menchinelli, F. Ingiosi, et. al. (2018). A Reliability Engineering Approach for Managing Risks in CubeSats. *Aerospace*, 5(4), 121.
- [84] B.T.C. Zandbergen. (2015). *Aerospace Design & Systems Engineering Elements I. Part: Launcher Design and Sizing* (1.05 ed.). Delft University of Technology, Faculty of Aerospace Engineering.
- [85] ESA: SRE-PA, D-TEC staff. (2015). Margin philosophy for science assessment studies.
- [86] D. Agnolon. (2012). *MarcoPolo-R Mission Requirements Document*. ESA.
- [87] Guillaume Schimmel, et. al. (2018). Free space laser telecommunication through fog. *Optica*, 5(10), 1338–1341.

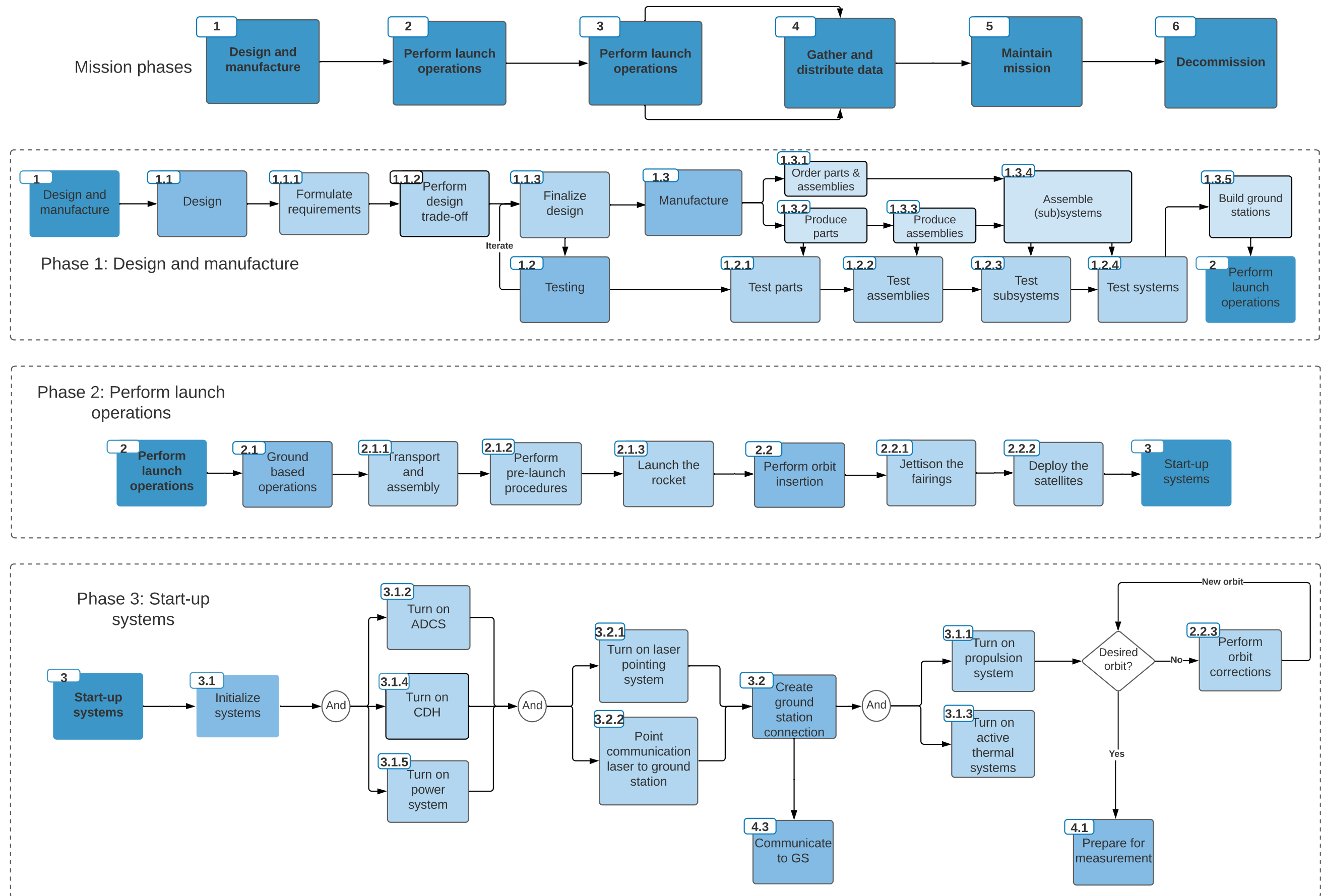


Figure A.1a: Functional Flow Diagram (phase 1-3).

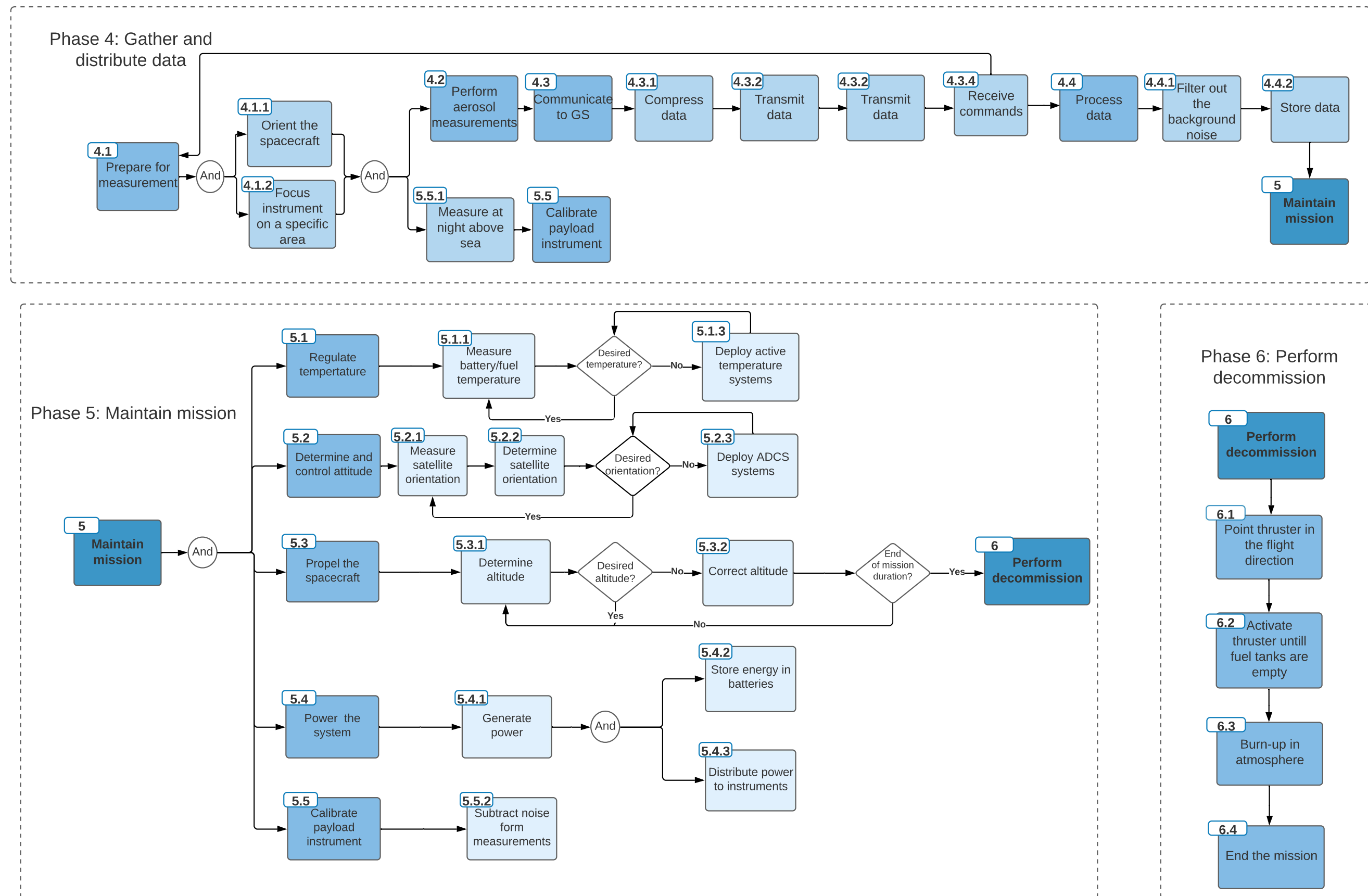


Figure A.2b: Functional Flow Diagram (phase 4-6).

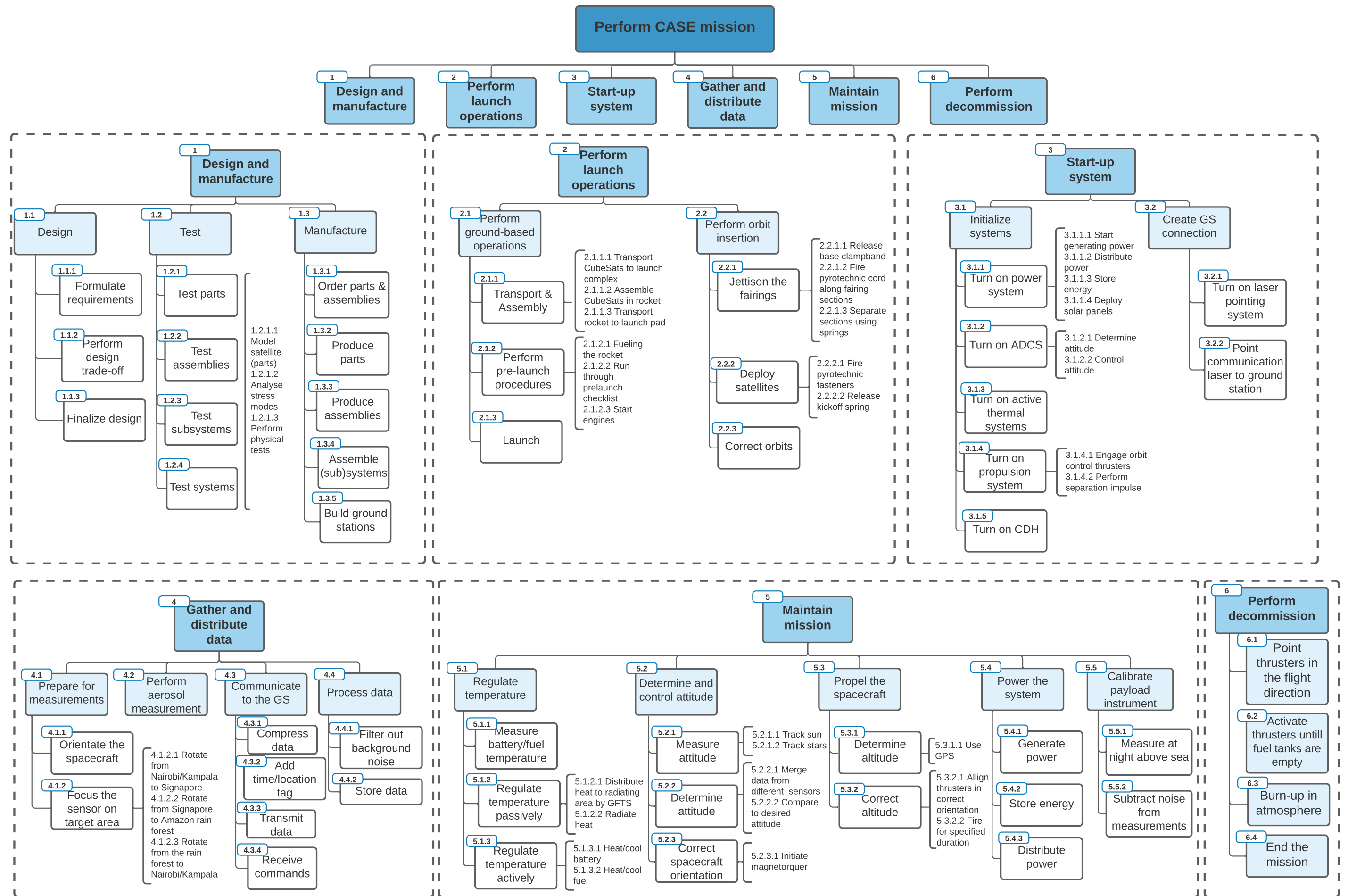


Figure A.2 Functional Breakdown Structure.

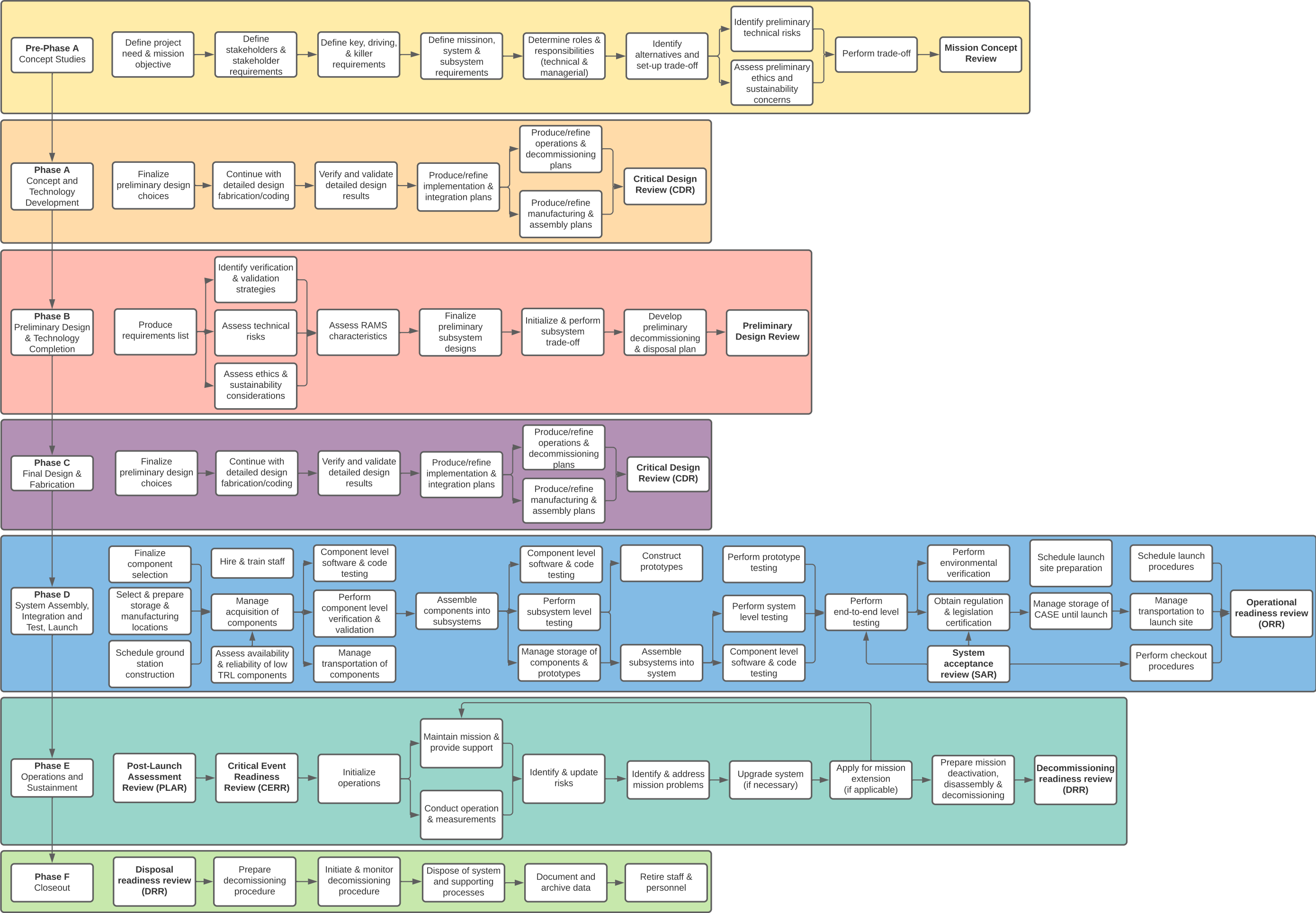
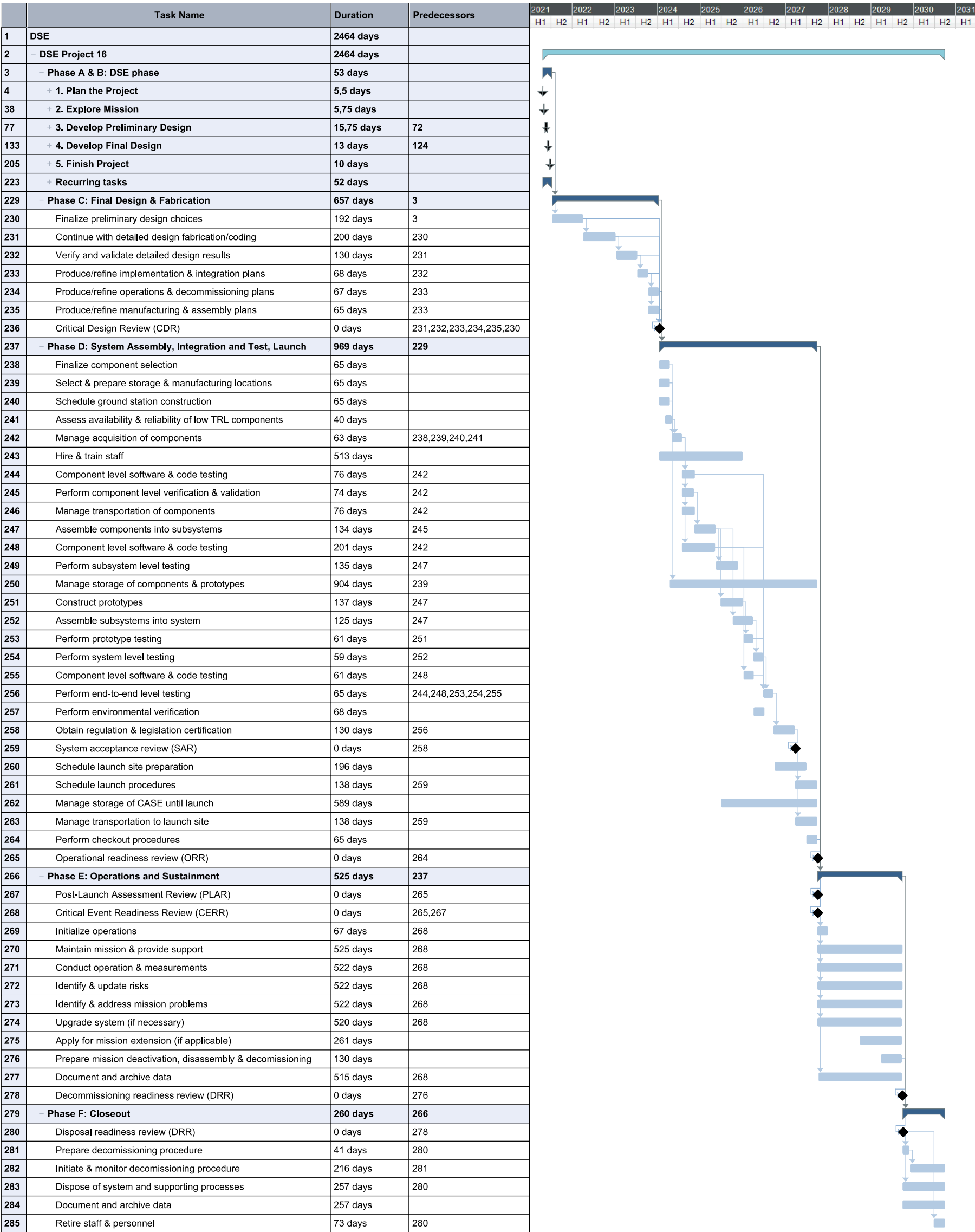
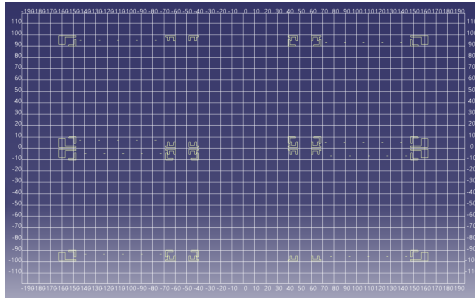


Figure 27.1: Project Design Logic Concept Diagram

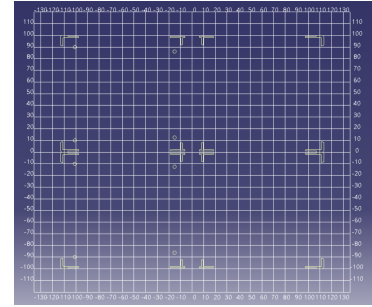


B. Second Moment of Area

In the Figure B.1 cross sections of the primary 12U structure can be seen. The axial cross section is shown on the left and lateral on the right. The coordinates on the axes are shown in millimeters.



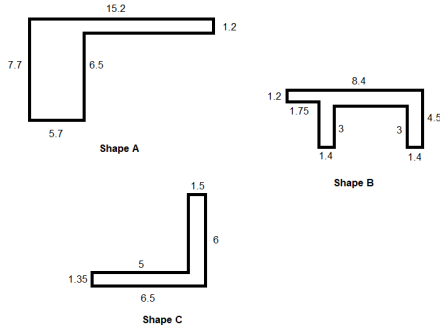
(a) Perpendicular to the axial direction.



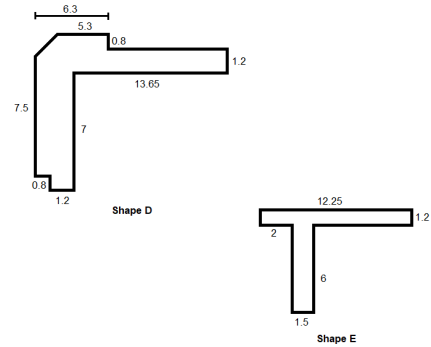
(b) Perpendicular to the lateral direction.

Figure B.1: Cross sections of the primary 12U structure.

The axial cross section can be divided into 3 different geometrical shapes: 8 shapes A, 16 shapes B and 16 shapes C. The lateral cross section consists of 8 shapes D and 8 shapes E. The shapes with the dimensions can be seen in Figure B.2.



(a) Shapes A, B and C.



(b) Shapes D and E.

Figure B.2: Cross sections shapes with dimensions in mm.

As each shape can be divided into basic simple rectangles, the basic second moment of are calculated:

$$I_0 = \sum \frac{1}{12}bh^3 \quad (\text{B.1})$$

where b is rectangle's dimension parallel to rotation axis and h is perpendicular to it. Then the total second moment including Steiner term is:

$$I = I_0 + \sum Ar^2 \quad (\text{B.2})$$

where A is a area and r is its distance to the centroid.